Stability, Structure, and Barrier Properties of Self-Assembled Films on Metal Supports

by

G. Kane Jennings

B.S., Chemical Engineering (1993)

Auburn University

M.S. in Chemical Engineering Practice (1996)

Massachusetts Institute of Technology

Submitted to the Department of Chemical Engineering
in Partial Fulfillment of the Requirements for the Degree of
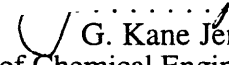Doctor of Philosophy in Chemical Engineering

at the

Massachusetts Institute of Technology

September, 1998

© 1998 Massachusetts Institute of Technology

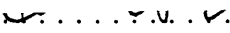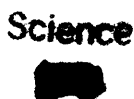Signature of Author . . . .

G. Kane Jennings
Department of Chemical Engineering
July 16, 1998

Certified by . . . .

Paul E. Laibinis
Doherty Assistant Professor of Chemical Engineering
Thesis Supervisor

Accepted by . . . .

Robert E. Cohen
St. Laurent Professor of Chemical Engineering
Chairman, Committee for Graduate Students

1

Stability, Structure, and Barrier Properties of Self-Assembled Films on Metal Supports

by

G. Kane Jennings

ABSTRACT

The first part of this thesis details the use of self-assembled monolayers (SAMs) derived from the adsorption of n-alkanethiols $[CH_3(CH_2)_{n-1}SH]$ onto copper to protect the underlying metal from corrosion. Due to their dense packing and crystalline structure, these films provide a barrier that impedes the transport of oxygen and water to the copper surface. As measured by electrochemical impedance spectroscopy, the resistance provided by these films increases by 4.2 MΩ•cm^2 for each methylene unit in the adsorbate that forms the SAM for chain lengths n 16. Efforts to form thicker, more protective SAMs on copper utilized the assembly of long-chain ω-alkoxy-n-alkanethiols $[CH_3(CH_2)_{p-1}O(CH_2)_mSH; m = 11, 19, 22; p = 18, 22]$ that contain an internal ethereal unit. The barrier properties of these ether-containing SAMs depend on the chain length of the adsorbate and the position of the ethereal unit along the hydrocarbon chain. For all SAMs studied, the crystalline, densely packed structure of the film dramatically affects its resistance against the transport of corrosive agents. The eventual loss in protection of these films is attributed to oxidation and subsequent roughening of the underlying copper surface which perturbs the crystalline hydrocarbon lattice of the SAM. Upon prolonged exposure to 1 atm of O_2 at 100% relative humidity (RH), the SAMs that exhibited the most stable crystalline structures were more effective in maintaining their barrier properties at superior levels. The results indicate that the design of barrier coatings requires a selection of adsorbates that can achieve dense packing and high crystallinity and are able to maintain their structural properties.

The second part of this thesis discusses the use of underpotential deposition (upd) of silver and copper on gold to affect the structure and stability of an adsorbed n-alkanethiolate SAM. Thiols adsorb onto gold surfaces modified by submonolayer quantities of silver or copper and form SAMs with macroscopic properties similar to those of SAMs on gold, as evidenced by wetting and ellipsometric thickness measurements. Nevertheless, the molecular-level features of these films are distinct from those of SAMs on the native metals (gold, silver, or copper). First, the presence of the upd metal alters the binding and molecular structure of the adsorbed thiol, resulting in a more dense packing and a different orientation for the terminal methyl (-CH$_3$) group than on gold. In addition, the presence of a silver upd adlayer improves the thermal stability of the adsorbed monolayer while the presence of either a silver or copper upd layer improves the stability of the SAM against exchange with competing adsorbates at room temperature. The improved stability of the SAMs on upd-modified gold is attributed to a stronger ligation between the adsorbed sulfur and the upd metal. These results demonstrate that a single atomic layer of silver or copper is sufficient to achieve the adhesion of evaporated films of silver or copper films while alleviating the problems associated with oxidation of these substrates.

Thesis Supervisor: Paul E. Laibinis
Title: Doherty Assistant Professor of Chemical Engineering

To the memory of my grandfather, Alvin B. Whisenant, the greatest engineer I ever knew.

Acknowledgments

Many people have enriched my life and/or contributed to my progress as a researcher here at MIT. While it is impossible to thank all of them, the following people deserve special mention:

My thesis advisor, Prof. Paul E. Laibinis for his teaching, guidance, support, and friendship during these last 4.5 years. Deciding to become Paul's first student is probably the best career decision that I have ever made. I truly appreciate the time he devoted to me, especially all the time he spent in lab during my first year. As I embark on a similar career path, I can only hope to emulate his outstanding leadership skills.

My thesis committee members—Profs. Gleason, Hammond, Hatton, and Latanision—for their enthusiastic advice and encouragement concerning my projects.

Tseh-Hwan Yong and Jeff Munro, both undergraduates at MIT, who each worked with me for six months and synthesized the longest-chained thiol adsorbates that have produced the thickest SAMs yet reported. Without their hard work, this thesis would be 30% shorter and 100% less interesting. They are brilliant and dedicated young engineers who will become extremely successful in the career path they choose.

My fellow PEL group members in 66-425—Mark, Seok-won, Namyong, Ben, Ivan, Seiichi, and Inge—for all their assistance and our friendly discussions during these last few years. Special thanks are directed to my baymate Mark for allowing me to share his home (bay) for six days per week, Seok-won for his dedicated work on the IR simulation codes, Ben for his electrochemical expertise, and Seiichi for his AFM wizardry. Special thanks also go to Srivatsan Raghavan and Cristina Perez de-la-Cruz for helping me climb the learning curve that first year in lab.

The 1993-94 "Thursday night drinking/Seinfeld club"—Diane, John, Randy, etc.—for all the fantastic memories. My years at MIT were infinitely more enjoyable due to the close friendships we developed. I wish them all the best of luck, and I look forward to our occasional reunions.

My practice school colleagues—Matthew, Garrett, and Ginger—for helping me find amusement in our 100-h work weeks at Merck and Dow and for their friendship thereafter. If I ever have to spend two months in Michigan again, I hope those guys will be there with me.

Dr. Atul Parikh for providing pertinent discussions on the characterization of SAMs by IR spectroscopy and developing the Fortran codes to simulate the IR spectra. I also thank Rebecca Hung for the synthesis of several odd-chained thiol adsorbates that were used in these studies.

My parents, Nathan and Renae Jennings, for their neverending support and guidance throughout my life. I sincerely appreciate their encouragement for me to attend MIT and all their efforts in helping me achieve my goals.

And finally, my wife Laura for her continuous care, support, and patience throughout all my hard work and late hours. I truly appreciate her taking a very difficult job in order to support us through these first three years of marriage. I also thank her for allowing me the flexibility to achieve my career goals. I look forward to spending the rest of my life with her.

Table of Contents

List of Figures

14

List of Tables

Chapter 1. Introduction to Self-Assembled Monolayers

1.1. Chemical Modification of Surface Properties of Materials

Interfacial properties such as wetting, adhesion, and lubrication are often determined by the outermost few angstroms of material at an interface. The control of these and other properties requires an ability to manipulate the molecular-level structure and composition at the surface of a material. One of the most flexible systems for modifying the surface properties of an inorganic material is that of self-assembled monolayers (SAMs).[1] SAMs are formed by the spontaneous chemisorption of tailored adsorbates onto reactive metal or metal oxide surfaces (Figure 1.1). The formation of the SAM is driven by a chemical reaction between the adsorbate and the metal surface and produces a robust surface coating that can be stable in vacuum, air, or liquid environments. SAMs have been prepared on various substrates: alkanethiols on gold,[2,3] silver,[4] copper,[4] mercury,[5] iron,[6] GaAs,[7] and YBa_2CuO_x;[8] alcohols and amines on platinum;[9] trichlorosilanes on silica;[10] carboxylic acids on oxides of aluminum;[11] phosphonic acids on oxides of zirconium, titanium, and aluminum;[12] hydroxamic acids on copper, silver, titanium, aluminum, zirconium and iron.[13] The chemical constituency of the monolayer can be tailored by chemical synthesis to expose a high density of specified functional groups at the monolayer/air(or solution) interface.[3] These functional groups may be selected to provide the requisite surface properties for a given application. The use of SAMs can impact many areas including corrosion prevention,[14] sensor design,[15] microelectronics,[16] biocompatibility,[17] separations,[18] and waste remediation.[19]
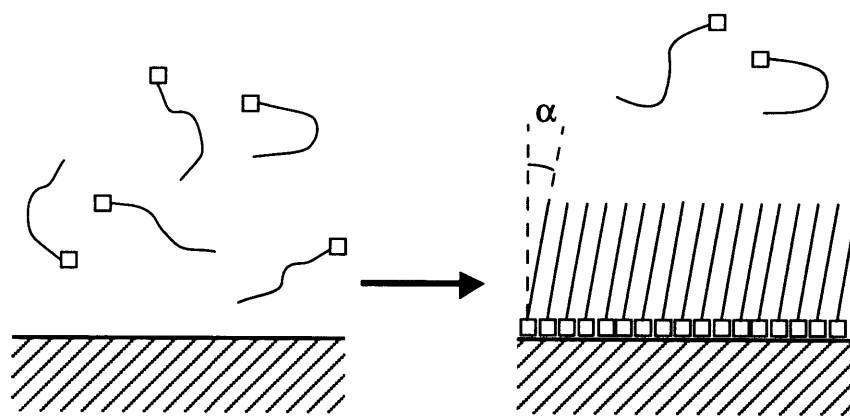
Figure 1.1. Schematic illustration of SAM formation from solution.

1.2. History of Self-Assembled Monolayers

The development of self-assembled monolayers (SAMs) can be traced to the seminal papers of Zisman et al. almost fifty years ago.[20-22] By exposing glass surfaces to dilute solutions of long-chained alcohols in hexadecane as the solvent, these researchers formed oriented monolayer films that were not wet by the solvent medium and exhibited wetting properties similar to those of oriented Langmuir-Blodgett monolayers. Zisman and coworkers extended this system to include a range of metal and metal oxide surfaces and various surfactant-like molecules including long-chained amines, carboxylic acids, and primary amides. The driving force for the assembly was the large interfacial free energy present between the metal (oxide) surface and the hydrocarbon solvent phase that was reduced upon directed adsorption of the amphiphilic species. In these cases, the polar species adsorbed to the solid support and the nonpolar alkyl tails oriented away from the substrate to expose a low energy surface of CH_3 groups[20] (and later CF_3 groups for perfluoroalkane-based amphiphiles[21]).

Shafrin and Zisman provided demonstration that ligating chemical interactions between the head group of a molecule and a metal surface could drive the formation of an oriented monolayer film by adsorbing alkyl amines onto platinum from water.[22] The resulting SAMs were hydrophobic and exhibited wetting properties that were the same as those for films formed from hexadecane (an inert solvent). The formation of this coating in water by a self assembly process is notable as it showed a preference toward adsorption of one chemical group over another (a preference of $> 10^6$ by the amine group for platinum vs. the hydroxyl groups of water[22]) and demonstrated the ability to produce oriented films from polar solvents. The systems developed by Zisman had low energies of adsorption (5 - 15 kcal/mol),[23] exhibited only modest stabilities, and were limited in that they only generated low-energy surfaces.

Nuzzo and Allara and coworkers extended the Zisman approach in a dramatic way by relying on the strong and specific interactions between gold and sulfur to form oriented organic films that exposed both high- and low-energy surfaces, depending on the tail group present in adsorbing organic disulfides,[24] and later for sulfides[9] and thiols.[2,25] The general inertness of gold toward many chemical species allowed the adsorption of organosulfur compounds to occur exclusively through the sulfur atom(s) and without concurrent adsorption of any non-sulfur-based moieties. The specificity of the interaction between gold and sulfur—a "soft-soft" chemical acid-base ligation between the soft ligand (sulfur) and a soft late transition element (gold)[26]— accommodates the presence of many "hard" polar groups that are typically encountered in organic and biological systems. This tolerance allowed formation of organized two-dimensional assemblies expressing these types of functionalities for the first time by a single adsorption step.

The adsorption of thiols to form densely packed, oriented monolayer films is not limited to gold surfaces but also occurs on silver,[4,27] copper,[4] mercury,[5] and GaAs[7] surfaces. Although the tolerance of these substrates for polar tail groups has only been demonstrated for silver and copper, it is likely that the assemblies that are the result of soft-soft chemical ligation would have similar abilities to accommodate hard polar tail groups and produce both high- and low-energy organic surfaces on other soft metal substrates. While the high flexibility of the self-assembly method is expected for these other substrates using thiols, the packing density, structure, and stability of the monolayers may be different from those formed on gold due to the specific geometric and electronic aspects of these other metal surfaces.

1.3. Motivation

While scientists have primarily studied SAMs as model systems, their use in applied research has been limited, due in part to their untested stabilities under industrially relevant conditions. The typical mode of use by researchers has been to prepare the monolayer immediately before use and discard it soon afterwards. Investigation of the long-term stability of the film has been a neglected area of research. Are SAMs destined to become restricted for use solely as model systems? Are there practical issues regarding the stability of SAMs that may better enable their use in applied research?

This thesis addresses pertinent engineering issues of SAM stability and technological application. The first part of the thesis investigates the use of SAMs on copper to provide a protective barrier against the diffusion of corrosive species (Chapters 2 - 7).[28,29] Part II focuses on a novel method for promoting metal-organic adhesion using the electrochemical method of underpotential deposition to provide an atomic-level, metal adhesive that enhances the stability of the SAM (Chapters 8 -12).[30,31]

1.4. References

1) Ulman, A. *An Introduction to Ultrathin Organic Films From Langmuir-Blodgett to Self-Assembly*; Academic Press: Boston, 1991.

2) Bain, C. D.; Troughton, E. B.; Tao, Y.-T.; Evall, J.; Whitesides, G. M.; Nuzzo, R. G. *J. Am. Chem. Soc.* **1989**, *111*, 321-335.

3) Laibinis, P. E.; Palmer, B. J.; Lee, S.-W.; Jennings, G. K. *The Synthesis of Organothiols and their Assembly into Monolayers on Gold*; In Thin Films, vol. 24; Ulman, A., Ed.; Academic Press: Boston, 1998; Vol. 24, pp 1-41.

4) Laibinis, P. E.; Whitesides, G. M.; Allara, D. L.; Tao, Y.-T.; Parikh, A. N.; Nuzzo, R. G. *J. Am. Chem. Soc.* **1991**, *113*, 7152-7167.

5) Demoz, A.; Harrison, D. J. *Langmuir* **1993**, *9*, 1046-1050.

6) Volmer, M.; Stratmann, M.; Viefhaus, H. *Surf. Interface Anal.* **1990**, *16*, 278-282.

7) Sheen, C. W.; Shi, J. X.; Martensson, J.; Parikh, A. N.; Allara, D. L. *J. Am. Chem. Soc.* **1992**, *114*, 1514-1515.

8) Mirkin, C. R.; Chen, K.; Lo, R. K.; Zhao, J.; McDevitt, J. T. *J. Am. Chem. Soc.* **1995**, *117*, 6374-6375.

9) Troughton, E. B.; Bain, C. D.; Whitesides, G. M.; Allara, D. L.; Porter, M. D. *Langmuir* **1988**, *4*, 365-385.

10) Plueddemann, E. P. *Silane Coupling Agents*; 2nd ed.; Plenum Press: New York, 1991.

11) Allara, D. L.; Nuzzo, R. G. *Langmuir* **1985**, *1*, 45-52.

12) Gao, W.; Dickinson, L.; Grozinger, C.; Morin, F.; Reven, L. *Langmuir* **1996**, *12*, 6429-6435.

13) Folkers, J. P.; Gorman, C. B.; Laibinis, P. E.; Buchholz, S.; Whitesides, G. M.; Nuzzo, R. G. *Langmuir* **1995**, *11*, 813-824.

14) Laibinis, P. E.; Whitesides, G. M. *J. Am. Chem. Soc.* **1992**, *114*, 9022-9027.

15) Creager, S. E.; Olsen, K. G. *Anal. Chim. Acta* **1995**, *307*, 277-289.

16) Jain, A.; Farkas, J.; Kodas, T. T.; Chi, K.-M.; Hampden-Smith, M. J. *Appl. Phys. Lett.* **1992**, *61*, 2662-2664.

17) Prime, K. L.; Whitesides, G. M. *Science* **1991**, *252*, 1164-1167.

18) Wirth, M. J.; Fairbank, R. W. P.; Fatunmbi, H. O. *Science* **1997**, *275*, 44-47.

19) Feng, X.; Fryxell, G. E.; Wang, L.-Q.; Kim, A. Y.; Liu, J.; Kemner, K. M. *Science* **1997**, *276*, 923-926.

20) Bigelow, W. C.; Glass, E.; Zisman, W. A. *J. Colloid Sci.* **1946**, *1*, 513-538.

21) Schulman, F.; Zisman, W. A. *J. Colloid Sci.* **1952**, *7*, 465-481.

22) Shafrin, E. G.; Zisman, W. A. *J. Colloid Sci.* **1949**, *5*, 571-590.

23) Bigelow, W. C.; Glass, E.; Zisman, W. A. *J. Colloid Sci.* **1947**, *2*, 563-591.

24) Nuzzo, R. G.; Allara, D. L. *J. Am. Chem. Soc.* **1983**, *105*, 4881-4883.

25) Nuzzo, R. G.; Fusco, F. A.; Allara, D. L. *J. Am. Chem. Soc.* **1987**, *109*, 2358-2367.

26) Pearson, R. G. *J. Am. Chem. Soc.* **1963**, *85*, 3533-3539.

27) Walczak, M. M.; Chung, C.; Stole, S. M.; Windrig, C. A.; Porter, M. D. *J. Am. Chem. Soc.* **1991**, *113*, 2370-2378.

28) Jennings, G. K.; Laibinis, P. E. *Colloids Surf., A* **1996**, *116*, 105-114.

29) Jennings, G. K.; Munro, J. C.; Yong, T.-H.; Laibinis, P. E. *Langmuir* **1998**, in press.

30) Jennings, G. K.; Laibinis, P. E. *Langmuir* **1996**, *12*, 6173-6175.

31) Jennings, G. K.; Laibinis, P. E. *J. Am. Chem. Soc.* **1997**, *118*, 5208-5214.

Part I. Protection of Copper Surfaces with Self-Assembled Monolayers of n-Alkanethiols

Chapter 2. Introduction

2.1. Uses of Copper and Factors that Limit its Application

Copper has become the material of choice for forming highly conductive interconnects within integrated circuits because of its low electrical resistivity and superior electromigration resistance.[1] A primary obstacle associated with the conversion to copper for this application includes the susceptibility of copper to corrosion. While copper-wired computer chips are typically not subjected to extremely corrosive conditions, the margin of error for chip corrosion is extremely small due to the sub-micron linewidths and even smaller thicknesses of the copper wires.[2] The development of methods to protect the surface of copper during the processing of the chip and the lifetime of the device could be extremely important in advancing its use for these applications.

Copper is also a commonly used material in heat exchanging applications[3] due to its high thermal conductivity and malleability. An important limitation for copper is that it readily corrodes in aqueous, oxygenated environments that are characteristic of heat exchanger operations.[4] Efforts to minimize the corrosion of copper in such applications have ranged from the use of deoxygenated water streams in specialized applications[5] to the addition of corrosion inhibiting agents to the process streams.[6-9] In this latter case, molecules such as benzotriazole, mercaptobenzimidazole, and thiourea are continuously added to circulating water streams during process operation to inhibit copper corrosion. These molecules—frequently being low-molecular-weight aromatic compounds that contain polar moieties for ligation to the surface and improved water solubility—bind to the metal surface in mono- or multilayer quantities. The packing of these rigid molecules on the surface is often poor, and the resulting layers provide only modest transport resistance for molecules such as O_2 and H_2O to the metal surface. In most cases, the coordination of the inhibitor molecules to the surface is weak, and their presence in the water streams is required to maintain the desired concentration of these agents at the metal surface.[6-9] As some inhibitor molecules also serve as reducing agents for the copper oxidation products, they must be continuously added to maintain the reducing potential of the water stream. The generation (and ultimately the disposal) of the contaminated waste water streams from these methods is an item of increasing environmental concern.

2.2 Self-Assembled Monolayers on Copper

A primary goal in this thesis is to develop robust coatings on copper that provide the requisite corrosion resistance for these applications, minimally impact the heat transfer characteristics of the metal, and remove the necessity for the continuous addition of inhibition agents to the contacting aqueous streams. In particular, this work focuses on systems that adsorb onto metal surfaces through strong chemical interactions and provide diffusional restrictions for small molecules (such as O_2 and H_2O) by nature of their densely packed, crystalline structure. Self-assembled monolayers (SAMs) offer many of the attributes needed for this application: (1) the film forms through a simple chemisorption process, enabling strong adhesion to the metal surface; (2) film formation is conformal allowing objects of any shape to be coated; (3) the thickness of the film can be controlled at the angstrom-level by selection of adsorbate; (4) the films are densely packed and crystalline; (5) the chemical composition of the film can be tailored by design and synthesis of adsorbates; (6) the molecular thickness of the films allows the use of x-ray photoelectron spectroscopy (XPS) and other surface analytical techniques to determine the chemical state and composition of species at the metal surface.

Due to the many attractive features of SAMs as coatings, our group[10,11] and others[12-16] have explored their application as films for inhibiting the corrosion on copper. Alkanethiols chemisorb to copper and form a densely packed monolayer of adsorbed thiolates where the hydrocarbon chains are oriented almost normal to the surface with an average tilt (or cant angle) of 12° or less.[17] The resulting SAMs can inhibit the oxidation of copper with thicker SAMs providing greater protection.[10] In specific, the oxidation rate of the copper substrate in air decreases by 50% for every four carbons in the adsorbate comprising the SAM.[10] These and other results[14] suggest that the cathodic process of corrosion is inhibited by the presence of the monolayer. In a study of the effects of humidity on the corrosion of copper, samples protected by a monolayer of $C_{22}SH$ oxidized at a rate that was independent of the water content in the contacting environment (see Chapter 3).[11] These results suggested that the SAM also acts as an effective barrier against the transport of water to the underlying copper surface for adsorbates of suitable chain length.

Aramaki and co-workers have modified hydroxyl-terminated SAMs on copper with alkyltrichlorosilanes to create films that contain an internal, cross-linked siloxane network (see Section 3.3). The resulting coatings exhibit protection efficiencies that are greater than for monolayer films formed from $C_{18}SH$ as evidenced by polarization measurements.[12,18,19] They have also extended this work to form a two-dimensional polymeric structure on copper by modification of a hydroxyl-terminated SAM with 1,2-bis(trichlorosilyl)ethane and subsequent treatment with an alkyltrichlorosilane to obtain further improvements in protection.[13] Feng et al.[15]

have combined electrochemical impedance spectroscopy (EIS), polarization, and XPS to determine that a thin SAM of $C_{12}SH$ is more protective than coatings formed from benzotriazole, a commonly used corrosion inhibitor for copper.

While the collective work from these groups demonstrates that SAMs can effectively inhibit the corrosion of copper, little is known about the stability of these films, the structural issues that govern the level of protection provided, or the mechanism of their eventual failure. The five other chapters that comprise this part of the thesis examine various engineering aspects concerning the use of SAMs to provide protection against the corrosion of copper. While SAMs offer many attributes needed for the requisite protection of copper, their efficacy on copper during extended exposure to water and oxidizing conditions had not been demonstrated prior to the work discussed in Chapter 3. Chapter 4 details the effect of film thickness on the protection provided by the SAM and the mechanism of the eventual breakdown in protection by combining electrochemical impedance spectroscopy and infrared spectroscopy. Chapters 5 and 6 report the formation, molecular structure, and barrier properties of a new class of SAMs formed from long-chain ω-alkoxy-n-alkanethiols. These systems represent the thickest and most protective SAMs yet formed from molecular adsorbates. Finally, the importance of dense packing and crystallinity on the protection provided by the SAM is discussed in Chapter 7.

2.3. References

1) Andricacos, P. C. *The Electrochem. Soc. Interface* **1998**, *7*, 23.

2) Frankel, G. S. "Corrosion of Microelectronic and Magnetic Storage Devices" In *Corrosion Mechanisms in Therory and Practice*, Marcus, P. and Oudar, J., Eds.; Marcel Dekker: New York, 1996, pp 547-579.

3) Blackman, L. C. F.; Dewar, M. J. S. *J. Chem. Soc.* **1957**, 162-176.

4) Torigoe, Y.; Ichino, T.; Nakano, Y. *Corros. Eng.* **1979**, *28*, 343-347.

5) Moliere, M.; Verdier, Y.; Leymonie, C. *Corros. Sci.* **1990**, *30*, 183-188.

6) Brunaro, G.; Parmigiani, F.; Perboni, G.; Rocchini, G.; Trabanelli, G. *Br. Corros. J.* **1992**, *27*, 75-79.

7) Gonzalez, S.; Laz, M. M.; Souto, R. C.; Salvarezza, R. C.; Arvia, A. J. *Corrosion* **1993**, *49*, 450-456.

8) Carron, K. T.; Lewis, M. L.; Dong, J.; Ding, J.; Xue, G.; Chen, Y. *J. Mater. Sci.* **1993**, *28*, 4099-4103.

9) Al-Kharafi, F. M.; Al-Hajjar, F. H.; Katrib, A. *Corros. Sci.* **1990**, *30*, 869-875.

10) Laibinis, P. E.; Whitesides, G. M. *J. Am. Chem. Soc.* **1992**, *114*, 9022-9027.

11) Jennings, G. K.; Laibinis, P. E. *Colloids and Surface, A: Physicochemical and Engineering Aspects* **1996**, *116*, 105-114.

12) Yamamoto, Y.; Nishihara, H.; Aramaki, K. *J. Electrochem. Soc.* **1993**, *140*, 436-443.

13) Itoh, M.; Nishihara, H.; Aramaki, K. *J. Electrochem. Soc.* **1995**, *142*, 3696-3704.

14) Ishibashi, M.; Itoh, M.; Nishihara, H.; Aramaki, K. *Electrochimica Acta* **1996**, *41*, 241-248.

15) Feng, Y.; Teo, W.-K.; Siow, K.-S.; Gao, Z.; Tan, K.-L.; Hseih, A.-K. *J. Electrochem. Soc.* **1997**, *144*, 55-64.

16) Scherer, J.; Vogt, M. R.; Magnussen, O. M.; Behm, R. J. *Langmuir* **1997**, *13*, 7045-7051.

17) Laibinis, P. E.; Whitesides, G. M.; Allara, D. L.; Tao, Y.-T.; Parikh, A. N.; Nuzzo, R. G. *J. Am. Chem. Soc.* **1991**, *113*, 7152-7167.

18) Itoh, M.; Nisihara, H.; Aramaki, K. *J. Electrochem. Soc.* **1994**, *141*, 2018-2023.

19) Itoh, M.; Nisihara, H.; Aramaki, K. *J. Electrochem. Soc.* **1995**, *142*, 1839-1846.

Chapter 3. Self-Assembled Monolayers of Alkanethiols on Copper Provide Corrosion Resistance in Aqueous Environments

3.1. Background

Laibinis and Whitesides have demonstrated the ability of self-assembled monolayer films derived from n-alkanethiols to inhibit oxidation of an underlying copper substrate under ambient conditions (air at room temperature and low humidity).[1] In this work, they observed that the films exhibited dramatic improvements in their ability to inhibit corrosion with only modest increases in the thickness of the self-assembled film: a 50% decrease in oxidation rate for every increase of 5 Å in film thickness. This improvement was attributed to the ability of the self-assembly method to form crystalline layers on the copper surface. In this chapter, the effectiveness of these adsorbed layers as barrier films against corrosion in the presence of water—both in the liquid and vapor phase—is presented. As the corrosion rate of untreated copper (and other metals) is known to be dramatically faster in the presence of an aqueous phase,[2] water could seriously affect the corrosion-resistant abilities of these layers. To address this issue, SAM-treated copper samples that were exposed to 1 atm of O_2 at 10 and 100% relative humidity levels and to oxygen-saturated water for periods up to two weeks were characterized.

Figure 3.1 displays a schematic illustration of the experimental approach. Self-assembled monolayers (SAMs) on copper were prepared by exposing freshly evaporated copper films supported on silicon wafers to deoxygenated solutions of alkanethiols. The evaporated copper samples were handled under nitrogen and anaerobically transferred to the adsorbate solution. These conditions produce well-defined monolayer films on the copper surface.[3,4] (When less stringent conditions are used, multilayer films can be produced on the copper surface.[5]) After exposure of the samples to the above oxidizing conditions for various periods of time, the samples were characterized by wetting measurements and x-ray photoelectron spectroscopy. These measurements provide information regarding the structural integrity of the barrier film and the extent of oxidation for the underlying copper substrate; the effectiveness of these layers as corrosion inhibitors were determined from these data. As an extension of these studies, the use of multilayer strategies were also explored to generate thicker layers on the copper surface to improve the barrier properties of self-assembled films on copper.
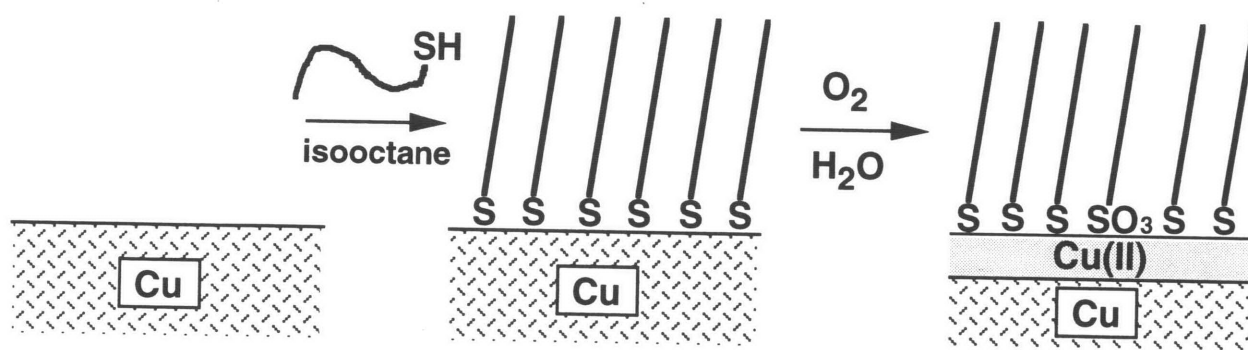
Figure 3.1. Schematic illustration of the formation of a self-assembled monolayer (SAM) on copper and the resulting species produced after exposure to oxidizing conditions. The assembly of the thiols (first step) was conducted under anaerobic conditions.

3.2. Results and Discussion

Figure 3.2 displays the results from x-ray photoelectron spectroscopy (XPS) for various bare and derivatized copper samples. XPS is well suited for these studies as it is highly surface sensitive and allows the detection of Cu(II) oxidation products at the sub-angstrom-level. In the Cu(2p$_{3/2}$) spectral region, Cu(0) and Cu(I) species exhibit a single peak at a binding energy of 932.6 eV. In comparison, Cu(II) species exhibit a peak that is shifted positively to a position of ~934.7 eV and also display the presence of less intense shake-up satellite peaks at 941.5 and 943.8 eV that are readily distinguished and well-separated from the primary Cu(2p$_{3/2}$) peaks. Changes in the relative intensities of these peaks can provide a quantitative monitor of an oxidation process (vide infra).

In these experiments, evaporated, polycrystalline copper films supported on silicon substrates were used. Immediately after evaporation, the chamber was backfilled with N_2 and the samples were transferred anaerobically to a solution of the adsorbate. XPS spectra for these samples exhibit no peaks in the Cu(2p3/2) region due to Cu(II) species (Figure 3.2a) and provide a starting point for these corrosion studies. Upon exposure to oxidizing conditions, the XPS spectra exhibit peaks due to Cu(II) species that increase in intensity with continued exposure (Figure 3.2b). A comparison of the level of oxidation for different samples provides information about the resistance of the system toward corrosion. For example, the XPS data in Figure 3.2 illustrate that a bare copper sample exposed to 1 atm of O_2 at 100% relative humidity (Figure 3.2d) oxidizes more rapidly than a bare copper sample exposed to 1 atm of O_2 at 10% relative humidity (Figure 3.2c). The presence of an adsorbed monolayer of hexadecanethiol on the copper sample (Figure 3.2b) is effective in decreasing the rate of oxidation of the copper substrate, even when the sample is exposed to oxidizing conditions of high humidity.

The relative intensities of the peaks in the Cu(2p$_{3/2}$) spectral region can be related to thicknesses through eq 3.1,[1]

$$d_{Cu(II)} = -\lambda \cos \phi \ln [1 - f_{Cu(II)}] \qquad (3.1)$$

where $d_{Cu(II)}$ is the thickness of the layer that contains Cu(II) species, λ is the inelastic mean free path of Cu(2p$_{3/2}$) photoelectrons through the CuO layer ($\approx$ 10.7 Å),[6] ϕ is the angle at which the detector is positioned relative to the surface normal (so-called "take-off angle" = 55°), and $f_{Cu(II)}$ is the fraction of the integrated peak area of the Cu(2p$_{3/2}$) spectral envelope that is due to Cu(II) species (both the primary and shake-up peaks). This analysis assumes that the Cu(II) species in the copper substrate are present in a uniform layer nearest the sample/air interface.[1] The use of eq 3.1, although not rigorous, is quite flexible for these investigations as it does not depend on the thickness or composition of any layers that separate the copper sample from the air (or vacuum) interface. The use of thickness measurements derived from eq 3.1 for the Cu(II) species allows
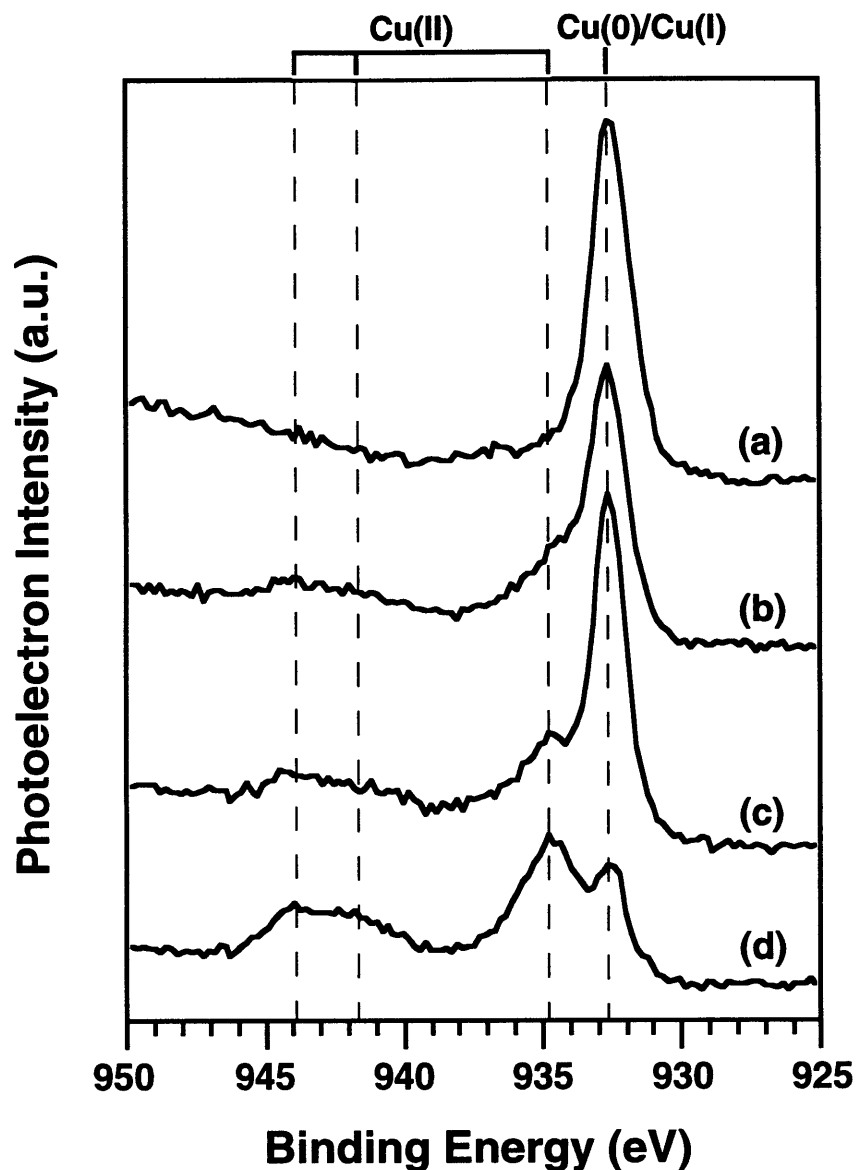
Figure 3.2. XPS spectra of the Cu($2p_{3/2}$) region for evaporated films of copper exposed to different oxidizing conditions. (a) Copper sample protected with $C_{16}H_{33}SH$ before exposure to oxidizing conditions. (b) Copper protected with $C_{16}H_{33}SH$ and exposed for 384 h to 1 atm of O_2 at 100% relative humidity. (c) Bare copper exposed for 144 h to 1 atm of O_2 at 10% relative humidity. (d) Bare copper exposed for 72 h to 1 atm of O_2 at 100% relative humidity. The dashed lines note the characteristic positions of the peaks for Cu(0)/Cu(I) and Cu(II)

direct quantitative comparison of the spectral results for different samples and oxidizing conditions. For example, application of eq 3.1 to the spectra in Figure 3.2 yields thickness for the Cu(II) species of 2.1 Å, 2.5 Å, and 9.3 Å for panels (b), (c), and (d), respectively.

Figure 3.3 summarizes the XPS results from experiments comparing the effectiveness of two adsorbates—$C_{16}H_{35}SH$ and $C_{22}H_{45}SH$—to impede corrosion of a copper substrate under common oxidizing conditions of 1 atm of O_2 at 100% relative humidity. The bare copper sample exhibits rapid oxidation under these conditions; the plateau in Figure 3.3 may be the result of transport limitations due to the formation of a 10-Å thick film of copper(II) oxide on the copper surface. For both adsorbates, the alkanethiolate monolayers are effective in inhibiting the corrosion process, with the longer-chained adsorbate ($C_{22}H_{45}SH$) providing the superior protection. The observation that longer-chained alkanethiols provide greater corrosion resistance under these humid conditions is similar to previous observations from related experiments conducted under ambient conditions. In Figure 3.3, the difference in the thickness of the two organic layers is only six methylene units (or ~7 Å in film thickness) and is sufficient to produce observable differences in the rate of oxidation to the underlying copper substrate. Laibinis and Whitesides previously asserted that the crystalline structure of the polymethylene chains in these adsorbed layers is responsible for the observations that changes in film thickness at the angstrom-scale can affect the diffusional rate of molecules (such as O_2 and H_2O) to the underlying substrate.[1]

Since copper oxidizes more rapidly in the presence of water,[2] the relative effectiveness of a SAM derived from $C_{22}H_{45}SH$ to inhibit corrosion under conditions where different concentrations of water are present were examined (Figure 3.4). In general, no differences were observed in the level of corrosion to the copper substrate when it was exposed to oxidizing conditions at different relative humidity levels or when the copper sample was placed in direct contact with oxygen-saturated water. Under these experimental conditions, underivatized copper samples exhibit significant differences in the formation of copper(II) oxides (see Figure 3.2c and d). The similarity of the data sets in Figure 3.4 illustrates the ability of these layers to limit the transport of water to the underlying copper substrate and suggests that these films remain structurally intact under these conditions. The use of hydrocarbon-based adsorbates provides suitable water repellency[4,7] (and in the case of samples immersed in water, poor water solubility) for the resulting layers to provide effective corrosion inhibition under these diverse conditions.

The stuctural integrity of the layers was examined during the corrosion process using wetting measurements. Laibinis et al. found that the wetting properties of the alkanethiolate SAM provided a highly sensitive probe of the changes occurring to the film during the oxidation process and that these measurements mirrored trends observed by XPS.[1] The wetting properties of hexadecane are a particularly sensitive indicator of structure as a densely packed surface expressing

29
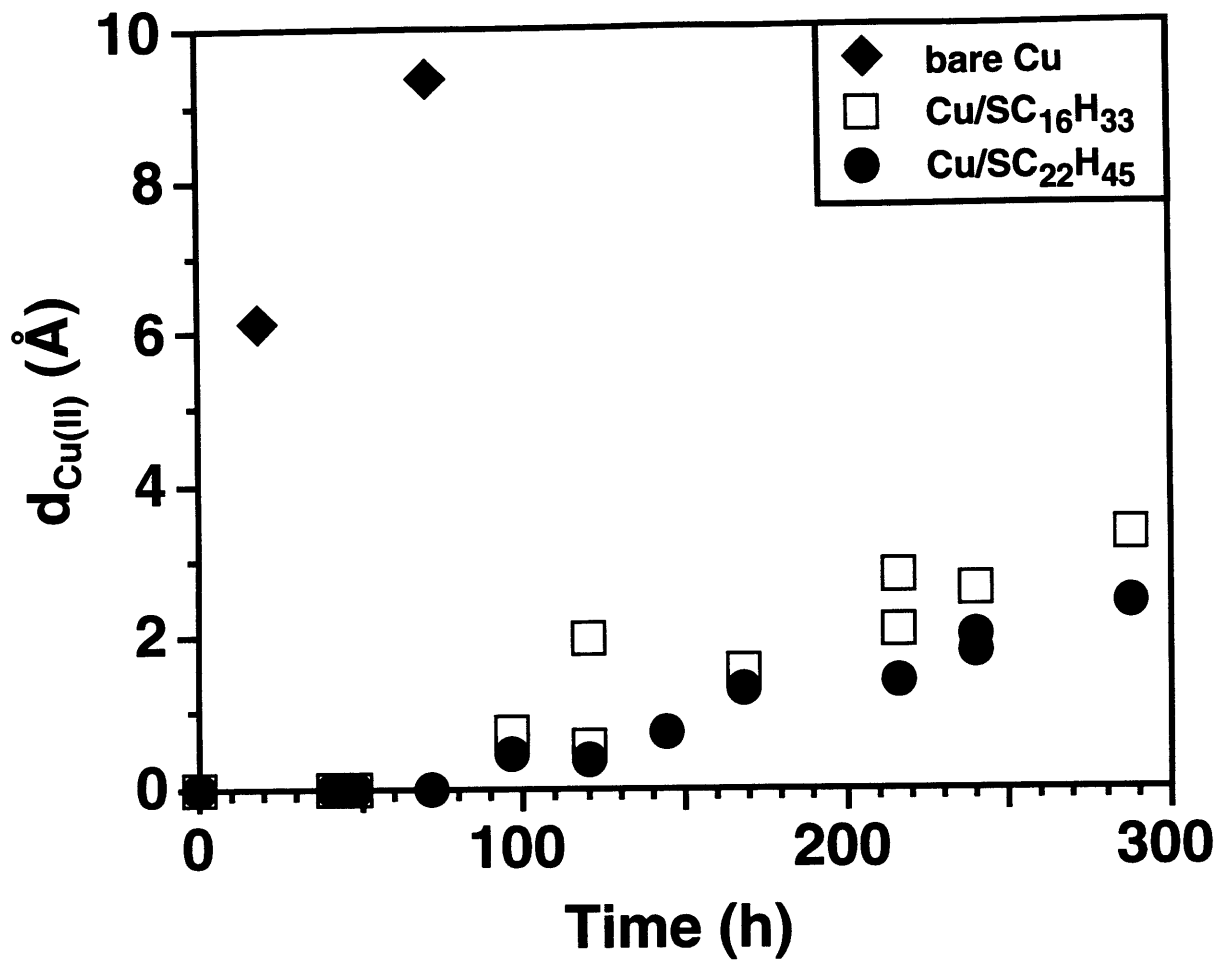
Figure 3.3. Extent of oxidation of the copper surface for bare copper samples and samples derivatized with $C_{16}H_{33}SH$ and $C_{22}H_{45}SH$ as a function of exposure time to 1 atm of O_2 at 100% relative humidity.
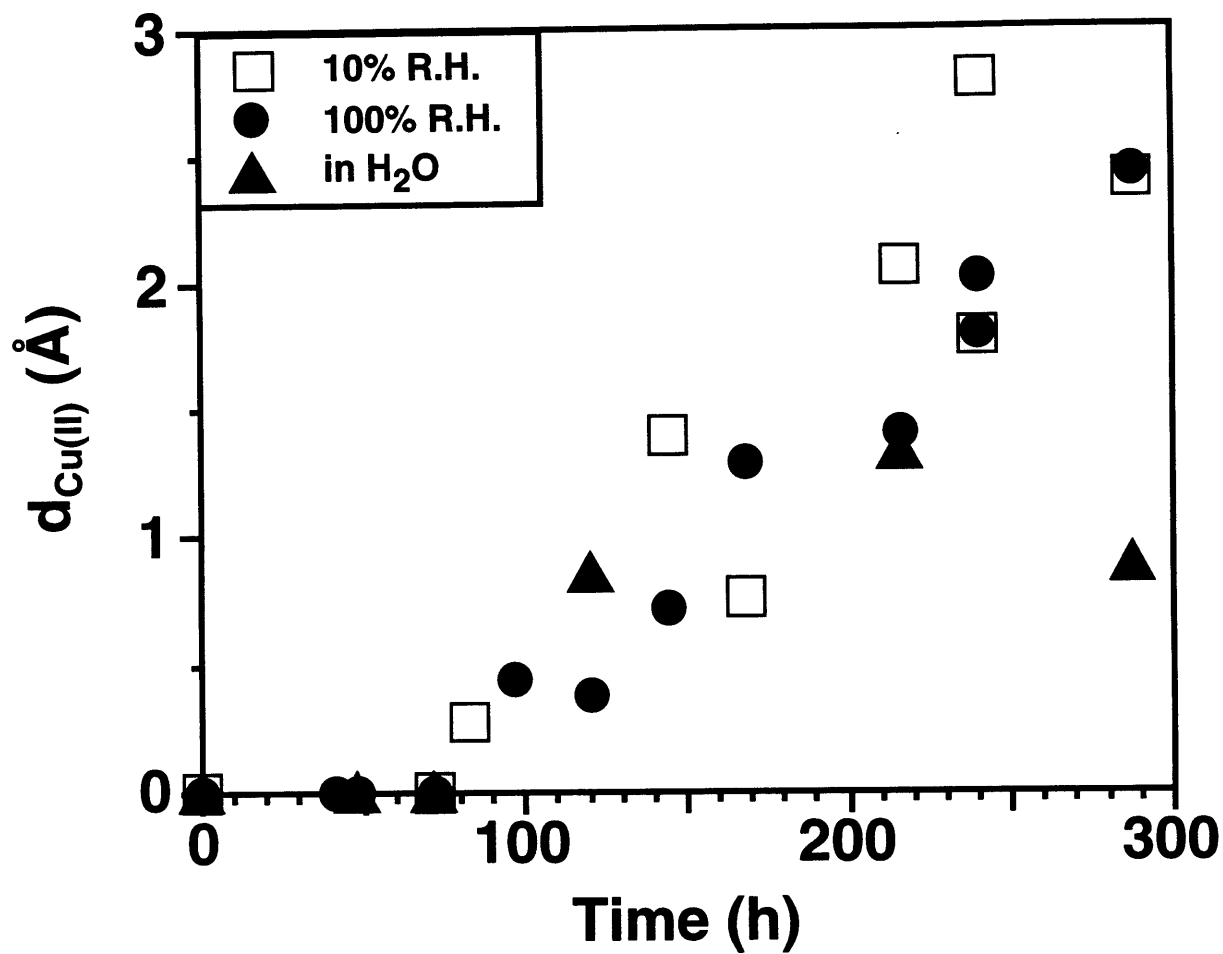
Figure 3.4. Comparison of the extent of oxidation for copper samples derivatized with $C_{22}H_{45}SH$ and exposed to 1 atm of O_2 at 10% and 100% relative humidity and to oxygen-saturated water at 1 atm.

methyl groups exhibits an advancing contact angle (θ_a) of ~45° whereas a surface exposing methylene units is wet by hexadecane (i.e., θ_a(HD) = 0°).[8]

Figure 3.5 displays the wetting properties by hexadecane for $C_{22}H_{45}SH$-derived SAMs on copper after exposure to various oxidizing conditions. The wetting properties of the layers decrease from their initial value and subsequently achieve a relatively constant value. This latter state is one largely exposing methyl groups at the surface, but is not as ordered as the initially formed SAM. The decreased contact angle reflects the availability of methylene units at the SAM/liquid interface for contact with the hexadecane and may be a result of surface reconstruction that occurs during the onset of oxidation. This drop in wettability occurs during a time period where no (or very little) formation of copper (II) species is observed by XPS (see Figure 3.4). The important feature of Figure 3.5 is that the wetting results for the samples are similar despite the differences in water concentration. This similarity suggests that the corrosion process using these SAMs as inhibitors is insensitive to the presence of water. For $C_{22}H_{45}SH$-derived samples immersed in oxygen-saturated water, the similarity of their wetting values to those under less harsh conditions provides evidence that the adsorbates (or their oxidized products) remain largely attached to the copper surface during extended exposure to an oxidizing aqueous environment.

When shorter-chained adsorbates are used, a more rapid decrease in the wetting properties of the film is observed (Figure 3.6). Shorter-chained adsorbates are less effective at maintaining their structure under oxidizing conditions than are longer-chained adsorbates and may also exhibit some sensitivity to the presence of water. This sensitivity may reflect the lesser degree of organization within these SAMs and the possible dissolution of these shorter-chained adsorbates into the contacting water. Over a two-week period of exposure, SAMs derived from adsorbates of chain lengths of hexadecanethiol or less were wet by hexadecane suggesting the presence of a highly disordered adlayer or its complete removal. From Figures 3.5 and 3.6, longer-chained adsorbates ($>C_{16}$) provide the greatest ability to maintain the film properties needed to impede corrosion processes. This observation may be the result of the high degree of crystallinity in these layers, the low solubility of these adsorbates in water, and the formation of a suitably thick layer of hydrocarbon that obstructs an interaction between the copper and water-containing phases.

The results in Figures 3.3 and 3.6 suggest that thicker films provide improved performance in inhibiting corrosion. Longer-chained adsorbates may be envisioned for further improving the properties of the layers; however, the use of these adsorbates becomes limited practically by difficulties in their synthesis and their poor solubilities in many solvents (see Chapter 5). To produce thicker, crystalline, hydrocarbon-based films on the copper surface for corrosion inhibition, self-assembling strategies for constructing multilayer assemblies on gold[9] were applied to these copper substrates. Figure 3.7 schematically illustrates the process for forming a bilayer
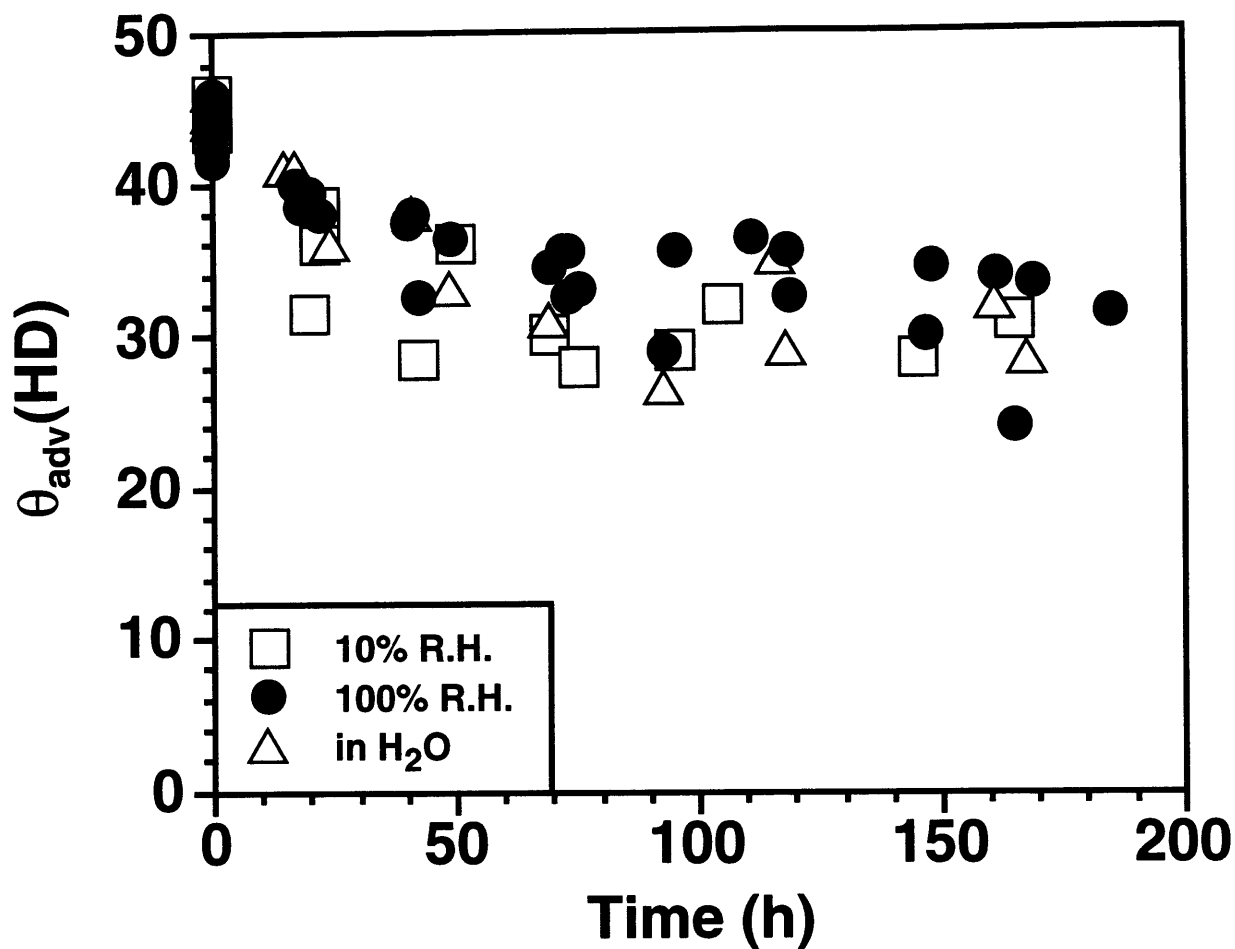
Figure 3.5. The advancing hexadecane contact angle on $C_{22}H_{45}SH$-protected copper samples as a function of exposure time to 1 atm of O_2 at 10% or 100% relative humidity or to oxygen-saturated water at 1 atm.
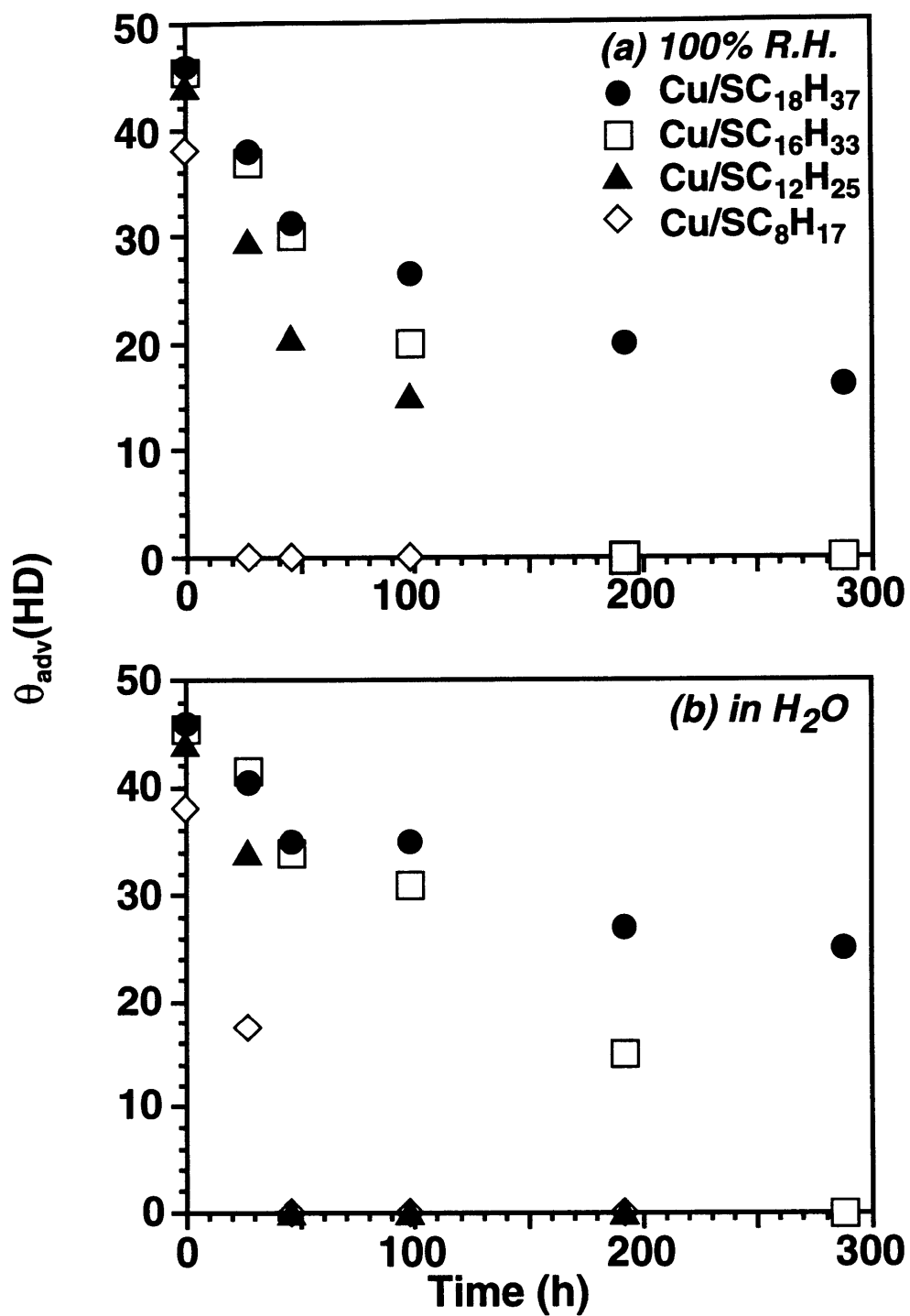
Figure 3.6. Extent of film integrity as probed by the advancing contact angle of hexadecane for copper samples derivatized with $C_8H_{17}SH$, $C_{12}H_{25}SH$, $C_{16}H_{33}SH$, and $C_{22}H_{45}SH$ and exposed to (a) 1 atm of O_2 at 100% relative humidity or (b) oxygen-saturated water at 1 atm.
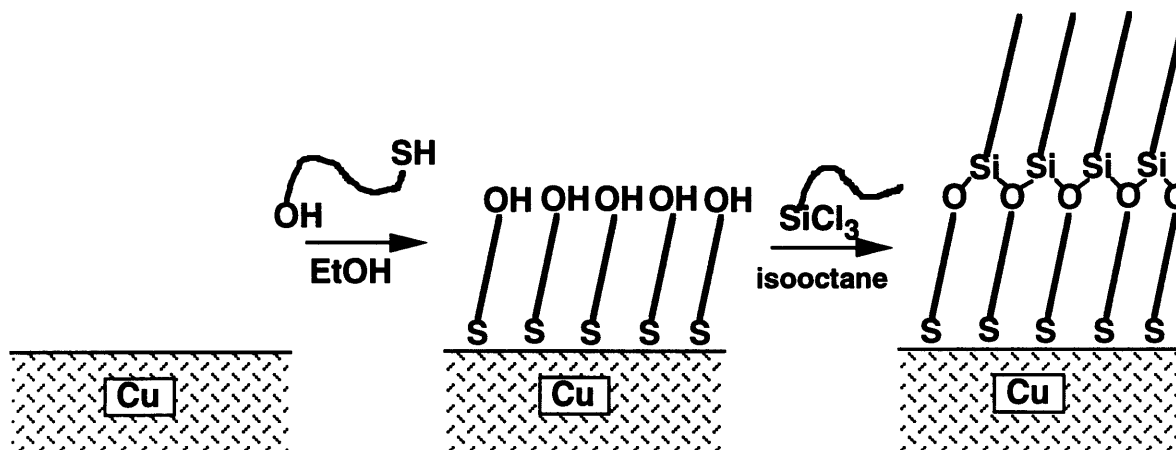
Figure 3.7. Schematic illustration of the assembly of a bilayer on copper. The assembly of the thiols (step 1) was conducted under anaerobic conditions, while the assembly of the trichlorosilanes (step 2) was performed in a dry box.

film on the copper surface using a mercapto-alcohol—$HS(CH_2)_{11}OH$ or $HS(CH_2)_{22}OH$—for the first layer and an alkyltrichlorosilane— $CH_3(CH_2)_{17}SiCl_3$—for the second layer. By using trichlorosilanes that terminate in vinyl or ester groups, other researchers have prepared multilayers on various substrates by this strategy (primarily for proposed non-linear optical applications).[10,11]

Figure 3.8 displays a comparison of the wetting properties for SAMs formed from $C_{22}H_{45}SH$ and for bilayer samples formed from the sequential adsorption of $HS(CH_2)_{22}OH$ and $CH_3(CH_2)_{17}SiCl_3$ that have been similarly exposed to 1 atm of O_2 at 100% relative humidity. In these samples, the thicknesses of the SAMs and bilayers are approximately 3 and 5 nm, respectively. For the initially formed layers, the wetting properties of the SAM by hexadecane are superior to those of the bilayer and may reflect a more well-defined structure for the SAM. (The differences may also be a reflection of the orientational differences that exist between the hydrocarbon chains in these systems.) Upon exposure to the oxidizing conditions, the quality of the C_{22} SAM, as reflected in its wetting properties by hexadecane, decreases to expose a greater number of methylene groups at the SAM/air(hexadecane) interface. This change indicates some level of film or surface reconstruction that occurs during the initial stages of oxidation. In contrast, the wetting properties of the bilayer remain unchanged over the entire week of exposure to these conditions. The presence of a cross-linked siloxane backbone within the bilayer may prevent any reconstruction within the film and yield an assembly that is more robust for these conditions. The development of crystalline hydrocarbon layers that contain stabilizing cross-links may prove to be a beneficial strategy for preparing robust, thin barrier films for corrosion inhibition.

The ability of the bilayer to inhibit corrosion of the underlying copper substrate was examined by exposing the assembly to 1 atm of O_2 at 100% relative humidity (Figure 3.9). XPS results showed that the bilayer, despite its improved stability (Figure 3.8) and greater thickness, was inferior in performance to that of a SAM derived from $C_{22}H_{45}SH$. The primary difference between these two samples was the presence of Cu(II) peaks in the XPS spectra for the initially formed bilayer sample. XPS spectra for a SAM on copper formed from $HS(CH_2)_{11}OH$ or $HS(CH_2)_{22}OH$ displayed no Cu(II) signals; however, Cu(II) signals were clearly evidenced in these samples after exposure to the trichlorosilane. For the samples derived from $HS(CH_2)_{11}OH$, XPS results showed the incorporation of chlorine into the resulting bilayer assemblies. Visible pitting of the copper substrate was also observed from some preparations. The amount of chlorine could be lessened by forming the bilayer in solutions containing scavengers (KOH and Na_2CO_3) for the HCl produced during the reaction between the trichlorosilane and the terminal hydroxyl groups; however, the films exhibited poor barrier properties toward oxidation of the copper substrate. The use of the longer-chained $HS(CH_2)_{22}OH$ for the initial layer dramatically reduced the amount of chlorine on the copper substrate to the level that samples (such as those used in
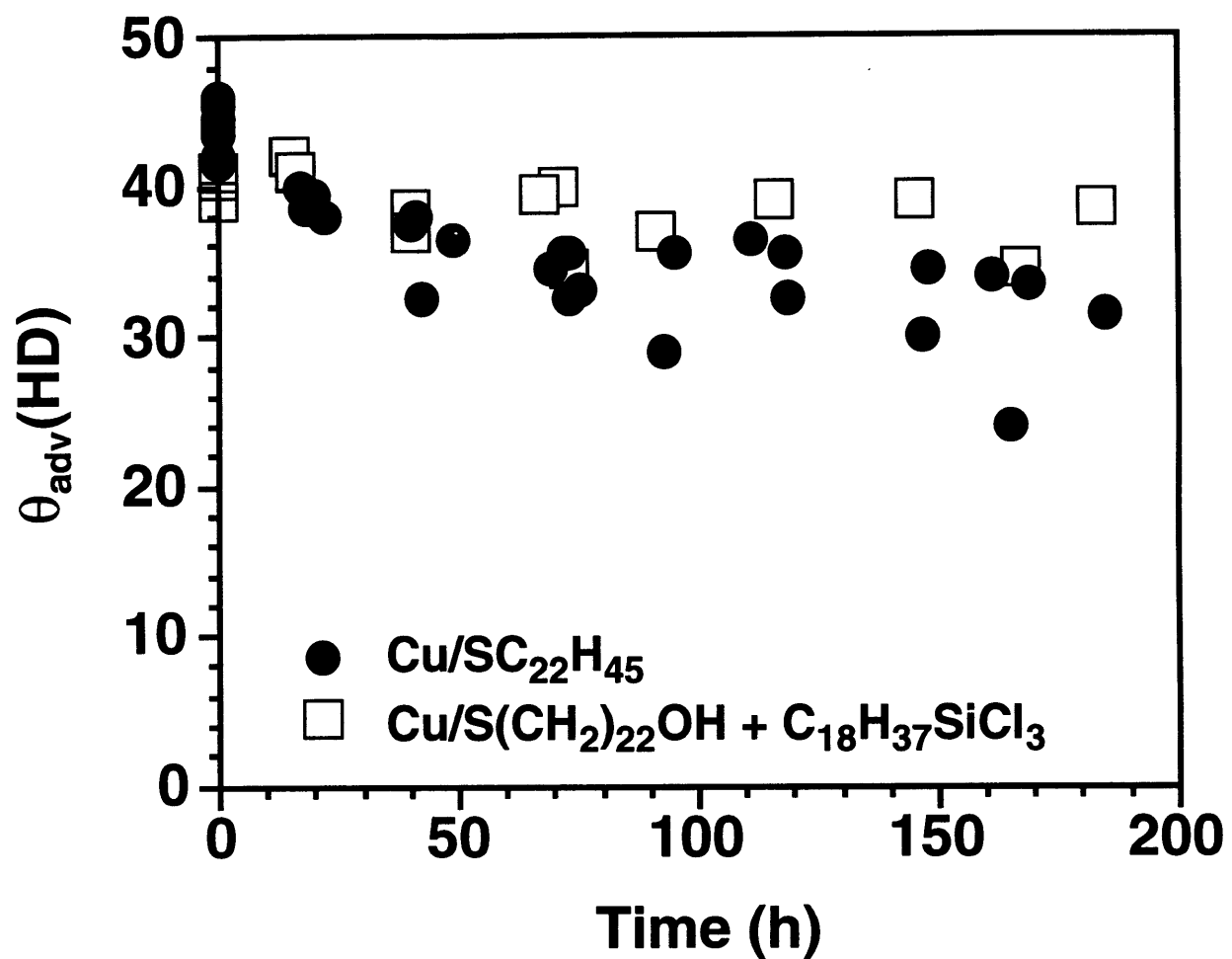
Figure 3.8. Extent of film integrity as probed by the advancing contact angle of hexadecane for copper samples functionalized with $C_{22}H_{45}SH$ or a bilayer formed from sequential treatments with $HS(CH_2)_{22}OH$ and $C_{18}H_{37}SiCl_3$ as a function of exposure time to 1 atm of O_2 at 100% relative humidity.
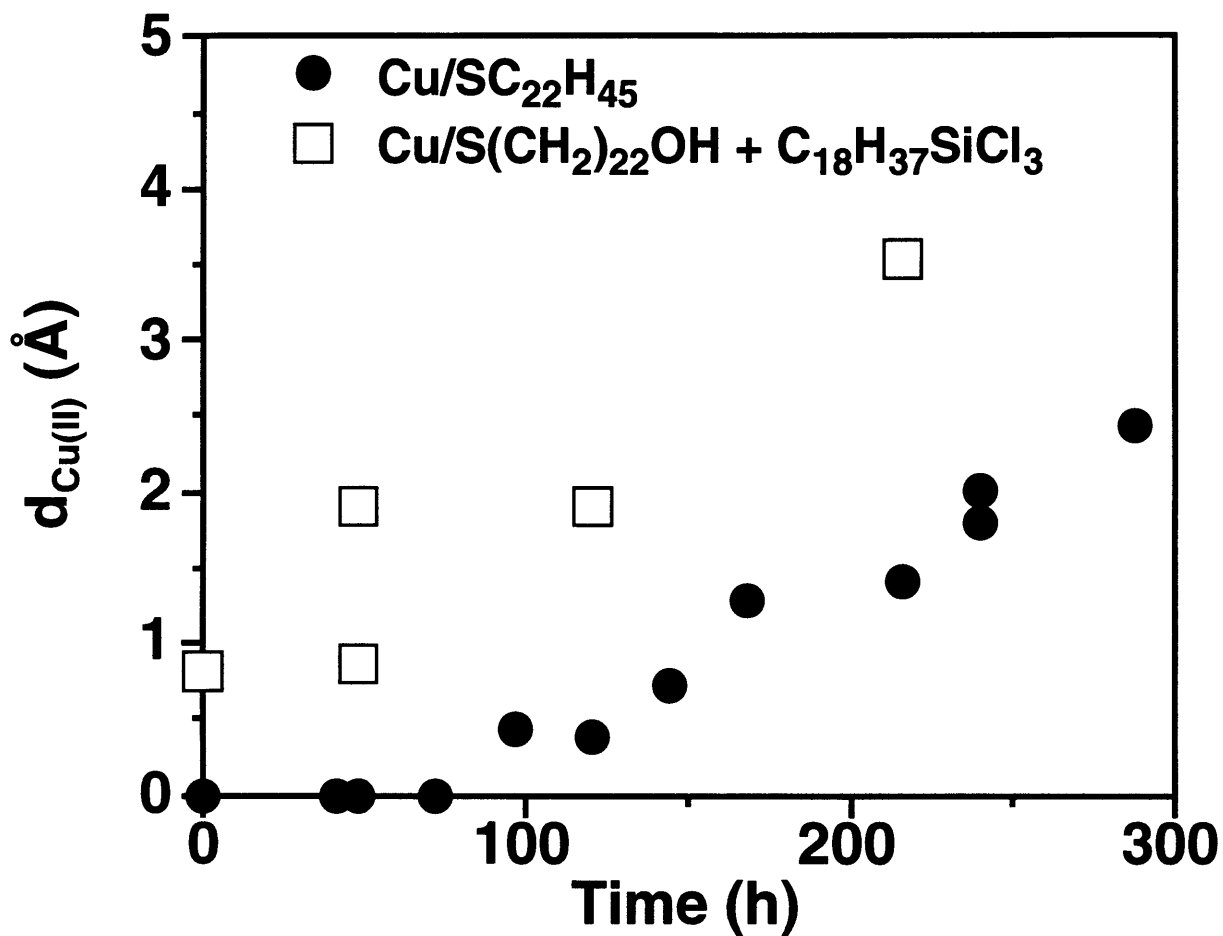
Figure 3.9. Extent of oxidation of the copper surface for copper samples derivatized with $C_{22}H_{45}SH$ or a bilayer formed from sequential treatments with $HS(CH_2)_{22}OH$ and $C_{18}H_{37}SiCl_3$ as a function of exposure time to 1 atm of O_2 at 100% relative humidity.

Figure 3.9) could be prepared that exhibited no chlorine signals by XPS; the lack of chlorine signal may also reflect the greater level of attenuation of photoelectrons by the thicker bilayer assembly. In all cases of forming bilayers on copper using trichlorosilanes, the samples exhibited a greater degree of oxidation by XPS than for samples derivatized using simple n–alkanethiols. The inferior performance of the bilayer systems stems from the use of chlorine-containing agents in the preparation of the second layer. The use of non-chlorine agents for forming bi- and multilayer assemblies on copper may circumvent this problem.

The use of SAMs and bilayers on copper for corrosion resistance have also been investigated by Aramaki et al.[12-15] In a series of papers, they have examined methods for generating bilayer assemblies on copper using the sequential adsorption of $HS(CH_2)_{11}OH$ and an alkyltrichlorosilane. Using polarization measurements in aerated 0.5 M Na_2SO_4(aq), they concluded that the bilayers could provide significantly greater protection abilities to the copper substrate than an octadecanethiolate monolayer.[13] This increased protection is probably a result of the enhanced stability of the siloxane-linked bilayer under the conditions of measurement. The results of Figure 3.8 also indicate improved stability for the bilayer; however, the abilities of the bilayer to impede corrosion was less than that for thinner films formed using simple n-alkanethiols (Figure 3.9). Aramaki et al. have recently used XPS to compare the effectiveness of bilayers on copper based on $HS(CH_2)_{11}OH$ for inhibiting substrate oxidation in air with SAMs formed from just $HS(CH_2)_{11}OH$.[14] From their experiments, they concluded that the addition of the second layer improved the corrosion resistance of the coating compared to that for the relatively short film prepared from just the mercapto-alcohol. Their results are compatible with those presented here that thicker layers generally provide greater corrosion resistance (Figures 3.3 and 3.6) and the bilayers prepared to date on copper are less effective in inhibiting corrosion on copper than are monolayer films of similar thicknesses prepared from n-alkanethiols. For example, Aramaki et al. have observed that the XPS spectra of copper that had been protected with a bilayer formed from the sequential adsorption of $HS(CH_2)_{11}OH$ and $C_8H_{17}SiCl_3$ exhibited mostly Cu(II) species in the $Cu(2p_{3/2})$ spectral envelope after a 231-hr exposure to air.[14] In contrast, for a longer exposure (384 hr) to harsher conditions (1 atm of O_2 at 100% relative humidity), the XPS spectra for a thinner $C_{16}H_{33}SH$-protected copper (Figure 3.2b) showed only minor contributions from Cu(II) species. Of these two systems, films formed from long-chained n-alkanethiols presently provide the greater level of protection for corrosion inhibition to copper. Bilayer and multilayer strategies may provide a means for improving the effectiveness of these self-assembling strategies for corrosion inhibition; however, work remains to establish the proper synthetic methods for generating high quality, crystalline multilayers on copper for this application.

3.3. Conclusions

Self-assembled monolayers adsorb onto copper and inhibit oxidation of the underlying substrate in dry, humid, and wet oxidizing conditions. The performance of the SAMs under these conditions was insensitive to the concentration of water, suggesting that the layers are effective in screening the interaction between water and the metal substrate. This result is important for the potential application of these systems as barrier layers that contact aqueous streams. Longer-chained n-alkanethiols yielded thicker SAMs on the copper substrate that exhibited superior abilities to impede corrosion than did shorter-chained adsorbates. The use of longer-chained adsorbates is preferred for maximizing the effectiveness and lifetimes of the adsorbed coatings under these conditions. Efforts using existing multilayer strategies are effective for producing thicker, more robust films on the copper surface; however, bilayer films derived from the adsorption of alkyltrichlorosilanes onto hydroxyl-terminated SAMs were not effective in improving the corrosion resistance abilities of the assembled coating beyond those of related SAMs derived from n-alkanethiols. The development of multilayer strategies that are compatible with the chemical reactivity of copper should allow formation of corrosion-resistant coatings on copper that remain stable under a wide variety of oxidizing conditions and require one-time chemical application for their generation and effective operation.

3.4. Experimental

3.4.1. Materials

Copper (99.99+%) and chromium (99.99+%) were obtained from Aldrich and R.D. Mathis, respectively. Octyl, dodecyl, and octadecyl thiols (Aldrich) were purified by vacuum distillation before use. Hexadecyl and docosyl thiols were prepared from the corresponding alkyl bromides (Aldrich) by nucleophilic displacement with thioacetate and subsequent solvolysis in HCl/MeOH.[16] 11-Hydroxy-undecanethiol was prepared via a literature procedure,[16] and 22-hydroxy-docosanethiol was available from previous studies.[4] Octadecyltrichlorosilane (United Chemical Technologies) was purified by vacuum distillation prior to use. Prepurified N_2 and O_2 were obtained from Middlesex. Isooctane (Mallinckrodt) and ethanol (Pharmco, 90%) were purged with N_2 for 5 min prior to use as solvents for the alkyl thiols. Silicon (100) wafers (75 mm diameter) (Silicon Sense) were rinsed with ethanol and dried with N_2 prior to use in the evaporator. Anhydrous hexadecane (Aldrich) and deionized H_2O (pH = 5.5) (Millipore) were used as liquids for contact angle measurements.

3.4.2. Sample Preparation

Cr (150 Å) and Cu (1000 Å) were sequentially evaporated from resistively heated tungsten filaments at 1.5 Å/s and 10 Å/s, respectively, onto Si wafers (75 mm diameter) in a diffusion-pumped evaporation chamber with a base pressure of 8×10^{-7} Torr and an operating pressure of 2×10^{-6} Torr. Immediately following evaporation of copper, the chamber was backfilled with N_2, and the freshly evaporated samples were transferred under a positive flow of N_2 to 1 mM deoxygenated isooctane solutions of the n-alkanethiols that were brought inside the evaporator. Polyethylene strips were placed around the circumference of the evaporator to reduce the effective exposed area of the open chamber for air diffusion during the transfer. After remaining in solution for 40 min, the samples were removed, rinsed with ethanol, and blown dry in a stream of N_2. XPS analysis of the $Cu(2p_{3/2})$ region for these functionalized samples exhibited a peak at 932.6 eV corresponding to Cu(0) and/or Cu(I) species and no peak at 934.7 eV for Cu(II) species. The wetting properties of the freshly prepared samples by water and hexadecane were comparable to those of n-alkanethiols on gold.[3]

Bilayer films were prepared on copper via a two-step process. The copper samples were anaerobically transferred from the evaporator (as described above) to ~1 mM ethanol solutions of $HS(CH_2)_{11}OH$ or $HS(CH_2)_{22}OH$. After 40 minutes of exposure to the adsorbate solutions, the samples were removed from solution, rinsed with ethanol, and blown dry in a stream of N_2. The samples exhibited advancing contact angles of water of 15-20° and 25-35° for copper functionalized with $HS(CH_2)_{11}OH$ and $HS(CH_2)_{22}OH$, respectively. The hydroxyl-terminated monolayers were treated with a mixture of 0.5 mM isooctane solution of octadecyltrichlorosilane ($C_{18}H_{37}SiCl_3$) and solid Na_2CO_3 in dry air for 5 min; longer exposure times resulted in films of lower quality as evidence by their wetting properties and physical appearance (pitting). The samples were rinsed with isooctane and blown dry. All manipulations involving the silane were performed in a glove box using dry air.

3.4.3. Oxidation Studies

Immediately after assembly of the monolayers, the silicon wafers were cut into 1 x 3 cm^2 samples using a diamond-tipped scribe, and the samples were placed into either a "dry" (10% R.H.) or a "humid" (100% R.H.) chamber. Humidity levels were determined using a digital hygrometer (Fisher). The chambers were subsequently evacuated and then backfilled with O_2 to atmospheric pressure. A steady stream of O_2 flowed through each chamber at 10 cm^3/min during the experiments. Within the "humid" chamber, a subset of samples was immersed in vials that contained deionized water. The chambers were stored at room temperature (20 °C) and kept in the

dark to minimize any possible effects due to light. After various periods of exposure, samples were removed from the chambers, rinsed with ethanol, dried in a stream of N_2, and characterized by either wetting or XPS. After characterization by either method, the samples were discarded. Data in the figures represent measurements on individual slides that had been continuously exposed to the listed oxidation conditions and had undergone no previous analysis. In most cases, the data represent at least two independent preparations and oxidations of the SAMs.

3.4.4. Wetting Measurements

Advancing contact angles were measured on both sides of a static drop using a Ramé-Hart manual goniometer. The drop was advanced prior to measurement by a Matrix Technologies electro-pipette (1 μL/s). The pipette tip remained in the drop during measurement. The data represent the average of at least three measurements, with the reproducibility across a sample being ± 3°.

3.4.5. X-ray Photoelectron Spectroscopy (XPS)

XPS spectra were obtained with a Surface Science X-100 spectrometer using a monochromatized Al Kα X-ray source (spot size = 600 μm) and a concentric hemispherical analyzer (pass energy = 50 eV). The detector angle with respect to the surface parallel was 35°. Copper spectra were accumulated over 5 scans (~10 min) with a 25-eV window. The spectra were fitted using 70% Gaussian/30% Lorentzian profiles and a Shirley background. Reduction of copper oxides did not occur on the time-scale of spectral accumulation due to the use of a monochromatized X-ray beam which does not contain the Bremsstrahlung.[1]

3.5. References

1)   Laibinis, P. E.; Whitesides, G. M. *J. Am. Chem. Soc.* **1992**, *114*, 9022-9027.

2)   Jones, D. A. *Principles and Prevention of Corrosion*; 2nd ed.; Prentice Hall: Upper Saddle River, NJ, 1996.

3)   Laibinis, P. E.; Whitesides, G. M.; Allara, D. L.; Tao, Y.-T.; Parikh, A. N.; Nuzzo, R. G. *J. Am. Chem. Soc.* **1991**, *113*, 7152-7167.

4)   Laibinis, P. E.; Whitesides, G. M. *J. Am. Chem. Soc.* **1992**, *114*, 1990-1995.

5)   Keller, H.; Simak, P.; Schrepp, W.; Dembowski, J. *Thin Solid Films* **1994**, *244*, 799-805.

6)   Tanuma, S.; Powell, C. J.; Penn, D. R. *Surf. Interface. Anal.* **1988**, *11*, 577-589.

7)   Blackman, L. C. F.; Dewar, M. J. S. *J. Chem. Soc.* **1957**, 162-176.

8)   Holmes-Farley, S. R.; Reamey, R. H.; McCarthy, T. J.; Deutch, J.; Whitesides, G. M. *Langmuir* **1985**, *1*, 725-740.

9)   Ulman, A.; Tillman, N. *Langmuir* **1989**, *5*, 1418-1420.

10) Netzer, L.; Iscovic, R.; Sagiv, J. *Thin Solid Films* **1983**, *99*, 235-242.

11) Tillman, N.; Ulman, A.; Penner, T. L. *Langmuir* **1989**, *5*, 101-111.

12) Yamamoto, Y.; Nishihara, H.; Aramaki, K. *J. Electrochem. Soc.* **1993**, *140*, 436-443.

13) Itoh, M.; Nishihara, H.; Aramaki, K. *J. Electrochem. Soc.* **1994**, *141*, 2018-2023.

14) Itoh, M.; Nishihara, H.; Aramaki, K. *J. Electrochem. Soc.* **1995**, *142*, 1839-1846.

15) Itoh, M.; Nishihara, H.; Aramaki, K. *J. Electrochem. Soc.* **1995**, *142*, 3696-3704.

16) Bain, C. D.; Troughton, E. B.; Tao, Y.-T.; Evall, J.; Whitesides, G. M.; Nuzzo, R. G. *J. Am. Chem. Soc.* **1989**, *111*, 321-335.

Chapter 4. Electrochemical Impedance Study on the Effect of Chain Length on the Protection of Copper by n-Alkanethiols

4.1. Background

The results in Chapter 3 demonstrated that self-assembled monolayers (SAMs) based on the adsorption of alkanethiols onto copper can provide protection against oxidation of the underlying metal that is independent of the moisture level in the environment. Nevertheless, little is known about the stability of these films and the mechanism of their eventual loss of performance. In this chapter, the barrier properties of various n-alkanethiols [$CH_3(CH_2)_{n-1}SH$; n = 8, 12, 16, 18, 20, 22, 29] on copper are examined as they are affected by exposure to oxidizing conditions. By varying the chain length of the adsorbate, the effect of angstrom-level changes in film thickness from 10 to 40 Å on the barrier properties and structural stability of the SAMs have been investigated. Results from electrochemical impedance spectroscopy (EIS) and infrared (IR) spectroscopy have been coupled to correlate the structure of the film with its ability to provide protection against corrosion of the underlying substrate.

Finklea has reviewed the use of EIS in the characterization of self-assembled monolayers.[1] Much of the prior work has focused on electron transfer from solution-phase redox probes through monomolecular[2] or polymer-modified SAMs[3] on a gold electrode. In the use of EIS with SAMs on copper substrates, Aramaki et al.[4] have studied capacitance and conductance properties of self-assembled bilayer films while Feng et al. have investigated the charge transfer resistance provided by a SAM of $C_{12}SH$.[5] In constructing an equivalent circuit for these films, the SAM has often been modeled as an incomplete film in which charge transfer occurs at random pinholes that approximate a microelectrode array. While this analysis may be accurate for some systems, such as SAMs on gold in the presence of bulky redox moieties, SAMs can instead be modeled as complete films in which through-film processes govern the electrochemical response. In a detailed investigation of SAMs derived from $CH_3(CH_2)_{n-1}SH$ on copper, Aramaki et al.[6] have shown that for n ≥ 10, the SAM can be modeled as a uniform, closely packed film through which oxygen permeates and participates in the cathodic corrosion reaction at the surface.

The equivalent circuit that best models the EIS data in this thesis is that of a solution resistance in series with a parallel network of a coating capacitance (C_c) and resistance (R_c) (Figure 4.1a). In this model, the coating capacitance and resistance should be functions of SAM thickness, and the coating resistance is that provided by the SAM against the transport of ionic species to the metal surface. Modeling EIS data with this equivalent circuit representation allows determination of the capacitance and resistance provided by the SAM during its lifetime and enables quantitative
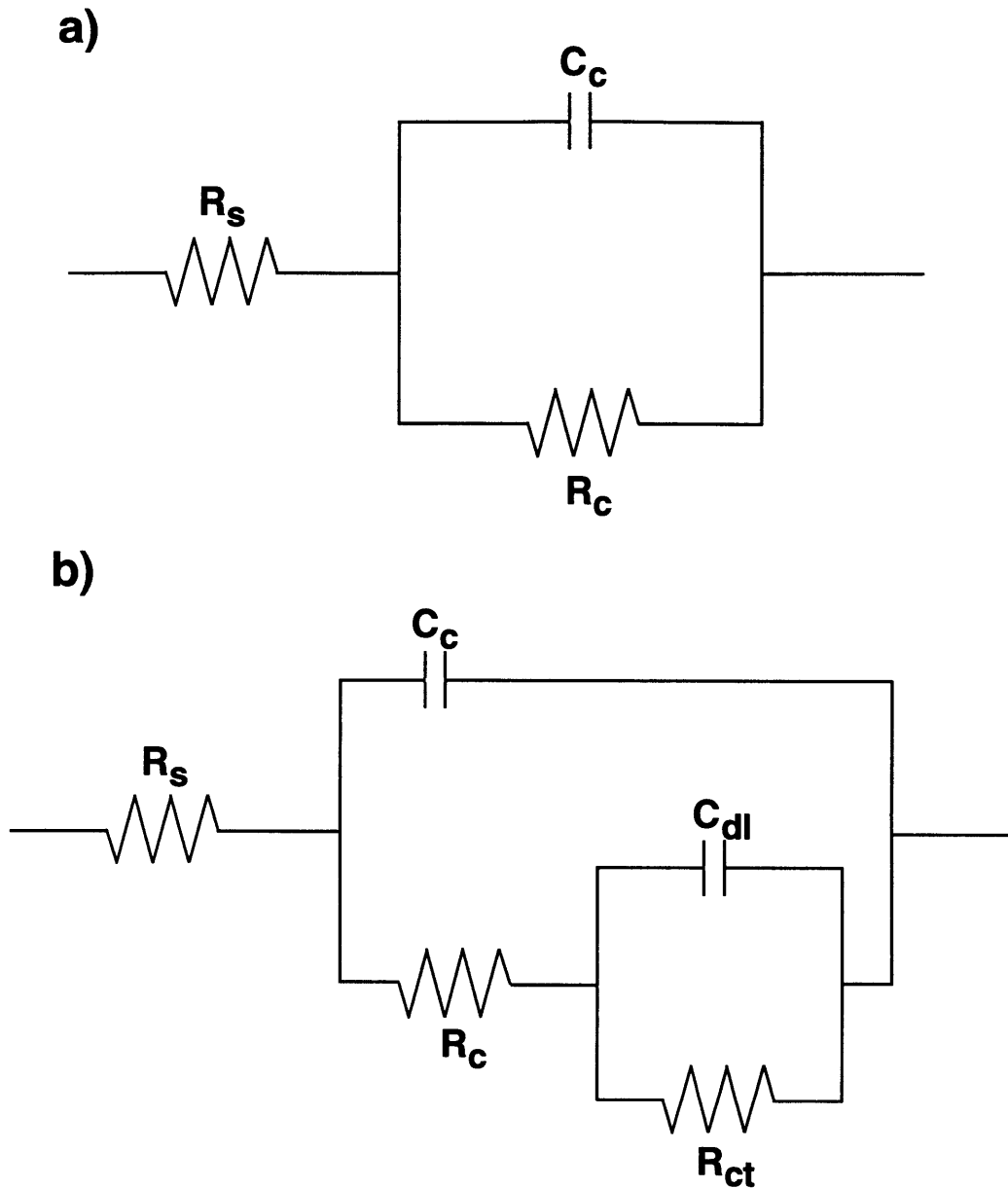
Figure 4.1. (a) Schematic illustration of the equivalent circuit used in this analysis. The model describes a complete coating that effectively separates the underlying metal from the contacting electrolyte. R_s = solution resistance, C_c = coating capacitance, and R_c = coating resistance. (b) The generally accepted equivalent circuit for a polymer-coated metal electrode that contains terms for the double layer capacitance (C_{dl}) and charge transfer resistance (R_{ct}) at the coating /metal interface.[7] The circuit in (b) simplifies to that in (a) if $R_c \gg R_{ct}$.

45

comparison between the performances of SAMs of different thickness and composition. The model circuit in Figure 4.1a is based on the assumption that the SAM is complete and homogeneous and that the metal is well separated from the contacting aqueous phase. The validity of this assumption is attributed to the nature of long hydrocarbon chains within the SAM to heal defects, such as adsorbate vacancies. This equivalent circuit representation is similar to that presented by Nahir and Bowden[8] for electron tunneling through a defect-free system on gold and is a reduced version of the generally accepted model for the corrosion of a polymer-coated metal in the absence of coating delamination (Figure 4.1b).[7] The model circuit of Figure 4.1a is valid as a simplified form of that in Figure 4.1b when the resistance for the coating (R_c) is much larger than the charge transfer resistance at the interface (R_{ct}) (Figure 4.1b). For SAM-coated copper substrates examined between 0.01 and 20,000 Hz, neither a second time constant nor any Warburg behavior indicative of corrosion at the metal/organic interface was observed over the timescales reported in this chapter.

4.2. Results

4.2.1. Properties of n-Alkanethiols on Copper

Ellipsometry has been a convenient technique for determining the thickness of SAMs on various substrates.[9] This method requires characterization of the substrate before and after formation of the SAM. The tendency of bare copper to oxidize rapidly when exposed to air complicates these measurements; furthermore, the necessity to minimize contact of the copper substrates with oxygen before SAM formation is inconsistent with the requirements for ellipsometric characterization. In contrast with ellipsometry, the use of XPS to determine thickness only requires analysis of the sample after SAM formation and thus, provides a method of characterizing the films that is compatible with the requisite experimental efforts to minimize oxidation of the uncoated copper substrate. XPS provides a convenient method for examining differences in relative thickness for n-alkanethiolate films by measuring their attenuation of photoelectrons from the underlying substrate.[10] Figure 4.2 shows the attenuation of the $Cu(2p_{3/2})$ signal in XPS by SAMs of various chain lengths from n = 8 to 29. The intensity of the underlying copper decreases exponentially as the chain length is increased, indicating a consistent and regular increase in the thickness of the SAM. The slope of the best-fit line through the data is $-0.095/CH_2$ and is equal to $-(d_{CH_2} / \lambda \sin \theta)$,[10] where d_{CH_2} is the incremental thickness of each methylene group in the monolayer ($d_{CH_2} = 1.27 \cos \phi = 1.24$ Å, where 1.27 is the incremental distance per CH_2 group in a trans-extended hydrocarbon chain[11] and ϕ is the average cant (12°) for the adsorbates within the SAM[10]), λ is the attenuation length of photoelectrons from the underlying metal through the hydrocarbon, and θ is
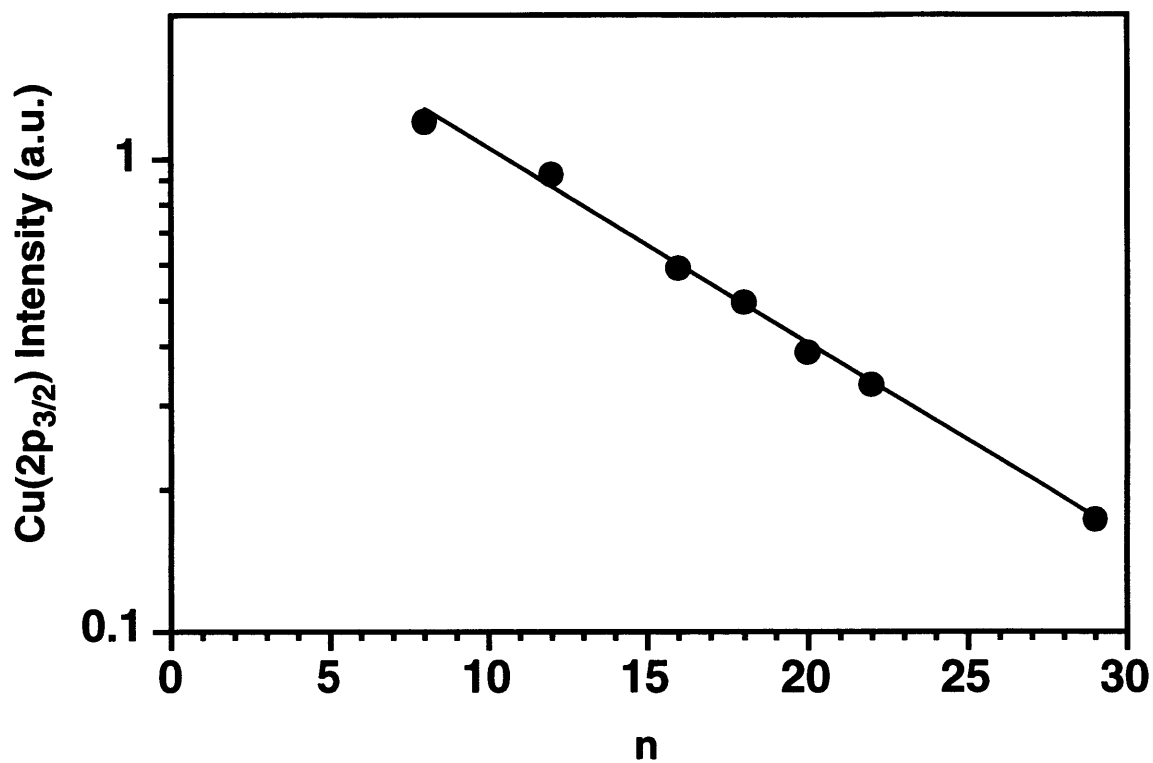
Figure 4.2. Attenuation of the $Cu(2p_{3/2})$ signal in XPS by SAMs formed from C_nSH. The line is a least-squares fit to the data and corresponds to an attenuation length of 23 Å for $Cu(2p_{3/2})$ photoelectrons through the hydrocarbon layer.

the angle of the photoelectron detector with respect to the surface parallel. From the data in Figure 4.2, the attenuation length of $Cu(2p_{3/2})$ photoelectrons through the n-alkanethiolate SAM is 23 Å, which agrees well with the value of 22 Å determined in a previous study.[12] These results suggest that the thickness of the hydrocarbon within these films can be varied from 10 to 36 Å by using adsorbates with chain lengths between 8 and 29 and demonstrate that the coating thickness on copper can be tuned at the angstrom-level by appropriate selection of adsorbate. This high level of control over film thickness is pertinent in investigating the effects of film thickness on barrier properties. It is important to note that the degree of oxidation of the copper surface must be minimized in order to form high-quality SAMs. XPS spectra taken immediately after SAM formation by the methodology used here indicate the absence of Cu(II) species.[13]

Since the capacitance of a film serves as an additional probe of its thickness, the chain length of the adsorbate should govern the capacitance of the resulting SAM.[14] The capacitance of SAMs formed from a series of n-alkanethiols were measured by electrochemical impedance spectroscopy, assuming the equivalent circuit shown in Figure 4.1a. Through a Helmholtz model of the interface, the capacitance of the film is related to its thickness by the following equation:

$$\frac{1}{C_c} = \frac{d_{SAM}}{\varepsilon_{SAM}\varepsilon_o} = \frac{d_{CH_2}n}{\varepsilon_{CH_2}\varepsilon_o} + \frac{d_{(S)}}{\varepsilon_{(S)}\varepsilon_o} \qquad (4.1)$$

where $d_{(S)}$ is the effective thickness of the ligating sulfur layer, d_{SAM} is the thickness of the monolayer ($d_{SAM} = d_{CH_2}n + d_{(S)}$), ε_{SAM} is the permittivity of the total film, ε_{CH_2} and $\varepsilon_{(S)}$ are the permittivities of the hydrocarbon and sulfur portions of the film, respectively, and ε_o is the permittivity of vacuum. The inverse capacitance increases linearly with increasing chain length of the adsorbate (Figure 4.3), suggesting that the Helmholtz model is valid. The slope of the best-fit line through the data in Figure 4.3 corresponds to a dielectric constant of 2.16 for the hydrocarbon portion of the monolayers. This value is similar to the value of 2.10 measured in situ with surface plasmon resonance for n-alkanethiols (n=16, 18) on gold[15] and compares well to the value of 2.30 for polyethylene.[16] The strong dependence of capacitance on chain length is consistent with the results from XPS attenuation (Figure 4.2) and demonstrates the high level of control over film thickness that is available with SAMs. In addition, these data support the equivalent circuit model presented in Figure 4.1a and discussed in Section 4.1.

Figure 4.4 shows reflection-infrared spectra of the C-H stretching region for SAMs derived from C_nSH on copper. For n > 12, the peak positions of the various modes—$v_a(CH_3) = 2965$ cm^{-1}, $v_a(CH_2) = 2918$ cm^{-1}, $v_s(CH_3) = 2879$ cm^{-1}, and $v_s(CH_2) = 2851$ cm^{-1}—are the same as those observed for n-alkanethiols on gold and indicate that the hydrocarbon chains predominately adopt a trans-zig-zag extended conformation. For n = 12, the peak positions indicate a less crystalline SAM with a greater density of gauche conformers that result from a less efficient packing of the

48
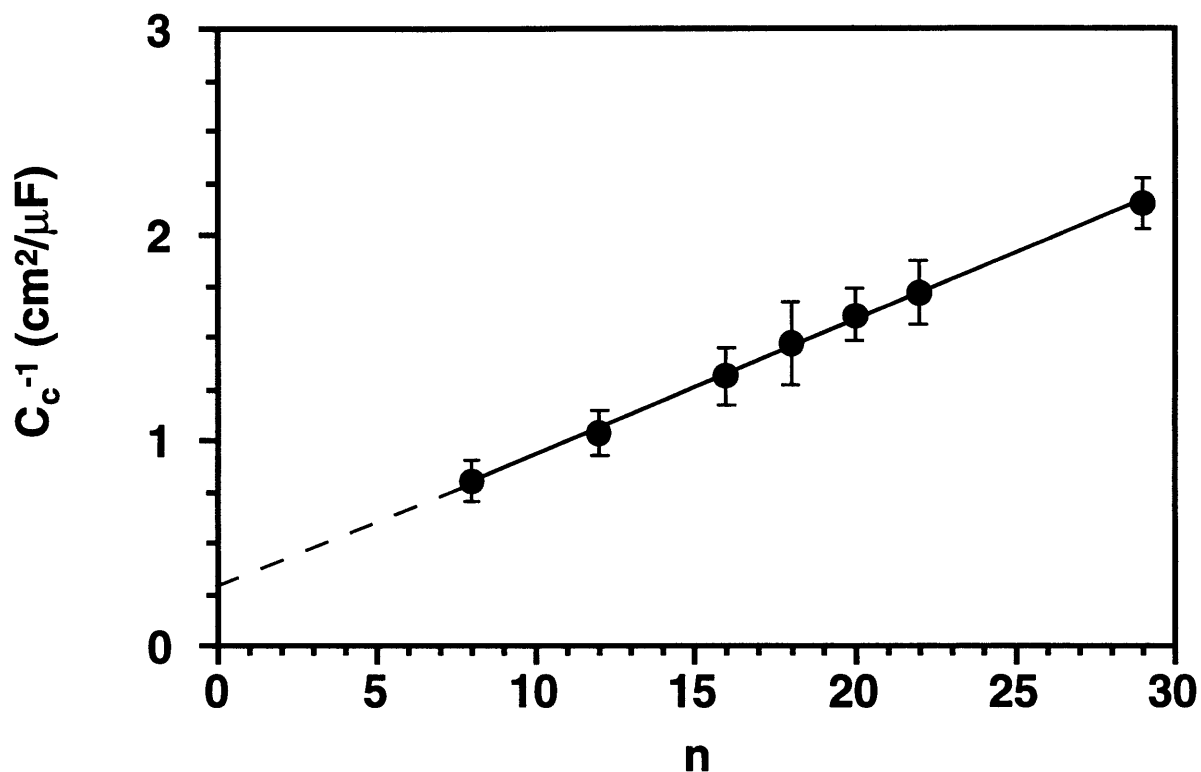
Figure 4.3. Inverse capacitance of SAMs of C_nSH on copper in oxygenated 50 mM
$Na_2SO_4(aq)$. Capacitance values were determined by fitting impedance data to the equivalent
circuit shown in Figure 4.1a. The line is a least-squares fit to the data and has a slope that
corresponds to a dielectric permittivity of 2.16. The dashed portion of the line represents an
extrapolation to n = 0. The nonzero intercept of C_c^{-1} is due to the capacitance provided by the thiol
head group and is similar to that observed by Porter et al. for thiols on gold.[14]

$\nu_a(CH_3)$ $\nu_a(CH_2)$ $\nu_s(CH_3)$ $\nu_s(CH_2)$

0.001

Absorbance

n

29

22

20

18

16

12

3000   2900   2800

Wavenumber (cm⁻¹)
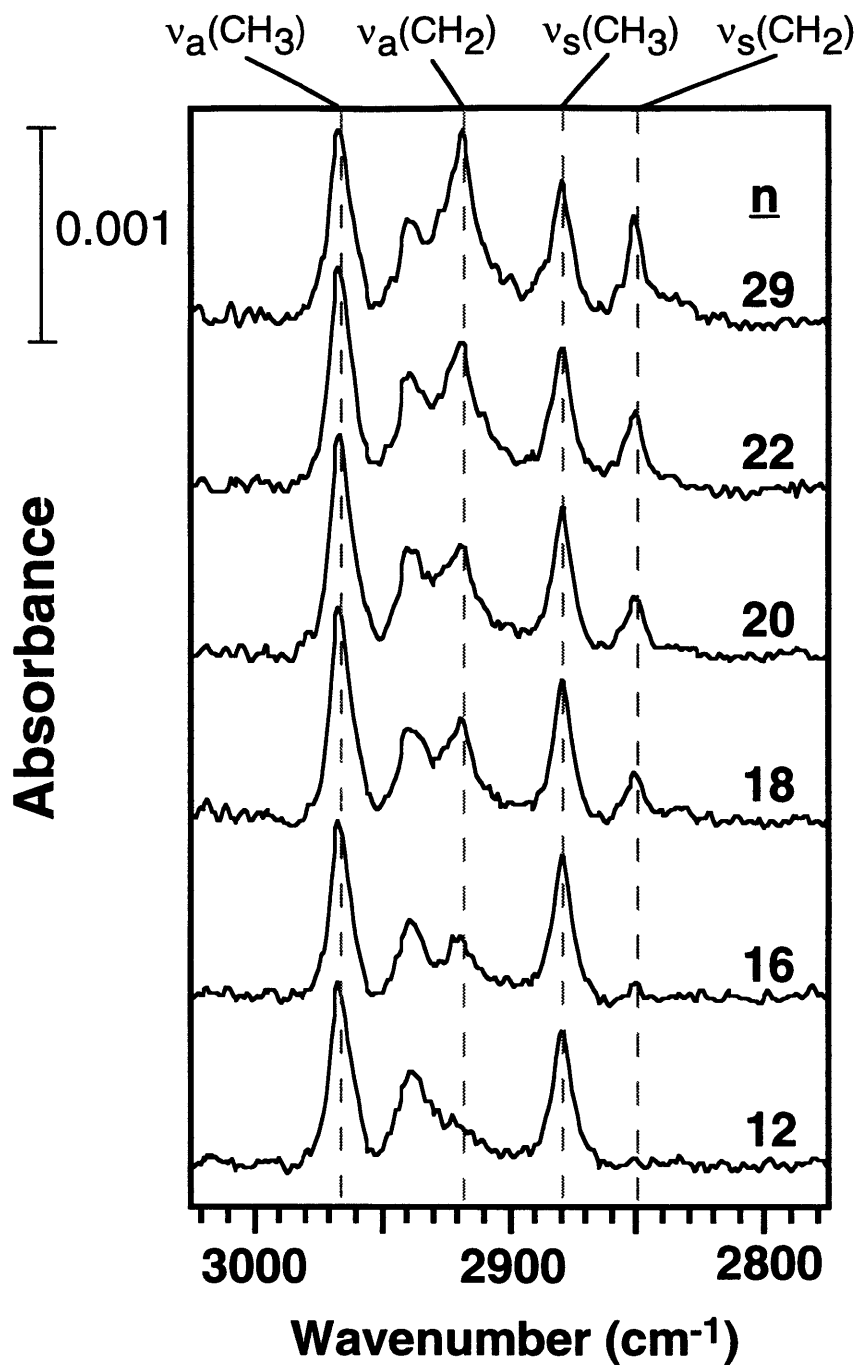
Figure 4.4. Grazing incidence polarized infrared spectra of the C-H stretching region for SAMs of C_nSH (n = 12, 16, 18, 20, 22, and 29) on copper. The dashed lines indicate the positions of the primary modes for a trans-extended monolayer with no gauche defects: $\nu_a(CH_3) = 2965$ cm⁻¹, $\nu_a(CH_2) = 2918$ cm⁻¹, $\nu_s(CH_3) = 2879$ cm⁻¹, and $\nu_s(CH_2) = 2851$ cm⁻¹. The spectra have been offset vertically for clarity.

shorter chains. For the series of n-alkanethiols, the intensities of the methylene stretching vibrations exhibit a linear dependence with chain length (not shown), as observed previously.[10] The intensities of the methylene stretching vibrations indicate that the hydrocarbon chains of the adsorbates tilt ~12° from the surface normal on the substrate; this nearly perpendicular orientation indicates the formation of a more densely packed system than is formed for thiols on gold where the chains tilt ~30 ° from the surface normal. The dense packing of these adsorbates on copper enables the formation of SAMs that can provide effective barriers against the diffusion of small molecules such as O_2[6,17] and H_2O[18] to the underlying copper surface.

Figure 4.5 shows electrochemical impedance spectra in the form of Bode magnitude (Figure 4.5a) and phase angle (Figure 4.5b) plots for copper, both bare and protected by SAMs derived from C_nSH. At high frequencies, the resistance of the solution dominates the impedance and thus, the Bode magnitude data exhibit a slope of zero while the phase angle is near 0°. In the intermediate frequency regime for coated samples, the capacitance of the films provides a significant impedance, and log |Z| increases linearly with a slope of 1 with decreasing log frequency (Figure 4.5a) while the phase angle is approximately 90° (Figure 4.5b). The smaller capacitance and greater impedance provided by the thicker films is evident in Figure 4.5a by comparing the various spectra in the intermediate frequency regime. At low frequencies, the plateaus in |Z| for C_8 and C_{12} films are consistent with the onset of ionic penetration into the SAM and correspond to the resistances (R_c) that the SAMs provide against the diffusion of these ions.[7] For copper protected by thicker films ($n \geq 16$), the coating resistance is sufficiently large that it is not directly observable on the magnitude plot; however, the slight decrease in phase angle (Figure 4.5b) at low frequencies suggests the onset of ionic penetration into these films. The coating resistances for these films are 30, 55, and 77 $M\Omega{\cdot}cm^2$ for C_{16}, C_{22}, and C_{29} films, respectively, and were determined by fitting Nyquist plots of the data (not shown) with the equivalent circuit model shown in Figure 4.1a. The greater protection provided by the longer-chained thiols is probably a result of the more effective packing, superior crystallinity, and greater thickness of these films. For all coatings, the impedance provided is orders of magnitude greater than that for unprotected copper (Figure 4.5a). The observed impedance of the bare metal at low frequencies in Figure 4.5 may be the result of a Warburg process indicating active corrosion at the surface during impedance characterization. A Warburg impedance corresponds to a phase angle of 45°, and the data in Figure 4.5b for bare copper approach this value. The results in Figure 4.5a show that a monolayer film can produce large (three to four orders of magnitude) enhancements of impedance and therefore provide significant protection against corrosion. Figure 4.6 shows the chain-length dependence of the coating resistance (R_c) for n-alkanethiols on copper; the values of R_c were obtained by fitting EIS data to the equivalent circuit shown in Figure 4.1a. The coating resistance is linearly related to chain length for $n \geq 16$, suggesting that each additional methylene group
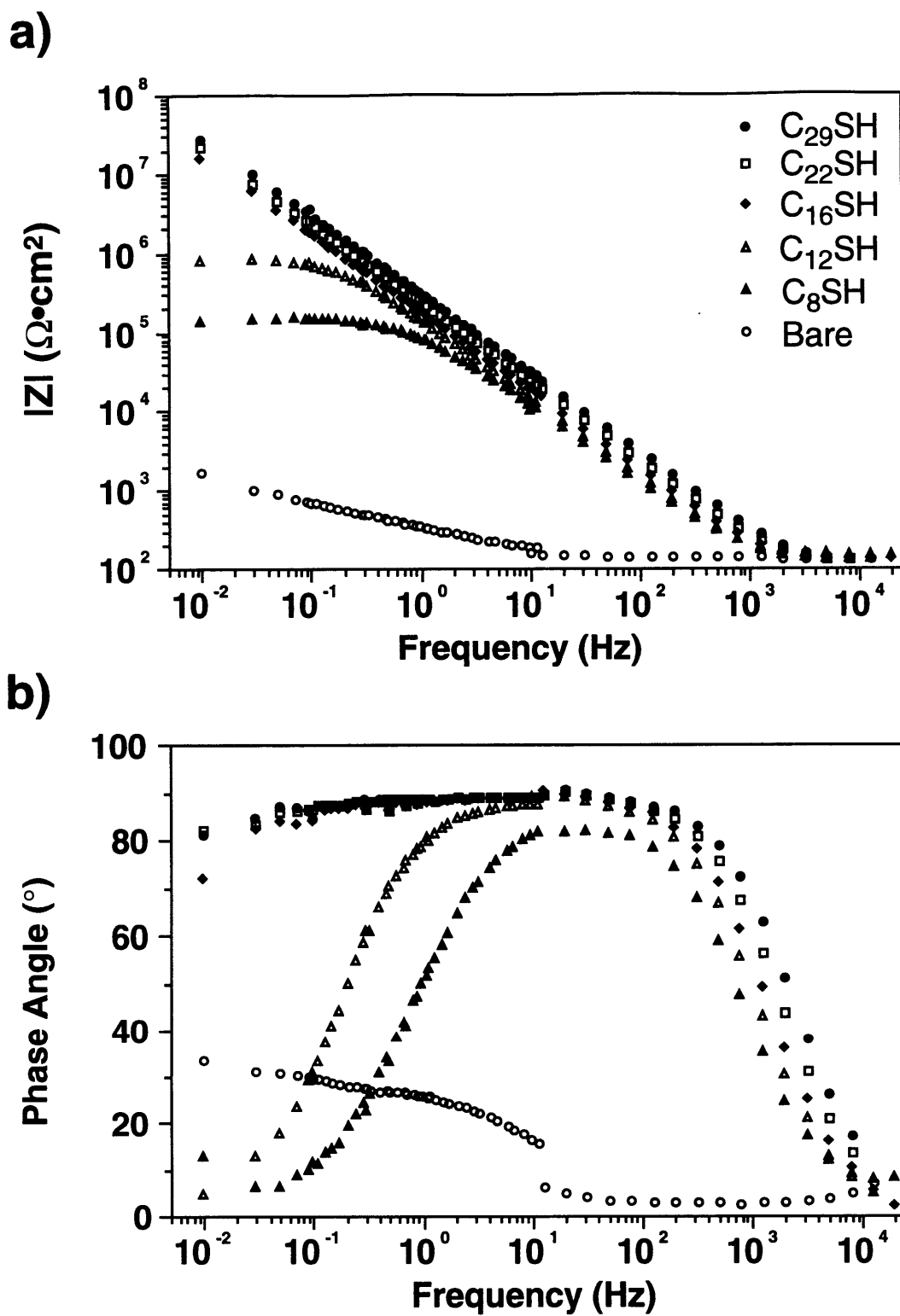
Figure 4.5. Bode magnitude (a) and phase angle (b) plots for copper protected with SAMs of C_nSH (n = 8, 12, 16, 22, 29) and unprotected in oxygenated 50 mM Na_2SO_4(aq).

within the SAM behaves as a resistance in series. The slope of a least-squares fit to the data for n $\geq$ 16 corresponds to an increase in R_c of 4.2 MΩ•cm^2/CH$_2$. This large incremental increase in R_c with each methylene is probably due to the close packing of the chains and their tendency to minimize free volume, as suggested by the IR results in Figure 4.4. The calculated value of conductivity for these films (n $\geq$ 16)—5.8±1.0 x 10^{-15} Ω^{-1}cm^{-1}—is nearly constant with chain length and indicates that the defect-free nature of these films prevents tunneling.[19] This value of conductivity agrees well with that of 4.6±3.0 x 10^{-15} Ω^{-1}cm^{-1} obtained for SAMs of alkyltrichlorosilanes on silicon[20] and is only roughly an order of magnitude greater than that of 2 x 10^{-16} Ω^{-1}cm^{-1} for bulk polyethylene.[20] For n = 8 and 12, the coating resistances were 0.14 and 0.81 MΩ•cm^2, respectively. The departure from the linear behavior in R_c for these thinner SAMs is attributed to the less ordered environment of their chains. That the line in Figure 4.6 intercepts the x-axis at n ~10 may approximate the minimum chain length necessary to form a SAM on copper that contains segments of hydrocarbon that are sufficiently crystalline to resist the penetration of ions. This value agrees well with results from Aramaki and co-workers who concluded that n-alkanethiolate SAMs with n $\geq$ 10 are more resistant to O$_2$ diffusion due to better packing of the hydrocarbon chains.[6] Computer simulations suggest that the crystalline portion of the SAM is likely to be along the middle of the polymethylene chain as gauche conformers concentrate at the chain ends.[21] Infrared data on SAMs show a predominately crystalline structure for chain lengths of n $\geq$ 16, with those of n = 12-15 having intermediate crystallinity based on the line shape and peak position of the asymmetric methylene [v_a(CH$_2$)] absorption band.[14] Combined with the resistance data, the structure of the SAMs may be considered to contain roughly n - 10 methylenes in a crystalline state that are encapsulated by less ordered hydrocarbon units at the Cu/SAM and SAM/air interfaces. The crystallinity determined from IR data would reflect a composite of the phase states within the SAM.

4.2.2. Properties of SAMs upon exposure to 1 atm of O$_2$ at 100% RH

After exposing SAM-coated copper to an environment of 1 atm of oxygen and 100% RH at room temperature for various periods of time, the barrier properties of the films deteriorated. Figures 4.7a and b show plots of the Bode magnitude and phase angle, respectively, for C$_{16}$, C$_{22}$, and C$_{29}$ films on copper after exposure to the humid, oxygen-rich conditions for 40 h. For the C$_{16}$ film, the resistive plateau decreased by two orders of magnitude after the 40-h exposure and the phase angle is 0° at the lowest frequencies. For thicker films of C$_{22}$ and C$_{29}$, the decrease in R_c over the exposure was less pronounced. The data in Figure 4.7 suggest that chain length is an important parameter governing the effectiveness of the films to maintain their barrier properties upon
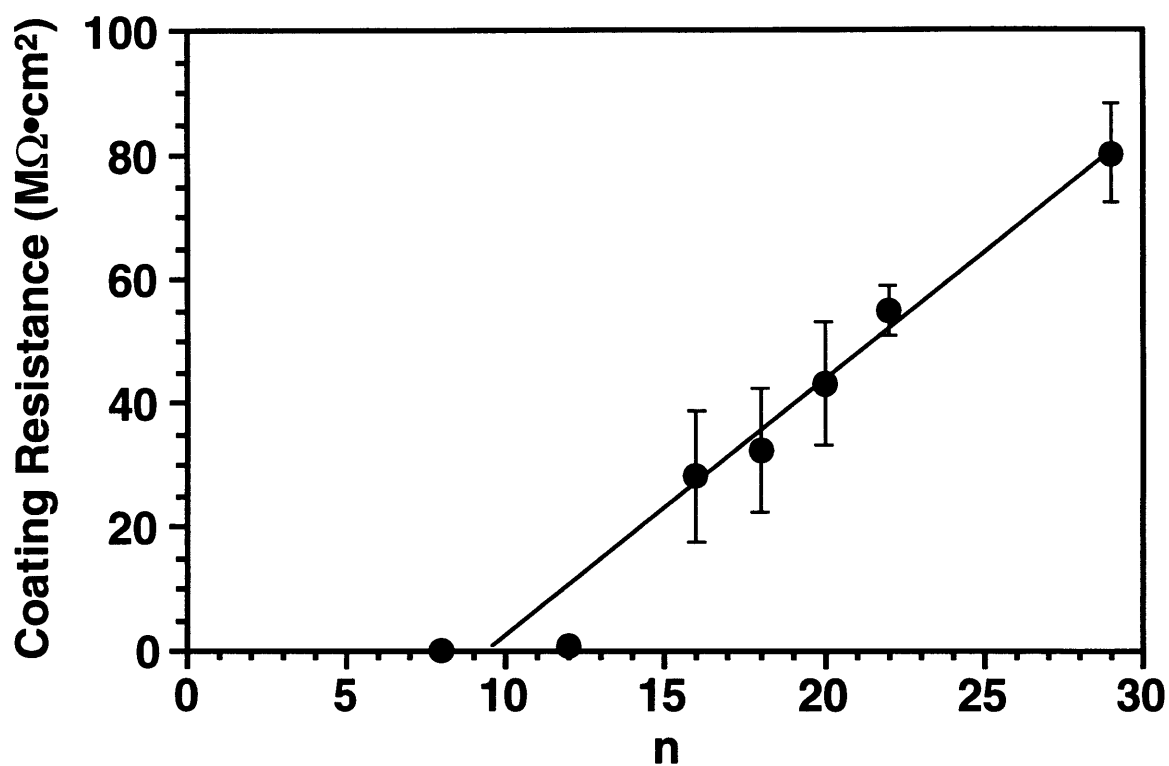
Figure 4.6. The effect of chain length (n) on the coating resistance of SAMs prepared from C_nSH on copper. Coating resistances were determined by fitting impedance data to the equivalent circuit shown in Figure 4.1a. The line is a least-squares fit to the data for $n \geq 16$.
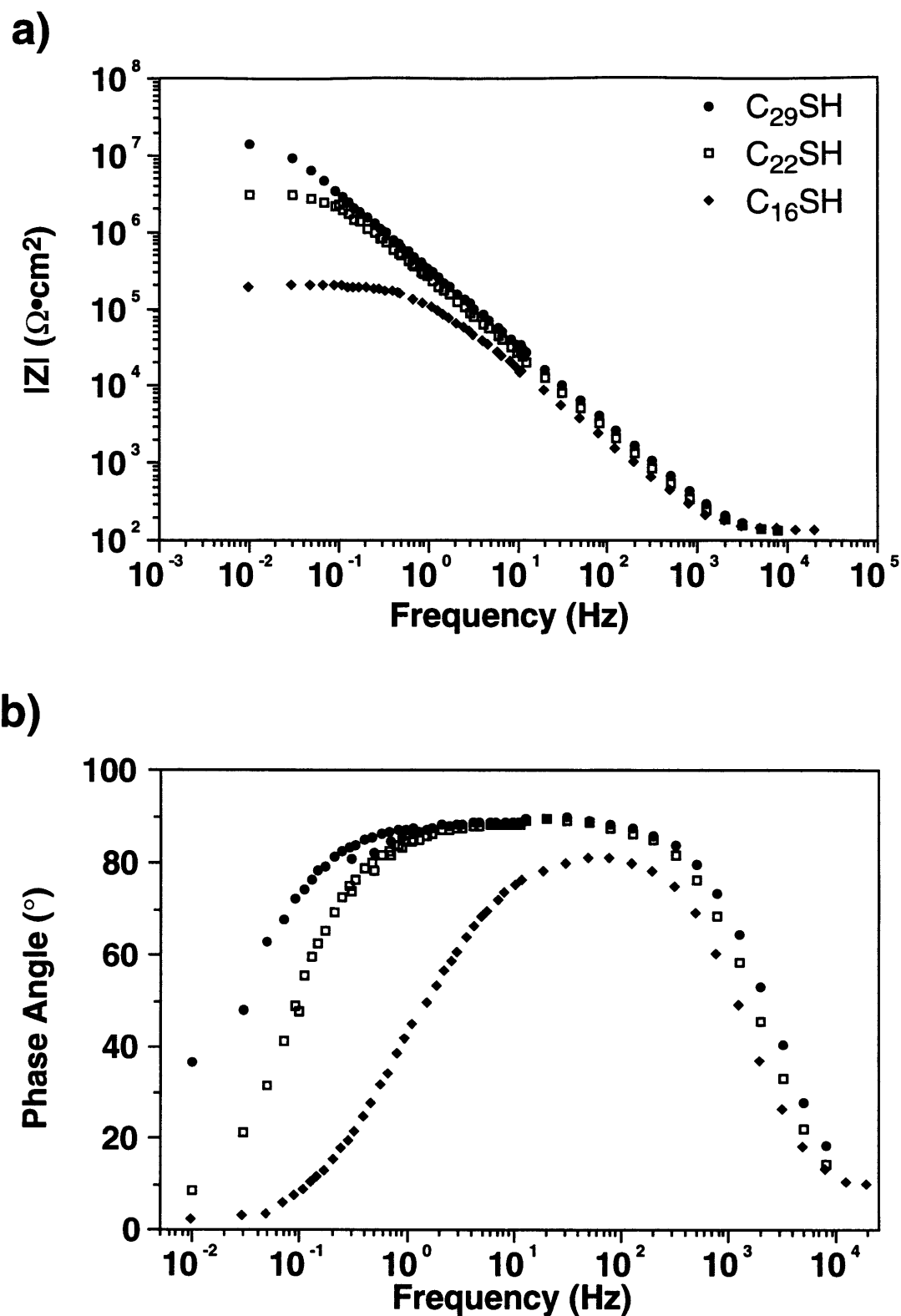
Figure 4.7. Impedance data obtained in oxygenated 50 mM Na_2SO_4(aq) for copper protected with SAMs of $C_{16}SH$, $C_{22}SH$, and $C_{29}SH$ after 40-h exposure to 1 atm of O_2 at 100% RH: (a) Bode magnitude and (b) phase angle plots.
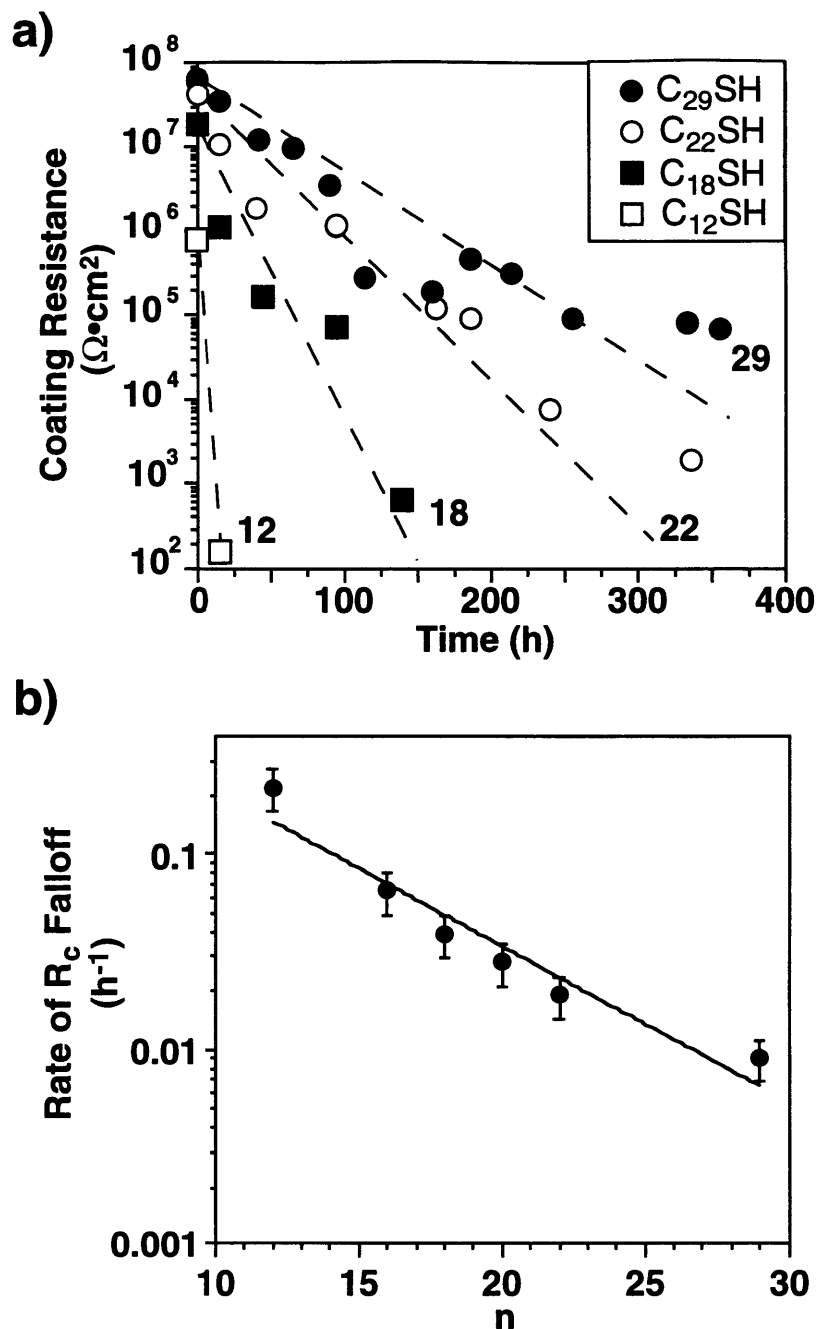
Figure 4.8. (a) Time-dependence of the coating resistance for SAMs of C_nSH (n = 12, 18, 22, and 29) on copper upon exposure to 1 atm of O_2 at 100% RH. Coating resistances were determined by fitting impedance data to the equivalent circuit shown in Figure 4.1a. The lines are least-squares fits to the data and were constrained to intersect the initial (t = 0) data point. (b) Relation between the rate of coating-resistance falloff (from Figure 4.7a) and the chain length (n) of the adsorbate that forms the coating for n = 12, 16, 18, 20, 22, and 29. The line represents a least-squares fit to the data. From the slope of the line, the incremental chain length that is required to reduce the coating-resistance falloff by a factor of 1/e is 6 CH_2 units.

exposure to a corrosive environment. This trend is illustrated in greater detail in Figure 4.8a where the coating resistance is plotted as a function of exposure time to 1 atm of O_2 at 100% RH. The data in Figure 4.8a illustrate that R_c decreases exponentially with time and that the thicker films are better able to maintain their protective properties over extended periods of exposure to the given conditions. This ability is likely a result of the increased number of van der Waals interactions for the thicker films (vide infra). In Figure 4.8b, the rate of falloff in R_c is plotted as a function of the chain length of the adsorbate. The slope of the line in Figure 4.8b indicates that the rate of R_c falloff decreases by 50% for every five carbons in the adsorbates forming the SAM. This result is comparable to that of Laibinis and Whitesides who observed that the rate of oxidation of the underlying copper decreases by 50% for every four carbons in the n-alkanethiol adsorbates.[17] The similarities in these results suggest that the phenomena affecting the loss in performance are related (vide infra).

The decrease in R_c with time may be the result of a structural change within the films. The structural properties of these films were monitored with IR spectroscopy as a function of exposure time to the oxidizing conditions (1 atm O_2 at 100% RH). Figure 4.9 displays the C-H stretching region of IR spectra for copper protected by C_{16}, C_{22}, and C_{29} films as initially prepared and after exposure to the corrosive conditions. After exposure for 22 h, the spectrum for the C_{16} film exhibits broadening of the peaks and an increased intensity in the methylene peaks, suggesting a less densely packed film in which the average orientation of the chain axis is more canted from the surface normal. This structural evolution is accompanied by a shift in peak position to higher wavenumbers for the CH_2 modes [i.e. $v_a(CH_2) = 2926$ cm^{-1}] that indicates a loss of crystallinity in the hydrocarbon film. Although broadened, the integrated intensity for the methyl peaks remains constant over the 22-h exposure. For the C_{16} film at longer times (not shown), the appearence of new peaks in the IR spectra at 3360, 1490, and 1405 cm^{-1} suggests the formation of $Cu(OH)_2$ and $CuCO_3$ species underneath the SAM. At these longer times, the peaks within the C-H stretching region continue to broaden, and $v_a(CH_2)$ shifts to 2930 cm^{-1}. For C_{22} and C_{29} films after 22 h of exposure, a related, albeit smaller, increase in integrated methylene peak intensities is observed due to a broadening of the bands; however, in contrast to the C_{16} film, the C_{22} and C_{29} films exhibit only a slight loss of crystallinity [$v_a(CH_2) = 2919$ cm^{-1}] during this time period.[22] Nevertheless, the coating resistance for the C_{22} and C_{29} SAMs decrease by factors of 5 and 2, respectively, after the 22-h exposure as shown in Figure 4.8a. That this large reduction in coating resistance occurs with a slight change in the structure of the film reveals the sensitivity of molecular structure on the barrier properties of a protective coating. At longer times, the spectra for the C_{22} (400 h) and C_{29} (640 h) films show a continued increase in the intensity of the methylene modes, suggesting greater tilt of the hydrocarbon chains within the film. A loss of intensity in the $v_s(CH_3)$ mode and a corresponding increase in intensity in the $v_a(CH_3)$ mode (both with considerable peak broadening)

57
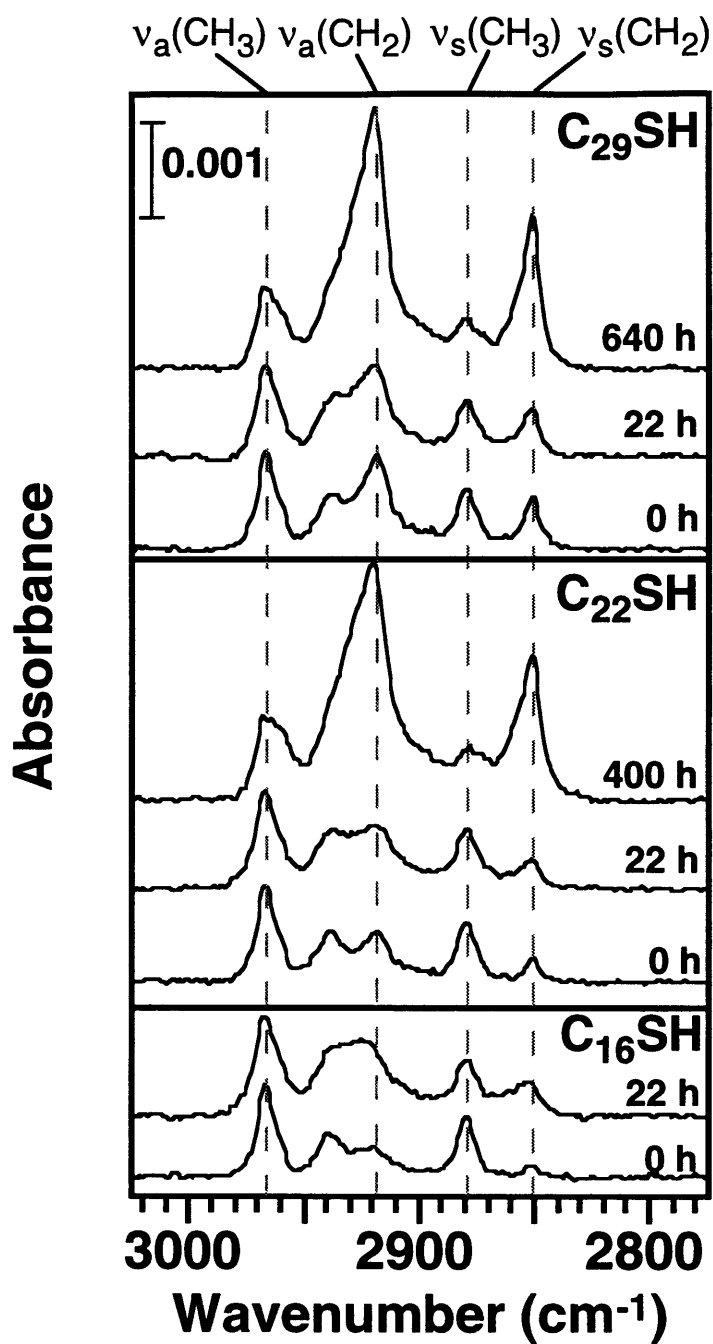
Figure 4.9. Grazing incidence polarized infrared spectra of the C-H stretching region for SAMs of $C_{16}SH$, $C_{22}SH$, and $C_{29}SH$ on copper before and after exposure to 1 atm of O_2 at 100% RH for various times. The dashed lines represent the positions of the primary modes for a trans-extended monolayer with no gauche defects: $v_a(CH_3) = 2965$ cm^{-1}, $v_a(CH_2) = 2918$ cm^{-1}, $v_s(CH_3) = 2879$ cm^{-1}, and $v_s(CH_2) = 2851$ cm^{-1}. The spectra have been offset vertically for clarity.

also suggest greater average cant of the molecular adsorbates but indicate that there is no loss of hydrocarbon adsorbates within the film during this structural evolution. The positions of the methylene modes at these longer times for the C_{29} film [$v_a(CH_2) = 2919$ cm^{-1}; $v_2(CH_2) = 2851$ cm^{-1}] and the C_{22} film [$v_a(CH_2) = 2920$ cm^{-1}; $v_2(CH_2) = 2851$ cm^{-1}] indicate only a slight loss in crystallinity throughout the exposure, and there was no appearance of peaks corresponding to $Cu(OH)_2$ or $CuCO_3$ in the spectra of either film. These spectra suggest that the adsorbates within the C_{22} and C_{29} SAMs also become more canted upon exposure to corrosive conditions, but in contrast to the C_{16} film, these adsorbates remain relatively crystalline for much longer periods of time.

As discussed above, the increase in the intensities of the methylene stretching modes suggests that the adsorbates within the SAM become more tilted and less densely packed with time. This structural transformation of the SAM can also be probed electrochemically since the coating capacitance should increase as the films become less densely packed and more permeable to ionic species. Figure 4.10 shows the effect of exposure to 1 atm of O_2 at 100% RH on both the sum of the integrated intensities for the asymmetric and symmetric methylene stretching modes (Figure 10a) and the coating capacitance (Figure 4.10b) for SAMs formed from $C_{16}SH$, $C_{22}SH$, and $C_{29}SH$ on copper. The methylene intensities have been normalized to the value for a freshly prepared SAM from the respective adsorbate. For a C_{16} SAM, the methylene intensity increases rapidly upon exposure to the corrosive conditions, indicating major structural changes for the hydrocarbon chains within the coating (Figure 4.10a). The capacitance of C_{16} films also increases sharply with exposure time (Figure 4.10b), indicating that structural changes within the hydrocarbon chains result in a film that is more permeable to ionic species. This increased capacitance could result from the SAM becoming effectively thinner and/or having an increased dielectric permittivity. For a C_{22} SAM with greater van der Waals interactions, the methylene intensities increase slightly for the first 70 h while the capacitance remains constant. On a similar timescale, the coating resistance for the C_{22} SAM decreases sharply (Figure 4.8a) suggesting that the subtle change in molecular structure affects the coating resistance of the film more strongly than the capacitance. After ~100 h, both the methylene intensities and the capacitance increase sharply indicating a transformation to a less densely packed film with a smaller effective thickness. The SAM derived from $C_{29}SH$ exhibits a slight increase in both methylene intensity and capacitance, but the rates of increase are far smaller than those for the thinner C_{16} and C_{22} films. These results demonstrate that structural changes within a coating can be correlated to its capacitance and that thicker SAMs with greater intermolecular interactions can better maintain a densely packed hydrocarbon lattice that is less permeable to ionic species.
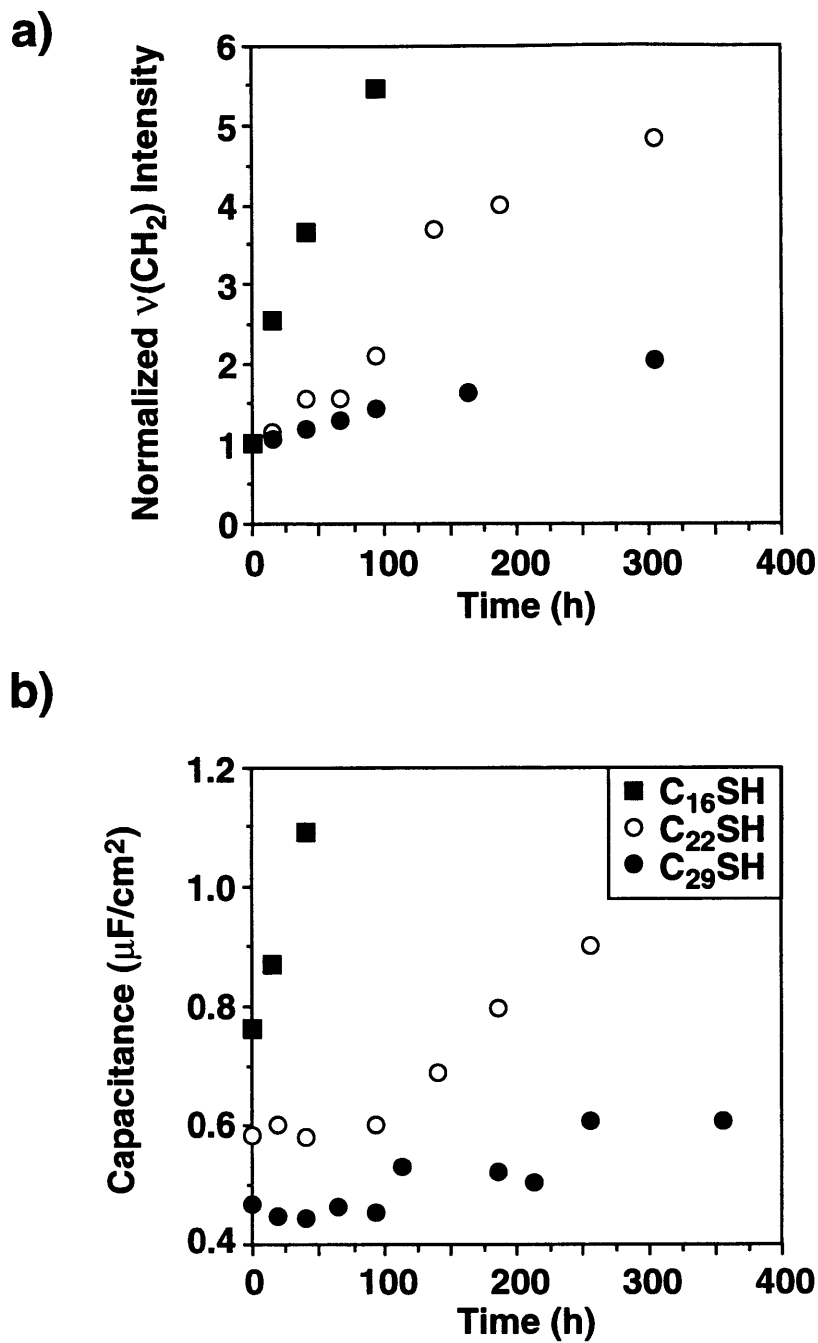
Figure 4.10. Effect of exposure to 1 atm of O_2 at 100% RH on (a) the sum of the integrated intensities for asymmetric and symmetric methylene stretching modes—$v_a(CH_2) + v_s(CH_2) =$ $v(CH_2)$—in IR and (b) the coating capacitance in oxygenated 50 mM Na_2SO_4(aq). The methylene intensities in (a) were normalized to the value for a freshly prepared coating of the same adsorbate. Capacitance values were determined by fitting impedance data to the equivalent circuit shown in Figure 4.1a.

4.3. Discussion

4.3.1. Chain-length Effects on the Protection of Copper by n-Alkanethiols

The barrier properties of initially formed SAMs on copper depend on the chain length of the adsorbates that form the film (Figures 4.5 and 4.6). SAMs formed from C_nSH with $n \leq 12$ provide coating resistances that are at least 30 times smaller than SAMs from $n \geq 16$. The poor barrier properties are likely a result of the inferior packing and crystallinity of the shorter-chained adsorbates as initially formed; the peak positions of $v_a(CH_2)$ for C_8 and C_{12} films on copper are 2924 and 2922 cm^{-1}, respectively, indicating films with predominately liquid-like characteristics. The initial impedance spectra for thicker films ($n \geq 16$) are primarily controlled by their capacitance (Figure 4.5), indicating that these films provide a greater physical barrier to the diffusion of ionic species present in the contacting aqueous phase. The superior barrier properties of these thicker films are attributed to the densely packed, crystalline hydrocarbon layer that separates the underlying copper from the external environment. Coating resistances for these SAMs increase linear with film thickness for $n \geq 16$ (as shown in Figure 4.6), suggesting that the CH_2 groups within the hydrocarbon chains behave as a series of resistors to the permeation of ionic species.

Upon exposure to 1 atm of O_2 at 100% RH, the thickest films exhibit the slowest transition to a less densely packed structure (Figure 4.10) and the slowest loss of coating resistance (Figure 4.8). Time-dependent infrared spectra demonstrate that the films formed from longer-chained adsorbates are more effective at maintaining their crystalline structure under oxidizing conditions than films formed from shorter-chained analogues. These IR data are consistent with results from Chapter 3 in which thicker SAMs were observed to be more effective in maintaining a low-energy methyl surface that was not wet by hexadecane.[18] The superior performance provided by SAMs with greater thickness is likely a result of their enhanced structural stability due to the greater number of intermolecular interactions within the hydrocarbon chains for these films; by analogy, the stability of structurally similar films (such as these) might be expected to scale with the melting points of the adsorbates. To test this hypothesis, the rate of falloff for the coating resistance of films derived from three linear alkanethiols were compared: $C_{22}SH$, $C_{29}SH$, and $C_{18}OC_{11}SH$ (Figure 4.11). While the chain length of the ether-linked thiol is similar to that of the $C_{29}SH$ (both have 29 carbons) and it produces a film of similar thickness, the melting point of $C_{18}OC_{11}SH$ (m.p. ~ 46 °C) is approximately the same as for $C_{22}SH$ (m.p. ~ 47 °C). Initial IR spectra of the C-H stretching region for SAMs formed from $C_{18}OC_{11}SH$ on copper reveal a crystalline, densely packed monolayer, similar to those from $C_{29}SH$. In Figure 4.11, the rate of coating-resistance falloff for the ether-substituted SAM is greater than that for the C_{29} SAM of similar thickness but nearly identical to that for the C_{22} SAM. This result suggests that the intermolecular interactions
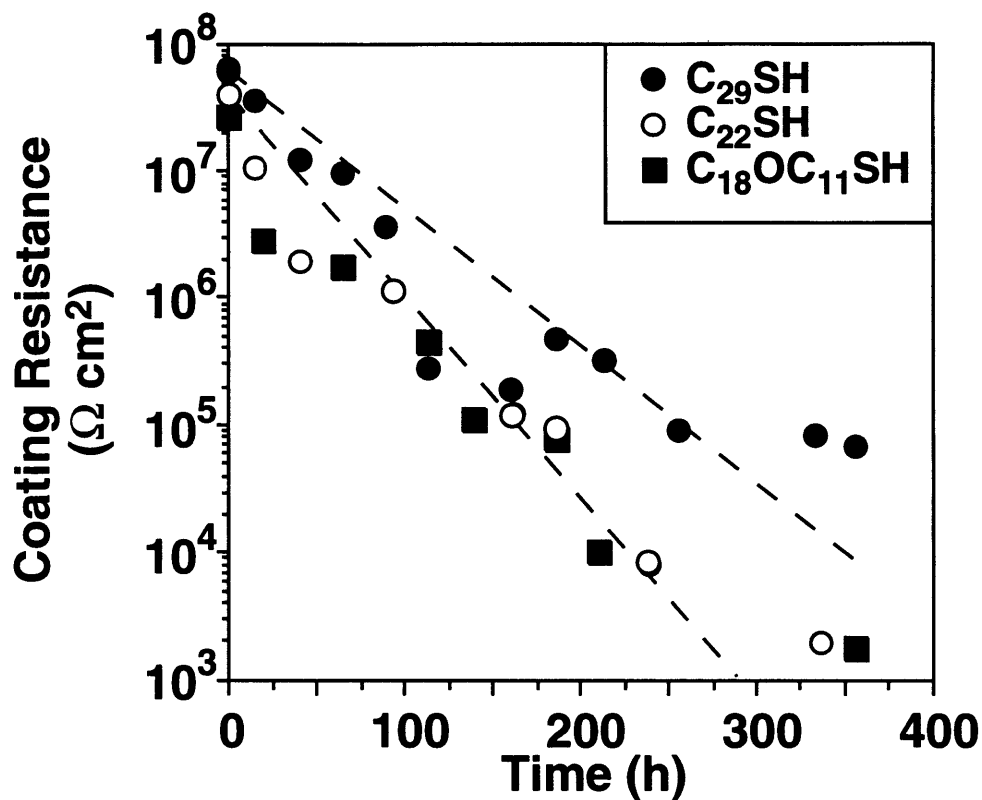
Figure 4.11. Time-dependence of the coating resistance for SAMs of $C_{22}SH$, $C_{29}SH$, and $C_{18}OC_{11}SH$ upon exposure to 1 atm of O_2 at 100% RH. Coating resistances were determined by fitting impedance data to the equivalent circuit shown in Figure 4.1a. The lines are linear least-squares fits to the data for C_{22} and C_{29} films and were constrained to intersect the initial (t = 0) data point.

that govern melting phenomena are also prominent factors that determine the structural stability of these thin films when exposed to oxidizing conditions.

4.3.2. Proposed Mechanism for Deterioration of SAM Barrier Properties

Comparison of data obtained from infrared and impedance spectra enables elucidation of the structural state of a SAM and its effect on barrier properties. Over the first 70 h of exposure to 1 atm of O_2 at 100% RH for C_{22} and C_{29} SAMs on copper, moderate changes in the structure of the films, as measured by the normalized intensity of methylene peaks in IR (Figure 4.10a), have no effect on their coating capacitance (Figure 4.10b) but can result in an exponential loss of their coating resistance (Figure 4.8a). Although the effective thickness of these SAMs as probed by capacitance remains essentially constant over the first 70 h, increased heterogeneity within the local environment of the hydrocarbon results in a SAM with a greater free volume that is less resistant to the transport of ions. These results demonstrate the sensitivity of ionic transport on subtle issues related to the densely packed structure of the hydrocarbon chains within the SAM. After 100 h of exposure to the oxidizing environment for a C_{22} SAM on copper, major changes in the structure of the film as indicated by an increase in the methylene intensity (Figure 4.10a) occur concurrent with an increase in the capacitance of the film (Figure 4.10b), indicating an effectively thinner SAM and/or an increased dielectric permittivity due to water and ionic uptake. These results are in contrast to the behavior of 1.2-μm-thick coatings of polyimide on aluminum where an increase in capacitance upon exposure to NaCl(aq) preceded breakdown of the barrier properties of the coating.[23] The different behavior for SAMs is attributed to their thinness in comparison to the much thicker polymeric coatings.

The time-dependent data presented in this paper provide insight into the mechanism of the corrosion process occurring on SAM-coated copper. The impedance data in Figures 4.7 and 4.8 illustrate that thicker films are more effective in protecting the copper surface from corrosion and that the performance of these thicker films deteriorates more slowly than that of thinner films upon exposure to O_2 (1 atm) at 100% RH. The infrared spectra (Figure 4.9) indicate that the SAMs become more heterogeneous and less densely packed upon prolonged exposure to the oxidizing conditions but that the thicker films are more effective in maintaining their levels of crystallinity and packing. Furthermore, the IR data suggest that there is no loss of the molecular adsorbates from the film during the corrosion process. The deterioration in the barrier properties for these films probably corresponds to an altered structure in which the hydrocarbon chains within the film become more canted and less densely packed. An increased free volume within polymer films has been shown to result in greater permeability to water.[24] That the transformation to a less densely packed SAM occurs without loss of molecular adsorbates suggests an increase in the surface area

of the underlying copper, most likely through roughening by oxidation. An increase in surface roughness is consistent with an increased hysteresis in the time-dependent wetting data for these films on copper.[17] This nanoscale roughness could affect the local environment of the hydrocarbon chains, rendering them less resistant to the transport of aqueous species.

These results are consistent with a mechanism in which O_2 and H_2O diffuse through the film and react at the surface during exposure to O_2(1 atm) at 100% RH. Because the SAM acts as a barrier to the transport of O_2[6,17] and H_2O,[18] oxidation (and surface roughening) will occur more rapidly through thinner films. In addition, oxidation of thiolates to less-adherent sulfonates occurs more rapidly with thinner films.[17] The atomic-level roughening of the underlying copper may distort the hydrocarbon lattice of the SAM and increase its permeability to the diffusion of aqueous ions (such as in the EIS measurement), resulting in films with inferior barrier properties. SAMs formed from longer-chain adsorbates provide a thicker barrier against the diffusion of small molecules and a more structurally stable hydrocarbon lattice that can better accommodate surface roughening.

Further experimental support of this mechanism can be illustrated by monitoring the structural properties for n-alkanethiols on gold and silver substrates. SAMs of C_nSH ($15 \leq n \leq 22$) on gold and silver exhibited no major structural changes and no loss of crystallinity after exposure to air for 43 days. The enhanced structural stability of these SAMs is likely a function of the greater resistance of these metals against oxidation, and thus surface roughening, in comparison to copper.

A less likely mechanism for the deterioration of the barrier properties within the films involves the oxidation of thiolates to sulfonates and the subsequent desorption of these loosely bound sulfonates into water, during either a rinsing step or the EIS measurement. The thiolate moieties of a SAM on copper can be converted to less adherent sulfonates upon extended exposure to oxygen.[17] Such a loss of adsorbate material from the film would result in a coating with a significant density of pinholes and defects and a corresponding decrease in the barrier properties. While the falloff in barrier properties could be rationalized by this mechanism, the structural properties of these films as probed by IR are not consistent with this hypothesis because they are independent of contact to water for the timescales investigated. For example, IR spectra accumulated before and after rinsing with water or characterization by EIS were identical, indicating no loss of material in the film upon contact to an aqueous phase. In addition, repetitive EIS measurements on the same sample were identical. These results and the consistency of the integrated methyl intensities in the time-dependent IR spectra reveal that the adsorbates remain bound to the underlying copper during exposure to the corrosive conditions and during characterization by EIS and suggest that the structural changes within the film are the result of oxidation of the underlying copper surface.

4.4. Conclusions

Self-assembled monolayers (SAMs) derived from unsubstituted n-alkanethiols [$CH_3(CH_2)_{n-1}SH$] on copper provide protection against corrosion of the underlying metal that scales with the chain length of the adsorbate. SAMs formed from longer-chained adsorbates (n ≥ 16) are highly crystalline and provide substantially greater initial coating resistances than thinner SAMs. Upon exposure to 1 atm of O_2 at 100% RH, thicker SAMs maintain their structural and barrier properties at a level superior to thinner SAMs. For these unsubstituted n-alkanethiolate SAMs, the thicker films have greater van der Waals interactions which contribute to the superior maintenance of their barrier properties. Addition of an ethereal oxygen in the self-assembling adsorbate ($C_{18}OC_{11}SH$ vs. $C_{29}SH$) can result in films with similar thickness but reduced intermolecular interactions (as estimated from melting points) and less effective maintenance of barrier properties. IR results show that the adsorbates within the SAM become less densely packed upon exposure to 1 atm of O_2 and 100% RH but that the adsorbates remain at the metal surface. These results are consistent with a mechanism in which oxidation of the underlying copper roughens the surface and perturbs the hydrocarbon lattice of the SAM into a less crystalline state, producing coatings that are more permeable to ionic species as measured with EIS.

4.5. Experimental

4.5.1. Materials and Synthesis.

Isooctane (J.T. Baker), anhydrous tetrahydrofuran (Aldrich), and hexadecane (Aldrich) were used as received. Octyl, dodecyl, and octadecyl thiols were purchased from Aldrich and were purified by distillation or recrystallization before use. Docosyl and hexadecyl thiols were available from a previous study,[18] and eicosyl thiol and 11-bromo-undecyl-*t*-butyldimethylsilyl ether were synthesized via a literature procedure.[25] The synthesis of 11-octadecyloxy-1-undecanethiol is noted in Chapter 5. Dilithium tetrachlorocuprate, octadecylmagnesium chloride, tetrabutylammonium fluoride, diisopropyl azodicarboxylate, and triphenylphosphine were purchased from Aldrich and used as received. All intermediates were characterized by ^{1}H NMR (400 MHz). NMR spectra were obtained in $CDCl_3$ and referenced to residual chloroform at 7.24 ppm.

Nonacosyl-t-butyldimethylsilyl ether. A solution of Li_2CuCl_4 in THF (5.2 mL, 0.1 M) was added to a solution of 11-bromo-undecyl-*t*-butyldimethylsilyl ether[25] (8.54 g, 20.7 mmol) in 100 mL of anhydrous THF at 0 °C. A solution of octadecyl magnesium chloride in anhydrous THF (45 mL, 0.5 M) was then added dropwise to the reaction mixture. After the reaction warmed

to room temperature overnight, it was quenched by dropwise addition to a saturated aqueous solution of $NH_4Cl(aq)$. The layers were separated and the aqueous fraction was extracted thrice with hexanes. The organic extracts were combined and concentrated to yield a yellow-brown oil. The title compound was obtained by chromatography (hexanes followed by 2% ethyl acetate/hexanes) over silica gel as a yellow oil (7.22 g, 13.4 mmol, 65%). ^{1}H NMR, δ 3.57 (t, 2 H), 1.53 (quint, 2 H), 1.2-1.4 (m, 52 H), 0.87 (m, 9 H), 0.85 (t, 3 H), 0.03 (m, 6 H).

Nonacosanol. A solution of tetrabutylammonium fluoride in THF (30 mL, 1.0 M) was added to nonacosyl-t-butyldimethylsilyl ether (7.23 g, 13.4 mmol) in 100 mL of THF. The reaction was stirred for 2.5 h and concentrated under reduced pressure. Column chromatography (2% methanol/chloroform) over silica gel yielded the title compound as a white solid (5.36 g, 12.6 mmol, 94% yield). ^{1}H NMR, δ 3.62 (t, 2 H), 1.55 (m, 2 H), 1.2-1.4 (m, 52 H), 0.86 (t, 3 H).

Nonacosyl thioacetate. Diisopropyl azodicarboxylate (1.52 g, 7.32 mmol) was added to a solution of triphenylphosphine (1.91 g, 7.32 mmol) in 200 mL of anhydrous THF at 0 °C.[26] A solution of nonacosanol (1.55 g, 3.67 mmol) and thiolacetic acid (0.556 g, 7.32 mmol) in 60 mL of anhydrous THF was added dropwise to the reaction mixture and stirred at 0 °C for 1 h. The reaction was stirred for an additional 2 h as it warmed to room temperature. The mixture was concentrated under reduced pressure, and the title compound was obtained by column chromatography (1% ethyl acetate/ hexanes) as a white solid (1.02 g, 2.1 mmol, 58% yield). ^{1}H NMR, δ 2.85 (t, 2 H), 2.30 (m, 3 H), 1.53 (quint, 2 H), 1.2-1.4 (m, 52 H), 0.86 (t, 3 H).

Nonacosyl thiol. Concentrated hydrochloric acid (0.77 g, 21 mmol) was added to a refluxing mixture of nonocosyl thioacetate (1.02 g, 2.1 mmol) in 25 mL of deoxygenated ethanol, and the reaction proceeded overnight. The mixture was concentrated under reduced pressure. Column chromatography (5:2 chloroform/hexanes) yielded the title compound as a white powder (0.324 g, 0.67 mmol, 32% yield). ^{1}H NMR, δ 2.52 (quart, 2 H), 1.58 (m, 2 H), 1.2-1.4 (m, 52 H), 0.86 (t, 3 H).

4.5.2. Oxidation Studies

Immediately after assembly of the monolayers, the Cu-coated Si wafers were cut into 1.5 x 3 cm^2 samples that were either characterized or placed into a chamber at 100% relative humidity (RH). Humidity levels were determined by a digital hygrometer (Fisher). The chamber was evacuated and then backfilled with O_2 to atmospheric pressure. A steady stream of O_2 flowed through the chamber at 10 cm^3/min during the experiment. The chamber was kept at room temperature and stored in the dark to minimize any possible effects due to the influence of light. After various periods of exposure, samples were removed from the chamber, rinsed with water, dried in a stream of N_2, and characterized by either IR, EIS, or XPS. After characterization by EIS or XPS,

the samples were discarded. Samples initially characterized by IR were often subsequently characterized by one of the other methods.

4.5.3. Electrochemical Impedance Spectroscopy (EIS).

Electrochemical impedance spectroscopy of SAM-coated copper samples was performed with an EG&G 1025 frequency response detector connected to an EG&G 263A potentiostat, both interfaced to a personal computer. A glass cell equipped with a platinum mesh counter electrode and a Ag/AgCl/sat'd KCl reference electrode contained an oxygenated solution of 0.050 M Na_2SO_4 as electrolyte. The electrolyte contacted only the center of the SAM-coated copper sample at an area of 1 cm^2 confined by an o-ring. The measurements were made at the corrosion potential with a 5 mV ac perturbation that was controlled between 10 mHz and 20 kHz. Film resistance and capacitance values were determined by fitting the EIS data with an appropriate equivalent circuit using software—Equivcrt.pas written by Bernard Boukamp—provided by EG&G.

4.5.4. Reflection-Absorption Infrared Spectroscopy (RAIRS).

IR spectra were obtained in single reflection mode with a Bio-Rad FTS 175 infrared spectrometer and Universal Reflectance Attachment. The p-polarized light was incident at 80° from the surface normal, and the reflected light was detected with a narrow-band MCT detector. Spectral resolution was 2 cm^{-1} after triangular apodization. Spectra were referenced to those of SAMs prepared from octadecanethiol-d_{37} on copper with 1024 scans being acquired for both the sample and reference. Integrated peak intensities were determined by fitting the spectra with Gaussian profiles.

4.6. References

1) Finklea, H. O. *Electrochemistry of Organized Monolayers of Thiols and Related Molecules on Electrodes*; In Electroanalytical Chemistry, vol. 19; Bard, A.J.; Rubinstein, I., Eds.; Marcel Dekker: New York, 1996; Vol. 19, pp 109-335.

2) Finklea, H. O.; Snider, D. A.; Fedyk, J.; Sabatani, E.; Gafni, Y.; Rubinstein, I. *Langmuir* **1993**, *9*, 3660-3667.

3) Zhao, M.; Zhou, Y.; Bruening, M. L.; Bergbreiter, D. E.; Crooks, R. M. *Langmuir* **1997**, *13*, 1388-1391.

4) Yamamoto, Y.; Nishihara, H.; Aramaki, K. *J. Electrochem. Soc.* **1993**, *140*, 436-443.

5) Feng, Y.; Teo, W.-K.; Siow, K.-S.; Gao, Z.; Tan, K.-L.; Hseih, A.-K. *J. Electrochem. Soc.* **1997**, *144*, 55-64.

6) Ishibashi, M.; Itoh, M.; Nishihara, H.; Aramaki, K. *Electrochimica Acta* **1996**, *41*, 241-248.

7) Mitton, D. B.; Latanision, R. M.; Bellucci, F. *J. Electrochem. Soc.* **1996**, *143*, 3307-3316.

8) Nahir, T. M.; Bowden, E. F. *Electrochimica Acta* **1994**, *39*, 2347-2352.

9) Ulman, A. *An Introduction to Ultrathin Organic Films From Langmuir-Blodgett to Self-Assembly*; Academic Press: Boston, 1991.

10) Laibinis, P. E.; Whitesides, G. M.; Allara, D. L.; Tao, Y.-T.; Parikh, A. N.; Nuzzo, R. G. *J. Am. Chem. Soc.* **1991**, *113*, 7152-7167.

11) Abrahamsson, S.; Larsson, G.; von Sydlow, E. *Acta Cryst.* **1960**, *13*, 770-774.

12) Laibinis, P. E.; Bain, C. D.; Whitesides, G. M. *J. Phys. Chem.* **1991**, *95*, 7017-7021.

13) The formation of high-quality SAMs from alkanethiols on copper is more difficult than for analogous SAMs on gold as the assembly is sensitive to the adsorption conditions. Feng et al.[9] demonstrate the importance of achieving an oxide-free copper surface before self-assembly as thiol adsorbates exhibit poor interaction with CuO and have been reported to form multilayers when assembled under aerobic conditions (see Keller et al. *Thin Solid Films* **1994**, *244*, 799-805).

14) Porter, M. D.; Bright, T. B.; Allara, D. L.; Chidsey, C. E. D. *J. Am. Chem. Soc.* **1987**, *109*, 3559-3568.

15) Peterlinz, K. A.; Georgiadis, R. *Langmuir* **1996**, *12*, 4731-4740.

16) Lanza, V. L.; Herrman, D. B. *J. Polym. Sci.* **1958**, *28*, 622-625.

17) Laibinis, P. E.; Whitesides, G. M. *J. Am. Chem. Soc.* **1992**, *114*, 9022-9027.

18) Jennings, G. K.; Laibinis, P. E. *Colloids Surf., A* **1996**, *116*, 105-114.

19) Conductivity is expected to decrease exponentially with film thickness if electron tunneling is the primary mode of charge transfer (Simmons, J.G. *J. Appl. Phys.* **1963**, *34*, 1793).

20) Boulas, C.; Davidovits, J. F.; Rondelez, F.; Vuillaume, D. *Phys. Rev. Lett.* **1996**, *76*, 4797-4800 and references therein.

21) Bareman, J. P.; Cardini, G.; Klein, M. L. *Phys. Rev. Lett.* **1988**, *60*, 2152-2155.

22) The increase in methylene intensity is not likely the result of adventitious carbon contamination, as all the samples studied expose low-energy methyl surfaces that are resistant to the adsorption of foreign species..

23) Bellucci, F.; Kloppers, M.; Latanision, R. M. *J. Electrochem. Soc.* **1991**, *138*, 40-48.

24) Nenov, K. *Impedance Spectroscopy Study of the Water Uptake and Long-Term Degradation of Immersed Polyimide Coatings*; Ph.D. Thesis, Materials Science and Engineering; Massachusetts Institute of Technology, 1994.

25) Bain, C. D.; Troughton, E. B.; Tao, Y.-T.; Evall, J.; Whitesides, G. M.; Nuzzo, R. G. *J. Am. Chem. Soc.* **1989**, *111*, 321-335.

26) Volante, R. P. *Tet. Lett.* **1981**, *22*, 3119-3122.

Chapter 5. Formation and Structure of Oriented Monolayers on Gold and Copper from Long-Chain ω-Alkoxy-n-Alkanethiols

5.1. Background

Although much effort has been devoted to controlling surface properties with SAMs in two dimensions,[1] a fine-tuned control over the third dimension (thickness) has only been demonstrated for film thicknesses less than 30 Å.[2] The ability to form SAMs from longer-chain adsorbates provides the opportunity to produce thicker films that may provide enhanced barriers against electron transfer or corrosive agents. In Chapter 4, the relationship between the structure and barrier properties of n-alkanethiolate $[CH_3(CH_2)_{n-1}SH]$ SAMs on copper with chain length as great as n = 29 was reported. The results obtained demonstrate that SAMs formed from adsorbates with longer chain lengths provide greater resistances against the diffusion of aqueous ions and are more effective in maintaining a high level of protection to the underlying substrate during prolonged exposure to a corrosive environment. Efforts to form thicker, more protective SAMs with unsubstituted n-alkanethiols having n > 29 are complicated by lengthy syntheses and poor solubility of the long-chained intermediates in many commonly used solvents. Grainger and co-workers have adsorbed disulfide-containing polymers on gold that include various side-chain compositions.[3,4] While the thermal stability of these films is superior to monolayer films due to their multipoint ligation, the films ranged in thickness from 10 - 40 Å and exhibited barrier properties that were inferior to those of monolayers films of similar thickness.[4]

In order to form SAMs with greater thickness, the synthesis of a series of long-chain ω-alkoxy-*n*-alkanethiol adsorbates $[CH_3(CH_2)_{p-1}O(CH_2)_mSH]$ was accomplished where an ethereal unit provides coupling between two n-alkyl chains. For this targeted goal, the Williamson ether synthesis provides a flexible synthetic methodology that enables the formation of these long-chain adsorbates with relatively few synthetic steps. The presence of the ethereal oxygen increases the polarity of the thiols and their synthetic intermediates and improves their solubility for assembly and purification. Substitution of an ether moiety within the hydrocarbon of the adsorbate does not dramatically affect the crystallinity of the resulting SAM due to the similarity of the ether in size and structure to a methylene group; while the presence of the ether oxygen causes a local disordering within the SAM, the gross structure of the SAM is largely insensitive to its presence when the ether unit is placed at least two methylene units away from the chain terminus.[5] Miller et al.[6] have used reflection-absorption infrared spectroscopy and electrochemical measurements to study the structural properties for SAMs on gold derived from ω-hydroxy-alkanethiols that contain an

70

internal ethereal oxygen. They correlated shifts in the potential of zero charge to the structural orientation of the ethereal oxygen unit in the crystalline monolayer.

In this chapter, the kinetics of formation and the structural properties of SAMs derived from ω-alkoxy-n-alkanethiols [$CH_3(CH_2)_{p-1}O(CH_2)_mSH$] on gold and copper are reported; for simplicity, the compounds are abbreviated as C_pOC_mSH. As summarized in Figure 5.1, the following adsorbates have been synthesized: $C_{18}OC_{11}SH$, $C_{22}OC_{11}SH$, $C_{18}OC_{19}SH$, $C_{22}OC_{19}SH$, and $C_{22}OC_{22}SH$. SAMs derived from these adsorbates have been characterized by ellipsometry and x-ray photoelectron spectroscopy (XPS) to determine thickness of the adsorbed film, infrared spectroscopy to determine the structural phase state of the hydrocarbon chains within the SAM, and electrochemical impedance spectroscopy to quantify the resistance provided by SAMs on copper against the diffusion of aqueous ions. In particular, the longest-chained adsorbates in this study have been used to produce the thickest SAMs formed to date from non-polymeric adsorbates.

The kinetics of formation for these long-chained adsorbates will be compared to those for shorter-chained n-alkanethiols (C_nSH) to assess the effect of chain length on the rates of assembly. The kinetics of assembly for alkanethiolate monolayers on gold from solution have been monitored previously in situ by surface plasmon resonance (SPR),[7] scanning probe microscopies (SPM),[8] and quartz crystal microbalance (QCM)[9] and ex situ by ellipsometry.[2] Peterlinz and Georgiadis[7] have used SPR to study the formation of n-alkanethiolate monolayers (n = 8, 12, 16, 18) on gold from ethanol and heptane as solvents. They found that the kinetics of assembly in a strong alkanethiol solvent (heptane) were rapid and consistent with a first-order, diffusion-limited Langmuir isotherm while the kinetics in a weaker alkanethiol solvent (ethanol) were slower and involved three kinetic steps. The first and final steps were consistent with a first-order, diffusion-limited Langmuir isotherm while the second step was zeroth order. They concluded that a physisorbed layer of alkanethiols is present on top of the partial chemisorbed film in ethanol and that the transport of thiol molecules from this layer limits the formation of the SAM. Karpovich and Blanchard have used in situ QCM to show that an equilibrium exists between free gold sites and alkanethiolate moieties and that the kinetics of formation for these films are consistent with a Langmuir isotherm over a limited range of concentrations.[9] Bain et al. have monitored the ellipsometric thickness of SAMs on gold from ethanol ex situ and observed an initial kinetic regime of rapid growth of the SAM followed by a slower ordering step in which the final 10% of the thickness is achieved after hours of adsorption.[2] Ex situ measurements typically reveal more rapid kinetics than in situ techniques; the effect of solvent during in situ formation may influence the properties of the SAMs,[10] as may the process of removing a partial SAM from solution for ex situ measurements.
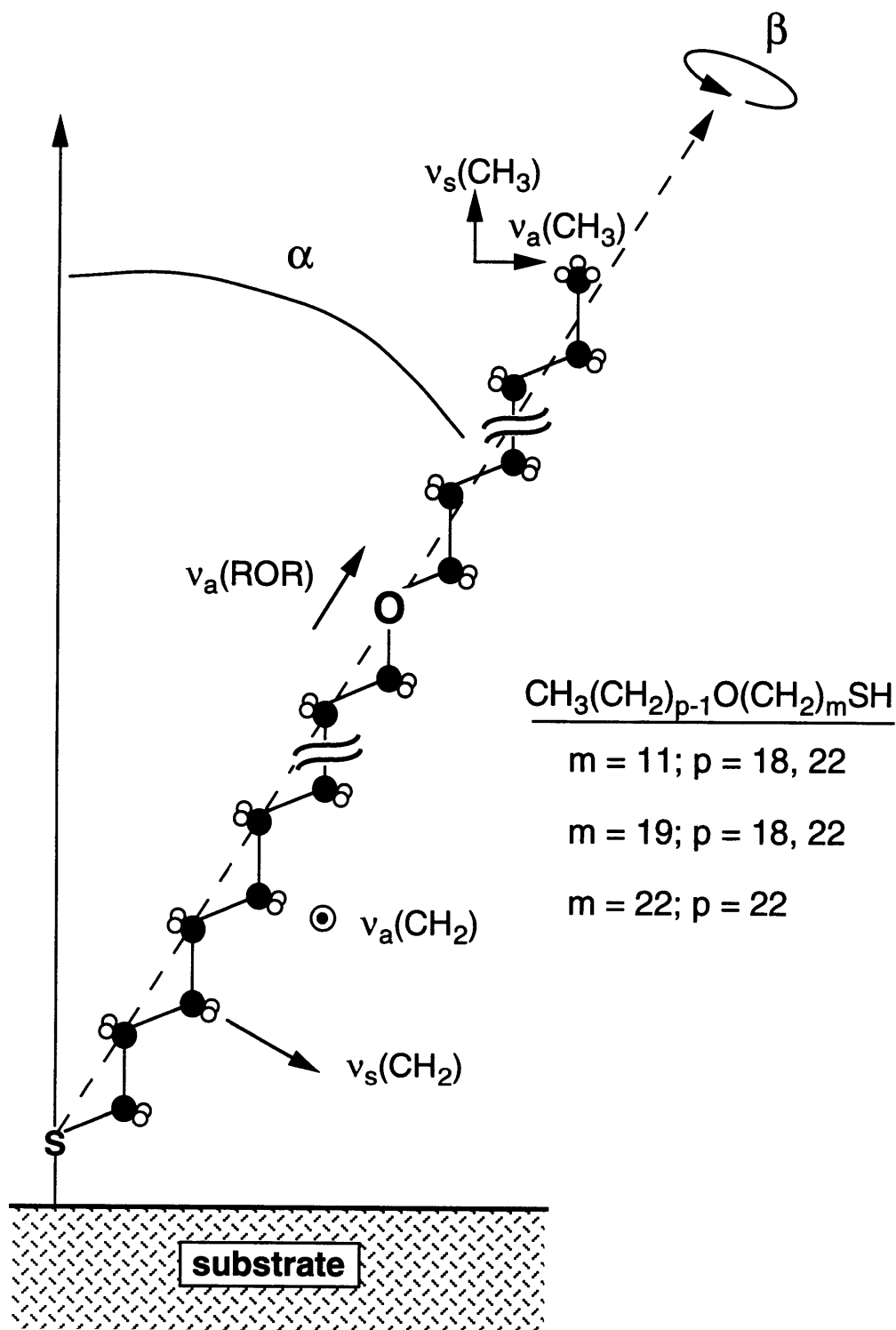
Figure 5.1. Schematic illustration of an ω-alkoxy-n-alkanethiolate adsorbate that is canted (tilted) 30° from the surface normal and twisted 0° around its molecular axis. The arrows indicate the dipole moments for the following stretching modes: $v_s(CH_2)$, $v_a(CH_2)$, $v_s(CH_3)$, $v_a(CH_3)$, and $v_a(ROR)$. The intensities of the infrared bands for these dipole moments depend on their projection along the z-axis.

72

In collaboration with Prof. Gang-yu Liu and co-workers at Wayne State University, the kinetics of formation for SAMs of $C_{18}OC_{19}SH$ on Au(111) from 2-butanol were studied in situ using atomic force microscopy (AFM).[8] Images obtained with AFM at dilute concentrations (2 μM, butanol) showed that the hydrocarbon chains lie flat on the gold surface at early times, adopt various structures on the gold surface at intermediate times—including adsorbates that are oriented, kinked at the ether bond, or lying flat—and become oriented and densely packed with continued exposure to the thiol solution. As observed by AFM, the kinetics of formation for $C_{18}OC_{19}SH$ in 2-butanol were more rapid than for shorter, unsubstituted thiols such as $C_{18}SH$. In this chapter, the kinetics of formation for $C_{18}OC_{19}SH$, as measured ex situ by ellipsometry, are correlated with the structural properties of the forming monolayers, as characterized ex situ by IR spectroscopy. In addition, the general structural aspects of ω-alkoxy-n-alkanethiols on copper and gold are examined.

5.2. Results and Discussion

5.2.1. Formation of Monolayers

The ω-alkoxy-n-alkanethiols were synthesized by a multistep process (eq 5.1):

$$H_2C=CH(CH_2)_{m\text{-}2}Br \xrightarrow[\substack{2.\ CH_3COSH/h\nu \\ 3.\ H^+/CH_3CH_2OH}]{1.\ CH_3(CH_2)_{p\text{-}1}ONa/THF} HS(CH_2)_mO(CH_2)_{p\text{-}1}CH_3 \tag{5.1}$$
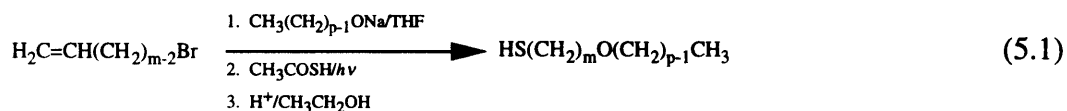
Self-assembled monolayers from these ω-alkoxy-n-alkanethiols were formed by immersion of freshly evaporated copper or gold substrates into 0.5 mM isooctane or 2-butanol solutions of the adsorbates at either 22 or 55 °C from 2 s to over 100 h. Since adsorbates with chain lengths p + m $\geq$ 37 were poorly soluble in the solvents at room temperature, the solutions were heated to solubilize the adsorbate before cooling to the adsorption temperature.

5.2.2. SAMs Derived from $C_{18}OC_{19}SH$ on Au

The formation of a densely packed SAM from alkanethiols requires that the adsorbates expel solvent molecules from near the metal surface and within a partially formed SAM. The effects of solvent on the formation of SAMs from $C_{18}OC_{19}SH$ on gold were investigated by comparing the kinetics of assembly in a stronger alkanethiol solvent (isooctane) and a weaker one (2-butanol). Based on *ex situ* ellipsometric measurements (Figure 5.2), the formation processes for the SAMs in these solvents are different. The thicknesses of the SAMs formed from $C_{18}OC_{19}SH$ on gold in either solvent (0.5 mM) increase with time, from 0.033 min (2 s) to 6000 min (100 h). The trend in film growth is similar to that shown by Bain et al.[2] who observed a rapid initial growth of octadecanethiolate SAMs onto gold over a few seconds. After only 2 s of exposure to
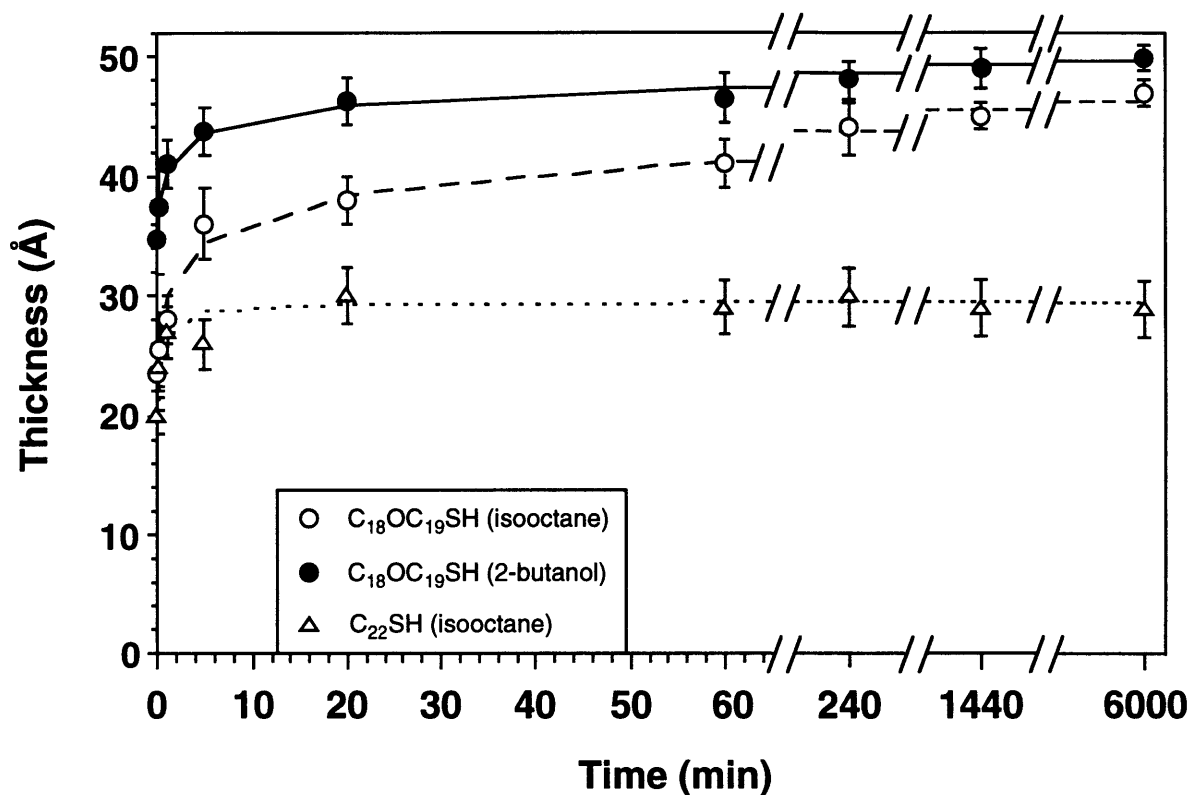
Figure 5.2. Time-dependence on the ellipsometric thickness of SAMs formed by immersion of gold substrates into solutions of $C_{18}OC_{19}SH$ (0.5 mM, isooctane or 2-butanol) or $C_{22}SH$ (0.5 mM, isooctane) at room temperature. The curves represent kinetic models that approximate the behavior of the data for $t > 0.033$ min (2 s). For the $C_{18}OC_{19}SH$ data sets, the curves are diffusion-limited, second-order Langmuir isotherms with kinetic rate constants (k_{2d}) of 0.08 and 0.05 $s^{-1/2}$ for assembly in 2-butanol and isooctane, respectively. The curve that best describes the $C_{22}SH$ data set is a second-order Langmuir isotherm with a rate constant (k_2) of 0.04 s^{-1}.

$C_{18}OC_{19}SH$-containing solutions, the thicknesses of the films formed from isooctane and 2-butanol were 23 Å and 34 Å, respectively. Upon continued exposure, the adsorption kinetics in 2-butanol were sharper and the film thickness achieved a greater asymptotic value on a more rapid timescale. The thicknesses of the SAMs after 100 h of adsorption in isooctane and 2-butanol were 47 and 50 Å, respectively, and did not change after 200 h of additional exposure to the thiol solution. These results indicate that the SAMs form more rapidly in the weaker 2-butanol solvent. This result contrasts that for short-chained, unsubstituted n-alkanethiols that form SAMs more rapidly in stronger solvents.[7] The more rapid initial film growth in 2-butanol is likely due to the tendency of long hydrophobic chains to dispel the moderately polar 2-butanol solvent by crystallizing out on the gold substrate. In isooctane, favorable interactions between the solvent and adsorbate (and also between the SAM and solvent) may contribute to the slower growth of the SAM. Bensebaa et al.[10] have reported that SAMs formed from $C_{22}SH$ in ethanol (5 μM) are significantly more crystalline than SAMs formed from hexanes for short (~2 min) adsorption times.

The curves in Figure 5.2 represent kinetic fits to the adsorption data. The earliest data in Figure 5.2 could not be modeled by any common Langmuir adsorption equations. In general, ex situ studies of SAM formation show more rapid growth than in situ studies at early times. This difference may be a result of the experimental process as the substrate is exposed to the solution-air interface and often retains a thinning film of the solution on its surface before being rinsed, dried, and subsequently characterized. Nevertheless, from 2 s to 100 h, the thickness data in Figure 5.2 for $C_{18}OC_{19}SH$ in both solvents are consistent with a diffusion-limited, second-order Langmuir adsorption model (eq 5.2):

$$d(t) = d^{\infty}[1 - \frac{1}{1 + k_{2d}t^{1/2}}] \qquad (5.2)$$

where d(t) and d^{∞} are the thicknesses of the SAM at any time (t ≥ 2s) and after 100 h of adsorption, and k_{2d} is the second-order, diffuison-limited rate constant. This model (eq 5.2) provides a superior fit to the data in Figure 5.2 in comparison to other models[7]—a diffusion-limited, first-order Langmuir model and a non-diffusion-limited, second-order Langmuir model— used by Peterlinz and Georgiadis to describe the assembly of shorter-chained n-alkanethiols. In the present case, the compatibility of the data with a second-order, diffusion-limited mechanism may reflect both the presence of a partial SAM that limits transport of adsorbates to reactive sites on the substrate and the presence of long, liquid-like chains of the adsorbed thiol that may interfere with further adsorption at adjacent sites. This impedance of further adsorption suggests that the adsorption rate will not be proportional to simply the number of unoccupied sites (first-order Langmuir) and may explain the consistency of the data with a higher-order Langmuir model. Rate

constants determined from fitting the experimental data in Figure 5.2 with these models are given in Table 5.1. After the initial 2 s of formation, the rate of formation in 2-butanol is 60% faster than in isooctane.

Table 5.1. Effect of solvent on the formation of $C_{18}OC_{19}SH$ onto gold at 22 °C.

Solvent	k_{2d} $(s^{-1/2})$
2-butanol	0.08 ±0.005
isooctane	0.05 ± 0.005

Figure 5.2 also allows comparison between the kinetics of formation of SAMs from $C_{18}OC_{19}SH$ with those for a shorter-chained $C_{22}SH$ in isooctane. The thickness of the $C_{22}SH$ film reaches a pseudo-asymptotic value within 20 min of adsorption, significantly less than the ~100 h required to achieve a constant film thickness for a SAM of $C_{18}OC_{19}SH$. The kinetics of assembly for $C_{22}SH$ on gold were fit with a non-diffusion-limited, second-order Langmuir isotherm, similar to that used to describe the kinetics of formation for shorter-chained n-alkanethiols.[7] The greater adsorption time required for the long-chained adsorbate is probably a function of the slow ordering of the longer hydrocarbon chains and their ability to limit the transport of further adsorbates to the gold surface. Peterlinz and Georgiadis[7] observed that SAMs formed from longer-chained n-alkanethiols formed at slower rates than shorter-chained thiols in the first kinetic regime.

During the formation of SAMs, their average structural properties change continuously until either an equilibrium state or a "complete" monolayer film is achieved. The structural properties of films formed from $C_{18}OC_{19}SH$ were characterized at various times during film formation by reflectance infrared spectroscopy (ex situ). Figure 5.1 schematically illustrates the orientation of the dynamic dipole moments for a trans-zig-zag extended adsorbate that is tilted from the surface normal by an angle of α and twisted around its molecular axis by an angle of β. The strengths of the bands corresponding to these dipoles are influenced by their orientation relative to the surface normal. Assuming that all chains are identical (single-chain model), Sinniah et al.[6] developed equations to relate the average cant (α) and twist (β) of ether-containing adsorbates within a SAM to its infrared intensities:

$$\tan \alpha = \frac{1}{\sin \beta} \left[\frac{I_{v_a(CH_2)}}{I_{v_a(ROR)}} \frac{I^{iso}_{v_a(ROR)}}{I^{iso}_{v_a(CH_2)}} \right]^{1/2} \tag{5.3}$$

76

$$\cot \beta = \left[\frac{I_{v_s(CH_2)}}{I_{v_a(CH_2)}} \frac{I^{iso}_{v_a(CH_2)}}{I^{iso}_{v_s(CH_2)}} \right]^{1/2} \tag{5.4}$$

where I^{SAM} and I^{iso} refer to the infrared intensities of the stretching modes for the SAM and for an isotropic sample of the adsorbate diluted with potassium bromide. While this single-chain model may not capture the structural complexities of the hydrocarbon chains in these SAMs, it still serves as a convenient guide to assess the relative packing densities of the adsorbates during formation. Based on the orientation of the dipoles, as the adsorbates within the film tilt less from the surface normal, the $v(CH_2)$ modes should decrease in intensity while the $v(ROR)$ mode should increase. A decreased tilt signifies the presence of more molecules on the surface and a more densely packed film. Figure 5.3 shows IR spectra of the C-H and R-O-R stretching regions for gold substrates after various exposures to 0.5 mM $C_{18}OC_{19}SH$ in 2-butanol. As adsorption time increases, the asymmetric methylene intensity decreases while the ether stretching intensity increases (Figure 5.3). These changes are consistent with the formation of a more densely packed film with smaller cant as the adsorption proceeds. Over the 100 h adsorption, the peak position for $v_a(CH_2)$ decreases from 2921 (at 2 s) to 2918 cm^{-1} while that for $v_a(ROR)$ increases from 1124 (at 2 s) to 1131 cm^{-1}. Both these shifts are consistent with a transition from a liquid-like to a crystalline state as the SAM becomes more densely packed. [6,11]

Figures 5.4a, b, and c display the temporal evolution in intensity for $v_a(CH_2)$, $v_s(ROR)$, and cant, respectively, for SAMs derived from $C_{18}OC_{19}SH$ (0.5 mM in isooctane or 2-butanol) on gold. At early times (< 1 min), the intensities of the $v_a(CH_2)$ modes(Figure 5.4a) for SAMs of $C_{18}OC_{19}SH$ adsorbed from 2-butanol are smaller than those at identical times for SAMs formed in isooctane while $v_s(ROR)$ intensities (Figure 5.4b) are larger than those for SAMs in isooctane. These intensities can be used to estimate the average cant of the adsorbates (eq 5.3) after various exposures to the thiol solutions (Figure 5.4c); in 2-butanol, the average cant is 8 -12° lower than that formed in isooctane during the first minute. These results are qualitatively consistent with the ellipsometric data (Figure 5.2) and indicate that a more densely packed film is formed from 2-butanol than from isooctane during the first few seconds. As the adsorption proceeds, the infrared intensities for the SAM formed from isooctane approach those from 2-butanol but do not achieve a state consistent with as densely packed a film on the timescale of 100 h. Upon 100 h of adsorption, the average cants are 31° and 35° as formed in 2-butanol and isooctane, respectively. While these values appear relatively similar, it is important to note that the film formed in 2-butanol has a thickness that is measurably (~3 Å) greater after the 100-h adsorption. A striking feature of Figure 5.4c is that significantly longer times—at least a factor of 30—are required to achieve the same cant (and therefore packing density) in isooctane as produced from 2-butanol.

Figure 5.3. Grazing incidence polarized infrared spectra of the C-H and R-O-R stretching regions for SAMs formed on gold by immersion into 0.5 mM $C_{18}OC_{19}SH$ in 2-butanol for various times. The horizontal lines to the right of the methylene and ether peaks denote the peak intensities for a film exposed to solution for 6,000 min (100 h). The vertical dashed lines represent the positions of the primary methylene and ether stretching modes for a trans-extended monolayer with no gauche defects: $v_a(CH_2)$ = 2918 cm^{-1}, $v_s(CH_2)$ = 2851 cm^{-1}, and $v_a(ROR)$ = 1132 cm^{-1}. The spectra have been offset vertically for clarity.
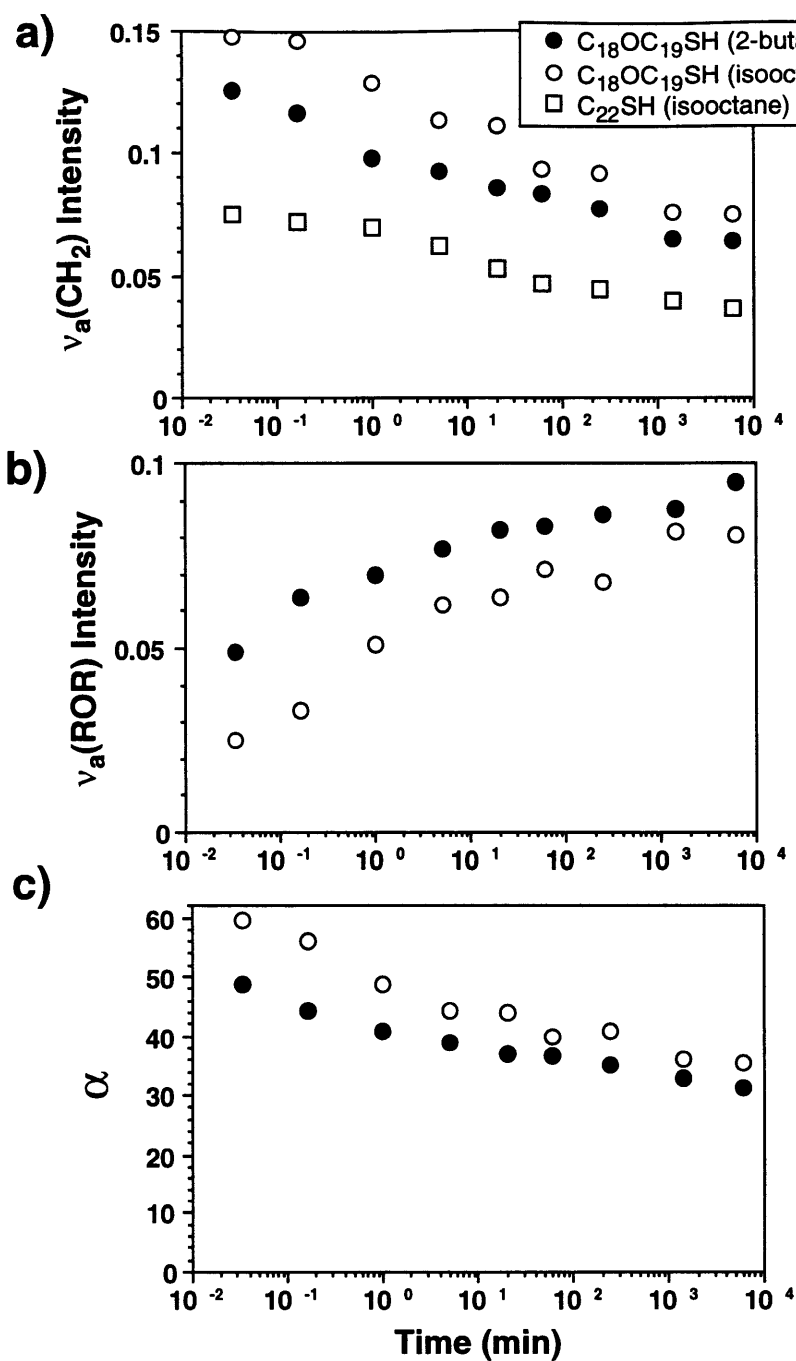
Figure 5.4. Time-dependence of the a) $\nu_a(CH_2)$ and b) $\nu_a(ROR)$ infrared intensities after various exposures of gold substrates to 0.5 mM solutions of $C_{22}SH$ in isooctane (Figure 5.4a only) or $C_{18}OC_{19}SH$ in either isooctane or 2-butanol. From these intensities, c) the average cant of the $C_{18}OC_{19}SH$ adsorbates were determined from eq 5.3 as a function of adsorption time in the isooctane or 2-butanol solutions.

The time-dependent variation in $v_a(CH_2)$ exhibited during the assembly of $C_{18}OC_{19}SH$ in isooctane is similar to that observed for $C_{22}SH$ (Figures 5.4a). The more gradual decrease in $v_a(CH_2)$ exhibited by the $C_{22}SH$ SAM may reflect the initial formation of a more complete film that required less structural change to produce the complete SAM. From the ellipsometric data in Figure 5.2, 70% of the $C_{22}SH$-SAM is formed in the first 2 s of adsorption while only 50% of the $C_{18}OC_{19}SH$-SAM is formed during the same time period.

5.2.3. SAMs Derived from $C_{18}OC_{19}SH$ on Copper

The conditions required for formation of SAMs from long-chained adsorbates such as the ω-alkoxy-n-alkanethiols have not been studied in great detail. Traditionally, SAMs have been formed at or near room temperature, but the formation of a densely packed SAM from these long-chained adsorbates may not be possible at such low temperatures. Hautman and Klein note that the rotational and conformational freedom of the chains increases at higher temperatures.[12] Therefore, formation of SAMs at higher temperatures may provide increased chain mobility needed to accommodate additional adsorbates within the SAM. To address these issues, RAIRS was used to characterize the structure of films formed at room temperature and at elevated temperatures. Figure 5.5 shows the C-H stretching region for films formed on gold and copper after 1-h immersion in 1 mM $C_{18}OC_{19}SH$ in isooctane at both 22 and 55 °C. The asymmetric and symmetric methylene peaks of each spectra are centered at 2918 and 2851 cm^{-1}, respectively, indicating a crystalline packing of the hydrocarbon chains. While the spectra for SAMs on gold are nearly identical at the different temperatures, those on copper suggest major structural differences between the two hydrocarbon films. The spectrum for the film formed at 55 °C on copper has reduced methylene intensities and an increased ether intensity compared to the spectrum for the film formed at 22 °C. Differences in these intensities correspond to different canted structures for the adsorbates within the SAM and indicate that the SAM formed at 55 °C is more densely packed and the adsorbates are less canted than for the SAMs formed at the lower temperature. Based on a single-chain model (eq 5.3), the average cant achieved at 55 °C is 17° while that at 22 °C is 32°. These cants suggest that the film formed on copper at higher temperature has 12% greater adsorbate density. This difference is likely a result of the increased conformational freedom of the long chains at the higher temperature; chains with increased energy can more effectively accommodate additional adsorbates into the partial film, thus forming a more complete, densely packed assembly. For shorter-chained adsorbates on copper (p + m ≤ 33), the structures of the resulting films were observed to be less dependent on adsorption temperature, and these SAMs were formed at room temperature. The insensitivity to temperature exhibited by the assembly of $C_{18}OC_{19}SH$ on gold could be a result of
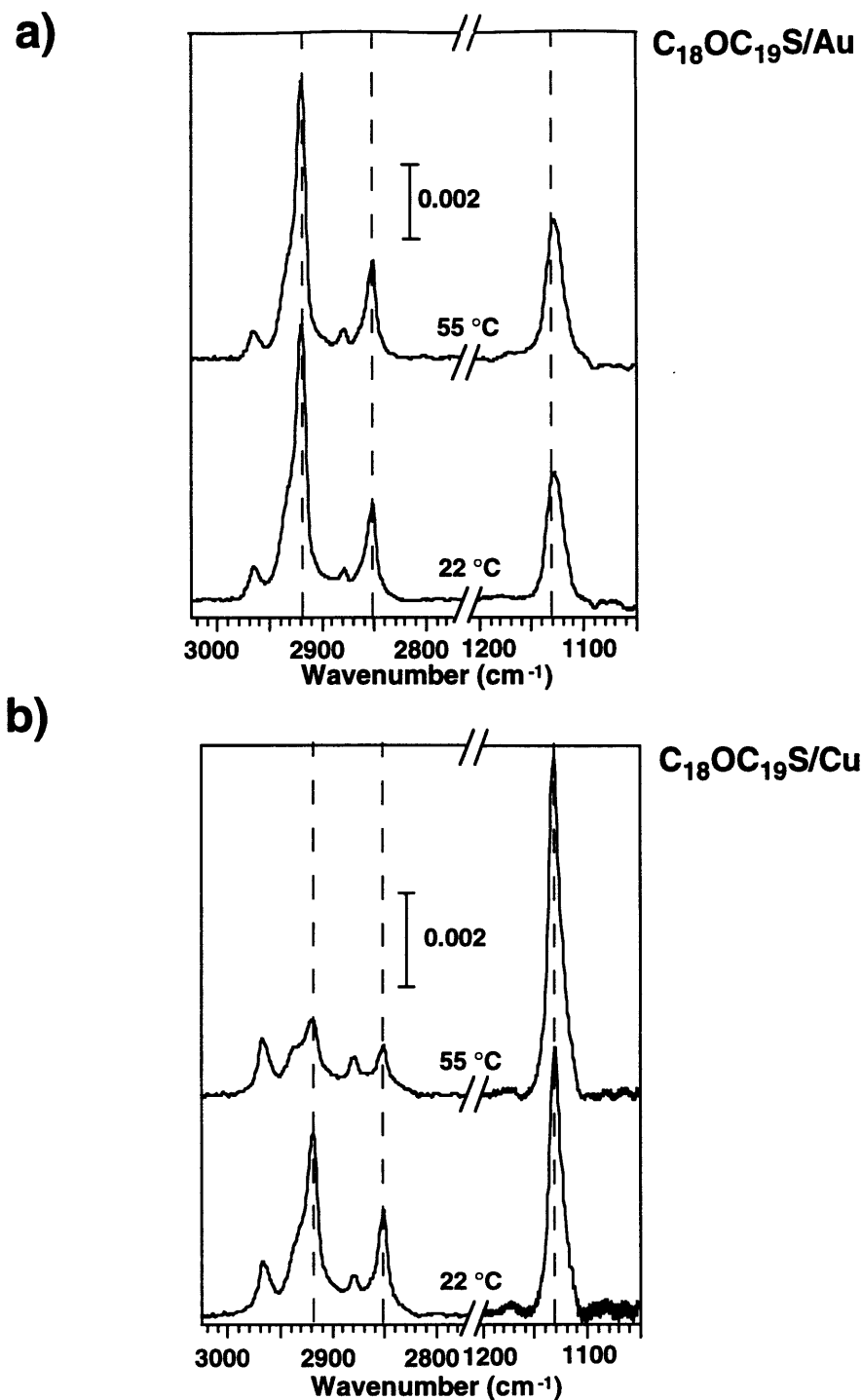
Figure 5.5. Grazing incidence polarized infrared spectra of the C-H and R-O-R stretching regions for SAMs formed from 0.5 mM $C_{18}OC_{19}SH$ in isooctane on (a) gold or (b) copper after 1-h adsorptions at either 22 or 55 °C. The dashed lines represent the positions of the primary methylene and ether stretching modes for a trans-extended monolayer with no gauche defects: $v_a(CH_2) = 2918$ cm^{-1}, $v_s(CH_2) = 2851$ cm^{-1}, and $v_a(ROR) = 1132$ cm^{-1}. The spectra have been offset vertically for clarity.

the tendency for thiols to form less densely packed films on gold than copper, perhaps due to the presence of fewer energetically favorable surface sites on gold.[13]

For SAMs formed from $C_{18}OC_{19}SH$ at 55 °C, the formation of a complete film is significantly faster on copper than on gold. IR spectra of SAMs from $C_{18}OC_{19}SH$ on copper reveal no change in cant or twist for films adsorbed from 2 min to 4 h. In contrast, spectra for $C_{18}OC_{19}SH$ on gold at 55 °C show constant changes in both $v_a(CH_2)$ and $v_s(ROR)$ intensities with time, similar to the spectra formed at 22 °C (Figure 5.3). Longer adsorption times (> 4 h) on copper resulted in films with dramatically increased $v_a(CH_2)$ and $v_s(ROR)$ intensities that indicate multilayer formation.[14]

The ability to tailor the packing density of ω-alkoxy-n-alkanethiolates on copper by adjusting the temperature of adsorption provides a convenient means of investigating the effect of adsorbate packing density on the barrier properties of the resulting SAM. Figure 5.6 shows electrochemical impedance spectra in the form of Nyquist plots—a relationship between the imaginary and real impedance—for SAMs formed from $C_{18}OC_{19}SH$ (0.5 mM, isooctane) on copper at 22 and 55 °C. These data take the form of partial semi-circles and can be modeled as a parallel combination of coating capacitance and resistance in series with a solution resistance, as shown in Figure 4.1. For this equivalent circuit, the diameter of the (partial) semi-circle corresponds to the resistance provided by the coating. The coating resistances are 2.1×10^7 and 2.4×10^8 $\Omega \cdot cm^2$ for films formed at 22 and 55 °C, respectively. The capacitance of the film formed at 55 °C is 18% lower than that formed at 22 °C, further indicating that an effectively thicker film is formed on copper at the higher temperature. Together with the IR spectra, these results (Figures 5.5 and 5.6) reveal that adsorption of long-chain thiols onto copper at 55 °C enables formation of a more densely packed film that provides a greater barrier against the diffusion of aqueous ions than is possible from adsorption at 22 °C.

5.2.4. Effect of Chain Length on the Properties of ω-Alkoxy-n-Alkanethiolates on Gold and Copper

Using the synthetic strategy of Williamson, a series of ω-alkoxy-n-alkanethiol adsorbates—$C_{18}OC_{11}SH$, $C_{22}OC_{11}SH$, $C_{18}OC_{19}SH$, $C_{22}OC_{19}SH$, and $C_{22}OC_{22}SH$—were synthesized to investigate the effect of adsorbate chain length on the structural and barrier properties of the resulting SAMs. Evaluation of film thickness with this series of adsorbates allows determination of the completeness of the films as the chain length is incrementally increased. Ellipsometry offers a simple, nondestructive method to determine film thickness and requires characterization of the substrate before and after film formation. Figure 5.7 shows the ellipsometric thickness for SAMs of C_nSH (0.5 mM, isooctane) and C_pOC_mSH (0.5 mM, 2-butanol or isooctane) on gold. For
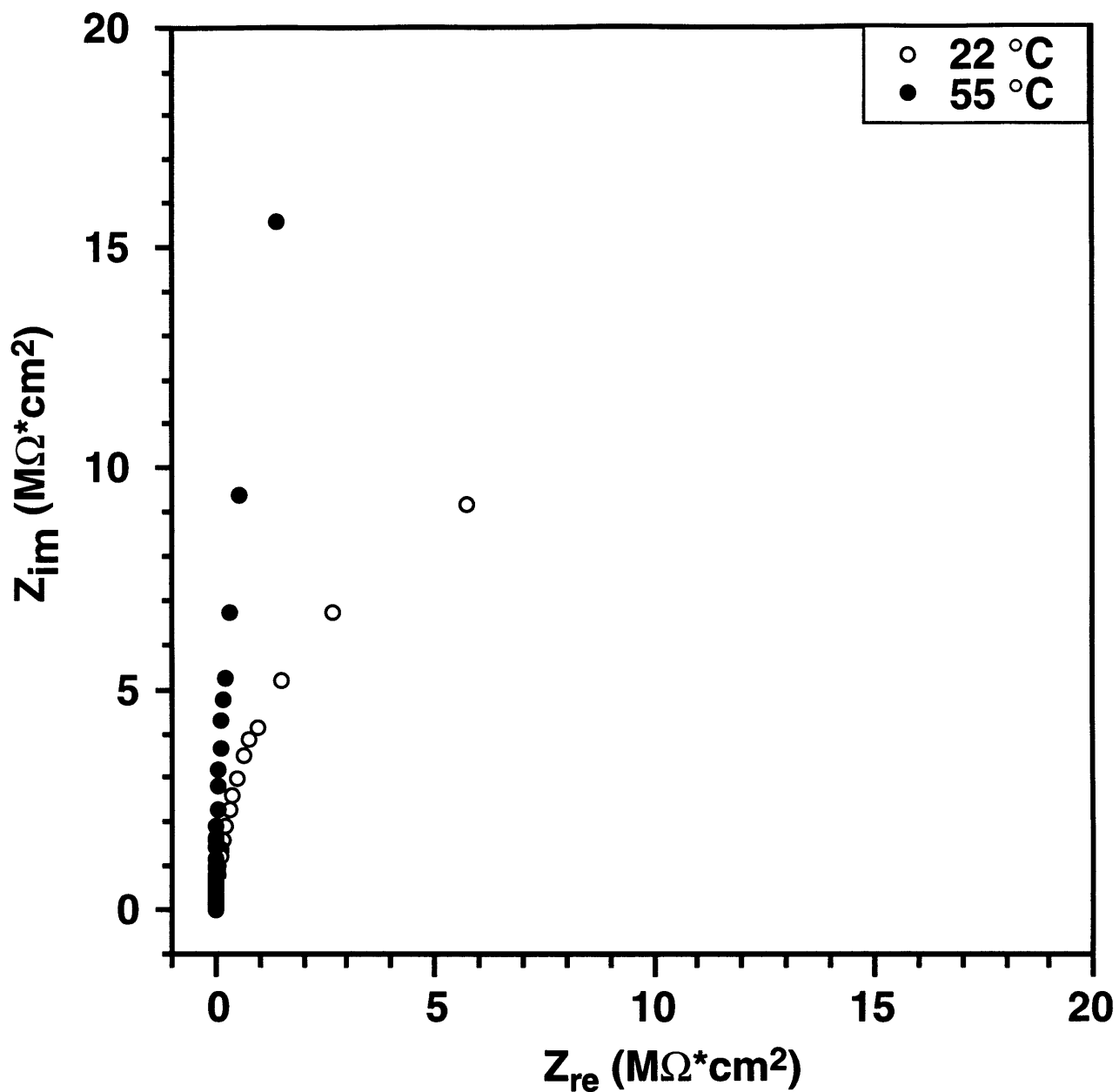
Figure 5.6. Nyquist plots for SAM-coated copper in oxygenated 50 mM Na_2SO_4(aq). The SAMs were formed by immersion of freshly evaporated copper in $C_{18}OC_{19}SH$ (0.5 mM, isooctane) for 1 h at either 22 °C or 55 °C.
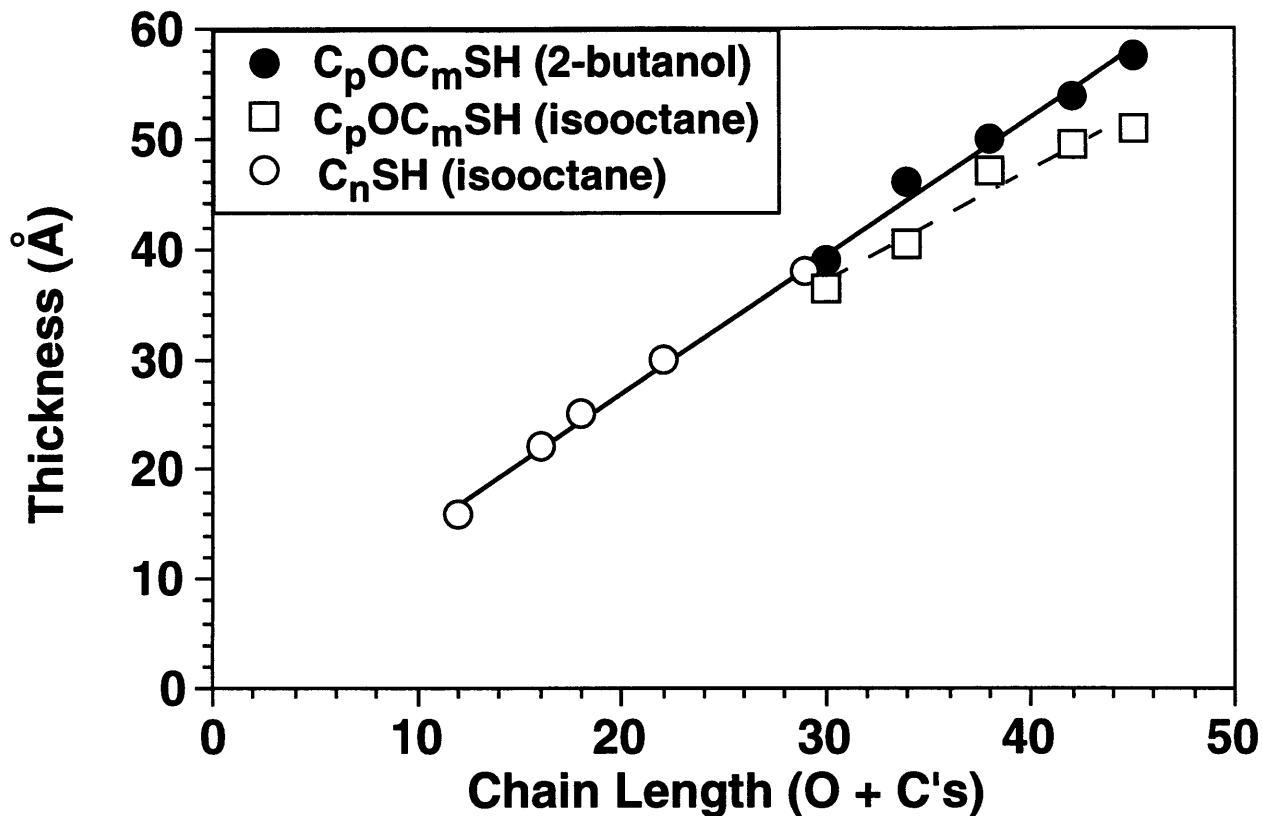
Figure 5.7. Ellipsometric thickness of SAMs of n-alkanethiols (C_nSH) and ω-alkoxy-n-alkanethiols (C_pOC_mSH) adsorbed onto gold from 0.5 mM solutions of the thiol in isooctane or 2-butanol. The solid line is a least-squares fit to the data for C_nSH (isooctane) and C_pOC_mSH (2-butanol) and has a slope of 1.3 Å per incremental unit. The dashed line is a least-squares fit to the data for C_pOC_mSH (isooctane) and has as slope of 1.0 Å per incremental unit.

ω-alkoxy-n-alkanethiols on gold formed from isooctane, the thickness data deviate from linearity for chain lengths (m+p) ≥ 37. This deviation reflects the difficulty in forming complete monolayers from the longest-chained adsorbates in isooctane due to the reduced ability to accommodate additional adsorbates into the partial film. When the ω-alkoxy-n-alkanethiolates are formed from 2-butanol, the film thicknesses are enhanced and increase linearly with chain length. These results are consistent with the kinetics data in Figure 5.2 and indicate that SAMs formed from ω-alkoxy-n-alkanethiols in 2-butanol are more complete than those formed in isooctane.

While ellipsometry is convenient for quantifying film thickness on substrates such as gold that do not change rapidly upon exposure to ambient conditions, it is less useful in characterizing SAM thickness on copper due to the tendency of bare copper to oxidize when exposed to air. Unlike ellipsometry, characterization by XPS is only required after SAM formation and thus, provides a more suitable method for estimating SAM thickness on copper. XPS allows qualitative assessment of SAM thickness (d_{SAM}) by measuring the attenuation of photoelectrons from an underlying substrate according to the following equation:

$$I = I_o \exp\left(\frac{-d_{SAM}}{\lambda \sin \phi}\right)$$
(5.5)

where I is the measured photoelectron intensity of the underlying metal substrate, I_o is the intensity of an infinitely thick substrate with no attenuating overlayer, λ is the attenuation length for substrate photoelectrons through the SAM, and ϕ is the angle of the detector with respect to the surface parallel. Figure 5.8 shows the attenuation of the $Cu(2p_{3/2})$ and $Au(4f_{7/2})$ signal in XPS for SAMs formed from C_nSH and C_pOC_mSH on copper and gold. SAMs on gold were formed from 2-butanol (0.5 mM) while those on copper were formed from isooctane (0.5 mM) at 22 (p + m ≤ 33) or at 55 °C (p + m ≥ 33). As the chain length of the adsorbate is increased, thicker SAMs are formed that attenuate the underlying metal substrate more. The slopes of the least-squares fits correspond to attenuation lengths (λ) of 23 and 45 Å for $Cu(2p_{3/2})$ and $Au(4f_{7/2})$ photoelectrons, respectively, for incident Al Kα x-rays at 1486 eV. These values are similar to attenuation lengths determined using a series of unsubstituted n-alkanethiols on gold and copper[15] and suggest that the SAMs formed from these long-chain ω-alkoxy-n-alkanethiols are of the expected thickness for a trans-extended configuration of the molecule on either substrate.

Figure 5.9 shows IR spectra of the C-H and R-O-R stretching regions for the SAMs formed from ω-alkoxy-n-alkanethiols on gold and copper by the conditions noted above. In comparison with the ω-alkoxy-n-alkanethiolates on copper, the SAMs on gold exhibit more intense methylene stretching peaks and less intense ether stretching peaks. These features of the spectra indicate that the hydrocarbon chains within the SAMs on gold have a greater average cant than

85
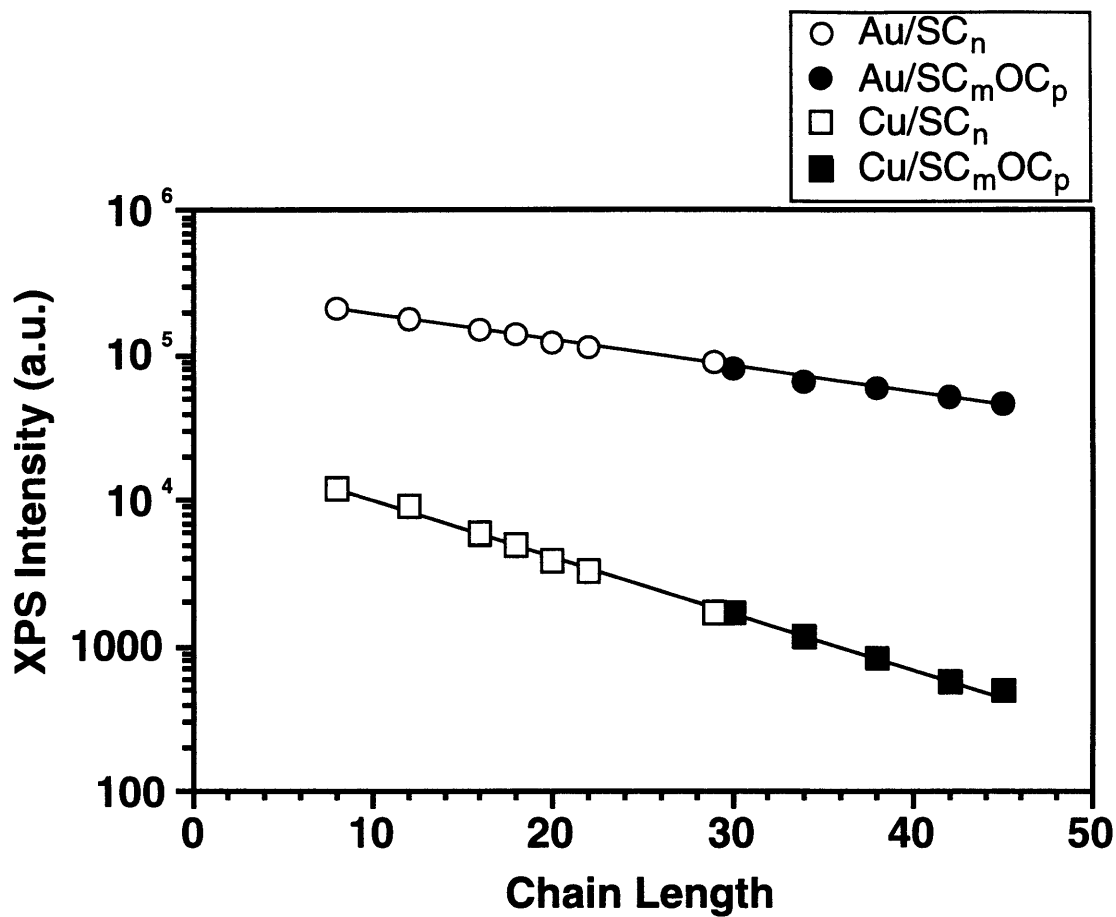
Figure 5.8. Attenuation of the $Cu(2p_{3/2})$ and $Au(4f_{7/2})$ XPS signals with SAMs formed from C_nSH and C_pOC_mSH on copper and gold. The lines represent least-squares fits to the data and correspond to attenuation lengths of 23 and 45 Å for SAMs on copper and gold, respectively.
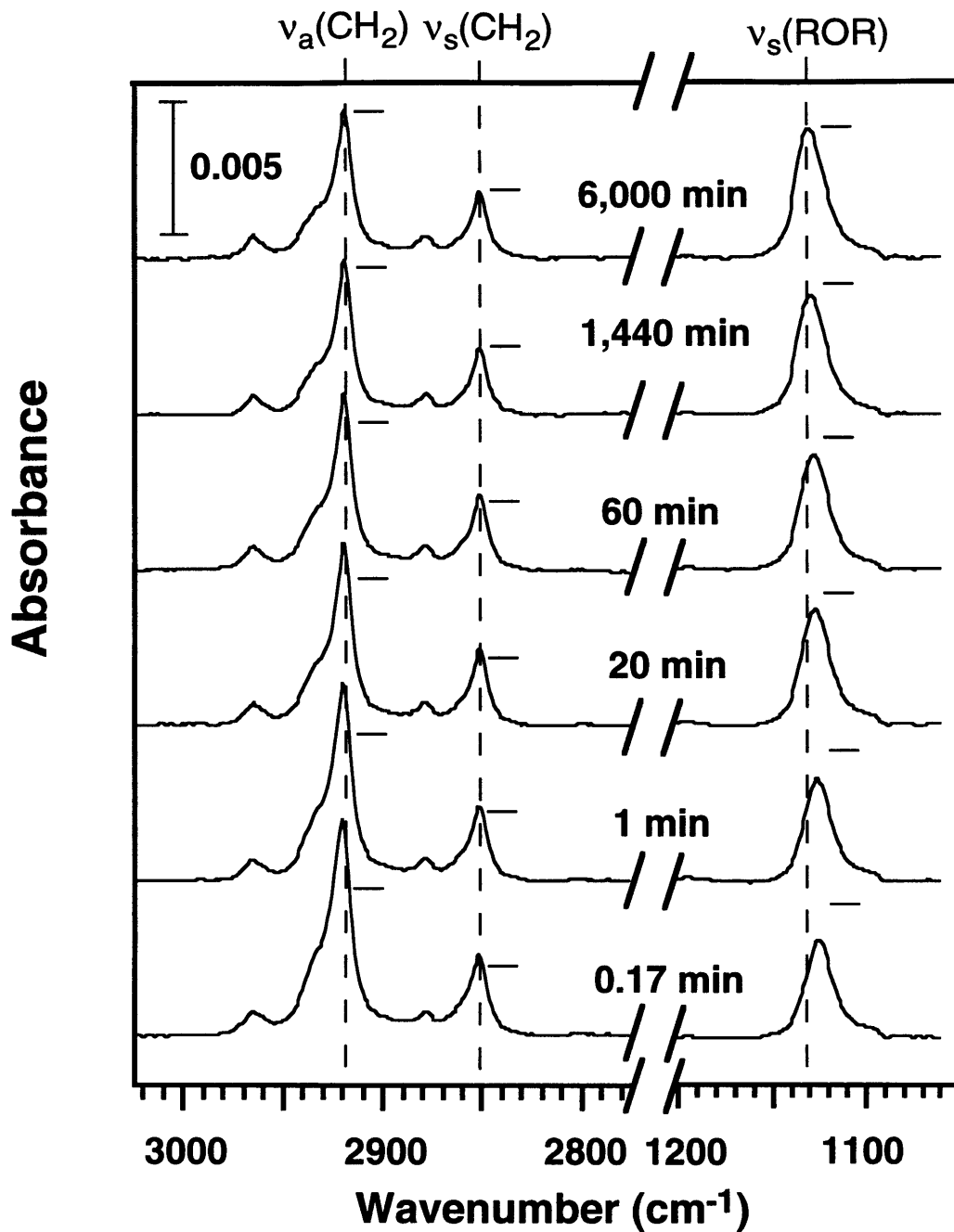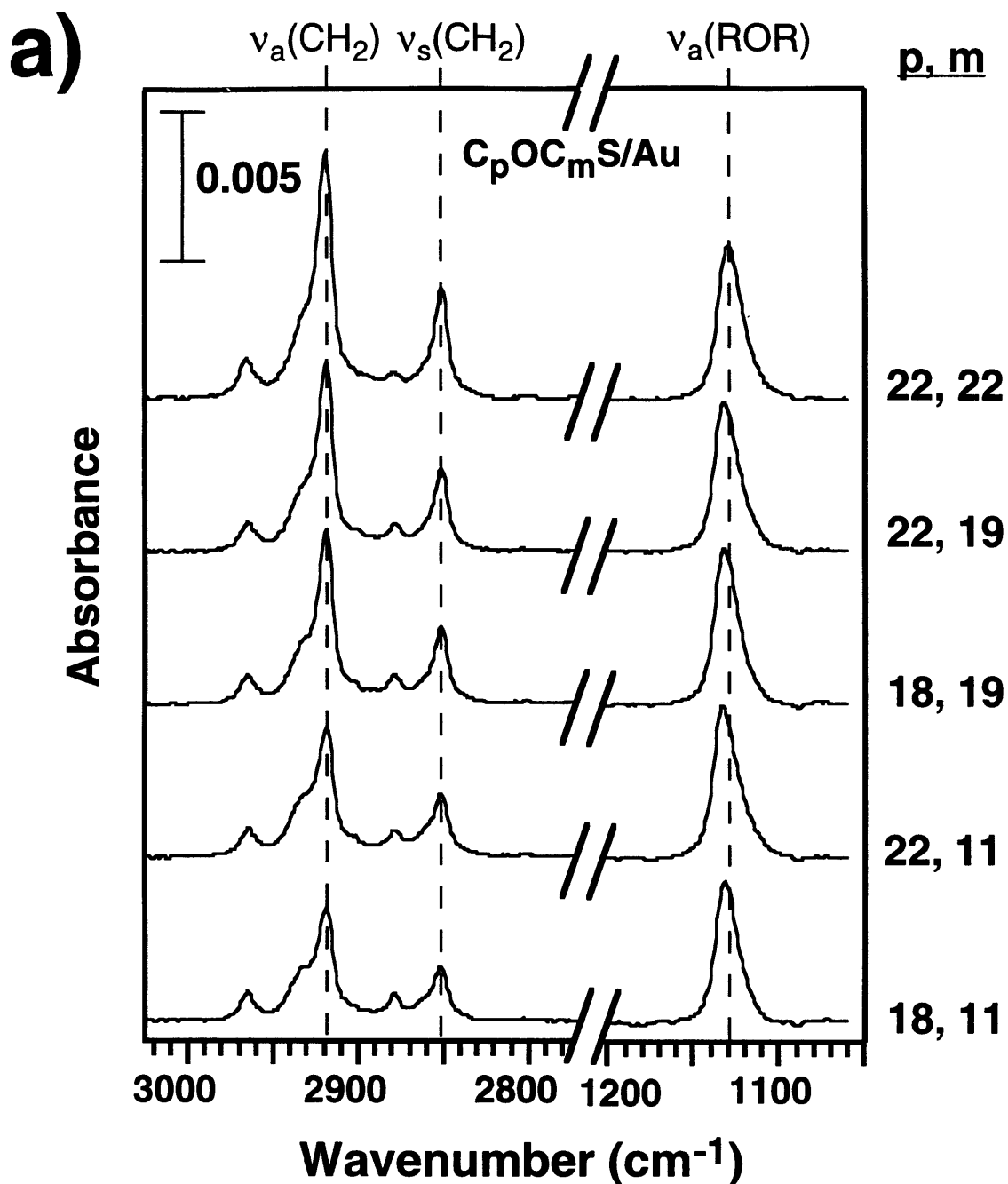
Figure 5.9. (a) Grazing incidence polarized infrared spectra of the C-H and R-O-R stretching regions for SAMs formed from C_pOC_mSH on gold. The dashed lines represent the positions of the primary methylene and ether stretching modes for a trans-extended monolayer with no gauche defects: $v_a(CH_2) = 2918$ cm^{-1}, $v_s(CH_2) = 2851$ cm^{-1}, and $v_a(ROR) = 1132$ cm^{-1}. The spectra have been offset vertically for clarity. The positions of the primary modes and the average cants and twists of the adsorbates are summarized in Table 5.2.
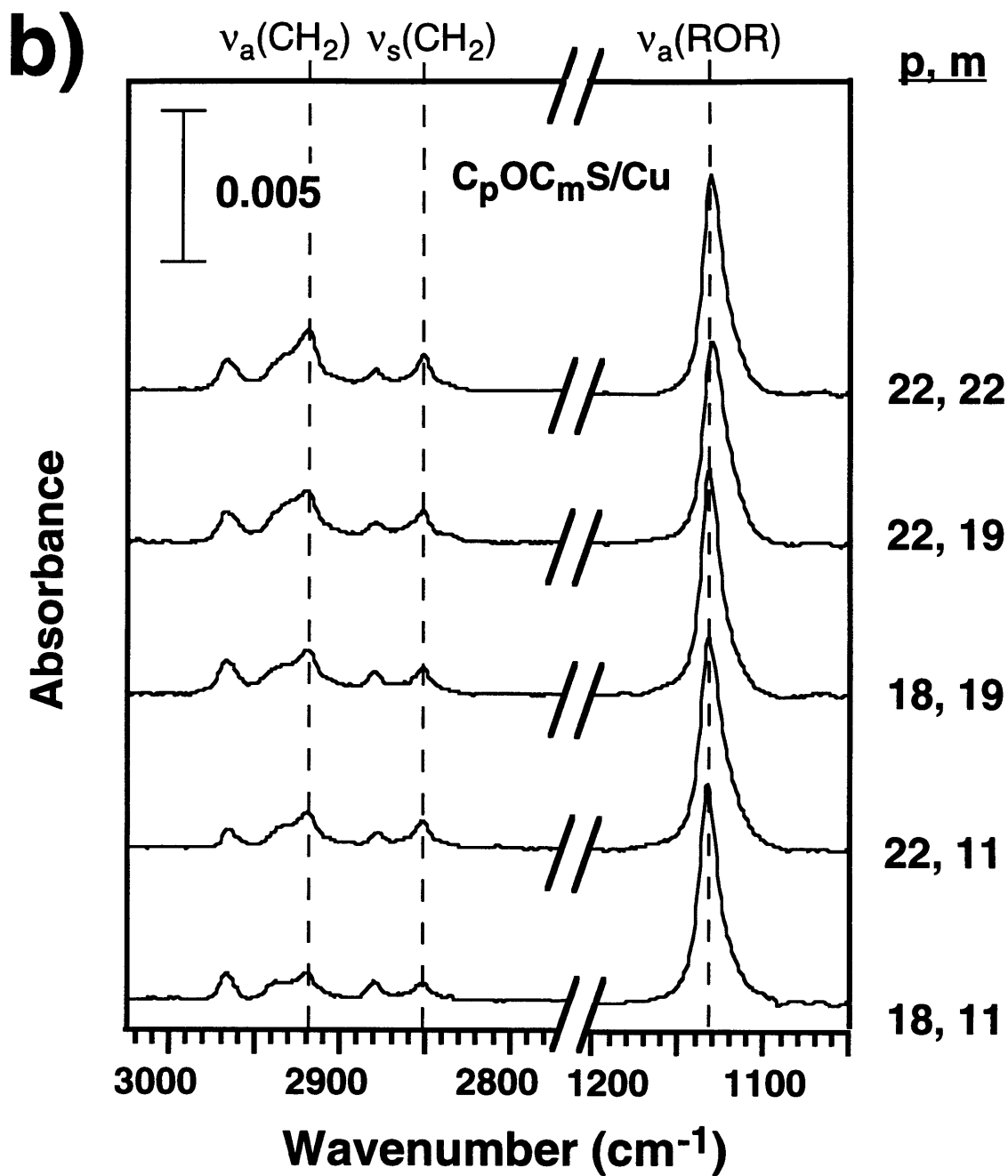
Figure 5.9. (b) Grazing incidence polarized infrared spectra of the C-H and R-O-R stretching regions for SAMs formed from C_pOC_mSH on copper. The dashed lines represent the positions of the primary methylene and ether stretching modes for a trans-extended monolayer with no gauche defects: $v_a(CH_2) = 2918$ cm^{-1}, $v_s(CH_2) = 2851$ cm^{-1}, and $v_a(ROR) = 1132$ cm^{-1}. The spectra have been offset vertically for clarity. The positions of the primary modes and the average cants and twists of the adsorbates are summarized in Table 5.2.

those on copper. The peak positions of the $v(CH_2)$, $v(CH_3)$, and $v(ROR)$ modes and the average cant and twist angles (calculated from eqs. 5.3 and 5.4, respectively) for these SAMs on gold and copper are shown in Table 5.2. On copper, the average calculated cants of the adsorbates are ~16° for all the SAMs, suggesting that the density of adsorbates within these different films is constant. This agrees well with values of ~13° reported for shorter-chained, unsubstituted n-alkanethiols on copper.[16] The average cants for the SAMs on gold show more variability, but they are all approximately ~30°, which again compares well with the value of ~27° reported for unsubstituted n-alkanethiols on gold.[16] These results are compatible with the thickness and XPS attenuation data in Figures 5.7 and 5.8, respectively, that suggest a linear relationship between the chain length of the adsorbate and film thickness for SAMs on both copper and gold. For ω-alkoxy-n-alkanethiolates on gold formed in 0.5 mM isooctane, increasing the chain length of the adsorbate resulted in decreasing ether intensities (not shown), suggesting that the adsorbates with longer chains yielded incomplete films with less dense packing.

Table 5.2. Positions of the primary modes in IR spectra of Figure 5.9 and the average cant (α) and twist (β) of the adsorbates.

Adsorbate/substrate	Peak Positions (cm⁻¹)						
	$v_a(CH_2)$	$v_s(CH_2)$	$v_a(ROR)$	$v_a(CH_3)$	$v_s(CH_3)$	α	β
$C_{18}OC_{11}S/Au$	2919	2852	1132	2965	2878	33	51
$C_{22}OC_{11}S/Au$	2918	2851	1133	2965	2878	28	52
$C_{18}OC_{19}S/Au$	2918	2851	1132	2965	2878	32	53
$C_{22}OC_{19}S/Au$	2918	2851	1131	2965	2878	27	51
$C_{22}OC_{22}S/Au$	2919	2851	1130	2966	2879	31	53
$C_{18}OC_{11}S/Cu$	2919	2851	1133	2965	2878	16	46
$C_{22}OC_{11}S/Cu$	2919	2851	1132	2965	2878	16	50
$C_{18}OC_{19}S/Cu$	2919	2851	1132	2966	2879	17	51
$C_{22}OC_{19}S/Cu$	2919	2851	1131	2966	2879	17	47
$C_{22}OC_{22}S/Cu$	2919	2851	1131	2966	2879	16	51

5.3. Conclusions

Self-assembled monolayers (SAMs) derived from ω-alkoxy-n-alkanethiols form oriented, crystalline films on gold and copper with thicknesses ranging from ~40 - 60 Å. On gold, the formation of these SAMs can be described by second-order, diffusion-limited Langmuir adsorption kinetics that are dependent on the solvent. These SAMs form more rapidly in a weaker hydrocarbon solvent (2-butanol) than in a stronger one (isooctane) due to the greater ease of the hydrocarbon chains to dispel the poorer solvent during film formation. The hydrocarbon chains in the SAM on gold are tilted at an average of ~30° from the surface normal while those on copper are canted ~16°. On copper, adsorption of these SAMs at higher temperatures (~55 °C) enables the

formation of a more densely packed hydrocarbon film that provides greater resistance against the permeation of aqueous electrolyte than is possible by adsorption at room temperature. The greater adsorption temperature likely provides increased mobility to the long chains of the adsorbed thiols, enabling the accommodation of additional adsorbates.

5.4. Experimental

5.4.1. Materials and Synthesis

Copper (99.99+ %) and gold (99.99+ %) shot and chromium-plated tungsten rods were obtained from Aldrich, Americana Precious Metals, and R.D. Mathis, respectively. Silicon (100) wafers (Silicon Sense) were rinsed with ethanol (Pharmco) and dried in a stream of N_2 (BOC) prior to use in the evaporator. The solvents, isooctane (J.T. Baker), 2-butanol (Aldrich), anhydrous tetrahydrofuran (Aldrich), hexanes (EM Science), ethyl acetate (EM Science), chloroform (Mallinckrodt), methanol (Mallinckrodt), and hexadecane (Aldrich) were used as received. Octyl, dodecyl, and octadecyl thiols were obtained from Aldrich and purified by distillation before use. The syntheses of docosyl and hexadecyl thiols were reported in Chapter 3.[17] 19-Bromo-1-nonadecene[8] and 19-octadecyloxy-1-nonadecanethiol[8] were available from previous studies, and eicosyl thiol[2] and 21-docosen-1-ol[18] were synthesized via literature procedures. NaH, octadecanol, 1-bromodocosane, docosanol, and thiolacetic acid were obtained from Aldrich and used as received. Undecylenic bromide and AIBN were obtained from Pfaltz and Bauer and were used as received. Na_2SO_4 and concentrated hydrochloric acid were obtained from Mallinckrodt and were used as received. Column chromatography was performed over silica gel (230-400 mesh ASTM, EM Science) using either an eluant of constant composition or a gradient of increasing polarity.

Synthesis of 11-octadecyloxy-1-undecanethiol [$CH_3(CH_2)_{17}O(CH_2)_{11}SH$]
11-Octadecyloxy-1-undecene. NaH (0.373 g, 15.6 mmol) was washed with 20 mL of hexanes and added to a solution containing octadecanol (4.0 g, 14.8 mmol) in anhydrous THF (150 mL). After addition of undecylenic bromide (3.80 g, 16.3 mmol), the reaction mixture was stirred for 50 h at 40 °C. After addition of water and hexanes to form a two-phase mixture, the layers were separated, and the aqueous fraction was extracted thrice with hexanes. The organic extracts were concentrated under reduced pressure. Column chromatography (hexanes to 2% ethyl acetate/hexanes) yielded the title compound (1.048 g, 2.48 mmol, 17% yield). ^1H NMR, δ 5.80 (m, 1 H), 4.96 (d, 1 H), 4.91 (m, 1 H), 3.37 (t, 4 H), 2.02 (quart, 2 H), 1.45 - 1.65 (m, 4 H), 1.2 - 1.4 (m, 42 H), 0.86 (t, 3 H).

11-Octadecyloxy-1-undecanethioacetate. A mixture of 11-octadecyloxy-1-undecene (1.048 g, 2.48 mmol), thiolacetic acid (0.754 g, 9.92 mmol), and AIBN (10 mg) in THF were photolyzed for 2 h with a medium-pressure Hg lamp. After addition of saturated NaCl(aq) and hexanes to form a two-phase mixture, the layers were separated, and the aqueous fraction was extracted thrice with hexanes. The organic fractions were combined and concentrated under reduced pressure. Column chromatography (1% to 4% ethyl acetate/hexanes) yielded the title compound (1.178 g, 2.37 mmol, 95% yield). ^{1}H NMR, δ 3.37 (t, 4 H), 2.85 (quart, 2 H), 2.30 (m, 3 H), 1.45 - 1.65 (m, 6 H), 1.2 - 1.4 (m, 44 H), 0.86 (t, 3 H).

11-Octadecyloxy-1-undecanethiol. Concentrated hydrochloric acid (0.863 g, 23.7 mmol) was added to a refluxing mixture of 11-octadecyloxy-1-undecanethioacetate (1.178 g, 2.37 mmol) in deoxygenated ethanol (25 mL), and the reaction proceeded overnight. After addition of water and hexanes to form a two phase mixture, the layers were separated. The aqueous fraction was extracted twice with hexanes, and the organic portions were combined and concentrated under reduced pressure. Column chromatography (1% ethyl acetate/hexanes) yielded the title compound (0.261 g, 0.572 mmol, 24.1% yield). ^{1}H NMR, δ 3.37 (t, 4 H), 2.54 (quart, 2 H), 1.45 - 1.65 (m, 7 H), 1.2 - 1.4 (m, 44 H), 0.86 (t, 3 H).

Synthesis of 11-docosyloxy-1-undecanethiol [$CH_3(CH_2)_{21}O(CH_2)_{11}SH$]

11-Docosyloxy-1-undecene. NaH (0.75 g, 31.2 mmol) was washed with 20 mL of hexanes and added to a solution of 10-undecene-1-ol (3.00 g, 17.6 mmol) in anhydrous THF (80 mL). After addition of 1-bromodocosane (7.00 g, 18.0 mmol), the mixture was stirred at 40 °C for 72 h. After addition of water and hexanes to form a two-phase mixture, the layers were separated, and the aqueous fraction was extracted twice with hexanes. The organic extracts were collected and concentrated under reduced pressure. Column chromatography (hexanes to 7% ethyl acetate/hexanes) yielded the title compound (1.953 g, 4.086 mmol, 23% yield). ^{1}H NMR, δ 5.80 (m, 1 H), 4.96 (d, 1 H), 4.91 (m, 1 H), 3.37 (t, 4 H), 2.02 (quart, 2 H), 1.45 - 1.65 (m, 4 H), 1.2 - 1.4 (m, 50 H), 0.86 (t, 3 H).

11-Docosyloxy-1-undecanethioacetate. Thiolacetic acid (1.180 g, 15.5 mmol) was added to a solution of 11-docosyloxy-1-undecene (1.953 g, 4.086 mmol) and AIBN (70 mg) in toluene (50 mL), and the resulting mixture was refluxed for 16 h. After addition of water to form a two-phase mixture, the layers were separated. The aqueous fraction was extracted twice with hexanes, and the organic extracts were combined and concentrated under reduced pressure. Column chromatography (hexanes to 2% ethyl acetate/hexanes) yielded the title compound (1.422 g, 2.567 mmol, 63% yield). ^{1}H NMR, δ 3.37 (t, 4 H), 2.85 (quart, 2 H), 2.30 (m, 3 H), 1.45 - 1.65 (m, 6 H), 1.2 - 1.4 (m, 52 H), 0.86 (t, 3 H).

<u>11-Docosyloxy-1-undecanethiol</u>. Concentrated hydrochloric acid (0.843 g, 23.1 mmol) was added to a solution of 11-docosyloxy-1-undecanethioacetate (1.422 g, 2.567 mmol) in deoxygenated ethanol, and the mixture was refluxed for 17 h. After the addition of water and hexanes to form a two-phase mixture, the layers were separated. The aqueous fraction was extracted twice with hexanes, and the organic extracts were combined and concentrated under reduced pressure. Column chromatography (hexanes to 2% ethyl acetate/hexanes) yielded the title compound (0.740 g, 1.445 mmol, 56% yield). ^{1}H NMR, δ 3.37 (t, 4 H), 2.54 (quart, 2 H), 1.45 - 1.65 (m, 7 H), 1.2 - 1.4 (m, 52 H), 0.86 (t, 3 H).

Synthesis of 19-docosyloxy-1-nonadecanethiol [$CH_3(CH_2)_{21}O(CH_2)_{19}SH$]

<u>19-Docosyloxy-1-nonadecene</u>. NaH (0.202 g, 8.4 mmol) was washed with hexanes and added to a solution containing docosanol (2.055 g, 6.3 mmol) in anhydrous THF (50 mL). 19-Bromo-1-nonadecene (1.45 g, 4.2 mmol) was then added, and the resulting mixture was heated to 40 °C for 72 h. After addition of water and hexanes to form a two-phase mixture, the layers were separated, and the aqueous fraction was extracted thrice with hexanes. The organic layers were collected and concentrated under reduced pressure. Column chromatography (hexanes followed by 5% ethyl acetate/hexanes) yielded the title compound (0.498 g, 0.844 mmol, 20% yield). ^{1}H NMR, δ 5.80 (m, 1 H), 4.96 (d, 1 H), 4.91 (m, 1 H), 3.37 (t, 4 H), 2.02 (quart, 2 H), 1.45 - 1.65 (m, 4 H), 1.2 - 1.4 (m, 66 H), 0.86 (t, 3 H).

<u>19-Docosyloxy-1-nonadecanethioacetate</u>. A solution of 19-docosyloxy-1-nonadecene (0.498 g, 0.84 mmol), thiolacetic acid (0.257 g, 3.3 mmol), AIBN (~50 mg), and toluene (20 mL) was photolyzed for 2 h. After addition of water to form a two-phase mixture, the layers were separated, and the aqueous fraction was extracted thrice with hexanes. The organic portions were collected and concentrated under reduced pressure. Column chromatography (hexanes to 2% ethyl acetate/hexanes) yielded the title compound (0.262 g, 0.39 mmol, 47% yield). ^{1}H NMR, δ 3.37 (t, 4 H), 2.85 (quart, 2 H), 2.30 (m, 3 H), 1.45 - 1.65 (m, 6 H), 1.2 - 1.4 (m, 68 H), 0.86 (t, 3 H).

<u>19-Docosyloxy-1-nonadecanethiol</u>. Hydrochloric acid (37%, 0.144 g, 3.9 mmol) was added to a solution of 19-docosyloxy-1-nonadecanethioacetate (0.262 g, 0.39 mmol) in absolute ethanol (15 mL), and the resulting solution was refluxed for 22 h. After addition of water and hexanes to form a two-phase system, the layers were separated, and the aqueous fraction was extracted with hexanes. The organic layers were collected and concentrated under reduced pressure. Column chromatography (hexanes to 3% ethyl acetate/hexanes) was used to purify the title compound (0.147 g, 0.236 mmol, 60% yield). ^{1}H NMR, δ 3.37 (t, 4 H), 2.53 (quart, 2 H), 1.45 - 1.65 (m, 7 H), 1.2 - 1.4 (m, 68 H), 0.86 (t, 3 H).

Synthesis of 22-docosyloxy-1-docosanethiol [CH$_3$(CH$_2$)$_{21}$O(CH$_2$)$_{22}$SH]

22-Docosyloxy-1-docosene. NaH (0.481 g, 20.1 mmol) was washed with 20 mL of hexanes, dissolved in 20 mL of anhydrous THF, and added to a solution of 21-docosen-1-ol (3.25 g, 10.0 mmol) in anhydrous THF (40 mL). A solution of 1-bromodocosane (4.292 g, 11.0 mmol) in anhydrous THF (40 mL) was added, and the resulting reaction mixture was heated at 40 °C for 45 h. After addition of saturated NH$_4$Cl (aq) and hexanes to form a two-phase mixture, the layers were separated. The aqueous fraction was extracted thrice with hexanes, and the organic extracts were combined and concentrated under reduced pressure. Column chromatography (hexanes to 1% ethyl acetate/hexanes) yielded the title compound (1.120 g, 1.77 mmol, 18% yield). ^{1}H NMR, δ 5.80 (m, 1 H), 4.96 (d, 1 H), 4.91 (m, 1 H), 3.37 (t, 4 H), 2.02 (quart, 2 H), 1.45 - 1.65 (m, 4 H), 1.2 - 1.4 (m, 72 H), 0.86 (t, 3 H).

22-Docosyloxy-1-docosanethioacetate. Thiolacetic acid (0.539 g, 7.1 mmol) was added to a solution of 22-docosyloxy-1-docosene (1.120 g, 1.77 mmol) and AIBN (10 mg) in THF (50 mL), and the reaction mixture was photolyzed for 3.5 h. After addition of saturated NaCl (aq) and hexanes to form a two-phase mixture, the layers were separated. The aqueous fraction was extracted thrice with hexanes, and the organic extracts were combined and concentrated under reduced pressure. Column chromatography (chloroform to 2% methanol/chloroform) yielded the title compound (0.374 g, 0.528 mmol, 30% yield). ^{1}H NMR, δ 3.37 (t, 4 H), 2.85 (quart, 2 H), 2.30 (m, 3 H), 1.45 - 1.65 (m, 6 H), 1.2 - 1.4 (m, 74 H), 0.86 (t, 3 H).

22-Docosyloxy-1-docosanethiol. Concentrated hydrochloric acid (0.193 g, 5.28 mmol) was added to a solution of 22-docosyloxy-1-docosanethioacetate (0.374 g, 0.528 mmol) in ethanol (20 mL), and the resulting mixture was refluxed for 15 h. After addition of saturated NaCl(aq) and chloroform to form a two-phase mixture, the layers were separated, and the aqueous fraction was extracted thrice with chloroform. The organic extracts were combined and concentrated under reduced pressure. Column chromatography (50% chloroform/hexanes) yielded the title compound (0.153 g, 0.230 mmol, 44% yield). ^{1}H NMR, δ 3.37 (t, 4 H), 2.54 (quart, 2 H), 1.45 - 1.65 (m, 7 H), 1.2 - 1.4 (m, 74 H), 0.87 (t, 3 H).

5.4.2. Preparation of Assemblies

Gold samples were prepared by evaporation of Cr and Au at 1 and 3 Å/s, respectively, onto Si wafers in a diffusion-pumped chamber with a base pressure of 2 x 10^{-6} Torr. To minimize the effects of adventitious carbon contamination on the kinetics of SAM formation, gold samples were used for adsorption studies within 10 min of removal from the evaporator. Copper samples were prepared by sequentially evaporating Cr and Cu at 1 and 12 Å/s, respectively, onto Si wafers. Immediately following the evaporation of copper, the chamber was backfilled with N$_2$ and the

freshly evaporated samples were transferred under a positive flow of N_2 to 1 mM solutions of n-alkanethiols that were taken inside the evaporator. Polyethylene strips were placed around the circumference of the bell jar to reduce the effective area for air to enter the open chamber during the transfer. Samples were transferred to adsorbate-containing solutions within 2 min after completion of the evaporation.

Freshly evaporated gold and copper substrates were immersed in 0.5 mM solutions of an alkanethiol in isooctane (copper and gold) or 2-butanol (gold) for various times. Adsorption temperatures were either 22 or 55 °C. Upon removal, the samples were rinsed with isooctane, ethanol, and water, and dried in a stream of N_2. The samples were characterized by RAIRS (see Chapter 4 for experimental details), ellipsometry, XPS (see Chapter 3), or EIS (see Chapter 4). Samples characterized by RAIRS or ellipsometry were often characterized by other techniques, whereas those characterized by XPS or EIS were discarded immediately after use.

5.4.3. Ellipsometry

The thicknesses of the SAMs on gold were determined using a Gaertner L116A automatic ellipsometer equipped with a He-Ne laser ($\lambda = 6328$ Å) at an incident angle of 70° and a refractive index for the organic film of 1.46. Samples were rinsed with ethanol and blown dry with N_2 before measurements were taken. Baseline values for upd assemblies were measured on unfunctionalized upd substrates within 2 min after emersion from the electrochemical cell. The reported thicknesses are the average of at least three independent experiments where each sample was characterized by ellipsometry at three different locations on its surface.

5.5. References

1)   Kumar, A.; Biebuyck, H. A.; Whitesides, G. M. *Langmuir* **1994**, *10*, 1498-1511.

2)   Bain, C. D.; Troughton, E. B.; Tao, Y.-T.; Evall, J.; Whitesides, G. M.; Nuzzo, R. G. *J. Am. Chem. Soc.* **1989**, *111*, 321-335.

3)   Sun, F.; Castner, D. G.; Grainger, D. W. *Langmuir* **1993**, *9*, 3200-3207.

4)   Sun, F.; Castner, D. G.; Mao, G.; Wang, W.; McKeown, P.; Grainger, D. W. *J. Am. Chem. Soc.* **1996**, *118*, 1856-1866.

5)   Laibinis, P. E.; Bain, C. D.; Nuzzo, R. G.; Whitesides, G. M. *J. Phys. Chem.* **1995**, *99*, 7663-7676.

6)   Sinniah, K.; Cheng, J.; Terretaz, S.; Reutt-Robey, J. E.; Miller, C. J. *J. Phys. Chem.* **1995**, *99*, 14500-14505.

7)   Peterlinz, K. A.; Georgiadis, R. *Langmuir* **1996**, *12*, 4731-4740.

8)   Xu, S.; Cruchon-Dupeyrat, S.; Garno, J. C.; Liu, G.-Y.; Jennings, G. K.; Yong, T.-H.; Laibinis, P. E. *J. Chem. Phys.* **1998**, *108*, 5002-5012.

9)   Karpovich, D. S.; Blanchard, G. J. *Langmuir* **1994**, *10*, 3315-3322.

10) Bensebaa, F.; Voicu, R.; Huron, L.; Ellis, T. H. *Langmuir* **1997**, *13*, 5335-5340.

11) Nuzzo, R. G.; Allara, D. L. *J. Am. Chem. Soc.* **1983**, *105*, 4881-4883.

12) Hautman, J.; Klein, M. L. *J. Chem. Phys.* **1989**, *91*, 4994-5001.

13) Sellers, H.; Ulman, A.; Shnidman, Y.; Eilers, J. *J. Am. Chem. Soc.* **1993**, *115*, 9389-9401.

14) Keller, H.; Simak, P.; Schrepp, W.; Dembowski, J. *Thin Solid Films* **1994**, *244*, 799.

15) Laibinis, P. E.; Bain, C. D.; Whitesides, G. M. *J. Phys. Chem.* **1991**, *95*, 7017-7021.

16) Laibinis, P. E.; Whitesides, G. M.; Allara, D. L.; Tao, Y.-T.; Parikh, A. N.; Nuzzo, R. G. *J. Am. Chem. Soc.* **1991**, *113*, 7152-7167.

17) Jennings, G. K.; Laibinis, P. E. *Colloids Surf., A* **1996**, *116*, 105-114.

18) Laibinis, P. E.; Whitesides, G. M. *J. Am. Chem. Soc.* **1992**, *114*, 1990-1995.

Chapter 6. Structural Effects on the Protective Properties of Self-Assembled Monolayers Formed from Long-Chain ω-Alkoxy-n-Alkanethiols on Copper

6.1. Background

In Chapter 4, electrochemical impedance spectroscopy (EIS) was used to determine that the coating resistances provided by n-alkanethiolate SAMs with chain lengths of 16 to 29 carbon atoms increase by 4.2 $M\Omega \bullet cm^2$ for each methylene ($-CH_2-$) in the adsorbate.[1] These dramatic chain-length effects on the barrier properties of the SAMs were related to the high level of dense packing and crystallinity within the hydrocarbon layer. The ability to form SAMs from longer-chain adsorbates would enable the opportunity to produce thicker films that should provide enhanced barriers to the transport of corrosive agents. In practice, efforts to synthesize n-alkanethiols with n > 29 are complicated by lengthy syntheses that are challenged by the poor solubility of the long-chained adsorbates in many common solvents. Chapter 5 described the synthesis and characterization of SAMs formed from long-chain ω-alkoxy-n-alkanethiols [$CH_3(CH_2)_{p-1}O(CH_2)_mSH$; m = 11, p = 18, 22; m = 19, p = 18, 22; m = 22, p = 22] on gold and copper. The ethereal oxygen in the adsorbate increases the polarity of the adsorbates and improves their solubility without dramatically affecting the crystallinity of the resulting SAM. Results from Chapter 5 indicate that SAMs as thick as 60 Å can be formed onto copper from these ω-alkoxy-n-alkanethiols and that the SAMs are densely packed and contain a crystalline hydrocarbon backbone that is canted at an average of ~16° from the surface normal. The formation of these SAMs at higher temperature (~55 °C) from a hydrocarbon solvent resulted in more densely packed films that provided superior barriers against the penetration of aqueous ions than were possible from adsorptions at room temperature.

In this chapter, chain-length effects on the inhibition of corrosion by SAMs formed from the adsorption of ω-alkoxy-n-alkanethiols onto copper are examined. EIS was used to determine the coating capacitances and resistances for these SAMs as a function of their exposure to 1 atm of O_2 at 100% RH. The results from EIS are coupled with those from grazing angle IR spectroscopy to correlate the structure of the SAMs to their barrier properties as a function of exposure time to the corrosive conditions. By comparing SAMs formed from these long-chained ether-containing adsorbates with those from shorter-chained, unsubstituted n-alkanethiols, the effect of the ethereal oxygen on the structure and barrier properties of these monolayer films is discussed. Particularly, while the ethereal unit might be a convenient synthetic linker for the synthesis of longer-chained

adsorbates, its inclusion may diminish the ability of the film to achieve dense packing and useful barrier properties.

6.2. Results

6.2.1. Properties of ω-Alkoxy-n-Alkanethiols on Copper

Freshly evaporated, polycrystalline copper substrates were transferred under anaerobic conditions to N_2-purged solutions of the ω-alkoxy-n-alkanethiols (0.5 mM) in isooctane. The assembly was performed at 22 or 55 °C depending on the chain length of the adsorbate (22 °C for p + m < 37 and 55 °C for p + m ≥ 37). Higher temperatures were required to provide sufficient thermal motion for the longer chains in the partial films to allow additional thiol adsorbates access to the underlying copper substrate, and thus, increase the packing density of these thicker SAMs, as detailed in Section 5.2. After adsorption for 1 h, the samples were removed, rinsed with isooctane and ethanol, and dried in a steam of N_2. Upon removal from solution, the samples exhibited no XPS signals for Cu(II) species. Furthermore, infrared peak positions of the $v_a(CH_2)$, $v_s(CH_2)$, and $v_a(ROR)$ modes appeared at ~2919, ~2851, and ~1131 cm^{-1}, respectively, and indicated that the films were crystalline, consisting primarily of trans-extended alkyl chains with few gauche conformers.

Electrochemical impedance spectroscopy (EIS) provides a method to assess the protective properties of SAMs by measuring their resistance against the diffusion of aqueous ions to the underlying metal surface. EIS has often been used to study the protection provided by polymeric coatings on metals[2,3] and to investigate the barrier properties of SAMs.[4] Figures 6.1a and b show Bode magnitude and phase angle plots, respectively, for SAMs formed from $C_{18}OC_{11}SH$, $C_{22}OC_{11}SH$, and $C_{22}OC_{19}SH$ on copper. In Figure 6.1a for frequencies less than 10^3 Hz, the log of the impedance magnitude increases linearly (slope of 1) with decreasing log frequency. This behavior indicates that the films behave primarily as a low dielectric layer that separates the corrosive solution from the underlying copper. The impedances provided by these SAMs and other unsubstituted n-alkanethiolate SAMs[1] on copper are significantly larger than those observed for thiols on gold[5] and may reflect the higher levels of interchain packing[6] in the former system. At the lowest frequencies in Figure 6.1, the impedance of the coating capacitance becomes sufficiently large that the resistance of the coating begins to control the response. This transition is illustrated best in Figure 6.1b in which the phase angle decreases from 90°—a value characteristic of capacitive behavior—at the lowest frequencies. The decrease in phase angle is most pronounced for the $C_{18}OC_{11}$S-SAM and least for the $C_{22}OC_{19}$S-SAM, suggesting that the thicker SAM provides a less permeable barrier to the diffusion of ions.
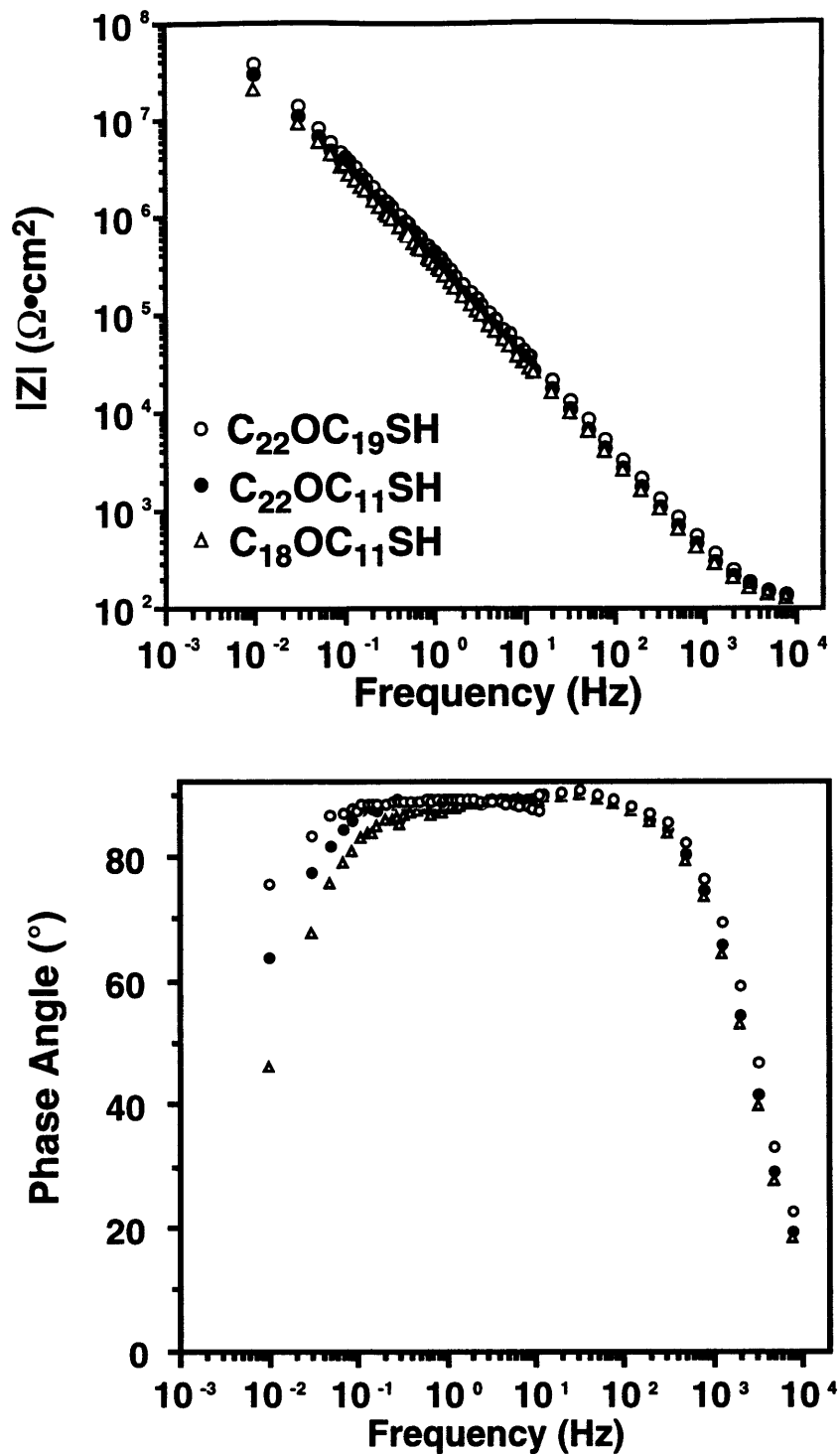
Figure 6.1. (a) Bode magnitude and (b) phase plots for copper protected with SAMs of $C_{18}OC_{11}SH$, $C_{22}OC_{11}SH$, and $C_{22}OC_{19}SH$ in oxygenated 50 mM Na_2SO_4 (aq).

Modeling the impedance data for these SAM on copper with an appropriate equivalent circuit model, that shown earlier in Figure 4.1a and discussed in Section 4.1, enables an estimation of the capacitance and resistance of the SAM. Since the SAM can be described as a low dielectric medium separating two parallel conductors (the metal and the solution), its capacitance should decrease as its thickness is increased. Figure 6.2 shows that the inverse capacitance is linearly related to the chain length (# carbons + # oxygens) for coatings derived from both unsubstituted n-alkanethiols and ω-alkoxy-n-alkanethiols adsorbed on copper. That these data sets lie approximately on the same line suggests that SAMs formed from the ether-linked thiols are similar in dielectric properties to those from the n-alkanethiols and that the effective thickness of the SAM can be increased incrementally by increasing the adsorbate chain length from 8 to 45. The thickness trends inferred from these capacitance data are consistent with results in Figure 5.8 where the $Cu(2p_{3/2})$ intensity in XPS decreased exponentially with increased chain length for both adsorbed n-alkanethiols and ω-alkoxy-n-alkanethiols. The dielectric permittivity (ε) of the coatings can be estimated from the slope of the line as described in Section 4.2; such an analysis gives values of ε of 2.16 for the purely hydrocarbon SAMs and 2.35 for the ether-substituted SAMs. These permittivities agree well with values of 2.3 determined for polyethylene[7] and 2.1 measured for C_nSH (n = 16, 18) on gold with surface plasmon resonance.[8]

Coating resistances for SAMs on copper derived from both unsubstituted n-alkanethiols and ω-alkoxy-n-alkanethiols are shown in Figure 6.3 as a function of the chain length of the adsorbate. As discussed in Section 4.2, the coating resistances for SAMs of C_nSH on copper increase linearly with chain length for n ≥ 16 with a slope of 4.2 $M\Omega\cdot cm^2$ for each incremental methylene. That the best-fit line through the alkanethiol data intersects the x-axis at n = 10 may reflect the minimum chain length required to achieve a region within the SAM that is sufficiently crystalline to impede the transport of corrosive species to the underlying copper surface.[1] For SAMs formed from ω-alkoxy-n-alkanethiols on copper, the coating resistance also increases with chain length, but these data are not a simple extension of the linear behavior of the C_nSH-systems as was the case for the capacitance data (Figure 6.2). In fact, the coating resistances for SAMs formed from $C_{18}OC_{11}SH$ (chain length = 30) and $C_{22}OC_{11}SH$ (chain length = 34) are significantly smaller than expected based on a linear extrapolation of the data for C_nS-films while resistances for SAMs formed from C_pOC_mSH (m + p ≥ 37) agree with those expected for a C_nS-SAM of similar chain length. The best-fit line through the data intersects the x-axis at a chain length of 24, considerably higher than that (n = 10) for SAMs formed from C_nSH. This observation suggests that a greater number of methylene units are required in these ether-linked thiols to form SAMs that are sufficiently crystalline to resist the penetration of corrosive agents. The disparity between the resistance and capacitance data is attributed to the greater sensitivity of resistance measurements on the structure of the SAM.
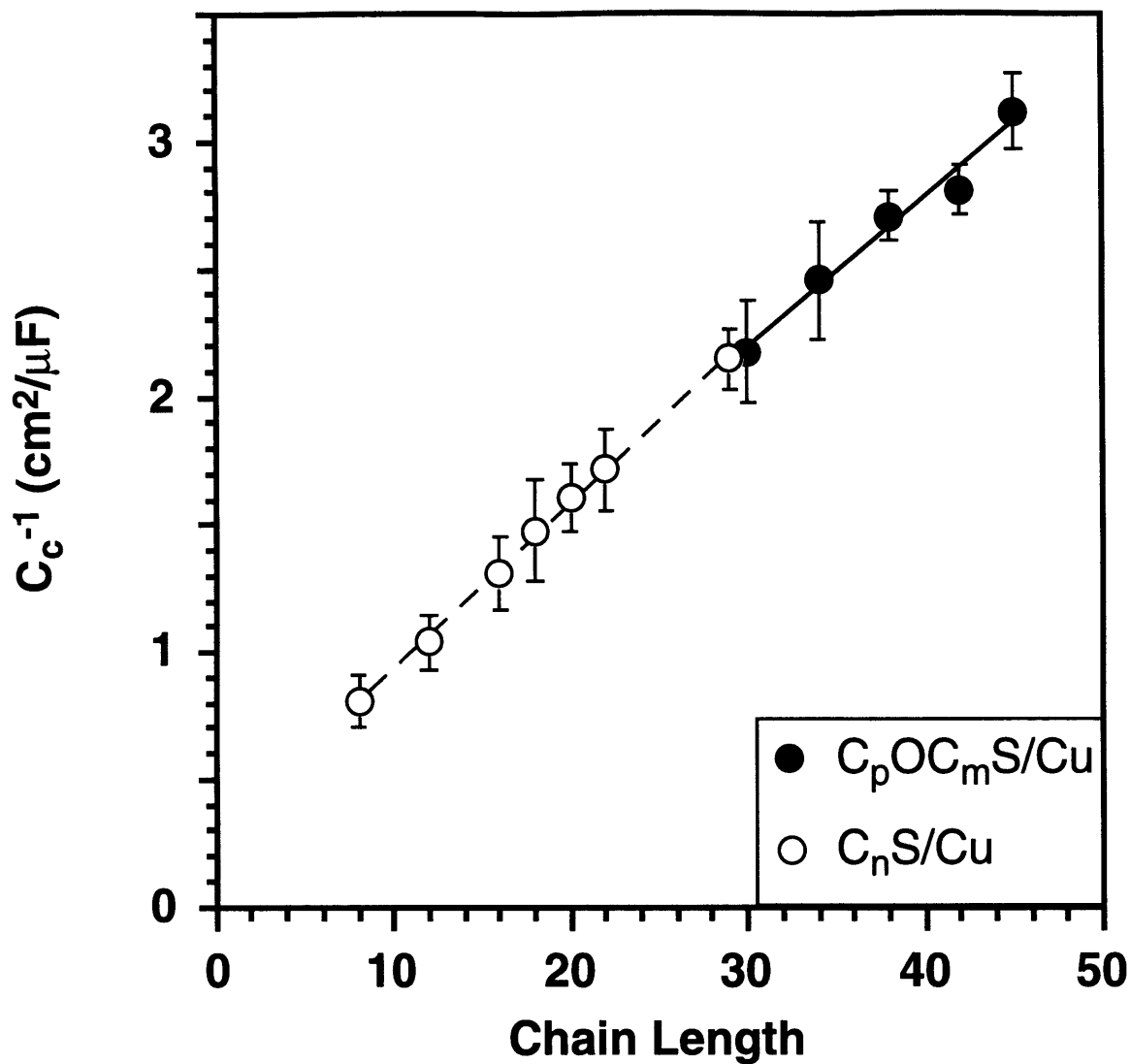
Figure 6.2. Inverse capacitance of SAMs of C_nSH and C_pOC_mSH on copper in oxygenated 50 mM Na_2SO_4 (aq). The lines are least-squares fits to the data and have slopes that correspond to dielectric permittivities (ε) of ~2.16 and ~2.35 for the C_nSH and C_pOC_mSH SAMs, respectively.
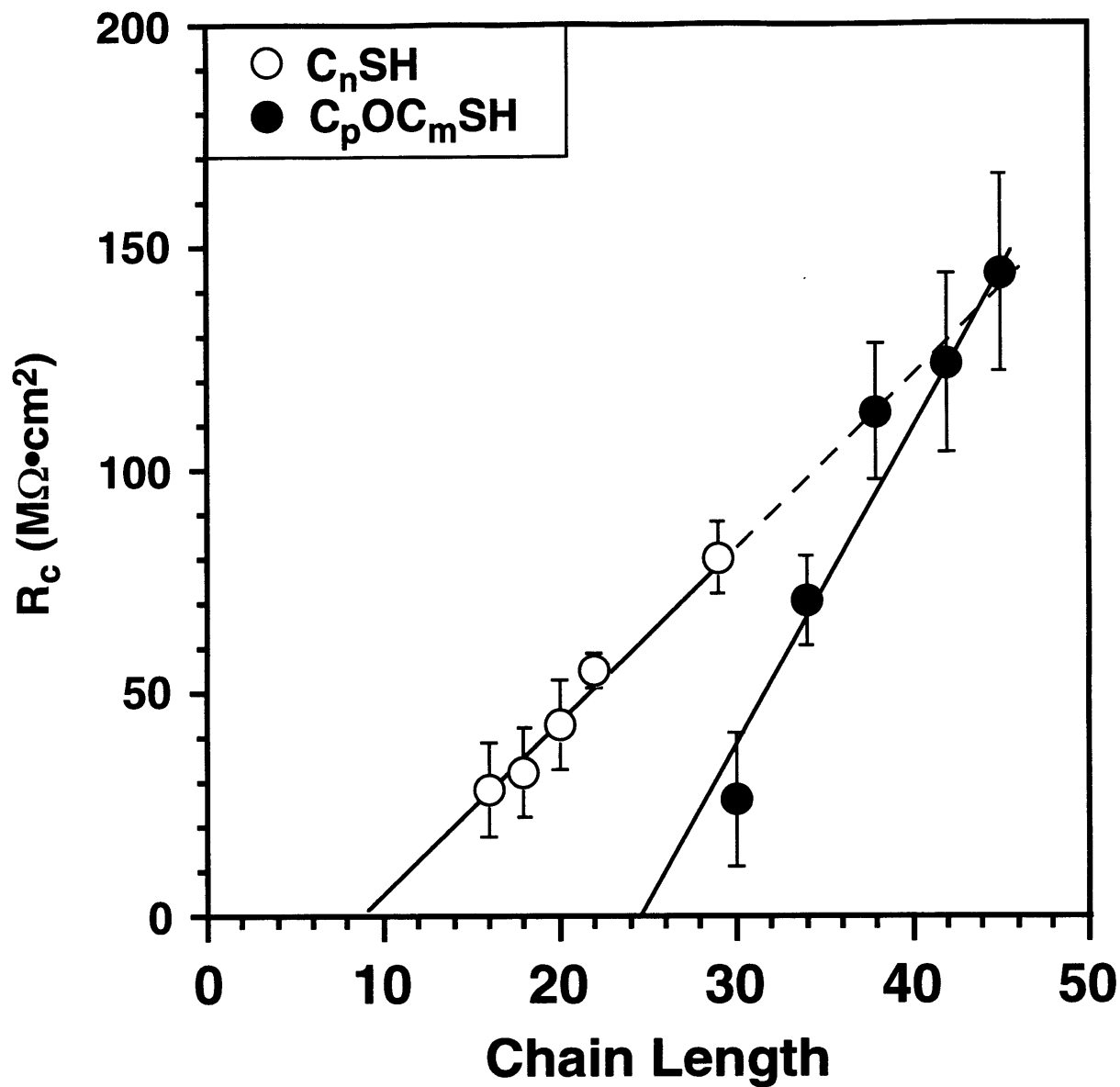
Figure 6.3. The effect of chain length on the coating resistance for SAMs prepared from C_nSH and C_pOC_mSH on copper. Coating resistances were determined by fitting the impedance data to an equivalent circuit consisting of a solution resistance in series with a parallel combination of coating resistance and coating capacitance (Figure 4.1). The lines are least-squares fits to the data.

6.2.2. Properties of SAMs Upon Exposure to 1 atm of O_2 at 100% RH

After exposing SAMs formed from ω-alkoxy-n-alkanethiols on copper to 1 atm of O_2 and 100% RH at room temperature, the protective properties of the films degraded; Figure 6.4a shows the coating resistance (R_c) for SAMs of $C_{18}OC_{11}SH$, $C_{22}OC_{11}SH$, and $C_{22}OC_{22}SH$ on copper as a function of exposure time to these oxidizing conditions. While the coating resistance for each SAM decreases exponentially with increased exposure, the thinnest SAM ($C_{18}OC_{11}SH$) exhibits the most rapid loss of coating resistance. Increasing the outer chain length by four methylene units ($C_{22}OC_{11}SH$) and then the inner chain length by eight methylene units ($C_{22}OC_{19}SH$) both result in films that exhibit slower losses in their coating resistance. From data such as those in Figure 6.4a, the rate of coating resistance falloff for SAMs formed from the various ω-alkoxy-n-alkanethiols was determined and compared to data from Figure 4.8b for unsubstituted n-alkanethiol systems (Figure 6.4b). The data for the ω-alkoxy-n-alkanethiols are similar to those for n-alkanethiolate SAMs in that thicker films are more effective in maintaining their barrier properties upon exposure to 1 atm of O_2 at 100% RH. Nevertheless, the slopes of the data sets in Figure 6.4b are distinctly different and indicate that each additional methylene unit added to an unsubstituted n-alkanethiol results in a greater reduction in the rate of R_c falloff for the SAM than one added to an ω-alkoxy-n-alkanethiol. Specifically, a decrease in the rate of R_c falloff by 50% requires the addition of only five methylene units to the unsubstituted thiol and thirteen methylene units to the ether-substituted thiol that forms the SAM.

Figure 6.5 shows capacitances for SAMs of $C_{18}OC_{11}SH$, $C_{22}OC_{11}SH$, and $C_{22}OC_{19}SH$ on copper upon exposure to 1 atm of O_2 at 100% RH. Increases in capacitance can correspond to the uptake of water or ions in the coating and/or the SAM becoming effectively thinner (vide infra). For these SAMs in Figure 6.5, C_c values change very little (if any) over the first ~70 h of exposure; however, R_c (Figure 6.4a) for all these SAMs decreases by nearly an order of magnitude over a similar time of exposure. The decrease in R_c is probably a result of slight structural perturbations in the film caused by oxidation of the underlying copper and subsequent roughening of the surface. After 70 h, the C_c values of the $C_{18}OC_{11}S$- and $C_{22}OC_{11}S$-SAMs increase more dramatically, suggesting the formation of larger defects within the coating that may serve as ion-conducting paths. The more subtle change in C_c for the $C_{22}OC_{19}S$-SAM over the entire exposure may reflect the greater structural integrity of this thicker film.

In Chapter 4, grazing angle IR spectroscopy was used to monitor the structural properties for SAMs derived from C_nSH (n = 16, 22, and 29) on copper upon exposure to 1 atm of O_2 at 100% RH. The results from this chapter suggested that the SAMs become less densely packed and less crystalline upon exposure to the corrosive environment but that the thicker SAMs (n = 29) exhibited a slower transition to the less crystalline state. Figure 6.6 shows grazing angle IR
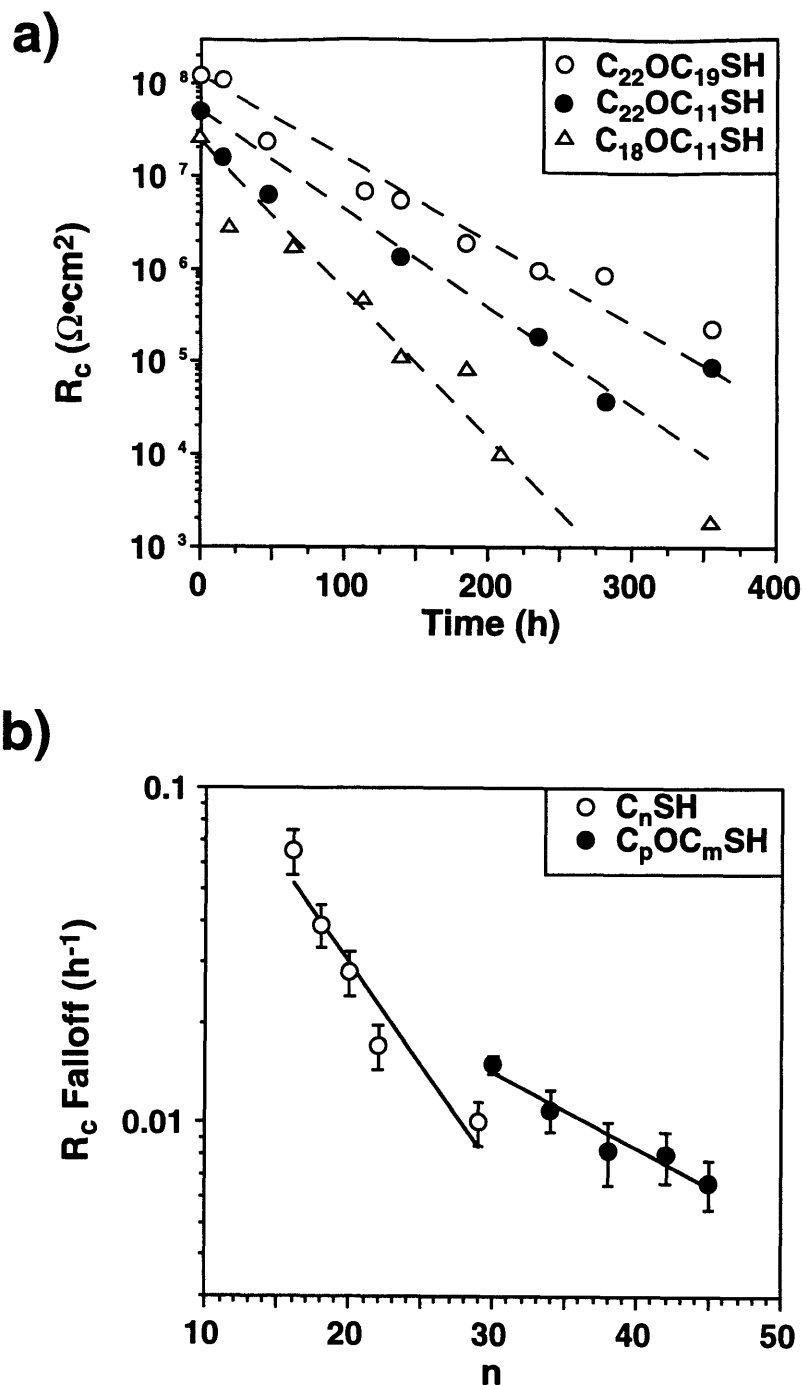
Figure 6.4. (a) Time-dependence of the coating resistance for SAMs formed from $C_{18}OC_{11}SH$, $C_{22}OC_{11}SH$, and $C_{22}OC_{19}SH$ on copper upon exposure to 1 atm of O_2 at 100% RH. The lines are least-squares fits to the data and were constrained to intersect the initial (t = 0) data point. (b) Relationship between the rate of coating resistance falloff (determined from Figure 6.4a) and the chain length of the adsorbate that forms the coating for SAMs of C_nSH and C_pOC_mSH on copper. The lines represent least-squares fits to the data. From the slope of the lines, the incremental chain lengths that are required to reduce the rate of R_c falloff by 50% are five and thirteen $-CH_2-$ units for the C_nSH and C_pOC_mSH systems, respectively.
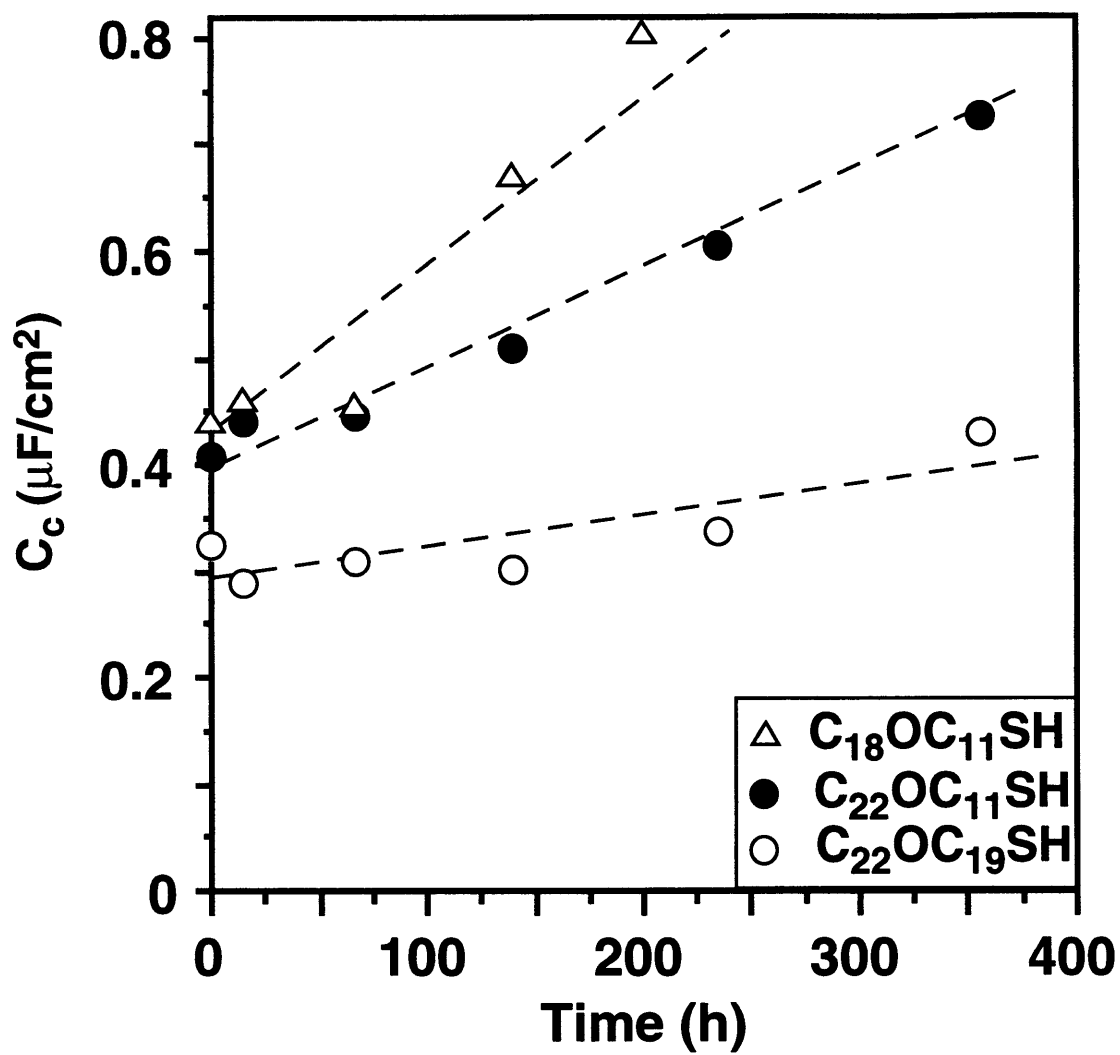
Figure 6.5. Time dependence of the coating capacitance (C_c) for SAMs formed from $C_{18}OC_{11}SH$, $C_{22}OC_{11}SH$, and $C_{22}OC_{19}SH$ on copper upon exposure to 1 atm of O_2 at 100% RH. The lines serve as guides to the eye.

spectra of the C-H and R-O-R stretching regions for SAMs formed from $C_{22}OC_{11}SH$ (Figure 6.6a) and $C_{22}OC_{19}SH$ (Figure 6.6b) on copper after various exposures to 1 atm of O_2 at 100% RH. The spectral changes observed for the $C_{22}OC_{11}S$-SAM are similar to those observed for the $C_{18}OC_{11}S$-SAM while changes for the $C_{22}OC_{19}S$-SAM are typical of those exhibited by coatings of the longer-chained adsorbates ($C_{18}OC_{19}SH$ and $C_{22}OC_{22}SH$). For the shorter-chained $C_{22}OC_{11}S$-SAM (Figure 6.6a), large increases in the intensities of the $\nu(CH_2)$ modes and a reduced intensity of the $\nu_a(ROR)$ mode upon increased exposure suggests that the adsorbates within the SAM become more canted and less densely packed, consistent with the increase in capacitance for this film (Figure 6.5). The peak positions for the $\nu(CH_2)$ modes remain at or near their initial values— $\nu_a(CH_2)$ at ~2919 cm^{-1} and $\nu_s(CH_2)$ at ~2851 cm^{-1}—during the 400-h exposure suggesting that the hydrocarbon maintains its primarily crystalline structure; however, $\nu_a(ROR)$ becomes broadened and shifts from 1132 to 1127 cm^{-1} indicating a less crystalline local environment near the ether substitution after 400 h of exposure.[9] While the methyl stretching modes provide no information about the cant of the adsorbates, they are useful for assessing the structural heterogeneity at the outermost region of the SAM. During the exposure, both the $\nu_a(CH_3)$ and $\nu_s(CH_3)$ modes become broadened with the $\nu_a(CH_3)$ increasing in intensity and the $\nu_s(CH_3)$ decreasing in intensity. These changes are consistent with an increased average tilt of the adsorbates within the SAM and the development of a more heterogeneous methyl environment at the surface. Clearly, exposure to the oxidizing conditions causes major structural changes in the $C_{22}OC_{11}S$-SAM.

In contrast to the $C_{22}OC_{11}S$-SAM on copper, the $C_{22}OC_{19}S$-SAM exhibits less dramatic structural changes during exposure to 1 atm of O_2 at 100% RH for 400 h (Figure 6.6b). The relatively constant intensities of the $\nu_a(CH_2)$, $\nu_s(CH_2)$, and $\nu_a(ROR)$ modes indicate that the adsorbates within the SAM remain densely packed during the 400-h exposure, but the broadening of the methylene modes suggest some loss in crystallinity. In comparing Figures 6.6a and 6.6b at 400-h exposure, it is evident that the addition of eight methylene units to the bottom portion of the SAM significantly enhances its ability to maintain its structure. Similar to the $C_{22}OC_{11}S$-SAM, the peak positions of the $\nu_a(CH_2)$ and $\nu_s(CH_2)$ modes for the $C_{22}OC_{19}S$-SAM remain essentially constant during the exposure while that for the $\nu_a(ROR)$ decreases from 1131 to 1128 cm^{-1}, indicating a local loss of crystallinity near the ether substitution. The outer surface of the SAM becomes more heterogeneous during the exposure, as evidenced by broadening of both the $\nu_a(CH_3)$ and $\nu_s(CH_3)$ modes.
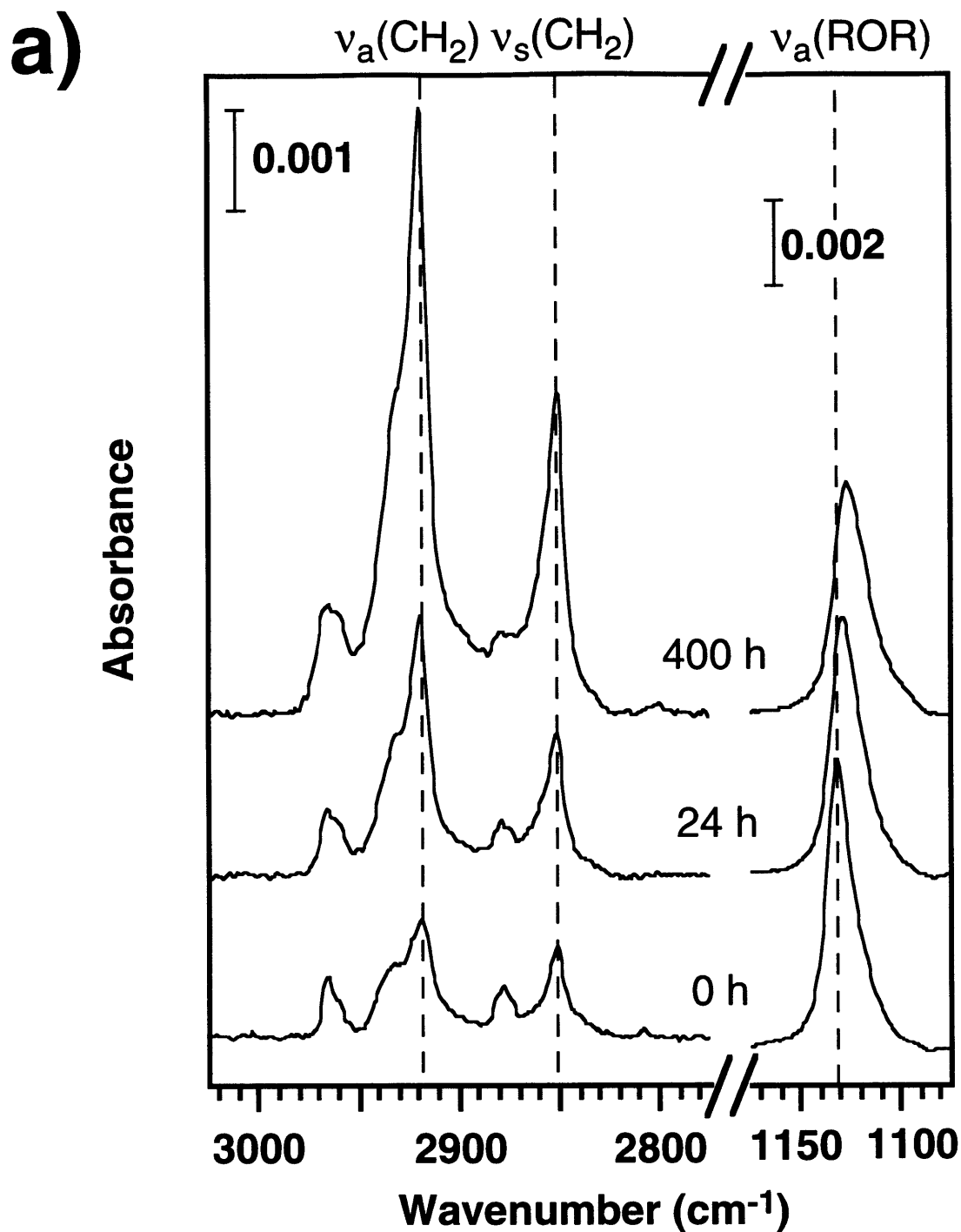
Figure 6.6. (a) Grazing incidence polarized infrared spectra of the C-H stretching region for SAMs of $C_{22}OC_{11}SH$ on copper before and after exposure to 1 atm of O_2 at 100% RH for various times. The dashed lines represent the positions of the primary modes for a trans-extended monolayer with no gauche defects: $v_a(CH_2) = 2918$ cm[-1], $v_s(CH_2) = 2851$ cm[-1], and $v_a(ROR) = 1132$ cm[-1]. The spectra have been offset vertically for clarity.
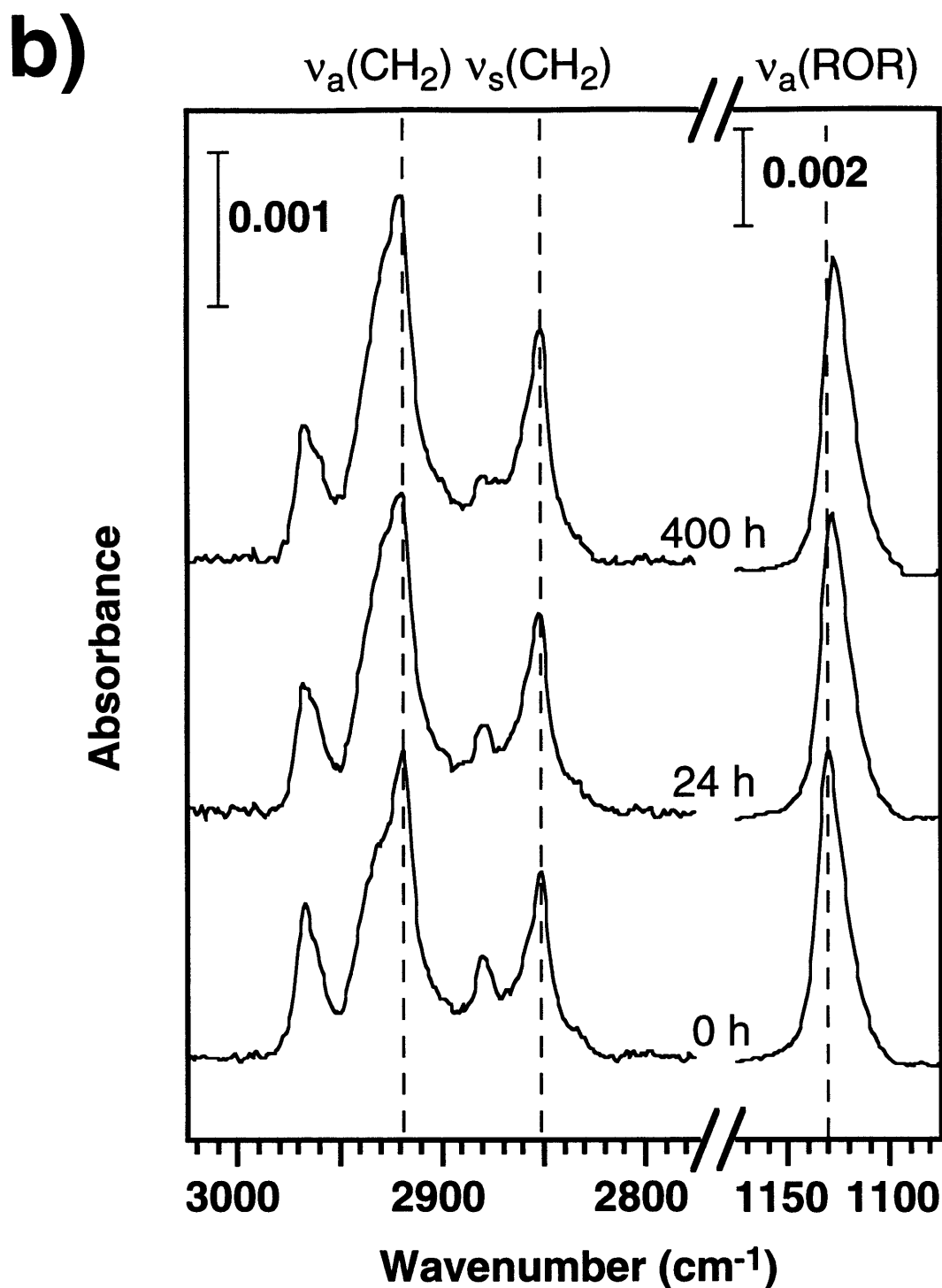
Figure 6.6. (b) Grazing incidence polarized infrared spectra of the C-H stretching region for SAMs of $C_{22}OC_{19}SH$ on copper before and after exposure to 1 atm of O_2 at 100% RH for various times. The dashed lines represent the positions of the primary modes for a trans-extended monolayer with no gauche defects: $v_a(CH_2) = 2918$ cm^{-1}, $v_s(CH_2) = 2851$ cm^{-1}, and $v_a(ROR) = 1132$ cm^{-1}. The spectra have been offset vertically for clarity.

6.3. Discussion

6.3.1. Effect of Ether Substitution on the Barrier Properties of SAMs

The results of Figures 6.1 - 6.6 consistently demonstrate that the chain length of the adsorbates forming the SAM significantly impacts the properties of the resulting films. The capacitance results in Figure 6.2 illustrate that effectively thicker SAMs can be formed on copper by use of long-chain ω-alkoxy-n-alkanethiols and that their thickness scales with the chain length of the adsorbates. While capacitance provides a measure of the bulk permeability of the SAMs toward simple ionic species, resistance measurements are more sensitive to the fine structural details of the film. In contrast to the capacitance data, coating resistances for the long-chain ω-alkoxy-n-alkanethiols are not linear extensions of the unsubstituted n-alkanethiol data (Figure 6.3). Coating resistances for SAMs of ω-alkoxy-undecanethiols ($C_{18}OC_{11}SH$ and $C_{22}OC_{11}SH$) are significantly less than that expected for n-alkanethiols of similar chain length while resistances for the longer-chained ether-containing thiols ($C_{18}OC_{19}SH$, $C_{22}OC_{19}SH$, and $C_{22}OC_{22}SH$) are much closer to a linear extrapolation of the C_nSH data. These data may be rationalized by considering the likely locations of gauche conformations within the hydrocarbon SAM. Hautman and Klein used molecular dynamics simulations to study the structure of SAMs of $C_{16}SH$ on gold and determined that gauche defects are concentrated near the chain termini.[10] In addition, Laibinis et al. used IR spectroscopy of SAMs on gold and silver and concluded that the presence of an ethereal oxygen along the hydrocarbon chain of a SAM causes a local disordering and increases the population of gauche conformations.[11] Their results also indicated that SAMs formed from $CH_3O(CH_2)_mSH$ on silver were significantly less crystalline for m = 8 and 11 than for m = 16. Thus, an accurate structural representation for these ω-alkoxy-n-alkanethiolate SAMs may include regions of reduced crystallinity near the metal surface, near the ether substitution, and near the outer portion of the SAM at the air interface. For SAMs in the present study formed from ω-alkoxy-undecanethiols, the close proximity of the lower and middle regions of higher gauche density may result in a less ordered layer of hydrocarbon between the ether linkage and the metal surface. For SAMs where the ether substitution is significantly further away from the surface, a higher degree of structural order is expected for the contiguous hydrocarbon portion between the ether linkage and the metal surface.

In Chapter 4, the eventual oxidation of copper upon exposure to 1 atm of O_2 at 100% RH was hypothesized to result in a nano-scale surface roughening that promotes a transition within the SAM to a less organized structure and negatively impacts its barrier properties.[1] Figure 6.4b indicates that the rate of coating resistance falloff for an ω-alkoxy-n-alkanethiolate SAM is greater

than that for an unsubstituted n-alkanethiolate SAM of similar chain length. Furthermore, the addition of incremental methylenes to the ether-linked adsorbates results in a smaller reduction in the R_c falloff than similar addition to unsubstituted n-alkanethiols. In other words, the rate of R_c falloff is not solely dependent on film thickness. If the structural stability of the monolayer affects its barrier properties, then the rate of R_c falloff should depend on the intermolecular interactions within the film. To test this hypothesis, the rate of R_c falloff was plotted as a function of the melting-point temperature of the parent compound for SAMs of C_nSH and C_pOC_mSH. The melting temperature (T_{melt}) is a highly sensitive, albeit qualitative, probe of the extent of intermolecular interactions within the SAM and provides a convenient comparison. For a constant chain length, ether-substituted thiols have lower melting points than unsubstituted n-alkanethiols due to the perturbation of interchain packing imposed by the ethereal substitution.[11] Figure 6.7 shows that the rate of R_c falloff decreases exponentially as the T_{melt} increases for both n-alkanethiols and ω-alkoxy-n-alkanethiols and that the data for the two systems exhibit a similar relationship with T_{melt}. This result indicates that the effectiveness of a SAM to maintain its barrier properties (R_c) depends on the intermolecular interactions within the monolayer and its ability to form a crystalline structure, rather than simply the thickness of the SAM. SAMs with a greater level of intermolecular interaction are superior in maintaining their structural integrity upon exposure to oxidizing conditions.

6.3.2. Mechanism for Breakdown in SAM Protection

Upon exposure of SAM-coated copper to 1 atm of O_2 at 100% RH, the adsorbates within the SAM undergo modest ($C_{22}OC_{19}SH$) or extensive ($C_{22}OC_{11}SH$) structural transformations (Figure 6.6), and the capacitance of the SAM increases (Figure 6.5) while its resistance decreases (Figure 6.4). Increases in the capacitance of the SAM can be related to a decrease in its thickness or an increase in its dielectric permittivity due to the uptake of aqueous species within the film or at defect sites. If the increases in capacitance are solely due to a reduction in the thickness of the SAM, these changes should occur with a concurrent increase in the average cant of the adsorbates on the surface. Thus, an estimation of the SAM thickness based on capacitance measurements should be similar to that estimated from the $v(CH_2)$ intensities in the IR spectra. For a $C_{22}OC_{11}S$-SAM exposed to 1 atm of O_2 at 100% RH for 350 h (Figure 6.5), the increase in capacitance would correspond to a 40% decrease in thickness from the initially prepared SAM. The increased intensity of the $v(CH_2)$ modes (Figure 6.6a) over the 400-h exposure suggests that the average cant of the film has increased from 17° to 39°, corresponding to a decrease in thickness of only ~20%. Since capacitance measurements suggest a greater reduction in film thickness than IR spectra the increase in capacitance is at least partially due to an increase in the dielectric permittivity (ε_{SAM}) of
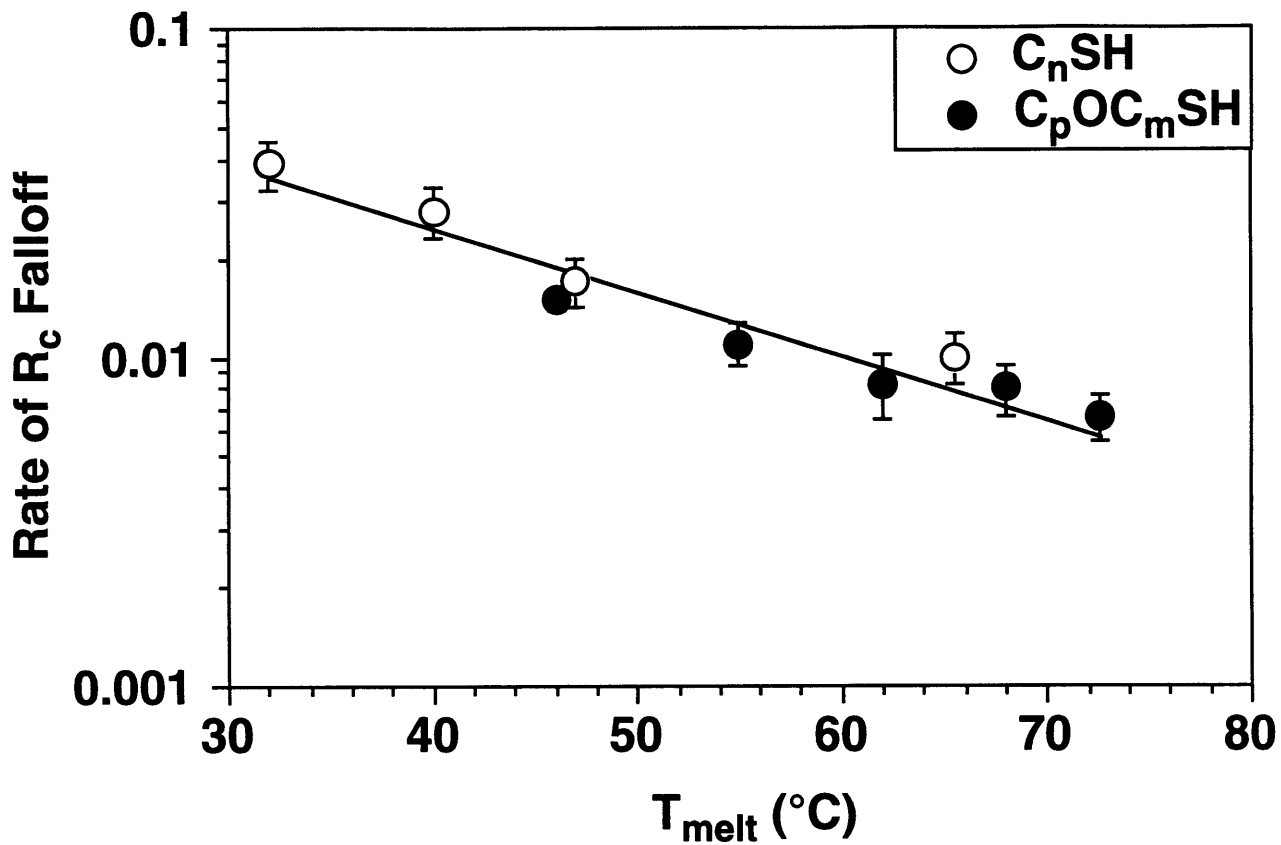
Figure 6.7. Relationship between the rate of coating resistance falloff for SAMs of C_nSH and C_pOC_mSH on copper from Figure 6.4b and the melting point of the adsorbate. The line is a least-squares fit to the data.

the coating. Whether the increase in ε_{SAM} is due to uptake of aqueous species throughout the SAM or their accumulation at specific defect sites within the SAM cannot be unequivocally determined from these results. Such a large increase in film capacitance ($\sim 40\%$) is not expected to result solely from the equilibrium uptake of electrolyte throughout the film as the solubility of water in these films is extremely low. Therefore, defects that form within the SAM upon exposure to 1 atm of O_2 at 100% RH likely become filled with electrolyte during the EIS measurement, increasing the capacitance of the films. Nevertheless, none of the experimental evidence suggests the existence of true pinholes defined as bare areas of the metal surface that are in direct contact with the electrolyte. For example, a Warburg impedance that is characteristic of solution-metal contact at pores in the film is not observed for these SAMs, even after prolonged exposure to 1 atm of O_2 at 100% RH. The presumed absence of pinholes is attributed to the tendency of long, flexible hydrocarbon adsorbates to form van der Waals interactions with neighboring molecules and reduce the size of any defects that may form.

The results in Figure 6.7 provide support for the proposed mechanism of film deterioration discussed in Chapter 4. After formation of the SAM and subsequent exposure to 1 atm of O_2 at 100% RH, oxygen diffuses through the film and reacts to convert copper to Cu(I) (and eventually Cu(II) oxide) and thiolates to sulfonates.[6,12] The oxidation of copper proceeds with roughening of the underlying substrate which effectively melts the crystalline lattice of the film and increases its density of defects. These structural changes within the SAMs have been revealed by IR spectroscopy and wetting measurements. Upon exposure to 1 atm of O_2 at 100% RH, IR spectra for these SAMs (Figure 6.6) indicate a broadening of the $v(CH_2)$ and $v(CH_3)$ absorptions, an increase in the intensity of the $v(CH_2)$ modes (for most SAMs), and a slight shift in the peak position of the $v(CH_2)$ modes to higher wavenumber. These changes are indicative of the transition from a purely crystalline film to a more heterogeneous one with a reduced packing density. In a similar manner, the contact angle of hexadecane decreases[13] and the contact angle hysteresis of water increases[6] upon exposure of these SAMs to oxidizing conditions, indicating the formation of a more chemically heterogeneous and roughened surface. When the SAM-coated samples are removed from the oxidizing conditions and exposed to an aqueous solution (during EIS measurement), penetration of water and electrolyte into the defects of the SAMs causes a reduction in the resistance and an increase in the capacitance of the SAM. The chain length trends described in this chapter demonstrate that SAMs containing adsorbates capable of greater intermolecular interaction (Figure 6.7) possess enhanced stability against the structural perturbations induced by oxidation of the copper substrate and thus, produce and maintain films with a lower density of defects. In support of these results, Zamborini and Crooks[14] and others[15,16] have demonstrated the importance of intermolecular interactions on film stability by

reporting that SAMs derived from thiols with H-bonding capabilities on gold are more stable to repeated oxidative electrochemical cycling and exposure to elevated temperatures.

6.4. Conclusions

The protection of copper by thiol-based self-assembled monolayers (SAMs) is sensitive to the chemical composition and molecular structure of the barrier film. The use of long-chain ω-alkoxy-n-alkanethiols provides a convenient strategy to prepare SAMs on copper with thicknesses of 40 - 60 Å that are thicker than those formed using presently available unsubstituted n-alkanethiols. The performances of these ether-containing films as barrier layers depends on the chain length of the adsorbate and the position of the ethereal unit along the hydrocarbon chain. For SAMs prepared from ω-alkoxy-undecanethiols ($C_{22}OC_{11}SH$ and $C_{18}OC_{11}SH$), the measured coating resistances are significantly lower than expected for unsubstituted n-alkanethiols of similar chain length, consistent with a structure containing a less crystalline region near the base of the SAM. In contrast to these SAMs, those prepared from ω-alkoxy-nonadecanethiols and ω-alkoxy-docosanethiols exhibit greater initial resistances (up to 150 MΩ•cm^2) and are superior in maintaining their structural properties during exposure to oxidizing conditions. The ability of a SAM to maintain its barrier properties during prolonged exposure to these conditions is related to the collective intermolecular interactions within the SAM rather than simply its thickness. The data suggest that the design of barrier coatings requires a selection of adsorbates that can achieve dense packing and high crystallinity and are able to maintain these structural properties. The melting points of the parent compounds can provide a useful comparative meter for the likely performance of these SAMs as barrier films after exposure to oxidizing conditions.

6.5. References

1) Jennings, G. K.; Munro, J. C.; Yong, T.-H.; Laibinis, P. E. *Langmuir* **1998**, in press.

2) Bellucci, F.; Kloppers, M.; Latanision, R. M. *J. Electrochem. Soc.* **1991**, *138*, 40-48.

3) Mitton, D. B.; Latanision, R. M.; Bellucci, F. *J. Electrochem. Soc.* **1996**, *143*, 3307-3316.

4) Finklea, H. O. *Electrochemistry of Organized Monolayers of Thiols and Related Molecules on Electrodes*; Bard, A.J.; Rubinstein, I., Eds.; Marcel Dekker: New York, 1996; Vol. 19, pp 109-335.

5) Finklea, H. O.; Snider, D. A.; Fedyk, J.; Sabatani, E.; Gafni, Y.; Rubinstein, I. *Langmuir* **1993**, *9*, 3660-3667.

6) Laibinis, P. E.; Whitesides, G. M. *J. Am. Chem. Soc.* **1992**, *114*, 9022-9027.

7) Lanza, V. L.; Herrman, D. B. *J. Polym. Sci.* **1958**, *28*, 622-625.

8) Peterlinz, K. A.; Georgiadis, R. *Langmuir* **1996**, *12*, 4731-4740.

9) Sinniah, K.; Cheng, J.; Terretaz, S.; Reutt-Robey, J. E.; Miller, C. J. *J. Phys. Chem.* **1995**, *99*, 14500-14505.

10) Hautman, J.; Klein, M. L. *J. Chem. Phys.* **1989**, *91*, 4994-5001.

11) Laibinis, P. E.; Bain, C. D.; Nuzzo, R. G.; Whitesides, G. M. *J. Phys. Chem.* **1995**, *99*, 7663-7676.

12) Schoenfisch and Pemberton have shown that (1) thiolate SAMs on gold convert to sulfonates upon exposure to air, (2) the sulfonates are not easily removed from the substrate, and (3) the barrier properties of the films are not affected by this oxidation. (see *J. Am. Chem. Soc.* **1998**, *120*, 4502-4513.) As no loss of adsorbate from the SAM is observed upon exposure to the aqueous electrolyte during impedance measurements (Chapter 4), the oxidation of thiolates to sulfonates is not expected to completely account for the exponential decrease in the resistance of these films.

13) Jennings, G. K.; Laibinis, P. E. *Colloids Surf., A* **1996**, *116*, 105-114.

14) Zamborini, F. P.; Crooks, R. M. *Langmuir* **1998**, *14*, 3279-3286.

15) Tam-Chang, S.-W.; Biebuyck, H. A.; Whitesides, G. M.; Jeon, N.; Nuzzo, R. G. *Langmuir* **1995**, *11*, 4371-4382.

16) Clegg, R. S.; Reed, S. M.; Hutchison, J. E. *J. Am. Chem. Soc.* **1998**, *120*, 2486-2487.

Chapter 7. Effect of Film Crystallinity on the Protective Properties of Self-Assembled Monolayers of Alkanethiols on Copper

7.1. Background

The molecular-level structure and composition of materials can dramatically affect their bulk and interfacial properties. In the design of coatings for corrosion inhibition, the molecular structure of the substituents controls the free volume within the coating and can often govern the provided level of protection. For example, polymeric coatings with high levels of crystallinity and dense packing are more effective in reducing the diffusion of water than similar polymers with greater free volume.[1] Crystallinity and dense packing are especially important in extremely thin coatings that are required to protect small device features or in situations where heat transfer from the underlying metal is important. For polymeric systems of these dimensions, controlling the molecular-level structure within the coatings can be challenging.[2]

This chapter provides a molecular-level examination of the effect of crystallinity on the protection of copper and demonstrates that molecular films can offer performance advantages over thicker polymeric coatings. In this chapter, two comparisons are made. In the first, the protection provided by SAMs of similar thickness but different levels of crystallinity is compared. To perform this comparison, a mixed SAM—a monolayer that consists of more than one adsorbate—was formed on copper containing equimolar amounts of $C_{12}SH$ and $C_{22}SH$, and its coating resistance was measured against that of a SAM of similar thickness formed from $C_{17}SH$. In the second, the barrier properties of a 30 Å SAM formed from $C_{22}SH$ on copper are compared with those of a 200 ± 10 Å film of polystyrene (PS). Polymeric coatings such as polyimides[3] and polystyrene[4] have been used to protect metals against corrosion. The polymeric layer functions as a thick, hydrophobic barrier that impedes the transport of water and other corrosive agents. SAMs, although thinner, could provide some advantages over polymers in that they are chemically bound to the underlying metal and can be applied to a wide range of substrates of various geometry.

7.2. Results and Discussion

7.2.1. Comparison of SAMs with Similar Thickness but Different Crystallinity

To compare the protection provided by thin films of similar thickness but different levels of crystallinity, a mixed SAM was formed on copper from $C_{12}SH$ and $C_{22}SH$ containing equal

Mixed SAM of $C_{12}SH$ and $C_{22}SH$
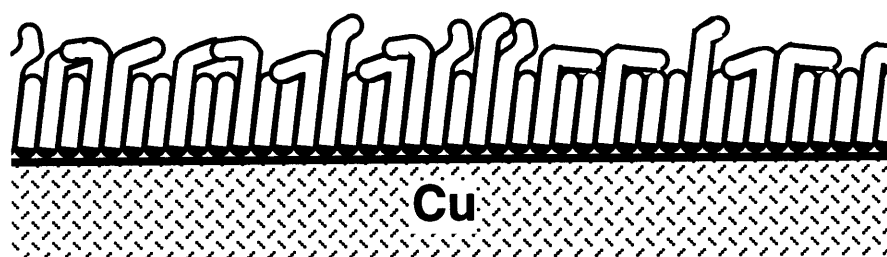
SAM of $C_{17}SH$
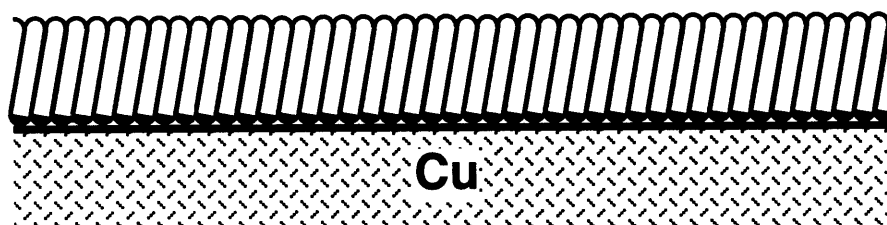
Figure 7.1. Schematic illustration of a mixed SAM containing both $C_{12}SH$ and $C_{22}SH$ ($\chi_{12} = \chi_{22} = 0.5$) and a SAM of $C_{17}SH$ on copper. The SAMs have similar thickness but different crystallinity.

surface mole fractions of the two components (Figure 7.1). The mixed SAM was designed to have the same effective thickness as the C_{17} SAM, but to be less crystalline, especially at the outermost few angstroms of the film. Previous results from IR spectroscopy for mixed SAMs formed from $C_{12}SH$ and $C_{22}SH$ on gold have demonstrated that the shorter thiol exists in a crystalline state with a low density of gauche conformers while the longer thiol contains both crystalline and liquid-like segments.[5] Specifically, the section of the longer adsorbate closer to the metal is crystalline while the terminal portion extending beyond the shorter alkanethiolate is disordered. Based on both wetting and IR data, the adsorbates within the SAM are well-mixed.

Grazing angle infrared spectroscopy allows determination of the structure and phase state of the hydrocarbon chains in the SAM. Figure 7.2 shows IR spectra for a SAM formed from $C_{17}SH$ and a mixed SAM composed of $C_{12}SH$ and $C_{22}SH$ ($\chi_{12} = 0.5$) on copper. For the C_{17} SAM, the $v_a(CH_2)$ and $v_s(CH_2)$ peaks are centered at 2918 and 2851 cm^{-1}, respectively, indicating primarily trans-extended hydrocarbon chains in a crystalline state. The $v_a(CH_3)$ and $v_s(CH_3)$ peaks are sharp and suggest a homogeneous arrangement of the methyl groups at the outer interface. For the mixed SAM, the methylene bands are more intense, broadened, and are shifted to higher wavenumber [$v_a(CH_2)$ at 2928 cm^{-1} and $v_s(CH_2)$ at 2855 cm^{-1}] while the methyl bands are poorly formed and broadened in comparison to those for the C_{17} SAM. These differences in the spectra are consistent with a heterogeneous film for the mixed SAM in which the longer C_{22}-chains are well-mixed on the surface and islanding is minimized,[6] as discussed previously.[5] The portion of these longer chains that extends above the shorter C_{12}-component is highly canted on average with the terminal methyl groups in a heterogeneous environment (Figure 7.1a).

Electrochemical impedance spectroscopy (EIS) enables determination of the resistance that SAMs provide against the transport of aqueous ions. Figure 7.3 displays EIS spectra in the form of Bode plots for SAMs formed from $C_{12}SH$, $C_{17}SH$, and $C_{22}SH$ and a mixed SAM composed of $C_{12}SH$ and $C_{22}SH$ ($\chi_{12} = 0.5$). At high frequencies, the solution resistance dominates the impedance and the impedance magnitude exhibits a slope of zero. In the intermediate frequency regime, the capacitance of the films governs the response, and log |Z| increases linearly (slope of 1) as log frequency is decreased for all SAMs. At low frequencies, the plateaus in |Z| for both the C_{12} film and the mixed SAM are consistent with the onset of ionic penetration into the monolayer and correspond to the resistances (R_c) that the SAMs provide against the diffusion of these ions. For copper protected by $C_{17}SH$ and $C_{22}SH$, the time constant for ionic penetration into the coating is sufficiently large that no resistive plateau is observed.

The spectra in Figure 7.3 can be fit with an equivalent circuit model that consists of a solution resistance in series with a parallel combination of coating resistance and coating capacitance (Figure 4.1a); Table 7.1 shows the values of these components for various SAMs in
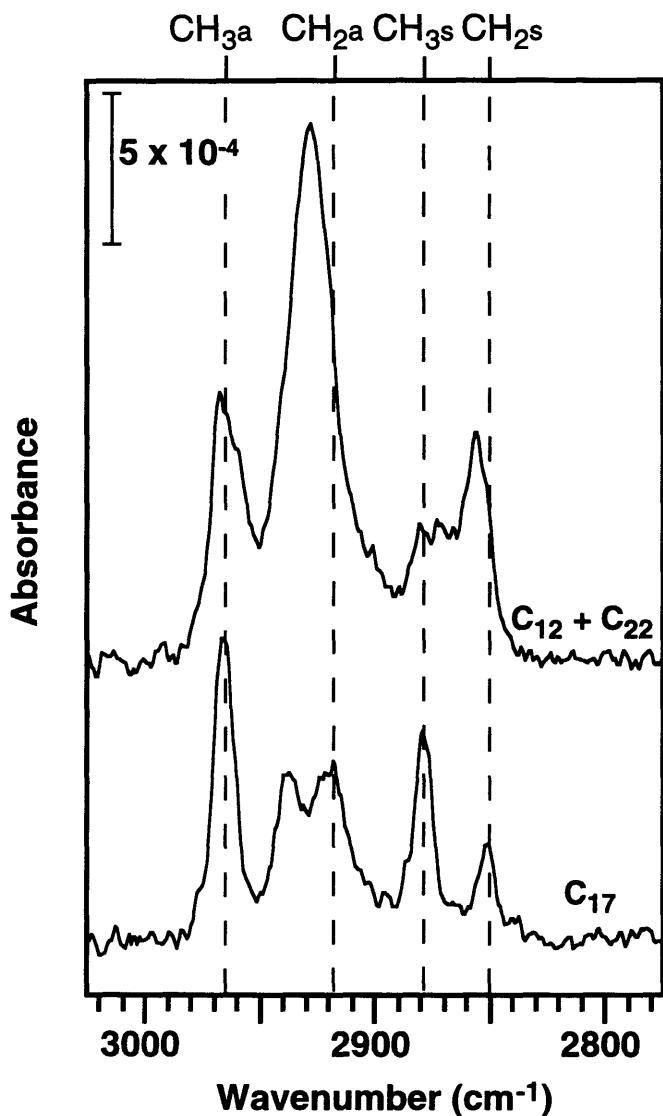
Figure 7.2. Grazing angle polarized infrared spectra of the C-H stretching region for a SAM formed from $C_{17}SH$ and a mixed SAM containing $C_{12}SH$ and $C_{22}SH$ ($\chi_{12} = \chi_{22} = 0.5$) on copper. The dashed lines indicate the peak positions of the primary modes for a trans-extended monolayer with no gauche defects: $\nu_a(CH_3) = 2965$ cm^{-1}, $\nu_a(CH_2) = 2918$ cm^{-1}, $\nu_s(CH_3) = 2879$ cm^{-1}, and $\nu_s(CH_2) = 2851$ cm^{-1}.
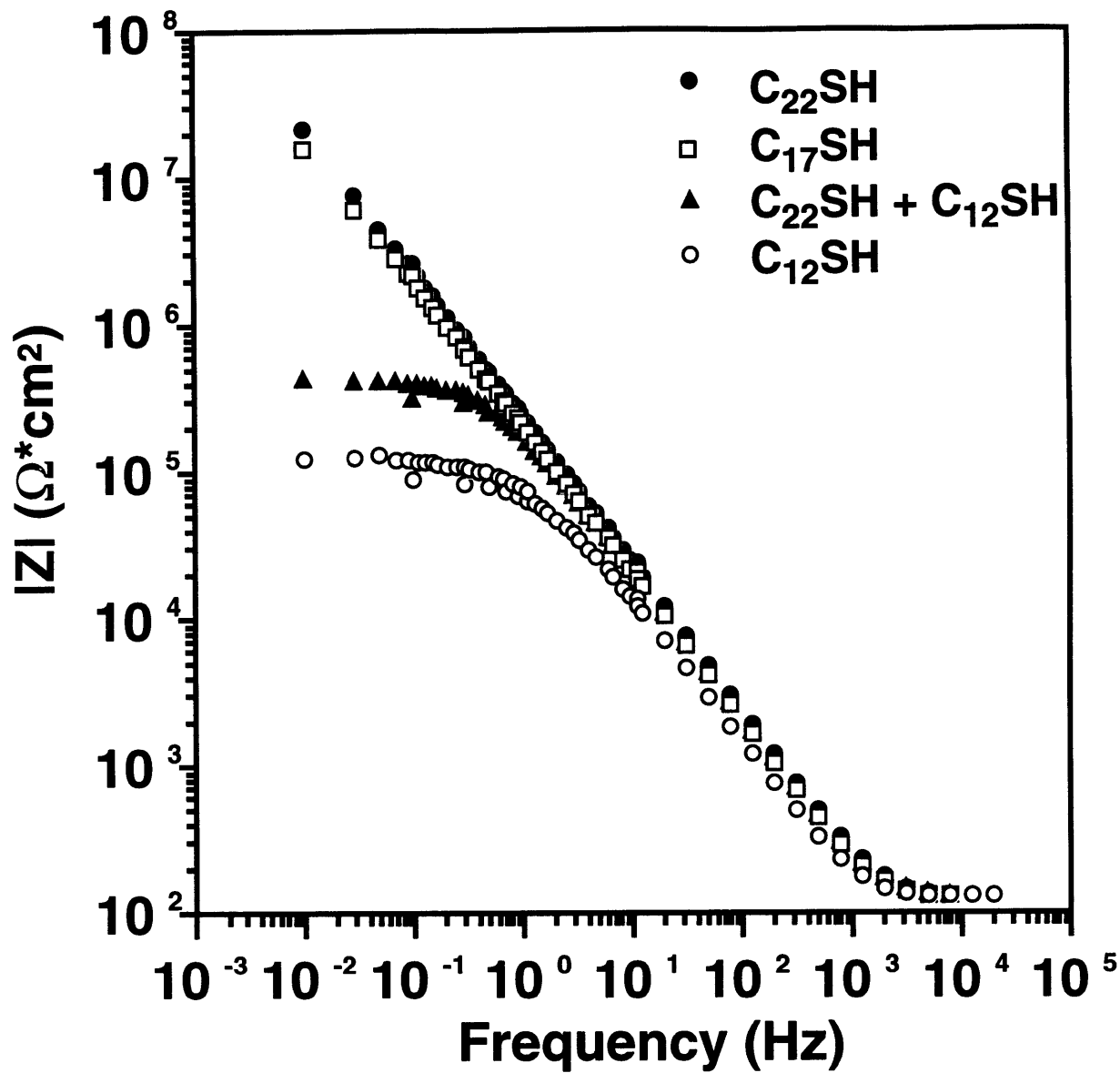
Figure 7.3. Bode magnitude plots for copper protected with SAMs of C_nSH (n = 12, 17, 22) and a mixed SAM of $C_{12}SH$ and $C_{22}SH$ ($\chi_{12} = \chi_{22} = 0.5$) in oxygenated 0.050 M Na_2SO_4.

Figure 7.3. As previously demonstrated in Figures 4.3 and 4.5 for a series of n-alkanethiolate SAMs on copper, the coating capacitances decrease while coating resistances increase as the chain length of the adsorbate is increased. The capacitances of the mixed SAM and the C_{17} SAM are approximately the same, indicating similar effective thicknesses; nevertheless, the coating resistance of the liquid-like mixed SAM is ~80 times smaller than for the crystalline C_{17} SAM. In comparison to the C_{12} SAM, the mixed SAM provides only modest improvement in coating resistance while the C_{17} SAM offers a ~250-fold enhancement. These results indicate that the degree of film crystallinity, which has been varied by the use of mixed SAMs, is an important factor in limiting the transport of corrosive species through SAMs.

Table 7.1. Coating capacitances (C_c) and resistances (R_c) determined from Figure 7.3 for SAMs on copper in oxygenated, 0.050 M Na_2SO_4(aq).[a]

Adsorbate(s)	C_c ($\mu F/cm^2$)	R_c ($M\Omega \cdot cm^2$)
$C_{12}SH$	1.0	0.11
$C_{12}SH + C_{22}SH$ (1:1)	0.77	0.38
$C_{17}SH$	0.78	29
$C_{22}SH$	0.52	48

[a] Values reported are ±5% for capacitances and ±10% for resistances.

7.2.2. Comparison of SAMs with a Thicker Polymeric Coating

In the second study to assess the importance of crystallinity on the protective properties of coatings, the barrier properties of a 30-Å SAM formed from $C_{22}SH$ on copper were compared with those of a 200 ± 10 Å polystyrene (PS) film, as shown schematically in Figure 7.4. Despite its molecular dimension, the densely packed nature of the SAM could provide performance advantages over thicker polymeric coatings. For this study, PS was chosen because it resists the transport of water, it can be easily spin-coated (unlike polyethylene),[7] and it does not pack as densely as a SAM. Here, the PS samples were prepared by spin-coating onto C_8SH-coated copper; the purpose of the SAM-primer was to improve adhesion between PS and copper and protect copper from oxidation while handling in air. Coating resistances for PS deposited directly onto copper were two orders of magnitude lower than those deposited onto the C_8-SAM. AFM images of the PS films revealed a complete film with no evidence of defects.

Figure 7.5 shows EIS spectra for SAMs on copper formed from C_8SH—both with and without a 200 Å over-layer of PS—and $C_{22}SH$. At intermediate frequencies, the greater |Z| exhibited by the PS + C_8 film is a result of its lower capacitance and increased thickness. At low

119
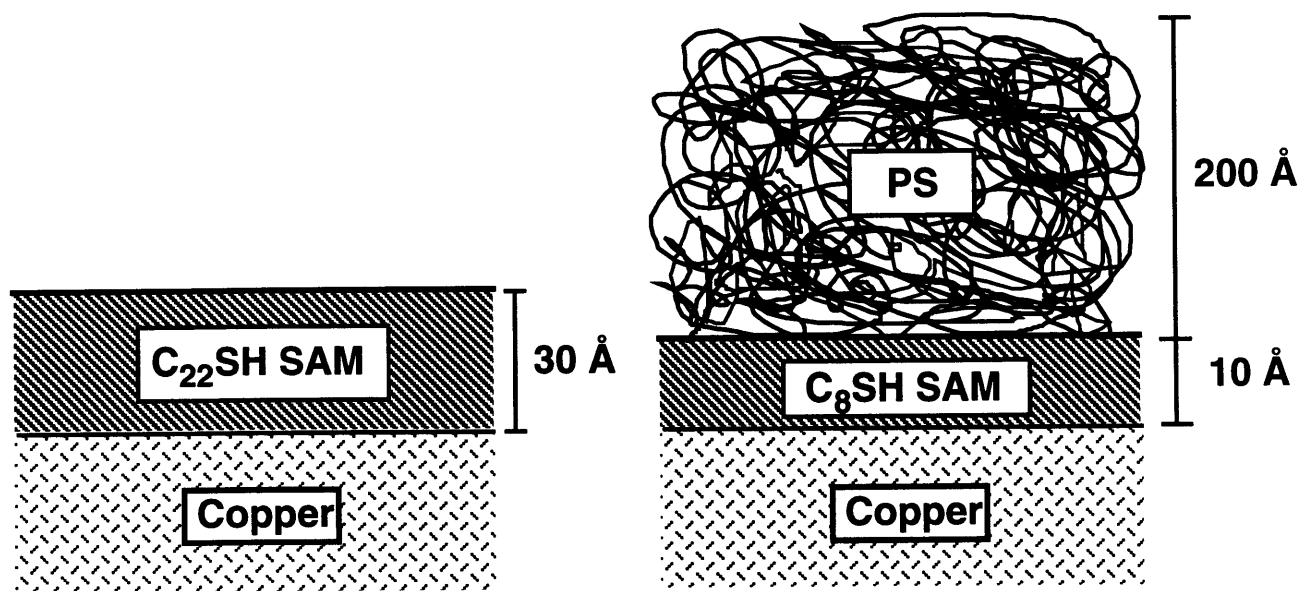
Figure 7.4. Schematic illustration of a SAM formed from $C_{22}SH$ on copper and a 200-Å PS film deposited onto a C_8SH-SAM.
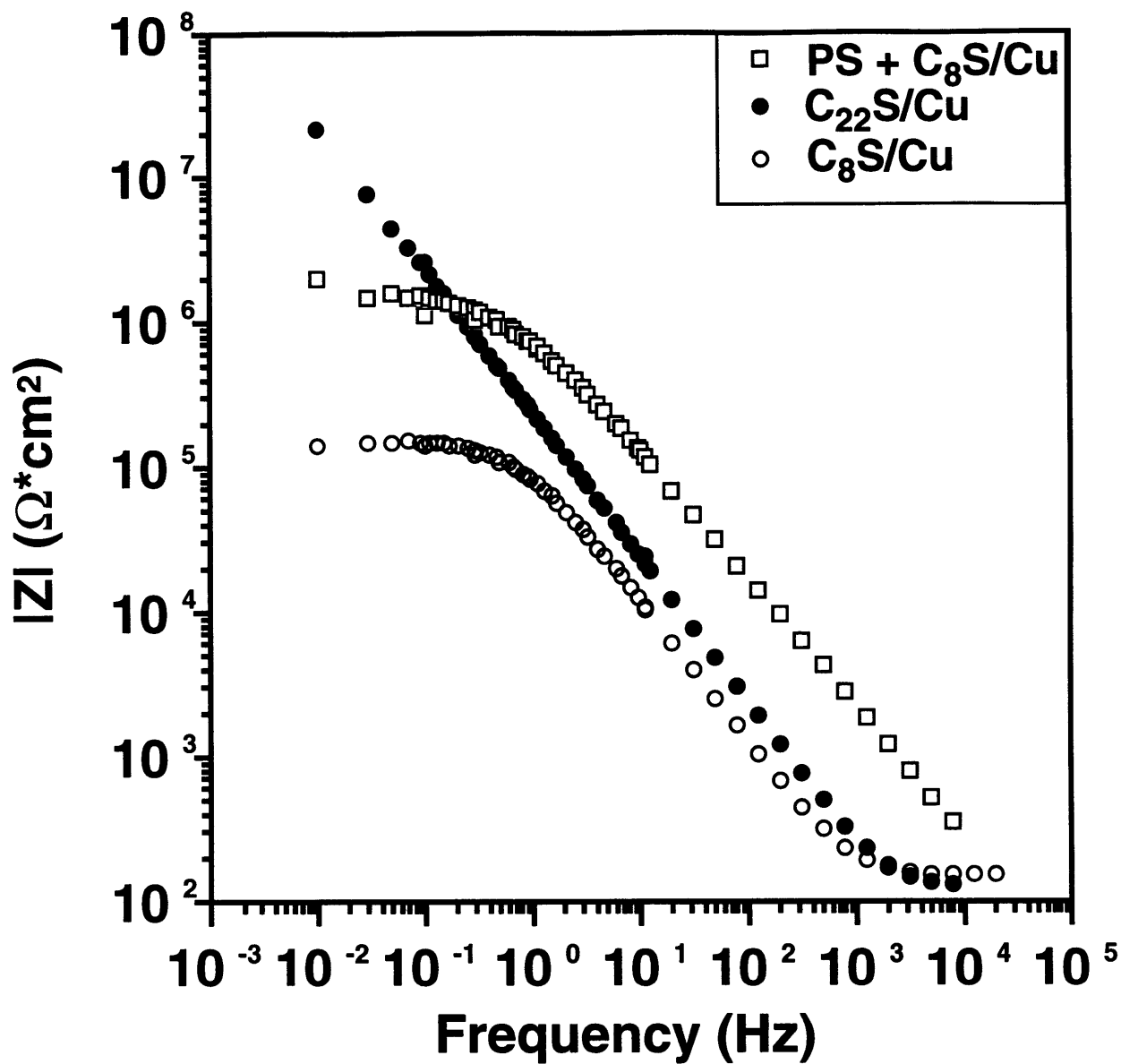
Figure 7.5. Bode magnitude plots for copper protected with SAMs of C_8SH—both with and without a 200 Å overlayer of PS—and $C_{22}SH$ in oxygenated 0.050 M Na_2SO_4.

frequencies, the PS + C_8 film exhibits a resistive plateau that is an order of magnitude greater than that for the C_8 SAM alone. Nevertheless, the 200 Å PS + C_8 coating is still far less protective than a 30 Å SAM formed from $C_{22}SH$ that shows no indication of ionic penetration at frequencies down to 0.01 Hz. Resistances for coatings derived from C_8SH, PS + C_8SH, and $C_{22}SH$ are 0.12, 1.1, and 48 MΩ•cm^2, respectively. For each angstrom of coating thickness, the C_{22} SAM provides 1.6 MΩ•cm^2 of coating resistance while PS provides only 5 x 10^{-3} MΩ•cm^2. These results illustrate the importance of achieving a densely packed, crystalline coating to provide a greater barrier against the transport of corrosive species. In comparison to polymeric films, SAMs provide a more flexible system with a greater ease of processing for forming crystalline barrier films on copper as their formation is the result of a simple chemisorption process. The self-assembly strategy offers a promising method for producing thin, adherent organic coatings with improved intrinsic barrier properties over polymer films.

7.3. Experimental

The experimental details of preparing SAMs on n-alkanethiols on copper (Chapter 3) and the characterization of these films with XPS (Chapter 3), IR spectroscopy (Chapter 4), and EIS (Chapter 4) have been discussed in previous chapters. Mixed SAMs of $C_{12}SH$ and $C_{22}SH$ (χ_{12}^{surf} = 0.5) were prepared by immersing freshly evaporated copper into an isooctane solution containing $C_{12}SH$ (χ_{12}^{soln} = 0.45) and $C_{22}SH$ (χ_{22}^{soln} = 0.55) for 1 h. The samples were removed from solution, rinsed with isooctane and ethanol, and dried in a stream of nitrogen. The surface mole fraction of the C_{12}-component in the mixed SAM (χ_{12}^{surf}) was determined by measuring the intensity of $Cu(2p_{3/2})$ photoelectrons from the underlying metal (I_{Cu}^{mixed}) with x-ray photoelectron spectroscopy and applying the following equation:

$$\chi_{12}^{surf} = \frac{\ln I_{Cu}^{mixed} - \ln I_{Cu}^{22}}{\ln I_{Cu}^{12} - \ln I_{Cu}^{22}} \qquad (1)$$

where I_{Cu}^{12} and I_{Cu}^{22} are the intensities of $Cu(2p_{3/2})$ photoelectrons for copper coated with SAMs of $C_{12}SH$ and $C_{22}SH$, respectively. I_{Cu}^{mixed} was compared with the $Cu(2p_{3/2})$ intensity for a SAM of $C_{17}SH$ on copper to make certain that the thickness of the mixed SAM was not less than that for the C_{17} SAM.

Polystyrene films were prepared by spin coating from a 0.4 wt% solution of polystyrene in THF onto Cu/SC_8 at 7000 rpm for 60 s. As noted by Stange et al.,[7] the concentration of PS used here is sufficient to achieve a complete film. AFM images of the PS surfaces indicated complete films on the various copper substrates. Some PS samples were heated at 50 °C for 30 min to

122

remove residual solvent and then cured at 100 °C for 60 min. Curing did not significantly change the impedance properties of the PS films.

The thicknesses of the PS films supported on C_8S/Cu were determined using a Gaertner L116A automatic ellipsometer equipped with a He-Ne laser ($\lambda = 6328$ Å) at an incident angle of 70°. The refractive index for the PS film was assumed to be 1.46. Baseline values for these films were measured on copper that was modified by a SAM of C_8SH. The reported thicknesses are the average of at least three samples where each sample was characterized by ellipsometry at three different locations on its surface.

7.4. References and Footnotes

1) Nenov, K. *Impedance Spectroscopy Study of the Water Uptake and Long-Term Degradation of Immersed Polyimide Coatings*; Ph.D. Thesis; Materials Science and Engineering; Massachusetts Institute of Technology, 1994.

2) Whitesides, G. M. *Chimia* **1990**, *44*, 310-311.

3) Bellucci, F.; Kloppers, M.; Latanision, R. M. *J. Electrochem. Soc.* **1991**, *138*, 40-48.

4) Kurbanova, R. A.; Mirzaoglu, R.; Kurbanov, S.; Karatas, I.; Pamuk, V.; Ozcan, E.; Okudan, A.; Guler, E. *J. Adhes. Sci. Tech.* **1997**, *11*, 105-112.

5) Laibinis, P. E.; Nuzzo, R. G.; Whitesides, G. M. *J. Phys. Chem.* **1992**, *96*, 5097-5105.

6) The spectrum for an islanded SAM of C_{12}/C_{22} would appear similar to that for the C_{17} SAM except for slight differences in the intensity (but not the position) of the $v(CH_2)$ modes.

7) Stange, T. G.; Mathew, R.; Evans, D. F.; Hendrickson, W. A. *Langmuir* **1992**, *8*, 920-926.

Part II. Self-Assembled Monolayers of Alkanethiols on Gold Modified by Underpotential Deposition of Silver or Copper

Chapter 8. Introduction and General Properties

8.1. Background

Advances in materials chemistry rely on the ability to tailor the structure and composition within the bulk and at interfaces at the nanoscopic level.[1] Indeed, the ability to generate systems with higher levels of organization and structural complexity is a focus of many areas of current research. Supramolecular assemblies,[2] self-assembled structures,[3] heteroelement composites,[4] and bimetallic catalysts[5] are examples where molecular (or atomic-scale) engineering has produced species with novel architectures, synthetic flexibility, and tailored properties.

At metal surfaces, two strategies—the formation of self-assembled monolayers (SAMs)[6] and the process of underpotential deposition (upd)[7]—have provided useful means for functionalizing the surface and tailoring its properties. These methods functionalize the surface with a highly organized single layer of material, where the composition of the layer is readily controlled. The difference between these methods is that the self-assembly method produces a thin organic layer on the metal surface and the upd procedure coats the metal surface with a one-atom-thick layer of a dissimilar metal.

Self-assembled monolayers (SAMs) form by the spontaneous adsorption of organic molecules onto a metal or metal oxide surface.[6] Various systems are presently available, with the assembly of n-alkanethiols onto copper,[8,9] silver,[8-12] and (particularly) gold[6,8,13] being the most investigated. On these metals, the thiols form a densely packed, oriented monolayer and the hydrocarbon chains pack in a trans-zig-zag-extended structure.[8,10] The assemblies are the product of strong metal-sulfur interactions that are also responsible for the robust nature of the SAM in liquid and vacuum environments. A notable feature of these assemblies is their ability to accommodate a wide range of polar and nonpolar functionalities in the tail group of the adsorbate.[9,13] This flexibility in their synthesis has allowed the formation of tailored organic surfaces for studies of wetting,[9,12,14] adhesion,[15] biocompatibility,[16] friction,[17] and interfacial electron transfer.[18]

The SAMs on copper, silver, and gold surfaces differ in structure: on gold, the axis of the hydrocarbon chain tilts ~30° from the surface normal (~5.0-Å spacing),[6,8] whereas it tilts ~13° from the surface normal on silver and copper (~4.7-Å spacing).[6,8,10,11] These differences in adsorbate packing density are a result of the bonding characteristics between the metal surface and the ligating

sulfur atoms, particularly their tendency to occupy specific sites on the metal surface.[6] Efforts for controlling the molecular packing density within SAMs have relied on the use of adsorbates that contain bulky substituents,[19] rigid architectures,[20] or multiple ligating functionalities[21] and often require lengthy syntheses. The development of methods that can manipulate the surface chemistry of the substrate—particularly at the sub-monolayer level—may offer a more flexible, synthetically simpler strategy for controlling the packing density, structure, and properties of these adsorbed films.

Underpotential deposition is an electrochemical process whereby a single metal adlayer is electroplated onto a dissimilar metal.[7,23-26] The process is driven by the formation of substrate-adatom interactions that are stronger than the adatom-adatom interactions that form during bulk electrodeposition. This difference in interaction allows easy preparation of adlayers with coverages no greater than a monolayer. Many substrate/adlayer combinations are known, and they have been characterized by a wide range of techniques, including surface scattering and diffraction methods (LEED, SEXAFS, etc.),[23,24] Auger and x-ray photoelectron spectroscopies,[23] and more recently by various scanning probe microscopies.[7,25] In many cases, the upd layer forms a highly ordered, epitaxial layer on the underlying substrate and the coverage of the upd layer and its structure are dictated by factors that limit access of the predeposited adlayer metal ions to the electrode surface.[27] The flexibility and control afforded by the upd technique allows access to a broad hierarchy of well-defined surface architectures. Of the various substrates that can be used for underpotential deposition, gold has been the most popular due to its general inertness, its resistance towards chemical oxidation, and the large number of elements that can form a upd layer on it.[28]

Self-assembled monolayers and underpotentally deposited layers share the common feature that they can form highly organized adlayers on the surface of an underlying material. To date, these highly structured monolayer-based systems, despite their functional similarities and analytical reliance on a common set of surface techniques (XPS, Auger, LEED, STM, AFM, etc), have remained separate areas of research. This work aims to determine whether the synthetic flexibility afforded by these two methods could be used together to generate a new class of self-assembled structures. In this chapter, polycrystalline gold films have been used as these substrates since they are widely used in the SAMs area and have direct analogs in device fabrication.[29] Copper and silver were selected for the upd layers as these systems have been widely investigated on both crystalline[7,25] and polycrystalline[7,26] gold substrates, and a wide variety of alkanethiols are known to form SAMs on surfaces of these bulk metals.[9] The result of this work is that underpotentially deposited films of copper and silver on polycrystalline gold substrates provide a new type of substrate for the self-assembly of adsorbed alkanethiolate monolayers. These substrates offer the high degree of synthetic flexibility associated with the assembly of thiols onto gold surfaces while providing a higher level of structural hierarchy to the assemblage and the ability to produce

126

supported SAMs with properties that are superior to those formed on gold.[30] The strategies employed in this chapter should be generalizable for many of the metals that can be underpotentially deposited on gold[7,28] and other substrates.[7]

8.2. General Properties of SAMs on Upd-Modified Gold

8.2.1. Au/upd/SAM Formation

In a two-step procedure, a polycrystalline gold substrate was functionalized first with a submonolayer amount of copper or silver (upd) and then a self-assembled organic monolayer to form the structures schematically illustrated in Figure 8.1;[29,30] all manipulations of the gold substrate were conducted in the laboratory ambient. Evaporated films of gold supported on silicon supports were functionalized with a layer of copper or silver atoms in a sulfuric acid solution (aq) of copper or silver sulfate, respectively; cyclic voltammograms for the underpotential deposition of silver and copper onto gold are shown in Figure 8.2. The gold substrates were first electrochemically cycled in these solutions as both a cleaning procedure and a means to provide information about the upd process on the substrate. During the second cathodic scan of this cycle, the potential was held just negative of the upd peak. The resulting derivatized gold substrates were emersed from the electrochemical cell under potential control, rinsed with ethanol, blown dry in a stream of nitrogen, and transferred through air to a 1 mM solution of the alkanethiol. Upon removal from the adsorbate solution, the slides were rinsed with fresh solvent and blown dry in a stream of nitrogen prior to characterization. Adsorption times between 5 min and 1 day in the thiol-containing solutions produced SAMs with similar properties; an adsorption time of 40 min was typically used for the systems reported in this chapter.

8.2.2. Characterization by X-ray Photoelectron Spectroscopy (XPS)

Table 8.1 displays the results from x-ray photoelectron spectroscopy (XPS) for the upd layers of silver and copper deposited onto the polycrystalline gold films and after their exposure to octadecanethiol. The untreated upd adlayers exhibit binding energies that are lower than those for the corresponding bulk metals due to their electronic equilibration with the underlying gold substrate.[31] The coverages of the copper and silver adlayers on the gold surface were sub-monolayer, based on coulometric[32] and XPS results, and exhibited good reproducibility across independent preparations. Upon assembly of the alkanethiol, XPS revealed that the copper and

127
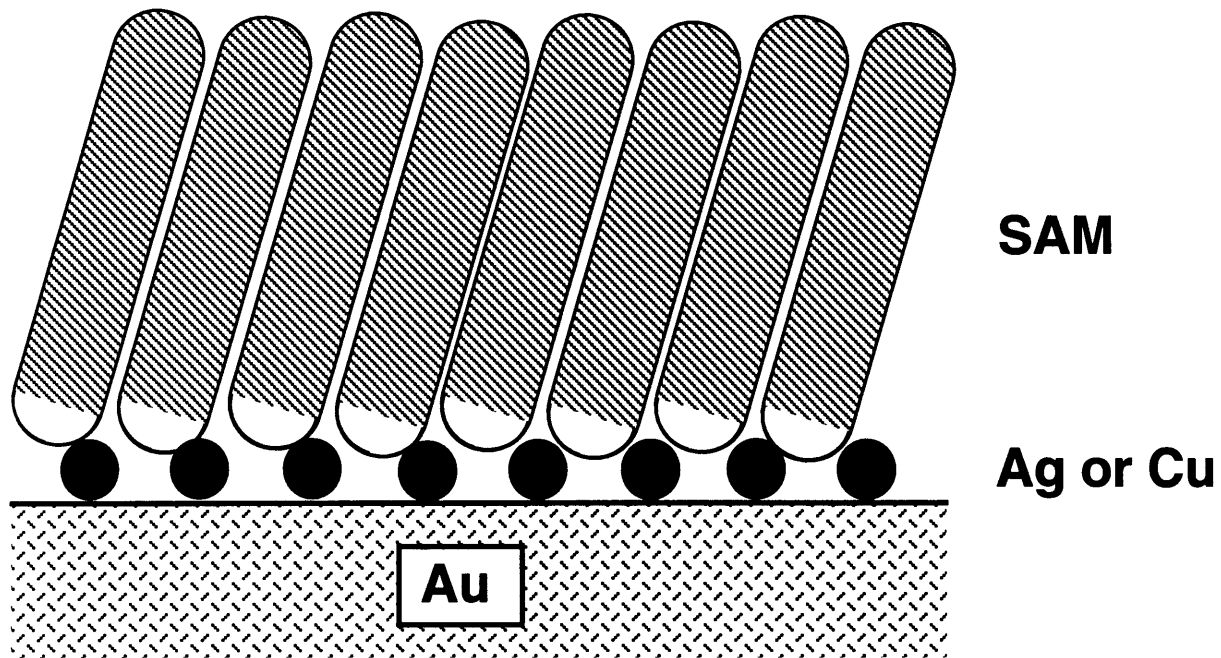
Figure 8.1. Schematic illustration of a gold/silver or copper (upd)/SAM assembly.
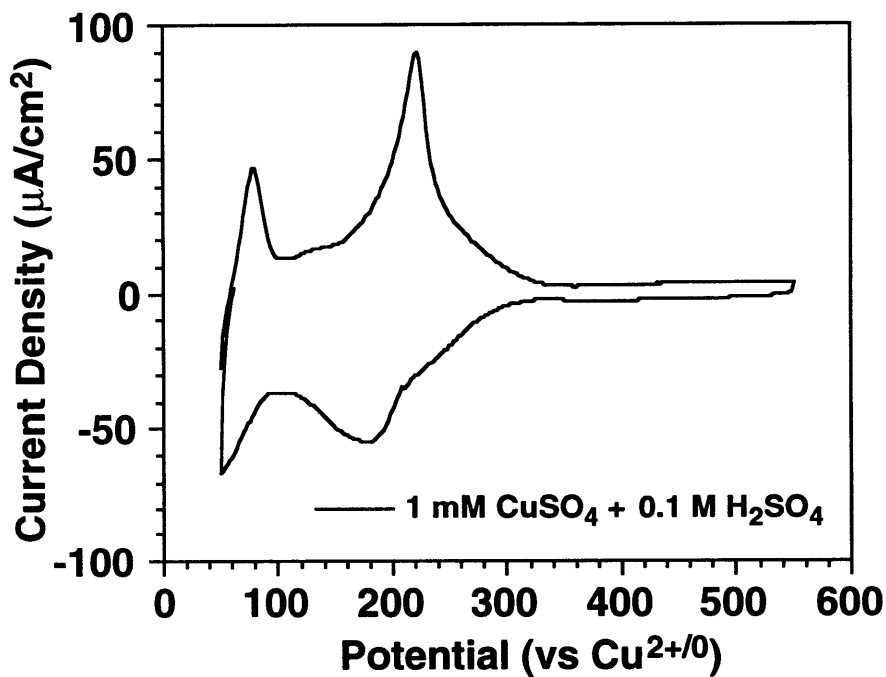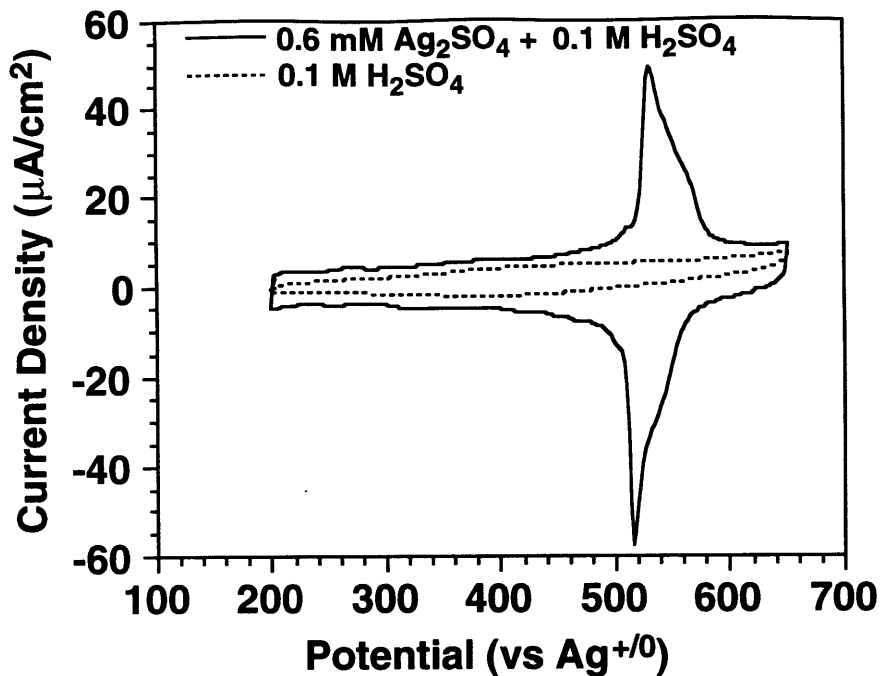
Figure 8.2. Cyclic voltammograms for supported polycrystalline gold films in 0.1 M H_2SO_4: 0.6 mM Ag_2SO_4 (upper panel) and 1 mM $CuSO_4$ (lower panel). For comparison, the upper panel also contains a cyclic voltammogram for the bare gold substrate in just 0.1 M H_2SO_4 (aq).

silver upd layers survive the assembly of the organic layer. The coverages of the upd layers exhibited little (or no) change upon adsorption of the thiol (Table 8.1), and only slight decreases in coverage (<10%) were observed during continued exposure to the thiol solution (5 days). These observations are in contrast with reports that the assembly of alkanethiols onto gold occurs with etching of the metal substrate.[33] The lack of change in the coverage of the upd layer (as derived from the relative XPS intensities of gold and copper or silver—see eq 8.1 in Section 8.3.5) during the assembly of the SAM suggests that the upd layers are not readily displaced by the thiol treatment, they remain at the gold/sulfur interface, and the upd metals do not diffuse into the gold substrate under these experimental conditions.

Upon adsorption of the thiol onto the upd substrates, the primary peaks of the adlayer elements shift to higher binding energies, and the $S(2p_{3/2})$ peak occurs at 162 eV indicating the presence of an adsorbed thiolate;[6,8] the binding energy data suggest that the adsorption of the thiol involves an oxidative-addition process at the upd metal surface. Such mechanisms have been suggested for the assembly of thiols onto copper, silver, and gold surfaces;[6] however, the presence of the oxidized metal species produced by this process could not be verified for these systems as its signals could not be distinguished from those due to the bulk metal.

Figures 8.3a and b show XPS survey spectra for Au/Ag(upd) and Au/Cu(upd) substrates, respectively, that were derivatized for 40 min with C_8SH (1 mM, ethanol). In both spectra, peaks indicative of gold, silver or copper, carbon, and sulfur species reveal that the expected elements are present. The XPS spectra for the Au/Ag(upd)/SC$_8$ sample exhibited no signals due to oxygen (Figure 8.3a). As the unfunctionalized Au/Ag(upd) substrate was exposed to air prior to adsorption of the thiol, the absence of oxygen signals suggests that the Au/Ag(upd) substrate is not prone to oxidation in air—the redox potential of the Ag(upd) layer is ~520 mV positive of $Ag^{+/0}$— or that the thiol reduces any oxidized species that do form. On the Au/Cu(upd) substrate, signals due to oxygen were regularly detected by XPS (Figure 8.3b) as well as trace signals in the Cu(2p) spectral region due to Cu(II) species.[8,9] The Au/Cu(upd) substrate is more prone to oxidation than the Au/Ag(upd) substrate; however, the properties of the resulting Au/Cu(upd)/SAMs were only moderately affected by the oxidation (noted by slightly larger hystereses in wetting, vide infra). The quality of the SAMs formed on the Au/Cu(upd) substrate formed in air were almost as good as those for SAMs formed on evaporated films of copper that were handled under anaerobic conditions[8] and superior to those for copper films handled in air.[34] In this latter case, the assembly produces poorly organized multilayers or low quality thin films.[34] Although the redox potential of the Au/Cu(upd) substrate is only ~100 mV positive of $Cu^{2+/0}$, the superior properties of this substrate in air to those of bulk copper probably reflect that oxidation on this substrate is limited to a maximum of one layer of copper.

Table 8.1. XPS Binding Energies and Coverages for Ag and Cu Adlayers on Au

Sample	Ag		Cu	
	Binding Energy (eV)[a]	Coverage[c]	Binding Energy (eV)[a]	Coverage[c]
bulk metal	368.0	-	932.0	-
Au/upd metal	367.4[b]	0.64	931.3[b]	0.56
Au/upd metal + $C_{18}H_{37}SH$	367.8[b]	0.59	931.8[b]	0.54

[a] Binding energies of Ag ($3d_{5/2}$) and Cu($2p_{3/2}$) peaks. [b] Binding energies referenced to Au($4f_{7/2}$) at 84.0 eV. [c] Coverages are ± 10%.
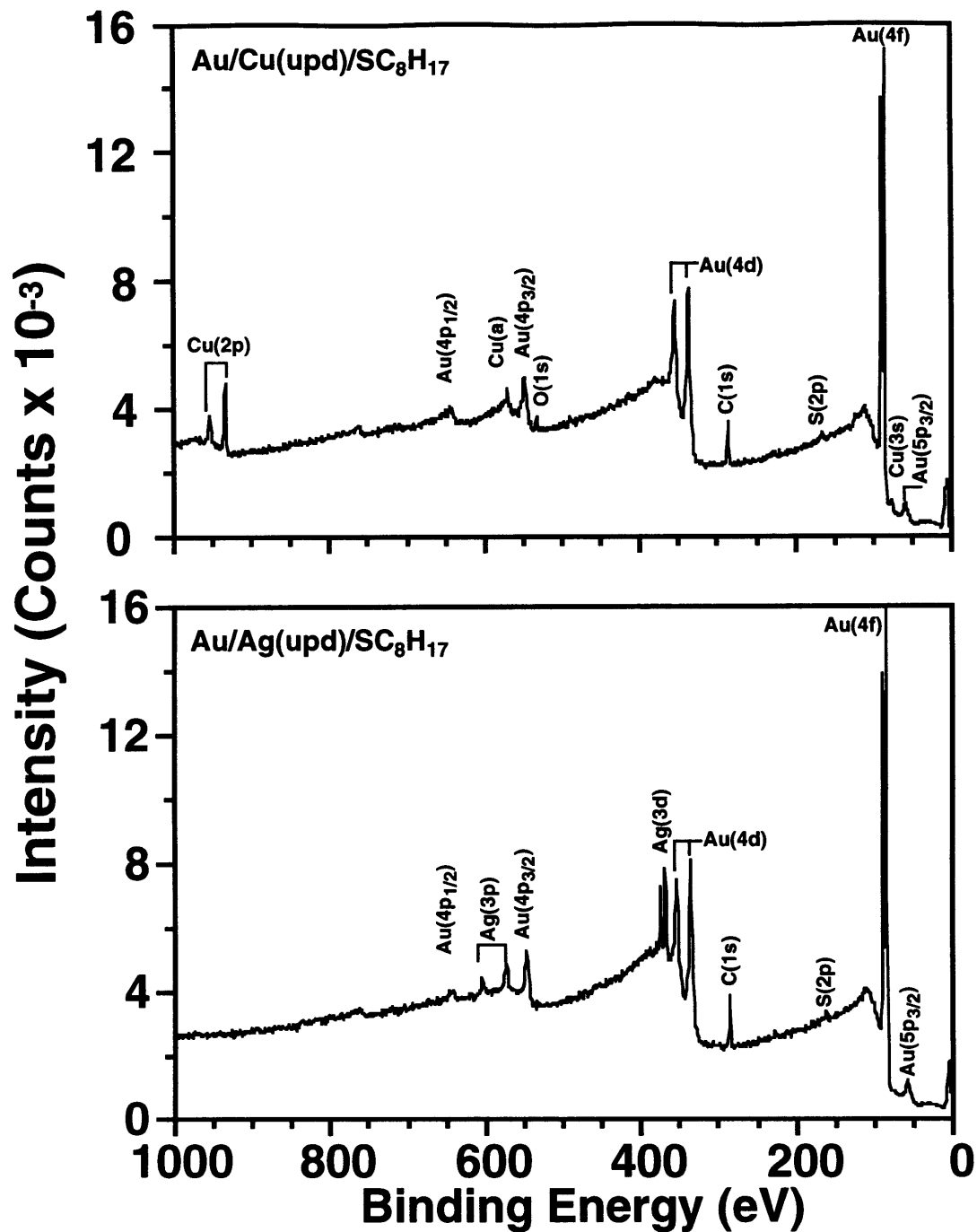
Figure 8.3. X-ray photoelectron spectra for Au/Ag(upd) and Au/Cu(upd) after derivatization with n-$C_8H_{17}SH$ in ethanol for 1 h. Surface coverages for the upd adlayers in related systems are given in Table 8.1.

8.2.3. Characterization by Ellipsometry and Wetting

The organic films formed from the assembly of alkanethiols onto copper and silver upd substrates exhibited properties similar to those produced on gold. For example, films formed on the copper and silver upd substrates and on gold using $C_{18}H_{37}SH$ had similar ellipsometric thicknesses (23 ± 3 Å, 23 ± 2 Å, and 21 ± 3 Å, respectively) and wettabilities (Table 8.2). The thickness of the SAM on the upd substrates could be varied by choice of adsorbate (Figure 8.4). The slope of the line in Figure 8.4 for silver upd samples is 1.4 Å/CH$_2$ and is comparable to the value for alkanethiols assembled onto bulk films of gold[13] and silver.[10a] Data with similar levels of reproducibility were obtained using copper upd substrates that also gave a slope of 1.4 Å/CH$_2$ (not shown). The ellipsometric data confirm that the alkanethiols form monolayer films on the silver and copper upd substrates.

Table 8.2 displays the wetting properties of SAMs prepared from alkanethiols that terminate in either polar or non-polar tail groups. The SAMs on the upd substrates exhibited wettabilities by water and hexadecane that were similar to those for SAMs formed from the same adsorbate on gold surfaces. This similarity indicated that the tail groups of the adsorbates were localized at the SAM/air(liquid) interface in a densely packed state. The wetting results indicate that the assembly on the silver and copper upd substrates can accommodate both polar and non-polar tail groups in the adsorbate and suggest that this system may have the synthetic flexibility associated with the thiols on gold system. Contact angle hystereses were comparable on the silver upd substrates and gold and slightly greater for SAMs on the copper upd substrates. The greater levels of hystereses on the copper upd substrates might reflect a greater sensitivity of the bare copper upd substrates to oxidation in air as less hysteresis was observed when the transfer time between the electrochemical cell and the adsorption solution was minimized. The level of hysteresis on the copper upd substrate is much lower than for assembly of these adsorbates onto freshly evaporated copper films that had been similarly exposed to air prior to monolayer assembly.[34]

The ability to form high and low energy organic surfaces on these substrates by selection of the tail group allows the generation of organic surfaces that span the range of wettability. Using 1 mM mixtures of $HS(CH_2)_{11}OH$ and $HS(CH_2)_{11}CH_3$, mixed SAMs were prepared on Au/Ag(upd) substrates that varied in surface composition between those for the pure SAMs. Figure 8.5 displays the wetting properties of the mixed SAMs and demonstrates the ability to tailor their composition and properties. The surface compositions of the mixed SAMs were determined from XPS by comparing the intensity of the O(1s) peak for the hydroxyl group to its intensity in a SAM

Table 8.2. Static wetting properties of water and hexadecane on films formed on gold and upd substrates.

	Contact Angles (advancing, receding; in degrees) [a]					
	Au		Au/Ag(upd)		Au/Cu(upd)	
Adsorbate	H_2O	HD	H_2O	HD	H_2O	HD
$HS(CH_2)_{11}OCH_2CF_2CF_3$	109, 102	69, 63	111, 104	71, 66	110, 103	73, 66
$HS(CH_2)_{17}CH_3$	111, 102	46, 41	113, 103	48, 42	112, 98	45, 35
$HS(CH_2)_{11}OCH_3$	81, 70	30, 20	80, 70	28, 18	81, 71	33, 22
$HS(CH_2)_{11}OH$	15, –	<5, –	17, –	<5, –	20, –	<5, –
$HS(CH_2)_{10}COOH$	<10, –	<5, –	<10,–	<5, –	<10, –	<5, –

[a] HD=hexadecane. A dash (–) indicates a receding angle for a contacting liquid that could not be removed from the surface. For these systems, $\theta_r \cong 0°$.
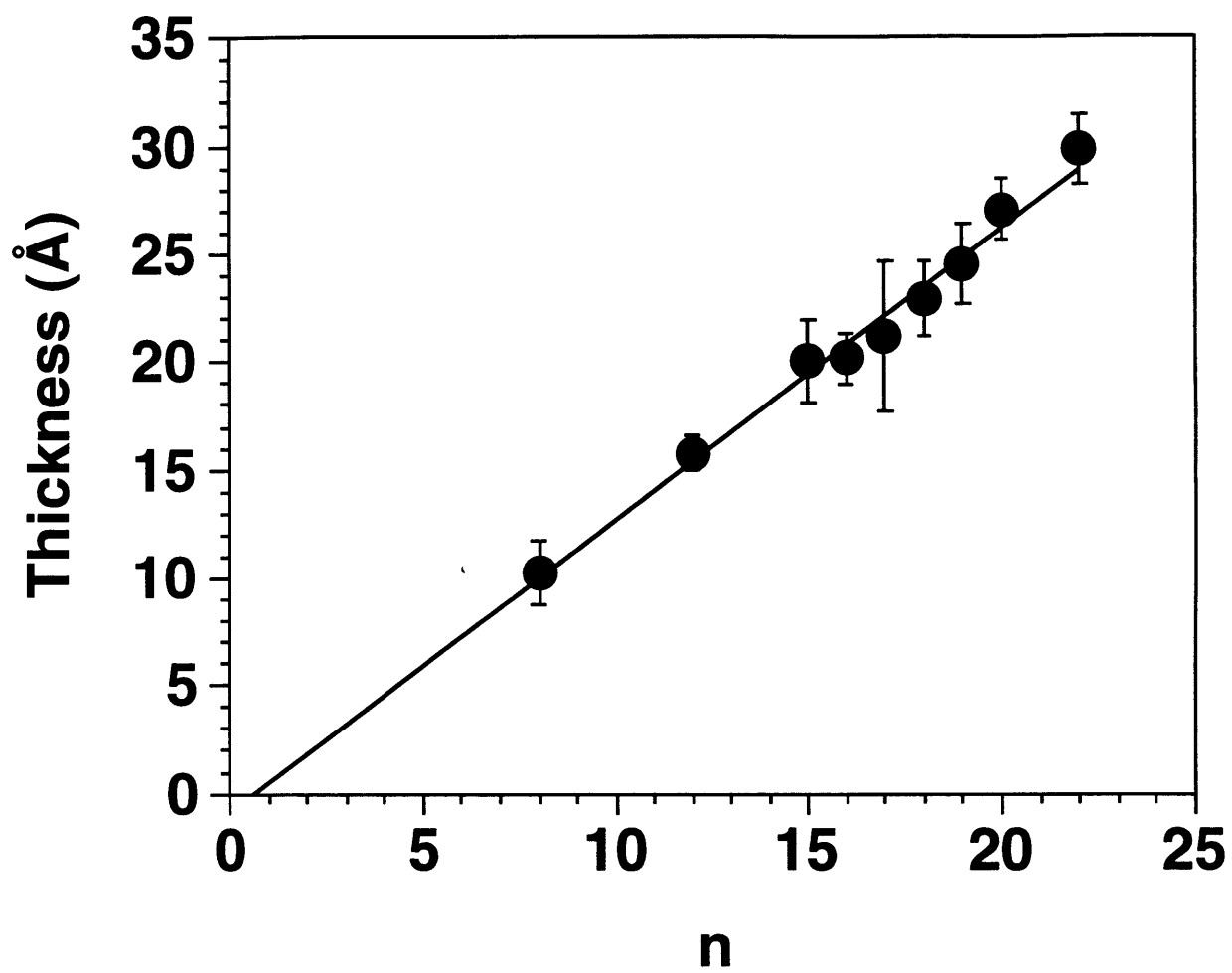
Figure 8.4. Ellipsometric thickness for SAMs of n-alkanethiols $(CH_3(CH_2)_{n-1}SH)$ adsorbed onto evaporated gold films containing an underpotentially deposited layer of silver. The line is a least-squares fit to the data and has a slope of 1.4 Å/CH$_2$. Thicknesses were calculated using a refractive index of 1.46.
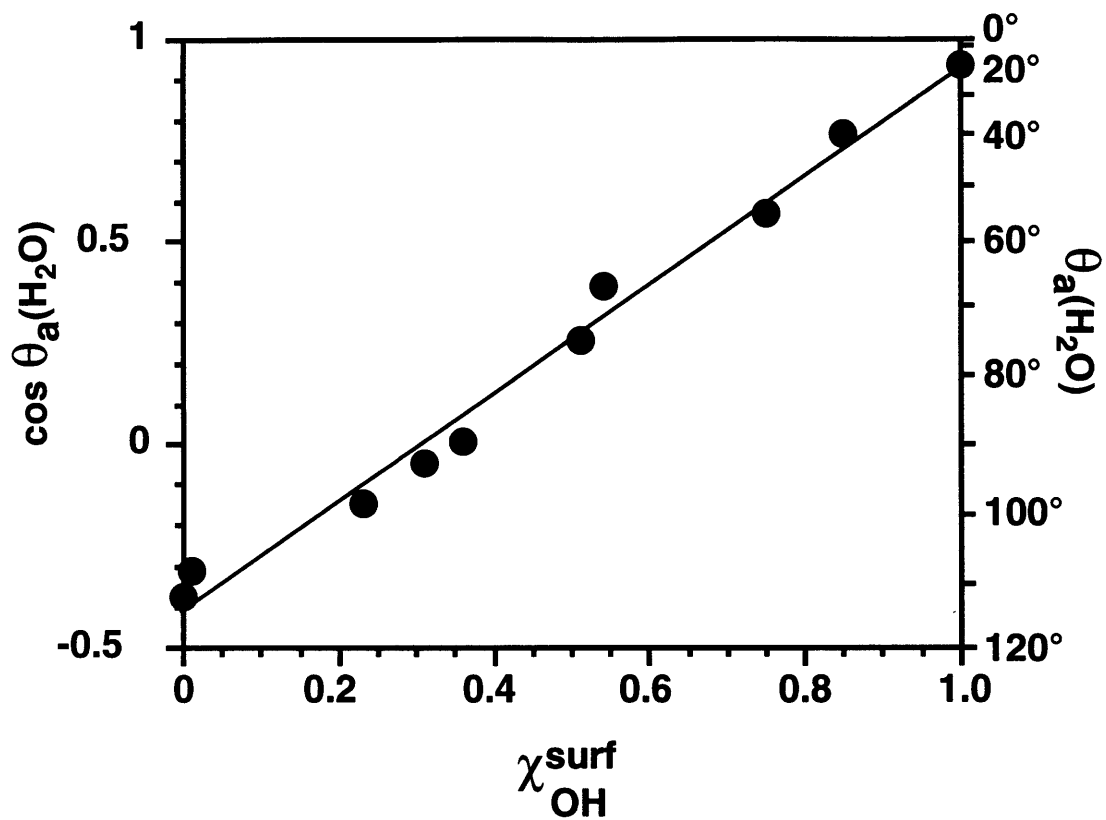
Figure 8.5. Advancing contact angles of water on mixed monolayers prepared from binary mixtures of $CH_3(CH_2)_{11}SH$ and $HO(CH_2)_{11}SH$ (1 mM total concentration in ethanol). The x-axis represents the mole fraction of the polar component on the surface, as determined by XPS.

derived from $HS(CH_2)_{11}OH$. In Figure 8.5, the relationship between wettability and surface composition on the upd substrates is the same as that observed using mixed SAMs of these adsorbates on evaporated films of copper, silver, and gold.[9]

8.2.4. Characterization by Reflectance Infrared Spectroscopy

Figure 8.6 displays reflectance infrared spectra for SAMs derived from octadecanethiol on Au, Ag, Au/Ag(upd), and Au/Cu(upd) substrates. In the upper three spectra of Figure 8.6, the asymmetric methylene peaks appeared at ~2918 cm^{-1}, indicative of a primarily trans-zig-zag extended hydrocarbon chain containing few gauche conformers.[35] The spectra demonstrate the ability to form highly crystalline monolayers by the assembly of alkanethiols onto these three substrates. For the various substrates, the intensities of the methylene peaks are greatest for SAMs on gold, the least intense for SAMs on silver, and intermediate for the upd substrates. The differences in intensity reflect different canted orientations for the polymethylene chains on these surfaces, with the tilts of the chains on upd substrates of silver and copper being intermediate (~20° from the surface normal) between those found for alkanethiolate SAMs on gold (~30°), silver (~13°), and copper (~13°).[6,8,10,11] The tilt of the hydrocarbon chain in SAMs is a result of the packing arrangement of the adsorbates on the metal surface, and the presence of the upd layer must alter the structural arrangement of the adsorbate on the upd surface from those on the parent metal surfaces (see Chapter 11).

On Au/Ag(upd), $v_a(CH_2)$ appears at 2918 cm^{-1}, suggesting that the hydrocarbon chains in the SAM are primarily trans-zig-zag extended and contain few gauche conformers. The structure of the adsorbed layer on the Au/Ag(upd) sample is distinct from those formed on the corresponding bulk metals as evidenced by the lower dichroic ratio [$v_a(CH_2)/v_s(CH_2)$] and less intense symmetric methyl peaks in its spectrum. These two features in the spectrum provide evidence that the SAM on the Au/Ag(upd) substrate has a structure that is not a composite of the structures that form on gold and silver.[36]

The SAMs formed on Au/Cu(upd) were less well defined, with $v_a(CH_2)$ appearing at 2921 cm^{-1}. This position suggests that the SAMs produced under these assembly conditions are structurally better ordered than SAMs formed on air-exposed copper, but include a higher degree of gauche defects within the SAM than on the Au/Ag(upd) substrate. As with the SAM on Au/Ag(upd), the $v_a(CH_2)$ peak had intermediate intensity to those for the octadecanethiolate SAMs on gold and copper. The greatest difference between the spectrum for the Au/Cu(upd) substrate and the other metals was that the dichroic ratio for the methylene absorption modes [$v_a(CH_2)/v_s(CH_2)$] was ~1 [vs. 1.5 on Au/Ag(upd) and 2 to 2.5 on copper, silver and gold]. These results are indicative of a different structure that forms on the Au/Cu(upd) surface.
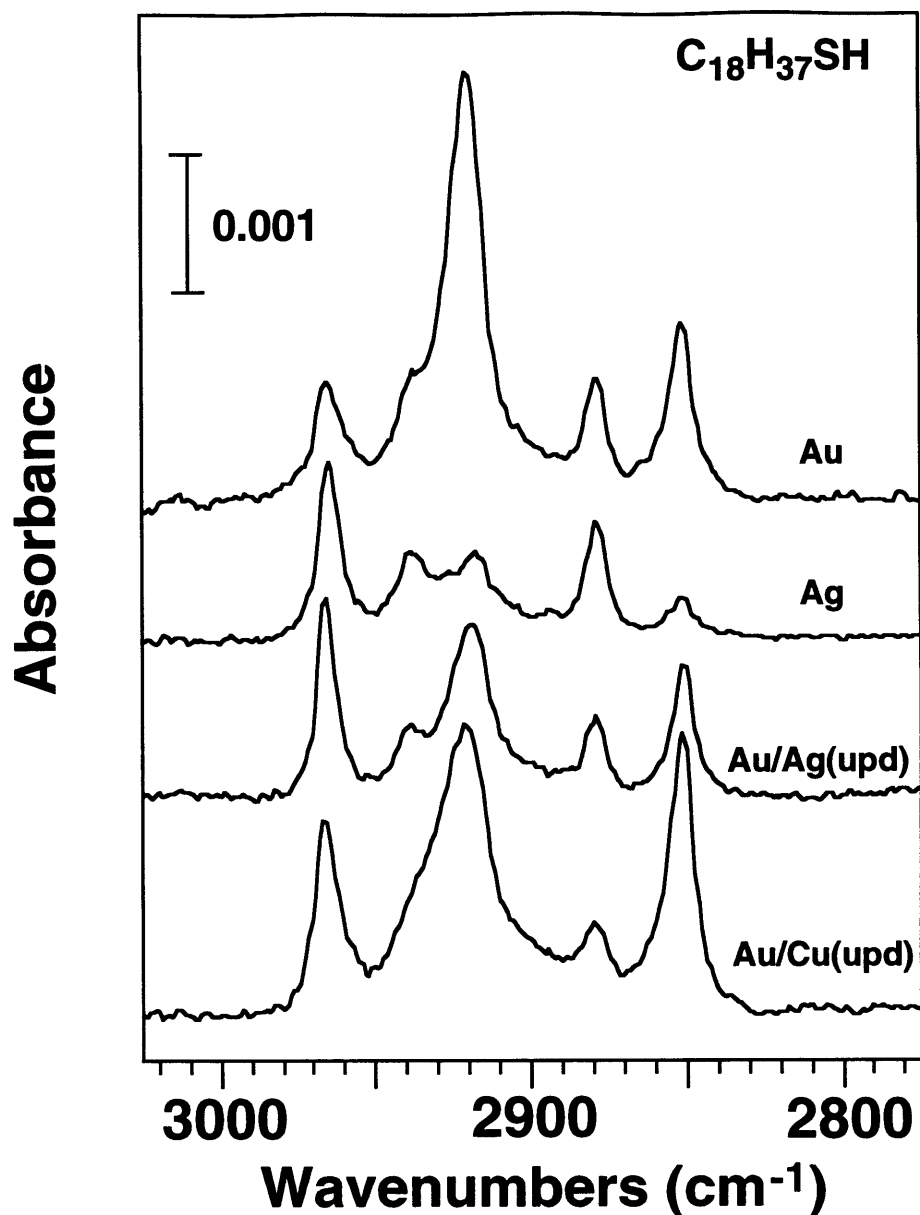
Figure 8.6. Grazing incidence polarized infrared spectra for SAMs of octadecanethiol adsorbed onto evaporated gold and silver surfaces and onto evaporated gold films that contain an underpotentially deposited layer of silver or copper. The approximate positions of the methylene modes are 2918 (asym) and 2850 (sym) cm^{-1}, and those for the methyl modes are 2964 (asym), 2935 (sym, Fermi resonance) and 2879 (sym) cm^{-1}. The spectra have been offset vertically for clarity.

In general, the use of upd layers may provide a means for controlling and manipulating the structure of SAMs. The relationships between the monolayer structure—crystallinity, canted orientation, chain twist, and packing density—and the composition and coverage of the upd layer in these two systems is reported in Chapter 11.

8.2.5. Electroactive SAMs

As the redox potential for the Au/Ag(upd) substrate is ~520 mV positive of $Ag^{+/0}$, this substrate offers useful applications as a substrate for the formation of electroactive SAMs. Figure 8.7 displays cyclic voltammograms for SAMs prepared by chemisorption of $FcCO(CH_2)_{10}SH$ (Fc = ferrocenyl) onto Au and Au/Ag(upd) substrates. The curves display the expected peaks corresponding to the oxidation of ferrocene and the reduction of ferrocenium, with the broadness of the peaks being comparable to that observed by others for SAMs of $FcCO_2(CH_2)_{11}SH$ and related adsorbates on gold.[37,38] The durability of the substrates modified with $FcCO(CH_2)_{10}SH$ is sufficiently great that routine electrochemical characterization is possible. The coverages obtained by coulometry for the ferrocenyl species were 4.3 and 4.5 x 10^{-10} (± 10 %) mol/cm^2 on Au/Ag(upd) and gold, respectively, and are comparable to those of prior studies for similar ferrocenyl-based adsorbates.[37,38] It is important to note that voltammetry for this monolayer cannot be performed on a bulk silver electrode at room temperature as the ferrocene$^{+/0}$ redox potential for this adsorbate is ~400 mV positive of that for silver oxidation and electrochemical cycling results in the anodization of silver and loss of the SAM.[39] XPS spectra for the SAM on the Au/Ag(upd) substrate both before and after electrochemical cycling displayed signals for silver and demonstrated that the Ag upd layer survives the assembly of the monolayer and the redox cycling of the surface-attached ferrocene couple. By depositing the silver layer on gold underpotentially, the $Ag^{+/0}$ redox potential on this modified electrode is increased by ~520 mV over that for a bulk silver electrode, thus, enabling the observation of ferrocene redox behavior.

In Figure 8.7, the potential was ramped to 650 mV positive of the $Ag^{+/0}$ redox potential for silver upd on gold. Nevertheless, silver oxidation was not observed in the cyclic voltammogram, and XPS results indicated that the silver coverage on the SAM-coated electrode did not change after being cycled to 650 mV. This added stability of the upd layer has been attributed to the presence of the SAM. Chidsey et al. have shown that an adsorbed organic monolayer can reduce electron transfer rates and thus lead to the requirement of more positive potentials to drive an oxidation process.[40] The cyclic voltammograms of a nonelectroactive monolayer (not shown) prepared from $C_{16}H_{33}SH$ on Au/Ag(upd) showed no evidence of silver oxidation until the potential reached ~+800 mV.
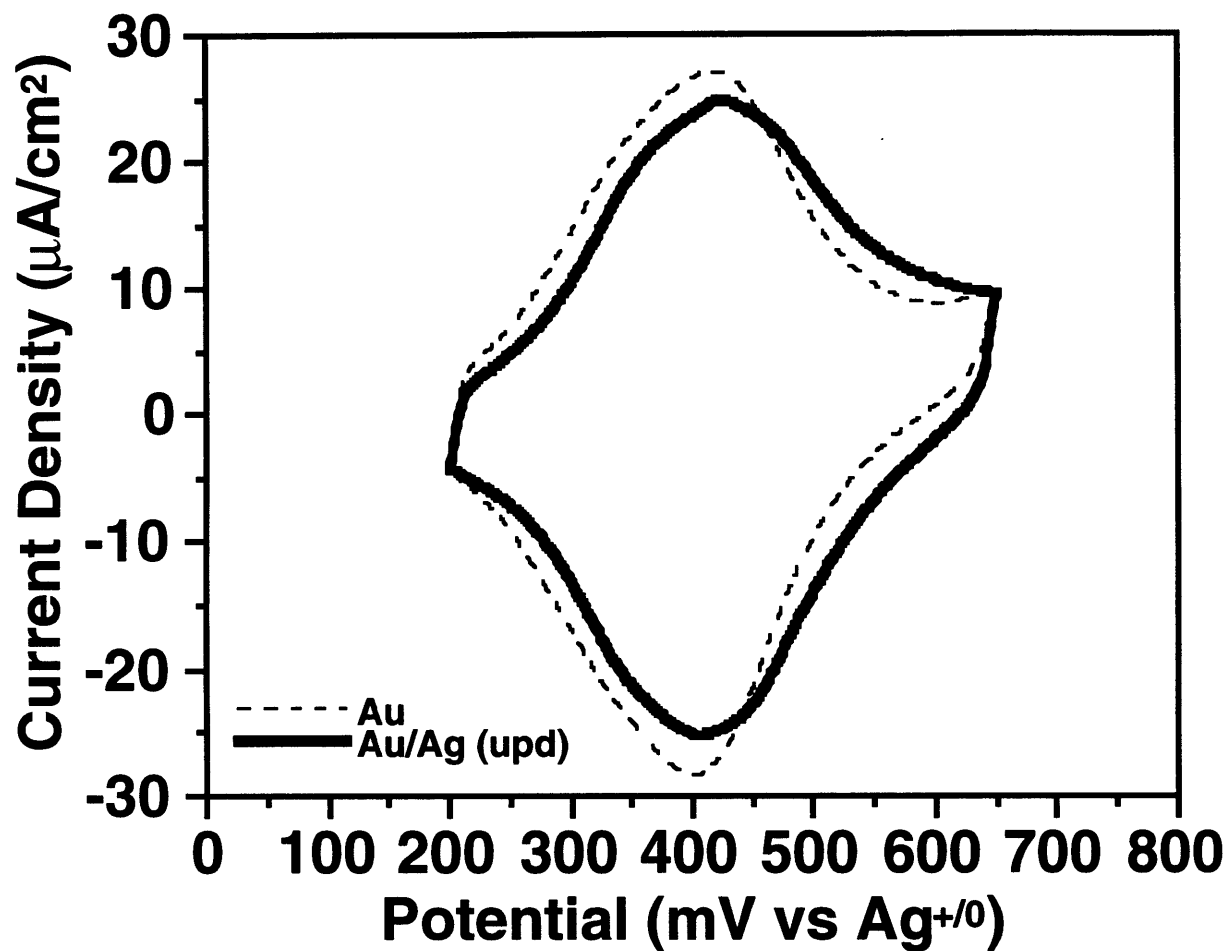
Figure 8.7. Cyclic voltammograms in 0.1 M $HClO_4$ of monolayers prepared from $FcCO(CH_2)_{10}SH$ (1 mM, ethanol) on gold and Au/Ag(upd). Scan rate = 100 mV/s.

8.3. Experimental

8.3.1. Materials

Gold shot (99.99%) and chromium-coated tungsten filaments were obtained from Americana Precious Metals Co. (East Rutherford, NJ) and R.D. Mathis (Long, Beach, CA), respectively. Silicon (100) wafers (Silicon Sense, Nashua, NH) were rinsed with ethanol and dried with nitrogen prior to use in the evaporator. Octyl, dodecyl, and octadecyl thiols (Aldrich) were distilled under vacuum prior to use. All other n-alkanethiols were prepared from the corresponding alkyl bromides (Aldrich) by nucleophilic displacement with thioacetate followed by solvolysis in HCl/MeOH. 11-Hydroxy-undecanethiol,[13] mercaptoundecanoic acid,[41] 11-(2,2,3,3,3-pentafluoropropoxy)-undecanethiol,[9] and octadecanethiol-d_{37}[14e] were prepared according to literature procedures. 11-Ferrocenyl-undecanethiol and 11-ferrocenoyl-undecanethiol were available from previous studies.[38] Ethanol (95%, Pharmco), isooctane (EM Science), and hexadecane (Aldrich) were used as received. Deionized water was purified with a Millipore-Q system.

8.3.2. Preparation of Assemblies

Chromium (100 Å) and gold (1000 Å) were evaporated in sequence at 1.5 and 4 Å/s, respectively, onto 100-mm silicon wafers in a diffusion-pumped chamber with a base pressure of 8×10^{-7} Torr and an operating pressure of 2×10^{-6} Torr. The gold-coated wafers were cut into 1 cm x 3 cm samples and were used for underpotential deposition and/or SAM formation within 3 days of evaporation. Copper and silver were underpotentially deposited onto evaporated gold surfaces in a glass cell using a supported gold film as counter electrode, a copper or silver wire as a reference electrode, and a computer-controlled PAR Model 263A potentiostat. The exposed area of the working electrode was either ~0.8 cm^2 for samples characterized by XPS, ellipsometry, and wetting or ~5 cm^2 for samples characterized by IR. Before deposition, the gold film was electrochemically cycled at 20 mV/s in a 0.1 M H$_2$SO$_4$(aq) solution of 0.6 mM Ag$_2$SO$_4$ or 1.0 mM CuSO$_4 \cdot$5 H$_2$O between 200 and 650 mV vs. reference for silver or between 50 and 550 mV vs. reference for copper. On the cathodic scan, the potential was held at a value just negative of the upd peak (460 mV for silver and 80 mV for copper). The electrode was emersed under potential control, rinsed with ethanol,[42] blown dry in a stream of N$_2$, and transferred rapidly through air to 1 mM isooctane or ethanol solutions of the alkyl thiols for 40 min. The resulting SAMs were rinsed with ethanol and blown dry with N$_2$ prior to characterization.

Mixed monolayers expressing methyl and hydroxyl termini were formed by immersing silver upd substrates into ethanolic solutions containing mixtures of dodecanethiol and 11-hydroxy-undecanethiol for 40 min. The mole fractions of the two thiols were varied while the total concentration of thiol in solution was held constant at 1 mM. The mole fraction of the hydroxyl-terminated component in the SAM was determined by normalizing the intensity of the O (1s) peak in the XPS spectrum to the peak obtained for a SAM composed solely of the hydroxyl-terminated species.[9]

8.3.3. Ellipsometry

The thicknesses of the SAMs were determined using a Gaertner L116A automatic ellipsometer equipped with a He-Ne laser (λ = 6328 Å) at an incident angle of 70° and a refractive index for the organic film of 1.46. Samples were rinsed with ethanol and blown dry with N_2 before measurements were taken. Baseline values for upd assemblies were measured on unfunctionalized upd substrates within 2 min after emersion from the electrochemical cell. The reported thicknesses are the average of at least five independent experiments where each sample was characterized by ellipsometry at three different locations on its surface; the averages of three measurements made at each location on the sample were used to calculate thicknesses.

8.3.4. Wetting Measurements

Advancing contact angles were measured on static drops of water or hexadecane with a Ramé-Hart manual goniometer equipped with video camera and computer monitor for viewing the drops. Contacting liquids were advanced or retreated (1 μL/s) prior to measurement with a Micro-Electrapette syringe (Matrix Technologies, Lowell, MA). The pipette tip remained in the drop during measurement. Both sides of ~5 μL drops were measured at three different locations on a sample, with the reproducibility across a sample being ± 2°.

8.3.5. X-ray Photoelectron Spectroscopy (XPS)

XPS spectra were obtained with a Surface Science Instruments Model X-100 spectrometer using a monochromatized Al Kα x-ray source (elliptical spot of 1.0 mm x 1.7 mm) and a concentric hemispherical analyzer (pass energy = 150 eV). The detector angle with respect to the surface parallel was 35°. Peak positions were referenced to Au($4f_{7/2}$) = 84.00 eV, and peaks were fit with 80% Gaussian/20% Lorentzian profiles and a Shirley background. Coverages of the upd adlayer

component (ϕ_{upd}) were calculated from measured intensities of the adlayer (I_{upd}) and substrate (I_{Au}) peaks using eq 8.1 (see appendix for derivation):[43]

$$\phi_{upd} = \left\{ \left(\frac{I_{Au}}{I_{upd}} \right) \left(\frac{I^o_{upd}}{I^o_{Au}} \right) C_{SAM} \left[1 - \exp\left(\frac{-a_{upd}}{\lambda_{upd(KE_{upd})}\cos\Theta} \right) \right] + \left[1 - \exp\left(\frac{-a_{upd}}{\lambda_{upd(KE_{Au})}\cos\Theta} \right) \right] \right\}^{-1} \quad (8.1)$$

where a_{upd} is the diameter of the adatom (2.56 and 2.89 Å for copper and silver, respectively); $\lambda_{upd(KE_i)}$ is the inelastic mean free path through the upd adlayer for electrons of kinetic energy (KE) from the upd layer or the gold substrate [λ_{Cu} for Au(4f$_{7/2}$) and Cu(2p$_{3/2}$) photoelectrons are 21 Å and 11 Å, respectively; λ_{Ag} for Au(4f$_{7/2}$) and Ag(3d$_{5/2}$) photoelectrons are 18 Å and 15 Å, respectively],[44] Θ is the angle of the detector to the surface normal, and I^o_{upd} and I^o_{Au} are sensitivity factors for the adlayer atoms and substrate atoms, respectively. Eq 8.2 gives C_{SAM}, the attenuation of the adlayer and substrate electrons by the SAM or adventitious carbonaceous material

$$C_{SAM} = \frac{\exp\left(\frac{-d_{SAM}}{\lambda_{SAM(KE_{upd})}\cos\Theta} \right)}{\exp\left(\frac{-d_{SAM}}{\lambda_{SAM(KE_{Au})}\cos\Theta} \right)} \quad (8.2)$$

where $\lambda_{SAM(KE_i)}$ is the attenuation length through the SAM for electrons of kinetic energy (KE) from the upd layer or the gold substrate [λ_{SAM} for Au(4f$_{7/2}$), Ag(3d$_{5/2}$), and Cu(2p$_{3/2}$) photoelectrons are 40 Å, 34 Å, and 21 Å, respectively],[45] and d_{SAM} is the thickness of the hydrocarbon layer for the SAM [$d_{SAM} = n\, d \cos\alpha$ where n is the number of methylene groups in the adsorbate, d is the incremental contribution of a methylene group to the length of an n-alkyl chain ($d = 1.27$ Å)[46] and α is the angle the hydrocarbon chain is canted relative to the surface normal as determined by IR (on copper and silver, $\alpha \cong 12°$; on gold, $\alpha \cong 30°$, on the upd systems, $\alpha \cong 20°$)]. For unfunctionalized upd samples, the thickness of adventitious carbonaceous material on its surface was quantified by comparing the intensity of the Au(4f$_{7/2}$) peaks for these samples with those of substrates coated with octylthiolate SAMs. The effective chain length of the carbonaceous material was determined by the slopes of a semi-logarithmic plot of substrate intensity versus SAM chain length. This treatment assumes that the inelastic mean free path through this carbonaceous material is similar to that of hydrocarbon.

8.3.6. Reflectance Infrared Spectroscopy

IR spectra were obtained in a single reflection mode using a Bio-Rad FTS 175 infrared spectrometer and Universal Reflectance Attachment. The p-polarized light was incident at 80° from the surface normal. The reflected light was detected with a narrow-band MCT detector cooled with liquid nitrogen. Spectral resolution was 2 cm^{-1} after triangular apodization. Spectra were referenced to those of SAMs prepared on the corresponding substrates from octadecanethiol-d_{37}, and 1024 scans of both the sample and the reference were collected to obtain good signal-to-noise ratios. Samples were rinsed with ethanol and blown dry with N_2 prior to characterization.

8.3.7. Electrochemistry

Cyclic voltammetry of ferrocene-terminated SAMs was performed in a glass cell using a supported gold film as the counter electrode, a silver wire as the reference electrode, and a PAR Model 263A potentiostat. A solution of 0.1 M $HClO_4$, prepared immediately before use with purified water (Millipore), served as the electrolyte. The exposed area of the working electrode was ~0.4 cm^2. The potential was cycled between 200 and 650 mV at a scan rate of 100 mV/s. The amount of charge passed between the electrode and the monolayer was determined by averaging the faradaic contributions to the anodic and cathodic peaks.

8.4. References

1) (a) Bard, A.J. *Integrated Chemical Systems: A Chemical Approach to Nanotechnology*; Wiley: New York, 1994. (b) Ball, P. *Designing the Molecular World: Chemistry at the Frontier*; Princeton University Press: Princeton, 1994.

2) (a) Vögtle, F. *Supramolecular Chemistry*; Wiley: Chichester, 1991. (b) Dietrich, B.; Viout, P.; Lehn, J.-M. *Macrocyclic Chemistry*; VCH: Weinheim, 1992. (c) Lehn, J.-M. *Supramolecular Chemistry: Concepts and Perspectives*; VCH: Weinheim, 1995.

3) (a) Whitesides, G.M.; G.M.; Mathias, J.P.; Seto, C.T. *Science* **1991**, *254*, 1312-1319. (b) Lehn, J.M. *Science* **1993**, *260*, 1762-1763 and references therein. (c) Whitesides, G.M. *Scientific American* **1995**, *273*, 146-149. (d) Philp, D.; Stoddart, J.F. *Angew. Chem., Int. Ed. Eng.* **1996**, *35*, 1154-1196.

4) (a) *Design of New Materials*; Cocke, D.L., Clearfield, A., Eds.; Plenum: New York, 1987. (b) George, E.P.; Yamaguchi, M.; Kumar, M.S.; Liu, C.T. *Annu. Rev. Mater. Sci.* **1994**, *24*, 409-451.

5) (a) Sinfelt, J.H. *Bimetallic Catalysts: Discoveries, Concepts and Applications*; Wiley: New York, 1983. (b) Lewis, L.N. *Chem. Rev.* **1993**, *93*, 2693-2730. (c) Wouda, P.T.; Nieuwenhuys, B.E.; Schmid, M.; Varga, P. *Surface Science* **1996**, *359*, 17-22 and references therein.

6) (a) Ulman, A. *An Introduction to Ultrathin Organic Films From Langmuir-Blodgett to Self-Assembly*; Academic Press: Boston, 1991; pp 237-301. (b) Dubois, L.H.; Nuzzo, R.G. *Ann. Rev. Phys. Chem.* **1992**, 43, 437-463. (c) Ulman, A. *Chem. Rev.* **1996**, *96*, 1533-1554.

7) (a) Kolb, D.M. In *Advances in Electrochemistry and Electrochemical Engineering*; Gerischer, H., Tobias, C.W., Eds.; Wiley-Interscience: New York, 1978; Vol. 11, pp 125-271. (b) Adzic, R. In *Advances in Electrochemistry and Electrochemical Engineering*; Gerischer, H., Tobias, C.W., Eds.; Wiley: New York, 1984; Vol. 13, pp 159-260.

8) Laibinis, P.E.; Whitesides, G.M.; Allara, D.L.; Tao, Y.-T.; Parikh, A.N.; Nuzzo, R.G. *J. Am. Chem. Soc.* **1991**, *113*, 7152-7167 and references contained therein.

9) Laibinis, P.E.; Whitesides, G.M. *J. Am. Chem. Soc.* **1992**, *114*, 1990-1995.

10) (a) Walczak, M.M.; Chung, C.; Stole, S.M.; Widrig, C.A.; Porter, M.D. *J. Am. Chem. Soc.* **1991**, *113*, 2370-2378. (b) Bryant, M.A.; Pemberton, J.E. *J. Am. Chem. Soc.* **1991**, *113*, 3629-3637.

11) (a) Fenter, P.; Eisenberger, P.; Li, J.; Camillone III, N.; Bernasek, S.; Scoles, G.; Ramanarayanan, T.A.; Liang, K.S. *Langmuir* **1991**, *7*, 2013-2016. (b) Dhirani, A.;

Hines, M.A.; Fisher, A.J.; Ismail, O.; Guyot-Sionnest, P. *Langmuir* **1995**, *11*, 2609-2614.

12) Laibinis, P.E.; Fox, M.A.; Folkers, J.P.; Whitesides, G.M. *Langmuir* **1991**, *7*, 3167-3173.

13) Bain, C.D.; Troughton, E.B.; Tao, Y.-T.; Evall, J.; Whitesides, G.M.; Nuzzo, R.G. *J. Am. Chem. Soc.* **1989**, *111*, 321-335.

14) (a) Bain, C.D.; Whitesides, G.M. *J. Am. Chem. Soc.* **1988**, *110*, 3665-3666. (b) Bain, C.D.; Whitesides, G.M. *Science* **1988**, *240*, 62-63. (c) Bain, C.D.; Whitesides, G.M. *J. Am. Chem. Soc.* **1988**, *110*, 5897-5898. (d) Ulman, A.; Evans. S.D.; Shnidman, Y.; Sharma, R.; Eilers, J.E.; Chang, J.C. *J. Am. Chem. Soc.* **1991**, *113*, 1499-1506. (e) Laibinis, P.E.; Nuzzo, R.G.; Whitesides, G.M. *J. Phys. Chem.* **1992**, *96*, 5097-5105. (f) Laibinis, P.E.; Bain, C.D.; Nuzzo, R.G.; Whitesides, G.M. *J. Phys. Chem.* **1995**, *99*, 7663-7676. (g) Drelich, J.; Wilbur, J.L.; Miller, J.D.; Whitesides, G.M. *Langmuir* **1996**, *12*, 1913-1922.

15) (a) Tarlov, M.J. *Langmuir* **1992**, *8*, 80-89. (b) Jung, D.R.; Czanderna, A.W. *Crit. Rev. Solid State Mater. Sci.* **1994**, *19*, 1-54 and references therein. (c) Willicut, R.J.; McCarley, R.L. *J. Am. Chem. Soc.* **1994**, *116*, 10823-10824. (d) Sayre, C.N.; Collard, D.M. *Langmuir* **1995**, *11*, 302-306.

16) (a) Prime, K.L.; Whitesides, G.M. *Science* **1991**, *252*, 1164-1167. (b) López, G.P.; Albers, M.W.; Schreiber, S.L.; Carroll, R.W.; Peralta, E.; Whitesides, G.M. *J. Am. Chem. Soc.* **1993**, *115*, 5877-5878. (c) Prime, K.L.; Whitesides, G.M. *J. Am. Chem. Soc.*. **1993**, *115*, 10714-10721. (d) Singhvi, R.; Kumar, A.; Lopez, G.P.; Stephanopoulos, G.N.; Wang, D.I.C.; Whitesides, G.M.; Ingber, D.E. *Science* **1994**, *264*, 696-698.

17) Green, J.B.T.; McDermott, M.T.; Porter, M.D.; Siperko, L.M. *J. Phys. Chem.* **1995**, *99*, 10960-10965.

18) (a) Chidsey, C.E.D. *Science* **1991**, *251*, 919-922. (b) Terrettaz, S.; Beck, A.M.; Traub, M.J.; Fettinger, J.C.; Miller, C.J. *J. Phys. Chem.* **1995**, *99*, 11216-11224 and references therein.

19) Chang, S.C.; Chao, I.; Tao, Y.-T. *J.Am. Chem. Soc*. **1994**, *116*, 6792-6805.

20) (a) Tour, J.M.; Jones II, L.; Pearson, D.L.; Lamba, J.J.S.; Burgin, T.P.; Whitesides, G.M.; Allara, D.L.; Parikh, A.N.; Atre, S.V. *J. Am. Chem. Soc.* **1995**, *117*, 9529-9534. (b) Dhirani, A.-A.; Zehner, R.W.; Hsung, R.P.; Guyot-Sionnest, P.G.; Sita, L.R. *J. Am. Chem. Soc.* **1996**, *118*, 3319-3320.

21) (a) Whitesell, J.K.; Chang, H.K. *Science* **1993**, *261*, 73-76. (b) Davis, F.; Stirling, C.J. *Langmuir* **1996**, *12*, 5365-5374.

22) (a) White, J.H.; Albarelli, M.J.; Abruna, H.D.; Blum, L.; Melroy, O.R.; Samant, M.G.; Borges, G.L.; Gordon, J.G. *J. Phys. Chem.* **1988**, *92*, 4432-4436. (b) Samant, M.G.; Borges, G.; Melroy, O.R. *J. Electrochem. Soc.* **1993**, *140*, 421-425. (c) Toney, M.F; Howard, J.N; Richer, J.; Borges, G.L; Gordon, J.G; Melroy, O.R; Yee, D.; Sorensen, L.B. *Phys. Rev. Lett.* **1995**, *75*, 4472-4475.

23) (a) Kolb, D.M. *Z. Phys. Chem. Neue Folge* **1987**, *154*, 179-199. (b) Kötz, R. In *Spectroscopic and Diffraction Techniques in Interfacial Electrochemistry*; Gutiérrez, C, Melendres, C., Eds.; Kluwer: Netherlands, 1990; pp 409-438.

24) Chen, C.; Kepler, K.D.; Gewirth, A.A.; Ocko, B.M.; Wang, J. *J. Phys. Chem.* **1993**, *97*, 7290-7294.

25) (a) Manne, S.; Hansma, P.K.; Massie, J.; Elings, V.B.; Gewirth, A.A. *Science*, **1991**, 251, 183-186. (b) Chen, C.; Vesecky, S.M.; Gewirth, A.A. *J. Am. Chem. Soc.* **1992**, *114*, 451-458. (c) Sneddon, D.D.; Sabel, D.M.; Gewirth, A.A. *J. Electrochem. Soc.* **1995**, *142*, 3027-3033. (d) Ogaki, K.; Itaya, K. *Electrochim. Acta* **1995**, *40*, 1249-1257.

26) (a) Lorenz, W.J.; Moumtzis, I.; Schmidt, E. *J. Electroanal. Chem. Interfacial Electrochem.* **1971**, *33*, 121-133. (b) Seo, M.; Aomi, M.; Yoshida, K. *Electrochim. Acta* **1994**, *39*, 1039-1044. (c) Salie, G.; Bartels, K. *Electrochim. Acta* **1994**, *39*, 1057-1065.

27) The structure and coverage of the upd layer can be selected by choice of counterion with bulkier anions yielding upd layers that have lower coverages and more open structures.[7,25]

28) The following metals form upd layers on gold: Ag, Bi, Cu, Hg, Li, Pb, Pd, Sb, Sn, Tl, and Zn (ref 7 and Gofer, Y.; Barbour, R.; Luo, Y.; Tryk, D.; Scherson, D.A; Jayne, J.; Chottiner, G. *J. Phys. Chem.* **1995**, *99*, 11739-11741).

29) Evaporated films of copper, silver, and gold are predominately (111) in texture.[9]

30) The presence of an upd film of silver on the gold substrate yields alkanethiolate SAMs that are more stable towards desorption at elevated temperatures (Chapter 9) and are less likely to exchange in the presence of a competing thiol (Chapter 10).

31) Kolb, D.M.; Michaelis, R. *J. Electroanal. Chem.* **1990**, *284*, 507-510.

32) Coverages determined by averaging the cathodic and anodic charges for the upd peaks are 0.41 ± 0.05 for silver upd and 0.45 ± 0.05 for copper upd on gold. Coulometric measurements frequently underestimate surface coverage.[7b]

33) (a) Edinger, K.; Gölzhäuser, A.; Demota, K.; Wöll, C.; Grunze, M. *Langmuir* **1993**, *9*, 4-8. (b) Schönenberger, C.; Sondag-Huethorst, J.A.M.; Jorritsma, J.; Fokkink, L.G.J. *Langmuir* **1994**, *10*, 611-614.

34) Keller, H.; Simak, P.; Schrepp, W.; Dembowski, J. *Thin Solid Films* **1994**, *244*, 799-805.

35) Snyder, R.G. *J. Mol. Spectrosc.* **1961**, *7*, 116-144.

36) The spectra for the Au/Ag upd and Au/Cu(upd) samples cannot be obtained by summing a weighted average of the spectra taken on the bulk metals.

37) (a) Chidsey, C.E.D.; Bertozzi, C.R.; Putvinski, T.M.; Mujsce, A.M. *J. Am. Chem. Soc.* **1990**, *112*, 4301-4306. (b) Hickman, J.J.; Laibinis, P.E.; Auerbach, D.I.; Zou, C.; Gardner, T.J.; Whitesides, G.M.; Wrighton, M.S. *Langmuir* **1992**, *8*, 357-359.

38) (a) Hickman, J.J.; Ofer, D.; Zou, C.; Wrighton, M.S.; Laibinis, P.E.; Whitesides, G.M. *J. Am. Chem. Soc.* **1991**, *113*, 1128-1132. (b) Hickman, J.J.; Ofer, D.; Laibinis, P.E.; Whitesides, G.M.; Wrighton, M.S. *Science* **1991**, *252*, 688-691.

39) The redox behavior of ferrocene has been observed at a silver electrode at 170 K and below where the rate of electron transfer to ferrocene becomes faster than the anodization of silver (Curtin, L.S.; Peck, S.R.; Tender, L.M.; Murray, R.W.; Rowe, G.K.; Creager, S.E. *Anal. Chem.* **1993**, *65*, 386-392).

40) Chidsey, C.E.D.; Loiacono, D.N. *Langmuir* **1990**, 6, 682-691..

41) Troughton, E.B.; Bain, C.D.; Whitesides, G.M.; Allara, D.L.; Porter, M.D. *Langmuir* **1988**, *4*, 365-385.

42) An ethanol rinse was found to remove residual electrolyte from the emersed electrode but did not change the coverage of the upd layer, as indicated by XPS.

43) Seah, M.P. In *Practical Surface Analysis: Volume 1. Auger and X-ray Photoelectron Spectroscopy*; Briggs, D., Seah, M.P., Eds.; Wiley: Chichester, 1990; p. 245.

44) Tanuma, S.; Powell, C.J.; Penn, D.R. *Surf. Interface Anal.* **1988**, *11*, 577-589.

45) Laibinis, P.E.; Bain, C.D.; Whitesides, G.M. *J. Phys. Chem.* **1991**, *95*, 7017-7021.

46) Abrahamsson, S.; Larsson, G.; von Sydlow, E. *Acta Crystallogr.* **1960**, *13*, 770-774.

Chapter 9. Underpotentially Deposited Metal Layers Provide Enhanced Thermal Stability to Self-Assembled Alkanethiol Monolayers on Gold

9.1. Background

Self-assembled monolayers (SAMs) derived from the spontaneous adsorption of alkanethiols onto gold surfaces are one of the most convenient and flexible systems for generating tailored organic interfaces and examining the structure/property relationships of organic surfaces.[1] The assembly produces chemisorbed monolayer films that can express a wide range of polar and nonpolar functionalities at the SAM/air(liquid) interface.[2,3] The robust behavior of these films in liquid and vacuum environments, coupled with the ease and flexibility in their synthesis, has been a primary factor in their increasing use in laboratory experiments. While this system exhibits useful stabilities at room temperature, the molecular components of the SAM are removed from the surface when the SAM is contacted with a thiol solution[4,5] or is exposed to elevated temperatures (~70 °C).[2] In general, the lack of stability of these films during long-term exposure to the atmosphere or to higher temperatures provide some restrictions to their application. Methods to improve the stability of these layers have focused on the design and multi-step synthesis of adsorbates that can achieve multiple gold/sulfur interactions,[6] or that incorporate polymerizable groups,[7] hydrogen bonding functionalities,[5] or aromatic moieties.[8] This chapter describes a straightforward method to increase the level of interaction at the gold/sulfur interface using an electrodeposited monolayer of silver as a one-atom-thick interlayer between the gold surface and the adsorbed SAM. This study focuses on polycrystalline gold films prepared by evaporation as these substrates are commonly used in studies and applications of alkanethiol-based SAMs and they have direct analogs in device fabrication.[9]

Underpotential deposition (upd) is an electrochemical method of depositing up to one monolayer of metal onto a more noble metal surface at potentials positive of bulk electrodeposition (see Section 8.1 for more details).[10] The upd process is the result of strong adatom-substrate interactions that are energetically more favorable than the adatom-adatom interactions formed during bulk electrodeposition.[10] Upd shares the common features with SAMs that the process yields robust layers of no greater than monolayer coverage, the system has a high degree of flexibility in the composition and coverage of the adlayer, and gold is a commonly used substrate. In Chapter 8,[11] the characterization of SAMs on upd substrates of copper and silver on gold were reported. The SAMs on the upd substrates are similar to those formed on gold in that the assembly can be performed in air and it accommodates both polar, nonpolar, and electroactive functionalities in the tail group of the adsorbate.[11] In these SAMs, the upd layer is present as an interlayer

between the gold surface and the adsorbed thiolate (refer to Figure 8.1), and it is not etched away during SAM formation nor does it alloy with the underlying gold.[11] The hydrocarbon chains in the SAM are primarily trans-zig-zag extended and cant ~20° from the surface normal[11] (vs. ~30° from the surface normal on gold, and ~10° from the surface normal on silver[12]).

9.2. Results and Discussion

The Au/Ag(upd) substrates were prepared by electrochemically cycling gold-coated silicon wafers in a 0.1 M H_2SO_4/0.6 mM Ag_2SO_4 aqueous solution and removing the substrates at potentials 50 mV cathodic of the upd peaks (460 mV vs. $Ag^{+/0}$; refer to Figure 8.2 for the cyclic voltammogram for Ag upd onto Au); the substrates were transferred rapidly through air to 1 mM solutions of the alkanethiol in isooctane or ethanol for 40 min. Under these conditions, the coverage of silver on the gold surface (ϕ_{Ag}) before and after adsorption of the SAM was 0.6.[14] Longer adsorption times for the thiol (up to 24 h) did not dramatically change the coverage of the upd layer or the properties of the SAM.

As the thiol-gold bond is not a fully covalent one, thiols desorb from the surface when contacted with solvents at temperatures above 70 °C.[2] The thrust of this chapter examines the effect of the substrate composition on the desorption rates of alkanethiolate SAMs when contacted with a heated solvent. The thermal stability experiments were conducted in heated solutions of a high boiling branched hydrocarbon solvent [decahydronaphthalene (DHN)]; this solvent was chosen to minimize possible solvent intercalation into the partial SAMs. Individual samples were each periodically removed from the DHN, rinsed with ethanol, blown dry in a stream of N_2, and characterized by *ex situ* by ellipsometry or x-ray photoelectron spectroscopy (XPS) to determine the remaining coverage of the SAM;[15] samples were discarded after analysis.

Figure 9.1a compares the desorption behaviors of *n*-docosanethiolate SAMs on gold and upd-modified gold surfaces at 103 °C in DHN; fractional coverages were determined *ex situ* by optical ellipsometry. After ~60 min at 103 °C, little adsorbate remained on the gold surface while most of the SAM remained on the upd-modified substrate. Similar improvements in thermal stability were also observed at lower temperatures (Figure 9.1b), with the rates of desorption (assuming first-order behavior) being 4 to 10 times slower for substrates that were modified by the upd process.[16] Least-squares fits to the data in Figure 9.1b yielded activation energies of 31 and 38 kcal/mol (± 10%) toward desorption of the SAM from the bare Au and Au/Ag(upd) substrates, respectively. The enhanced stability was also reflected by the wetting properties of the assemblies during these experiments. For example, after just 10 min of exposure to DHN at 103 °C, the *n*-docosanethiolate SAMs on gold were wet by ethanol (θ_a 0°); however, these SAMs on the upd-modified system remained autophobic to ethanol ($\theta_r > 0°$) through 90 min of exposure. Wetting is a sensitive probe

150
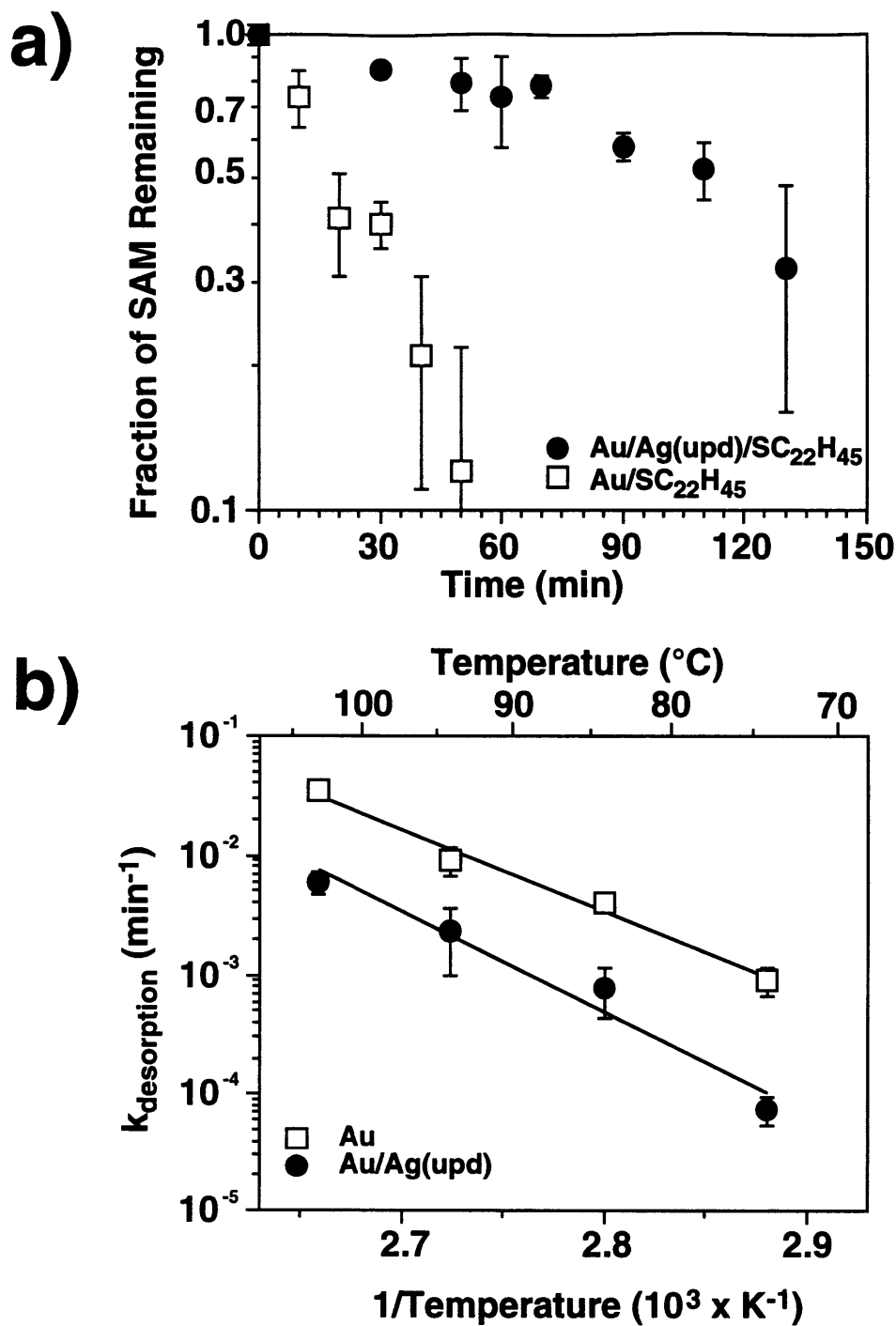
Figure 9.1. Desorption of n–docosanethiolate ($C_{22}H_{45}S-$) SAMs from Au and Au/Ag(upd) (ϕ_{Ag}= 0.6) substrates into decahydronaphthalene (DHN), as followed *ex situ* by ellipsometric measurements. (a) Fractional coverage of the docosanethiolate SAM remaining on the Au and Au/Ag(upd) substrates as a function of exposure time to DHN at 103 °C. (b) Arrhenius plot of the first-order rate constants for SAM desorption into DHN for the Au and Au/Ag(upd) (ϕ_{Ag}= 0.6) substrates. In all figures where error bars are not shown, they are approximated by the size of the symbol.

of film structure[1,17] and provides further indication that the upd layer can maintain the structure and integrity of the SAM under conditions where a native thiols-on-gold SAM is not stable.

The n-alkanethiolate SAMs on Au and Au/Ag(upd) substrates have a different canted structure, with the n-alkanethiolates being oriented more vertically on the Au/Ag(upd) substrate than on gold.[11] Considering this difference in structure, the increased van der Waals interactions associated with the Au/Ag(upd)/SAM structure could be responsible for the enhanced thermal stability of this system. To test this hypothesis, the desorption behaviors for a n-hexadecanethiolate monolayer on Au/Ag(upd) and a n-docosanethiolate monolayer on bare Au into DHN at 84 °C were compared (Figure 9.2). The adsorbates were selected so that the SAM on Au/Ag(upd) would be thinner (and contain fewer van der Waals interactions) than the longer-chained SAM on Au. In Figure 9.2, the SAM on the upd-modified substrate displayed better stability toward desorption than the thicker SAM on gold. These data demonstrate that the upd layer of silver is responsible for the improvements observed in the thermal stability of the SAMs.

Similar experiments were conducted using x-ray photoelectron spectroscopy (XPS) and SAMs derived from a fluorine-tagged thiol [$HS(CH_2)_{11}OCH_2CF_2CF_3$,[3] 1]; XPS has the advantages over ellipsometry as it can monitor the direct loss of material (from the intensity of the F(1s) peak[15]) and its measurement can distinguish between the tagged thiolate and adventitious materials that might adsorb onto the metal surface. In addition, XPS allowed complementary experiments to be conducted on bulk silver substrates as the XPS measurements were not sensitive to problems of substrate oxidation that could complicate ellipsometric determination of monolayer thickness on this substrate. Figure 9.3 shows the desorption behaviors for SAMs derived from 1 in DHN at temperatures between 70 and 100 °C.[18] The SAMs on the Au/Ag(upd) (ϕ_{Ag} = 0.6) substrate exhibited greater levels of thermal stability over this temperature range than did the corresponding SAMs on gold (by a factor of 3 to 5 in the rates of desorption). The results in Figures 2 - 4 demonstrate that the presence of a single layer of silver at the gold/SAM interface can impart improved stability to the alkanethiolate monolayers. XPS analysis of Au/Ag(upd) substrates after complete desorption of the SAM revealed some decrease in the coverage of the Ag adlayer (5-25%), suggesting that failure in the Au/Ag(upd)/SAM system is primarily at the metal/thiolate interface rather than at the Ag/Au interface.

The role of silver in the stabilization of the upd SAMs was investigated by using substrates with different coverages of silver. Assemblies from a bulk silver substrate were prepared, along with those from upd substrates that were emersed from the electrochemical cell at more reducing potentials, producing gold surfaces with intermediate submonolayer coverages of silver. Emersion at 250 mV and 100 mV vs $Ag^{+/0}$ yielded substrates with silver coverages of 0.75 and 0.85, respectively. Figure 9.4a shows that SAMs prepared from 1 on Au/Ag(upd) substrates where ϕ_{Ag} = 0.85 exhibited significantly greater stabilities than those where ϕ_{Ag} = 0.6. In addition, the

152
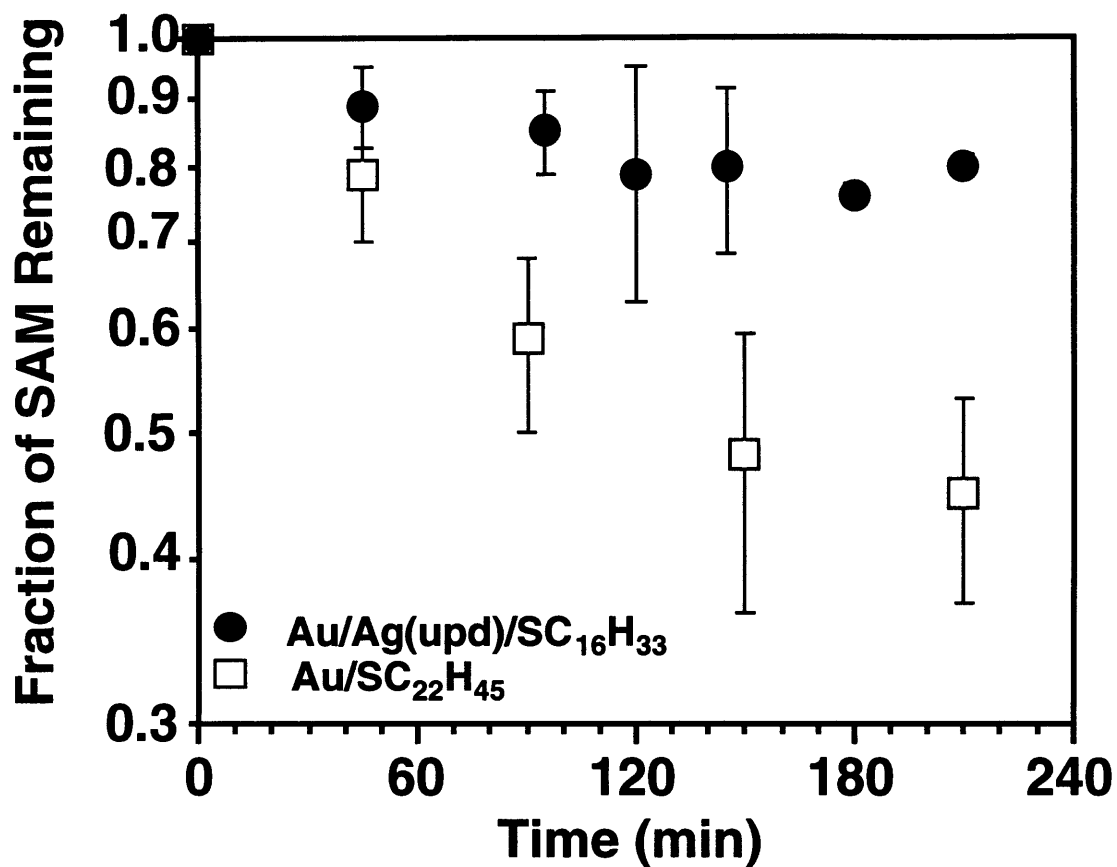
Figure 9.2. Comparison of the desorptive behaviors of n–docosanethiolate SAMs ($C_{22}H_{45}S$-) on Au and n–hexadecanethiolate SAMs ($C_{16}H_{33}S$-) on Au/Ag(upd) ($\phi_{Ag} = 0.6$) substrates into DHN at 84 °C, as followed *ex situ* by ellipsometric measurements. The chain lengths of the adsorbates were selected to produce a thicker SAM on the gold substrate.
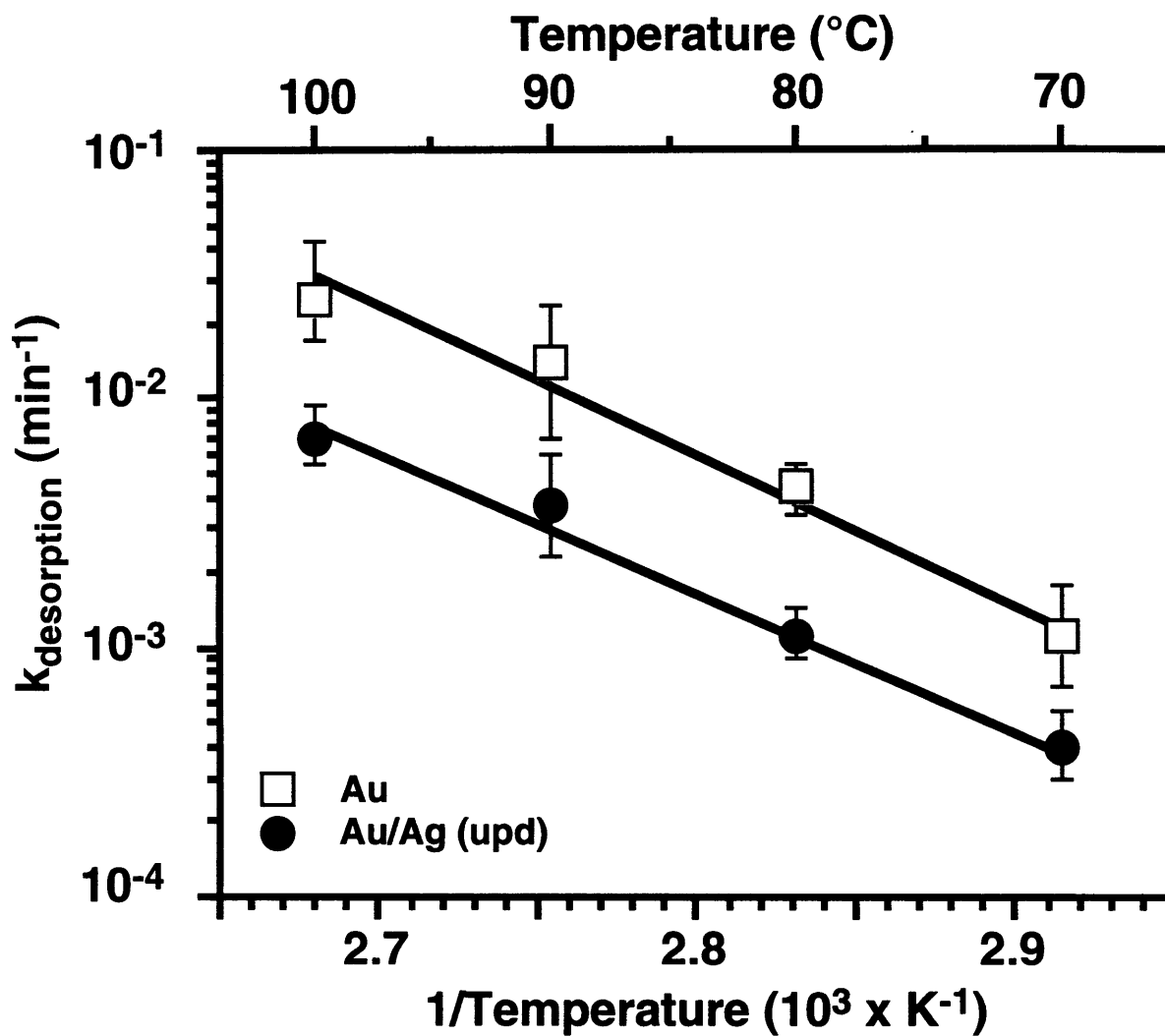
Figure 9.3. First-order rate constants for the desorption of SAMs derived from $CF_3CF_2CH_2O(CH_2)_{11}SH$ (**1**) on Au, Ag, and Au/Ag(upd) (ϕ_{Ag} = 0.6) substrates into decahydronaphthalene (DHN), as followed *ex situ* by x-ray photoelectron spectroscopy.

desorption behavior of the SAM on Au/Ag(upd) ($\phi_{Ag} = 0.85$) more closely approached that on bulk silver with ~ 70 % of the SAM remaining on the surface of both substrates after 400 min of exposure to DHN at 90 °C. In Figure 9.4b, the first-order rate constants for desorption of SAMs derived from **1** into 90° C DHN are shown as a function of the fractional coverage of silver at the SAM/metal interface.[19] As ϕ_{Ag} is increased, the stability of the SAMs toward desorption is enhanced as the SAM forms a greater number of thiolate-silver interactions and fewer of the weaker thiolate-gold interactions. At intermediate coverages of the Ag upd layer ($\phi_{Ag} = 0.6$), the interaction of the thiolate is probably largely due to interactions with the Ag upd layer and to a lesser degree, the underlying gold. The data in Figure 9.4b provide evidence that SAMs on silver are more thermally stable than those on gold and that a layer of silver (on the order of a monolayer) is sufficient to achieve the greater level of stability associated with a bulk silver substrate. From an experimental standpoint, the Au/Ag(upd) substrate provides the advantage over the use of bulk silver substrates as the underpotentially deposited silver is less prone to oxidation.[20]

9.3. Conclusions

Submonolayer amounts of underpotentially deposited silver provide enhanced stability to SAMs on polycrystalline gold substrates. The principal gain in adhesion results from an increase in the interaction between the sulfur headgroup and the upd-modified substrate. A single layer of metal on the surface of an electrode is sufficient to provide the adhesional properties of the bulk metal substrate. The advantage of the upd coating is that it offers these properties on a less air-sensitive, more noble version of the bulk substrate. As the assembly of thiols containing both polar and non-polar tail groups is compatible with the presence of the upd layer,[11] the strategy presented here for enhancing thermal stability should be directly applicable to the broad class of molecules that have been adsorbed onto gold.[21] The remaining chapters will explore the use of upd metal layers on gold to affect the room-temperature stability (Chapter 10) and structure (Chapter 11) of adsorbed organic monolayer films.
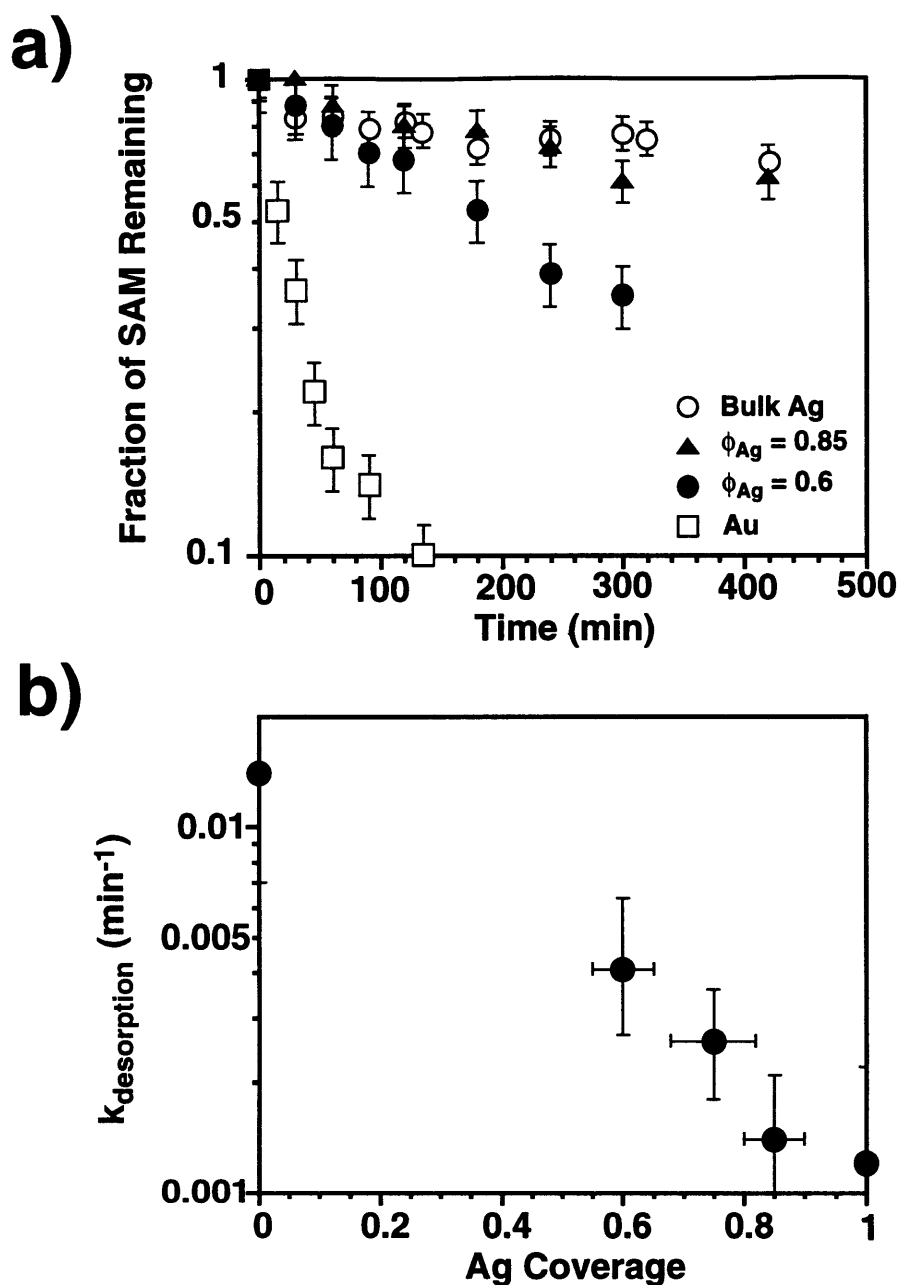
Figure 9.4. Effect of silver coverage on SAM stability. (a) Fractional coverage of the SAMs derived from $CF_3CF_2CH_2O(CH_2)_{11}SH$ (**1**) on Au, Ag, and Au/Ag(upd) (ϕ_{Ag} = 0.6 and 0.85) substrates as a function of exposure time to DHN at 90 °C. The fractional coverages of the substituents were determined *ex situ* by XPS. (b) First-order rate constants for data in the upper panel as a function of the fractional coverage of silver (ϕ_{Ag}) at the metal/organic interface. Evaporated silver is given as ϕ_{Ag} of 1.0.

9.4. References and Footnotes

1)   (a) Whitesides, G.M.; Laibinis, P.E. *Langmuir* **1990**, *6*, 87-96. (b) Dubois, L.H.; Nuzzo, R.G. *Annu. Rev. Phys. Chem.* **1992**, *43*, 437-463.

2)   Bain, C.D.; Troughton, E.B.; Tao, Y.T.; Evall, J.; Whitesides, G.M.; Nuzzo, R.G. *J. Am. Chem. Soc.* **1989**, *111*, 321-335.

3)   Laibinis, P.E.; Whitesides, G.M. *J. Am. Chem. Soc.* **1992**, *114*, 1990-1995 and references contained therein.

4)   Laibinis, P.E.; Fox, M.A.; Folkers, J.P.; Whitesides, G.M. *Langmuir* **1991**, *7*, 3167-3173.

5)   Tam-Chang, S.-W.; Biebuyck, H.A.; Whitesides, G.M.; Jeon, N.; Nuzzo, R.G. *Langmuir* **1995**, *11*, 4371-4382.

6)   (a) Whitesell, J.K.; Chang, H.K. *Science* **1993**, *261*, 73-76. (b) Sun, F.; Castner, D.G.; Grainger, D.W. *Langmuir* **1993**, *9*, 3200-3207. (c) Sun, F.; Castner, D.G.; Mao, G.; Wang, W.; McKeown, P.; Grainger, D.W. *J. Am. Chem. Soc.* **1996**, *118*, 1856-1866.

7)   (a) Batchelder, D.N.; Evans, S.D.; Freeman, T.L.; Haussling, L.; Ringsdorf, H.; Wolf, H. *J. Am. Chem. Soc.* **1994**, *116*, 1050-1053. (b) Kim, T.; Crooks, R.M.; Tsen, M.; Sun, L. *J. Am. Chem. Soc.* **1995**, *117*, 3963-3967.

8)   (a) Sabatani, E.; Cohen-Boulakia, J.; Bruening, M.; Rubinstein, I. *Langmuir* **1993**, *9*, 2974. (b) Chang, S.-C.; Chao, I.; Tao, Y.-T. *J. Am. Chem. Soc.* **1994**, *116*, 6792-6805. (c) Tour, J.M.; Jones II, L.; Pearson, D.L.; Lambda, J.J.S.; Burgin, T.P.; Whitesides, G.M.; Allara, D.L.; Parikh, A.N.; Atre, S.V. *J. Am. Chem. Soc.* **1995**, *117*, 9529-9534. (d) Dhirani, A.-A.; Zehner, R.W.; Hsung, R.P.; Guyot-Sionnest, P.; Sita, L.R. *J. Am. Chem. Soc.* **1996**, *118*, 3319-3320.

9)   The gold surfaces prepared by evaporation have a predominate (111) texure.

10)   (a) Kolb, D.M. In *Advances in Electrochemistry and Electrochemical Engineering*; Gerischer, H., Tobias, C.W., Eds.; Wiley-Interscience: New York, 1978; Vol. 11, pp. 125-271. (b) Chen, C.; Vesecky, S.M.; Gewirth, A.A. *J. Am. Chem. Soc.* **1992**, 114, 451-458 and references contained therein.

11)   Jennings, G.K.; Laibinis, P.E. *J. Am. Chem. Soc.* 1997, 119, 5208-5214.

12)   Laibinis, P.E.; Whitesides, G.M.; Allara, D.L.; Tao, Y.-T.; Parikh, A.N.; Nuzzo, R.G. *J. Am. Chem. Soc.* **1991**, *111*, 7152-7167 and references contained therein.

13)   For silver evaporations, the chamber was backfilled with N_2 and the substrates were transferred to the adsorbate solutions under a positive flow of N_2 to minimize oxidation of the substrate.

14) Silver coverages (ϕ_{Ag}) were determined using XPS data and Eq 8.1.

15) Fractional SAM coverages were determined by ratioing the ellipsometric thickness for a partial monolayer to the thickness for a freshly prepared SAM on the same substrate. Coverages of **1** were obtained by ratioing the integrated F(1s) intensity for a partial SAM to its value for a freshly prepared SAM of **1** on that substrate.

16) Higher temperatures were not examined as the rates of desorption were too fast to assume that the substrates achieved the desired temperature.

17) Laibinis, P.E.; Nuzzo, R.G.; Whitesides, G.M. *J. Phys. Chem.* **1992**, *96*, 5097-5105.

18) Figure 5a contains the desorption data at 90 °C for these samples.

19) Ag upd substrates with $\phi_{Ag} < 0.6$ could not be prepared with reproducible quality as ϕ_{Ag} changes from 0 to 0.6 over a narrow range of potential (~30 mV).

20) The redox potential of a silver upd layer on gold is ~520 mV positive of $Ag^{+/0}$ in 0.1 M H_2SO_4.

21) The upd strategy is also applicable to electroactive adsorbates. The persistent reversible electrochemistry for a SAM of Au/Ag (upd)/$S(CH_2)_{10}COFc$ (Fc = ferrocenyl) was demonstrated in Section 8.2 where the redox potential of the ferrocenoyl group (COFc) was 420 mV positive of $Ag^{+/0}$.[11]

Chapter 10. Exchange of Self-Assembled n-Alkanethiolate Monolayers on Gold Surfaces Modified by Underpotential Deposition of Silver or Copper

10.1. Background

While much work on self-assembled monolayers (SAMs) has focused on the development of systems of greater complexity through synthesis, little has been reported about the factors that affect their stability. Since the attachment of the thiols to the gold surface is not covalent, the components of alkanethiolate SAMs are known to desorb from gold surfaces into solvent to some degree at room temperature[1] and to a greater extent at elevated temperatures (> 70 °C).[2,3] The SAMs are also susceptible to exchange processes, where the components of an initially formed monolayer will be replaced on the surface with different adsorbed species when contacted with solutions of competing thiol adsorbates.[1,4-6] These exchange processes can affect the quality and composition of surfaces formed from solutions containing more than one thiol—so-called "mixed monolayers"—such as those used in the fabrication of chemically modified electrodes[4,5,7] or patterned interfaces.[8] Electrodes modified with these mixed SAMs exhibit superior electrochemical properties when the electroactive adsorbates are dispersed among electroinactive components, thereby enabling the active components to function as isolated redox sites on the electrode surface. However, exchange processes between surface-bound and solution-phase molecules can alter the composition of the electroactive groups on the surface. Another area in which exchange processes can impact the processing of SAMs-based systems is in microcontact printing. Whitesides and co-workers[8] have developed microcontact printing to create well-defined regions of chemical functionality by patterning one type of SAM on a metal surface and exposing the resulting patterned substrate to a solution of a second thiol adsorbate. The first patterned region is often formed by stamping the thiol onto selected regions of a gold surface with a polydimethylsiloxane stamp that is inked with a thiol solution. Upon exposure of the substrate to a solution containing a second thiol to derivatize the non-patterned, unfunctionalized areas, exchange processes can compromise the homogeneity of the preformed regions as the solution-phase thiols can exchange with the patterned thiols adsorbed in the first step.

Previous studies concerning the exchange kinetics of thiol adsorbates on gold have focused on the replacement of electroactive adsorbates by electroinactive ones[4,7] or of radio-labeled adsorbates by non-labeled molecules in solution.[1] These investigations consistently revealed an initial period of rapid exchange between surface-bound thiolates and thiols in solution followed by a slow ordering step in which the composition of the monolayer changed slowly over time. These distinct regimes in the exchange process suggest that some thiols are more easily removed from the

159

surface than others, perhaps resulting from different levels of interaction with the underlying gold substrate. Collard and Fox provided strong evidence to support this hypothesis by studying a two-step exchange of a surface-attached ferrocenyl alkanethiol by sequential exposure to 1) a ferrocenylcarbonyloxy-alkanethiol and 2) an unsubstituted alkanethiol from solution.[5] They concluded that the same molecules which replaced surface-bound species in the first step were, in turn, preferentially exchanged in the second step. While this observation suggests that distinct populations of thiols are present on the surface and interact at different levels with the substrate, some disagreement exists as to the nature of the fast-exchanging population. Chidsey et al. studied the exchange of electroactive ferrocenyl alkanethiols with inactive n-alkanethiols and hypothesized that thiols at domain boundaries exchanged more rapidly than thiols at the interiors of domains;[4] however, others have provided evidence suggesting that thiols bound at defect sites are more stable against exchange[1] and to electrochemical desorption[9] than thiols bound at terrace sites. Across these studies, there is agreement that the rate-determining step for desorption and exchange appears to be cleavage of the adsorbate-substrate bond (i.e. S-Au.). Thus, methods to increase the strength of adsorbate-substrate interactions could improve the stability of SAMs.

While these various studies have focused on understanding the mechanisms of exchange, there has been no report of a method that improves the stability of a SAM against exchange. In this chapter, underpotentially deposited metal adlayers of silver and copper are used to stabilize SAMs against exchange processes. In Chapter 8, alkanethiols were reported to adsorb on gold surfaces modified by upd of silver or copper and form densely packed, oriented monolayers with properties similar to those of SAMs on gold. A demonstrated advantage of these systems is that an upd adlayer of silver can act as an adhesive interlayer between gold and the thiol head group and increase the overall thermal stability of the SAM against desorption, as discussed in Chapter 9.

The ability to improve the room temperature stability of SAMs is also an important underlying need in this area of research, as these systems have been suggested to find use in devices that would require extended operation under ambient conditions. While monolayers of thiols on gold are stable for months in air,[10] they show significantly less stability toward desorption when contacted with a liquid phase.[1] Exchange experiments represent a useful means of studying the loss of a SAM in a liquid phase at room temperature. In this chapter, the kinetics of exchange are reported for various alkanethiol-based SAMs on substrates of gold, Au/Ag(upd), Au/Cu(upd), silver, and copper. The thiols that are exchanged from these substrates contained a variety of tail groups— -CH_3, -OH, -CO_2H, -$OCH_2CF_2CF_3$, and -COFc (Fc = ferrocenyl)—that differed in their specific size and polarity. These tail groups allowed the exchange process to be monitored by various techniques, including x-ray photoelectron spectroscopy (XPS), reflectance-infrared spectroscopy (RAIRS), electrochemistry, and wetting measurements. In addition, the use of terminal groups of varying size offers a method to tune the packing of the hydrocarbon tether

within the SAM. Investigation of the displacement of these different SAMs by competing adsorbates provides insight into the effects of monolayer packing and substrate composition on exchange rates.

10.2. Results

Polycrystalline gold substrates were functionalized with submonolayer amounts of silver or copper by underpotential deposition, as described in Chapter 8. Upd-modified gold, along with evaporated films of copper, silver, and bare gold, served as substrates for self-assembly and subsequent exchange studies. Upd-modified gold substrates were transferred from the electrochemical cell through air to thiol-containing solutions to form SAMs [Au/Ag(upd)/SR or Au/Cu(upd)/SR].[11] In all cases, the formed SAMs were exposed to air for less than five minutes before being placed in the exchanging solution to minimize oxidation of thiolates to sulfonates; SAMs that undergo this oxidation exhibit much faster rates of exchange.[6] As mentioned in Chapter 8, upd substrates that were derivatized with thiols exhibited no peaks for oxygen by XPS. In contrast, thiol-derivatized copper or silver films (~1000 Å) that were exposed to air for shorter times did exhibit peaks for oxygen by XPS. The greater resistance of the upd-modified substrates against oxidation in comparison to the bulk metals is a result of their more noble redox potential. The submonolayer coverage (ϕ_i) of the upd component in these systems was 0.55 ± 0.05 and 0.75 ± 0.06 for Au/Cu(upd) and Au/Ag(upd), respectively, based on calculations from XPS data (eq 8.1).

10.2.1. Exchange of $M/S(CH_2)_{11}OCH_2CF_2CF_3$ by $CH_3(CH_2)_{15}SH$.

SAMs derived from $CF_3CF_2CH_2O(CH_2)_{11}SH$ on gold, Au/Ag(upd), Au/Cu(upd), silver, and copper were exposed to solutions of n-$C_{16}SH$ (1 mM, ethanol), and the exchange rate of the fluorinated adsorbate was monitored *ex situ* by XPS from the intensity of the F(1s) peak (Figures 10.1a and b). In these semi-logarithmic plots, the lack of linearity in a data set illustrates a deviation from a first-order exchange process. The data for the gold substrate exhibited the strongest deviation from a simple first-order process, suggesting a more complex mechanism for exchange than for the other substrates (vide infra). The exchange on gold proceeded more rapidly than on silver or Au/Ag(upd). Over 80% of the SAM on gold was observed to exchange within 20 h of exposure to n-$C_{16}SH$, while the remaining 20% was displaced at a much slower rate. In contrast, 80% of the original SAM on silver remained on the surface during exposures to the n-$C_{16}SH$ solution for up to 120 h. When the gold substrate was modified by upd of silver [silver coverage (ϕ_{Ag}) = 0.75], the exchange rate was intermediate between that of silver and gold.
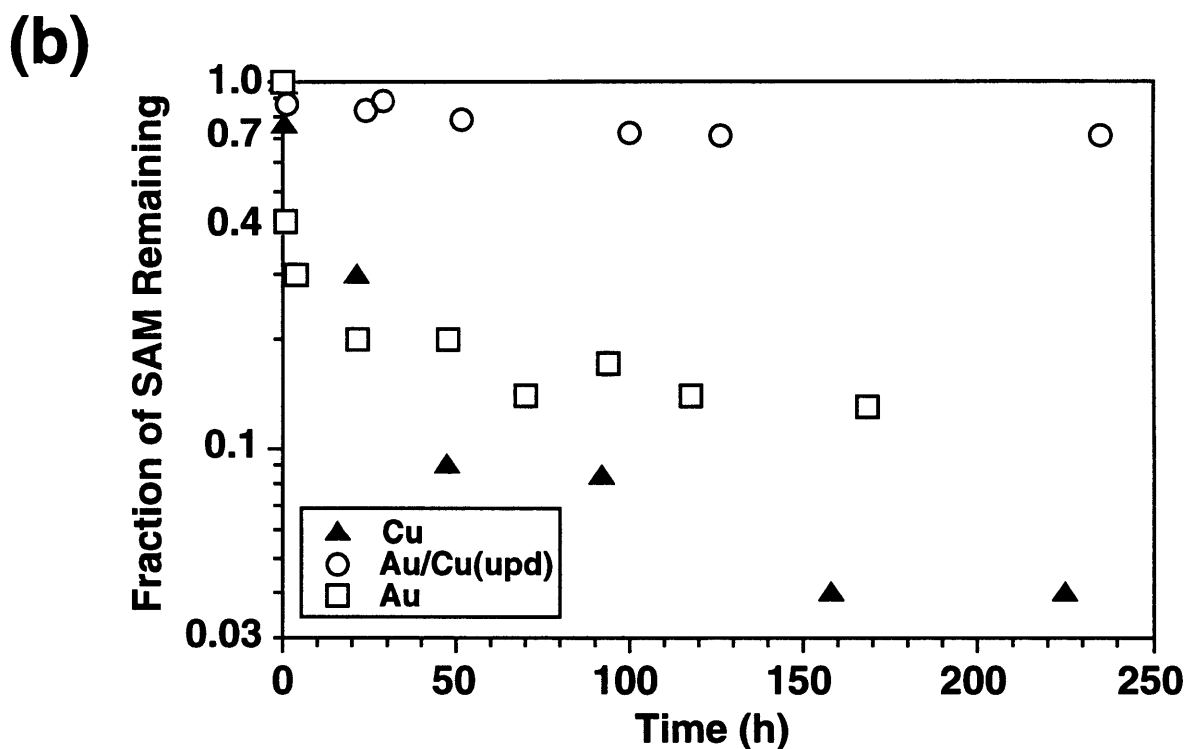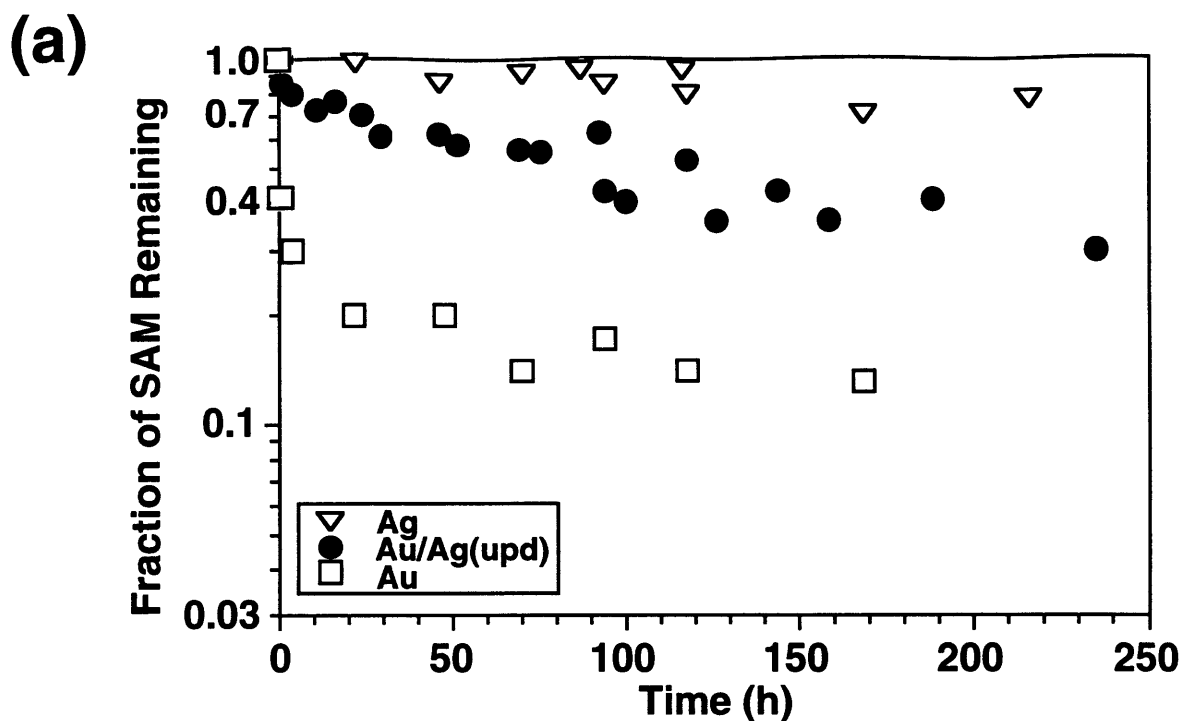
Figure 10.1. Surface coverage of SAMs derived from $CF_3CF_2CH_2O(CH_2)_{11}SH$ on various substrates as a function of exposure time to a 1 mM ethanolic solution of $C_{16}H_{33}SH$. Upper panel: Ag, Au/Ag(upd), and Au; lower panel: Cu, Au/Cu(upd), and Au. Surface coverages were determined *ex situ* using XPS by normalizing the F(1s) peak intensity to that of an initially prepared SAM on the same substrate. The data in Figures 10.1-10.4 have been plotted on semi-logarithmic axes to demonstrate compatibility or lack thereof with first-order kinetics.

Improvements in the thermal stability were also observed for SAMs derived from $CF_3CF_2CH_2O(CH_2)_{11}SH$ on Au/Ag(upd) substrates, as discussed in Chapter 9.

In Figure 10.1b, the exchange of $CF_3CF_2CH_2O(CH_2)_{11}S$- from either copper or gold occurs on a comparable timescale that is much shorter than that for exchange of this SAM on Au/Cu(upd) ($\phi_{Cu} = 0.55$). In fact, the exchange on Au/Cu(upd) is slower than on Au/Ag(upd) (Figure 10.1a). This difference contrasts the thermal stability of these monolayers on the upd substrates as the SAMs desorb from Au/Cu(upd) more rapidly than from Au/Ag(upd) (Chapter 9). A possible explanation for this difference in stability might be that the Au/Cu(upd) substrate is more susceptible to oxidation at the higher temperatures (70 - 100 °C) associated with the thermal stability studies. For the exchange studies performed at room temperature, the tendency for oxidation of the Au/Cu(upd) substrate is minimal.

10.2.2. Exchange of $M/S(CH_2)_{17}CH_3$ by $CD_3(CD_2)_{17}SH$

While Figure 10.1 shows the displacement with an unsubstituted n-alkanethiol of an ω-functionalized alkanethiol containing a tail group that is likely to affect interchain packing, Figure 10.2 displays data for the exchange of adsorbates with similar structure. For these experiments, reflectance-absorption infrared spectroscopy (RAIRS) was used to monitor the exchange of adsorbed n-$C_{18}H_{37}S$- by n-$C_{18}D_{37}SH$ (1 mM, ethanol) (Figure 10.2). Since the deuterated and protonated adsorbates would likely adopt identical structures on the substrate, this process resembles that of self-exchange. As the deuterated molecules displace the protonated adsorbates, diminution of the methylene stretching peaks in the RAIR spectra is observed. The coverage of the protonated adsorbates was estimated by normalizing the intensities of the $v_a(CH_2)$ and $v_s(CH_2)$ peaks (2919 and 2851 cm^{-1}, respectively) for a partially exchanged sample to their respective integrated intensities for a complete $C_{18}H_{37}S$- SAM on a particular substrate and averaging the resulting two values. The reduction in peak intensity is assumed to correlate linearly with -CH_2-coverage as the canted structures on the substrates are expected to remain unchanged as the composition of the protonated and deuterated species varies. Consistent with the results in Figure 10.1, the SAM on gold was replaced more rapidly than the SAMs on Au/Ag(upd) or Au/Cu(upd) (Figure 10.2); however, the displacement of the n-alkanethiolate SAM on gold (Figure 10.2) proceeded at a considerably slower rate than that of the F-tagged SAM (Figure 10.1). In comparison to the $CF_3CF_2CH_2O$- terminated SAM, the n-alkanethiolate SAM has a longer polymethylene chain and a smaller tail group (-CH_3), both of which may promote a higher degree of packing within the hydrocarbon portion of the SAM and thereby slow the exchange rates by limiting transport of competing adsorbates to the substrate.
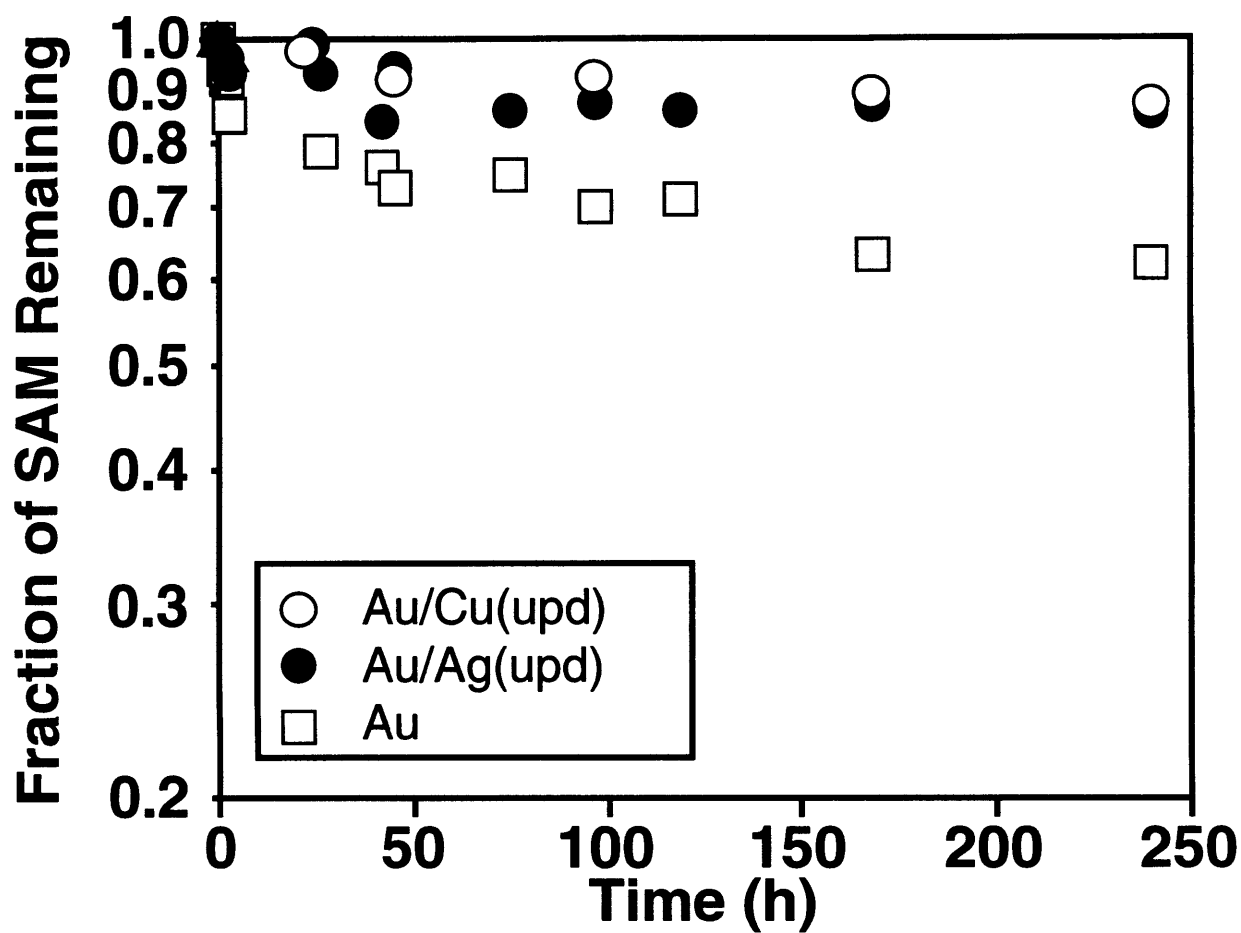
Figure 10.2. Surface coverage for SAMs derived from $C_{18}H_{37}SH$ on Au/Cu(upd), Au/Ag(upd), and Au after exposure to 1 mM ethanolic solutions of $C_{18}D_{37}SH$. Surface coverages were determined *ex situ* with IR spectroscopy by normalizing the integrated intensities of the asymmetric $[v_a(CH_2)]$ and symmetric $[v_s(CH_2)]$ methylene stretching peaks to those for an initially prepared SAM from $C_{18}H_{37}SH$ on the same substrate and averaging the two values.

10.2.3. Exchange of $M/S(CH_2)_{11}OH$ and $M/S(CH_2)_{10}CO_2H$ by $CH_3(CH_2)_{11}SH$

Monolayers derived from $HO(CH_2)_{11}SH$ and $HO_2C(CH_2)_{10}SH$ expose surface groups that are slightly different in size and provide systems for studying the effect of SAM packing on exchange rates. The exchange of $HO(CH_2)_{11}S$- SAMs with $CH_3(CH_2)_{11}SH$ has been previously monitored by the advancing contact angle of water.[12] As the relatively polar HO-terminated adsorbates are replaced by nonpolar CH_3-terminated adsorbates, the water contact angle on these surfaces increases, indicative of the formation of a lower energy surface. The measured contact angle on the exchanged surface (θ_{meas}) can be correlated with the composition of the binary surface through the Cassie equation:

$$\cos \theta_{meas} = \chi_p \cos \theta_p + \chi_{np} \cos \theta_{np} \qquad (10.1)$$

where θ_p and θ_{np} are the advancing contact angles for water on the polar-terminated surface and the CH_3-terminated surface, respectively, and χ_p and χ_{np} are the surface area fractions of the polar and nonpolar components on the surface, respectively. Equation 10.1 has been shown to accurately predict the surface concentration of these binary systems on copper, silver, and gold substrates.[13] Figures 10.3a and b show the surface coverage of the HO- and HO_2C-terminated SAMs, respectively, upon exposure to $C_{12}SH$ (1 mM, ethanol). The results of these exchange studies on the various substrates indicate more rapid replacement of the SAM on gold than on upd-modified gold or on silver. In addition, although the data in Figures 10.3a and b suggest that the rates are similar, the exchange of the HO-terminated SAM is slightly slower than that of the HO_2C-terminated monolayer on all substrates studied. While $HO(CH_2)_{11}SH$ forms a more crystalline SAM,[14] the HO_2C-terminated monolayer may form a hydrogen-bonded network[15] that could provide additional stability for the SAM. The similar exchange rates on the various substrates suggest that the stability of the SAMs are not dramatically affected by small differences in head group size.

10.2.4. Exchange of $M/S(CH_2)_{10}COFc$ with $CH_3(CH_2)_{11}SH$

If monolayer packing does indeed influence exchange, then replacement of an adsorbate with a bulkier tail group should proceed more rapidly than for a SAM with a smaller tail group. In this section, the exchange of SAMs formed from $FcCO(CH_2)_{10}SH$ (Fc = ferrocene) with 1 mM $C_{12}SH$ in ethanol is discussed. The cross-sectional area of ferrocene is 36 Å^2 and is greater than the packing density of unsubstituted alkanethiols on silver and gold. The exchange of these
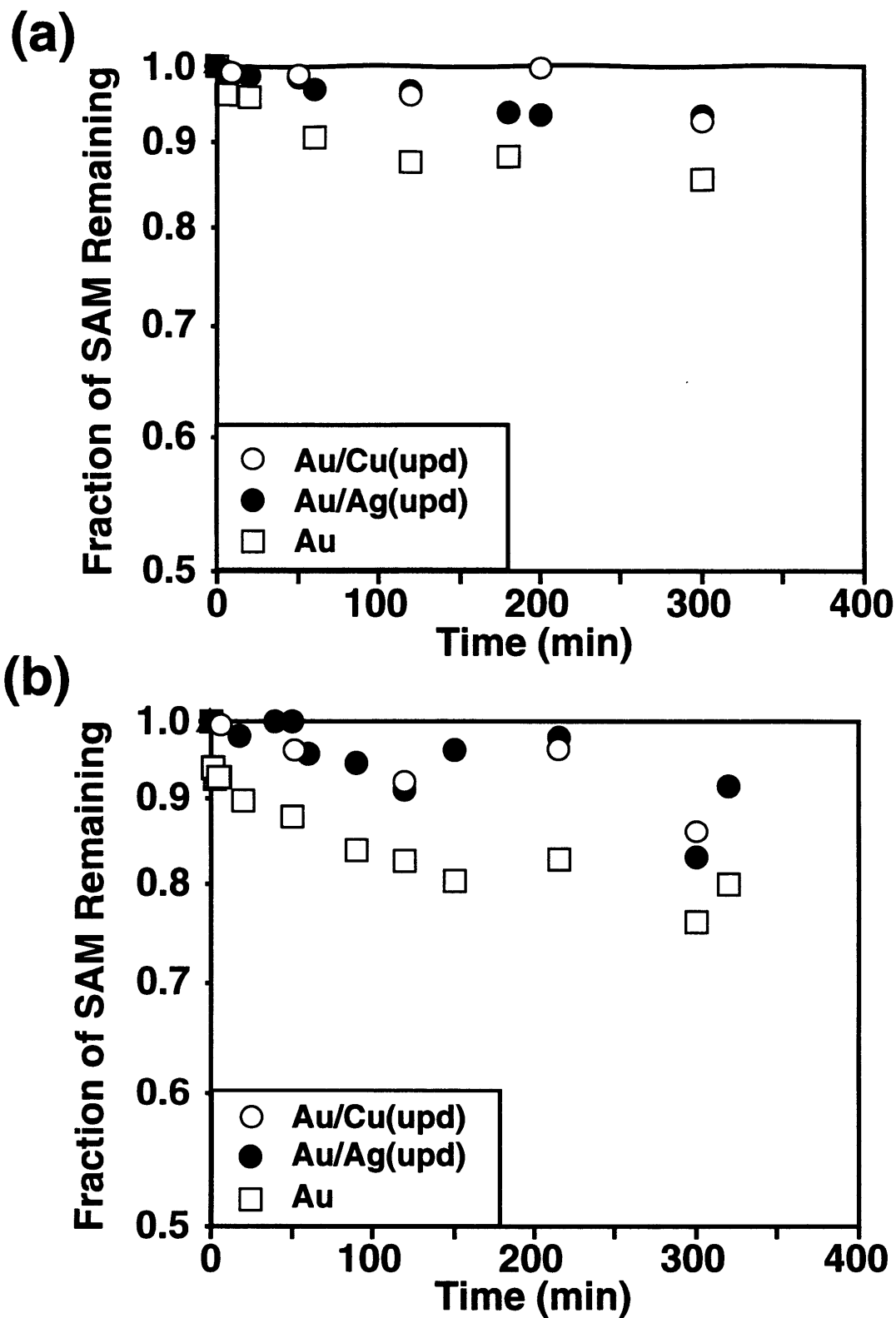
Figure 10.3. Surface coverage for SAMs derived from (a) HO(CH$_2$)$_{11}$SH and (b) HO$_2$C(CH$_2$)$_{10}$SH on Au/Cu(upd), Au/Ag(upd), and Au after exposure to 1 mM ethanolic solutions of C$_{12}$H$_{25}$SH. The surface coverage was estimated from the Cassie equation (eq 10.1) using the advancing contact angle of water on these partially exchanged SAMs.

electroactive SAMs was studied by determining the coverage of the ferrocene groups electrochemically after exposure to n-alkanethiol solutions. Reversible voltammetry has been reported for monolayers derived from $FcCO(CH_2)_{10}SH$ on gold,[16] Au/Ag(upd) (Chapter 8),[11] and Au/Cu(upd)[17] substrates. Voltammetry of these SAMs on copper and silver is not possible as the redox potential of the ferrocenoyl SAM is positive of $Ag^{+/0}$ and $Cu^{2+/0}$. The exchange data for SAMs derived from $FcCO(CH_2)_{10}SH$ on gold exposed to 1-mM n-$C_{12}SH$ (ethanol) show that 70% of the bulky adsorbates exchanged from gold within 6 h of exposure while few ($< 20\%$) of the adsorbates were displaced from Au/Ag(upd) or Au/Cu(upd) over 22 h (Figure 10.4).

The exchange process for $FcCO(CH_2)_{10}S$- monolayers on Au and Ag(upd) was examined by reflectance IR (Figure 10.5) to determine if the improved stability of the electroactive SAM afforded by the upd layers could be due to a difference in structure as unsubstituted n-alkanethiols form more densely packed films on the upd-modified substrates than on gold.[11] As the ferrocene-terminated SAM is initially formed on either substrate, the IR spectra contain methylene stretching peaks at 2925 [$v_a(CH_2)$] and 2853 cm^{-1} [$v_s(CH_2)$] for the polymethylene tether and an aromatic stretching peak at 3105 cm^{-1} for the terminal ferrocenyl moieties. The similar intensities and positions of these peaks on the different substrates suggest that the structure and organization of the Fc-terminated SAM are independent of substrate. This observation is not surprising since the bulky ferrocene group should govern the packing densities of the adsorbates on the substrates.[18]

After exposure of the Fc-terminated SAM on gold to 1 mM n-$C_{12}SH$ for 22 h (Figure 10.5), the IR spectrum revealed increased intensities of the methylene stretching peaks, the appearance of methyl stretching peaks, and a diminution of the aromatic peak. The position of the asymmetric methylene stretching peak [$v_a(CH_2)$] shifted from 2925 cm^{-1} to 2921 cm^{-1} after this exposure and indicated a more crystalline conformation of the alkyl chains within the SAM. These observations are consistent with the replacement of Fc-terminated thiolates with n-alkanethiols that can pack more densely. The spectrum for $FcCO(CH_2)_{10}S$/Ag(upd)/Au after the same 22-h exposure to n-$C_{12}SH$ (1 mM, ethanol) indicated no major changes in the peak intensities or positions. The intensity of the aromatic C-H stretching peak at 3105 cm^{-1} is approximately 90% of that found in the spectrum for the original SAM. The appearance of a weak peak in this spectrum at 2880 cm^{-1} corresponding to [$v_a(CH_3)$] suggests that only slight levels of exchange and/or incorporation have occurred with the methyl-terminated adsorbate. These results confirm those obtained by coulometry (Figure 10.4) and provide structural information about the exchange process.

167
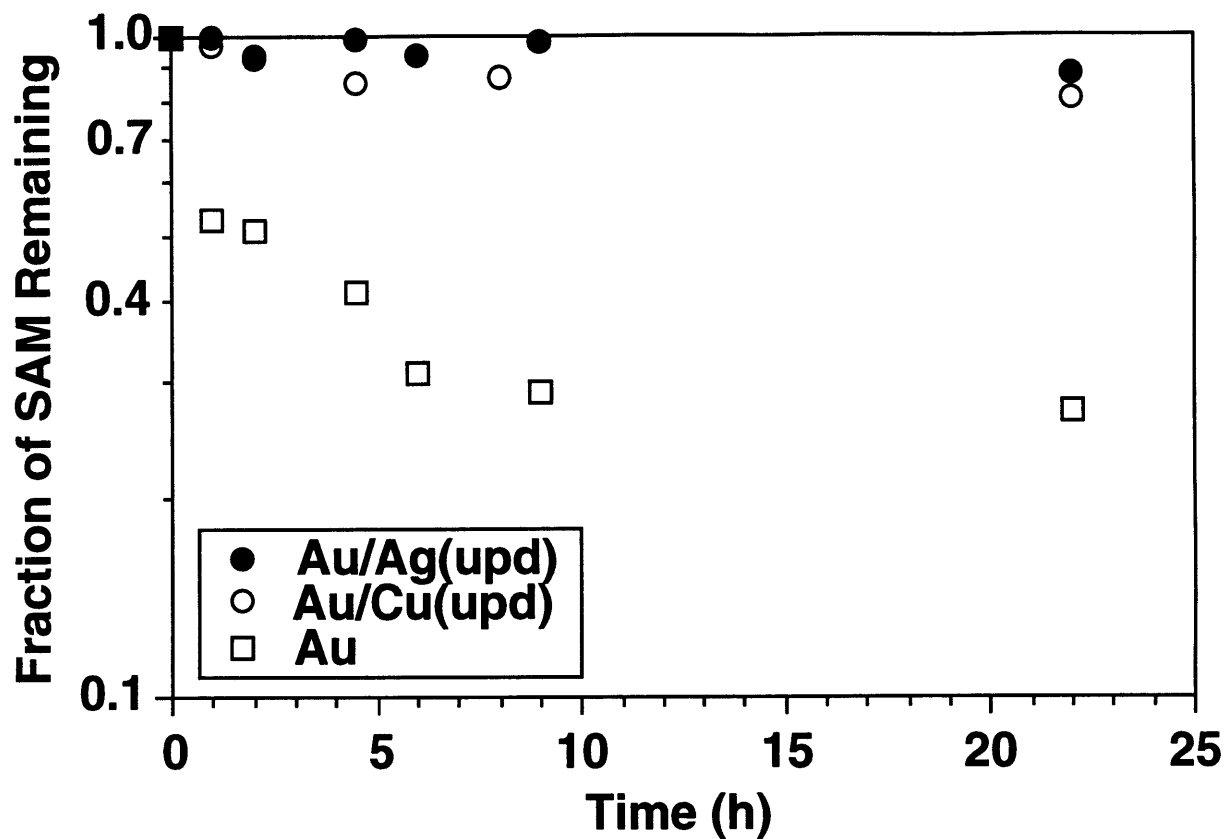
Figure 10.4. Surface coverage for SAMs derived from $FcCO(CH_2)_{10}SH$ on Au/Cu(upd), Au/Ag(upd), and Au after exposure to 1 mM ethanolic solutions of $C_{12}H_{25}SH$. The data are normalized to the coverages of initially formed SAMs on the respective substrates.

168
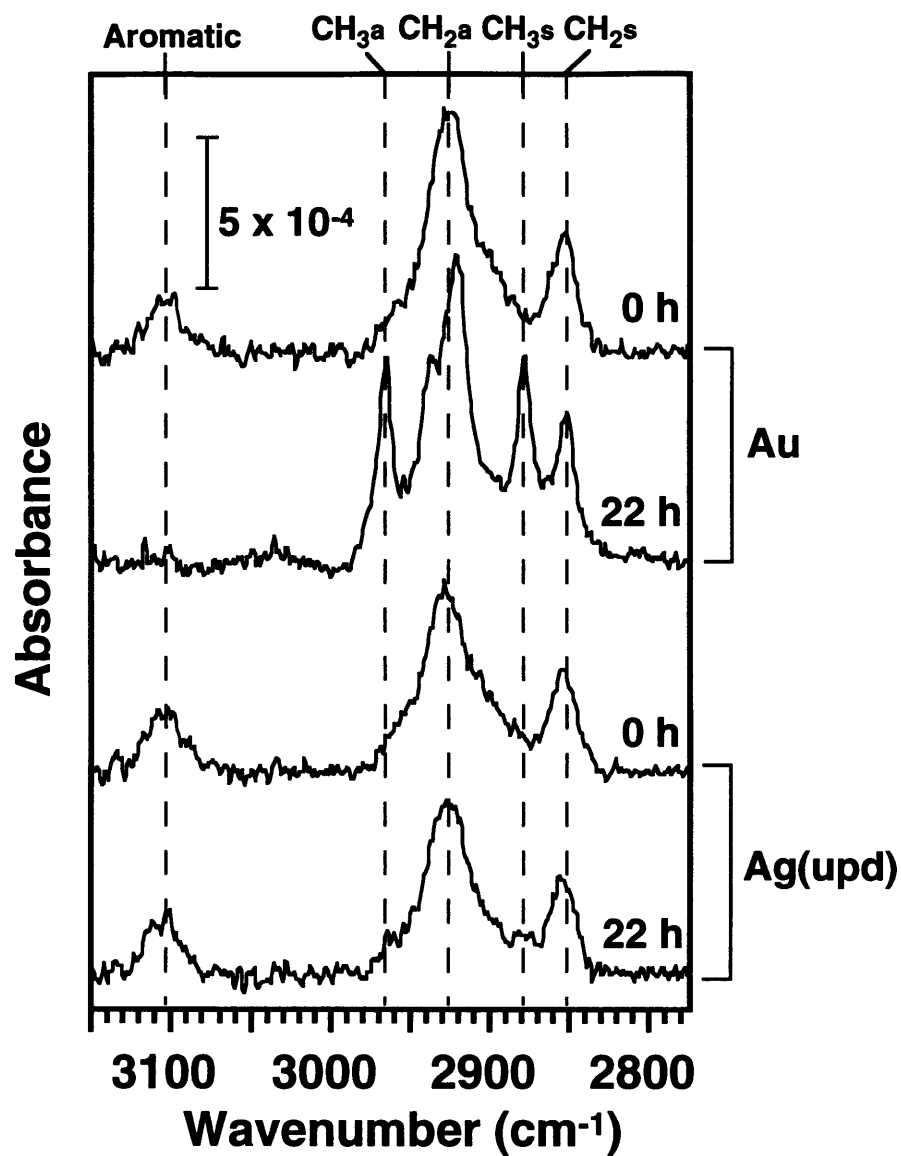
Figure 10.5. Grazing incidence polarized infrared spectra for SAMs of $FcCO(CH_2)_{10}SH$ on Au and Au/Ag(upd) before and after exposure to 1 mM ethanolic solutions of $C_{12}H_{25}SH$ for 22 h. The spectra have been offset vertically for clarity.

10.3. Discussion

The results shown in Figures 10.1 - 10.5 are consistent in that thiols exchange more rapidly from gold than from Au/Ag(upd) and Au/Cu(upd) and that adsorbates with bulkier tail groups are replaced from gold at a greater rate than adsorbates with smaller terminal groups. In order to compare the exchange rates for the different substrates and tail groups, the exchange was assumed to be a first-order process. This assumption appears to be valid for SAMs on the upd-modified gold and evaporated silver substrates as the data in Figures 10.1 - 10.4 exhibit a high degree of linearity which would suggest a first-order process. The data on gold and copper do not show the same linear behavior, suggesting a more complex process, but can be approximated as a first-order process in the following manner:

$$\ln [\theta(t) - \theta_{eq}] = -kt \qquad\qquad (10.2)$$

where k is a pseudo-first-order rate constant that accounts for the relatively constant solution-phase thiol concentration, $\theta(t)$ is the surface coverage of the original SAM, and θ_{eq} is a pseudo-equilibrium coverage in which the SAM concentration changes slowly with time. Table 10.1 lists the first-order rate constants for the data in Figures 10.1 - 10.4.

Table 10.1. Effect of tail group and substrate on exchange rates (k).

Adsorbate	Au	Ag(upd)	Ag	Cu(upd)	Cu
$HSC_{10}COFc$	200	8		9	
$HSC_{11}OCH_2CF_2CF_3$	120	6	2	3	100
$HSC_{10}CO_2H$	90	20		20	
$HSC_{11}OH$	40	14	12	12	
$HSC_{17}CH_3$	4	1		1	

k (h^{-1} x 10^3)

10.3.1. Exchange of SAMs on Gold

In these experiments, the size of the terminal group of the adsorbates was varied to generate SAMs with differing levels of packing. SAMs formed from adsorbates with bulky terminal groups— especially those with cross-sectional areas greater than the projected area of ~19.4 $Å^2$/ CH_2 for the polymethylene chain—are expected to pack less densely and contain more defects than those formed from adsorbates with smaller terminal groups. Exchange rates for these SAMs should depend on the degree of packing if the exchange mechanism is indeed mediated by defects within

the SAM. As summarized in Table 10.1, the exchange of SAMs on gold depends on the terminal group of the adsorbates comprising the SAM. For example, the rate of exchange of a SAM terminating in a bulkier -COFc group on gold is five times greater than for a SAM with a -CH$_2$OH terminus. This result cannot be explained by solubility differences because the alcohol adsorbate is more soluble in ethanol than the Fc adsorbate. The exchange rates for SAMs derived from CF$_3$CF$_2$CH$_2$O(CH$_2$)$_{11}$SH on gold are also considerably greater than for adsorbates with smaller terminal groups. This rapid exchange is attributed to the poor packing of the hydrocarbon within the SAM that results from the -OCH$_2$CF$_2$CF$_3$ tail groups. The ethereal and fluorinated units are likely to introduce gauche conformers in the tail group and cause the hydrocarbon chains of the SAM to pack less densely than for unsubstituted n-alkanethiolate SAMs. A comparison of IR spectra for CF$_3$CF$_2$CH$_2$O(CH$_2$)$_{11}$S- and CH$_3$(CH$_2$)$_{11}$S- SAMs on gold confirmed this difference as the methylene peaks revealed a less crystalline structure for the fluorinated SAM [v_a(CH$_2$) = 2921 cm^{-1}, v_s(CH$_2$) = 2852 cm^{-1}] than for the dodecanethiolate SAM [v_a(CH$_2$) = 2918 cm^{-1}, v_s(CH$_2$) = 2851 cm^{-1}]. Hickman et al. have also shown that the exchange of SAMs derived from different Fc-terminated adsorbates depends on the packing of the tether.[16]

Since exchange rates for SAMs on gold depend on the level of packing within the SAM, the mechanism for exchange is likely defect-mediated, as proposed by Collard and Fox. While they[5] and others[1] have concluded that dissociation of the adsorbed molecule from the substrate is rate-limiting, the results presented in this chapter indicate that the competing adsorbate is an active participant in the displacement. For example, less than 5% of adsorbed CF$_3$CF$_2$CH$_2$O(CH$_2$)$_{11}$S- desorbs from gold after 100 h exposure to blank ethanol, whereas 70% of the SAM was exchanged by C$_{16}$H$_{33}$SH (1 mM, ethanol) within 5 h. Clearly, the competing adsorbate must be present to promote dissociation. In addition, faster exchange rates have been observed when shorter-chained competing adsorbates are used,[5] even though longer-chained adsorbates are more favored on the substrate. Since shorter-chained thiols can more easily diffuse through defects within the SAM, this result further indicates that the exchange process on gold is mediated by defects within the SAM through which competing adsorbates can diffuse and promote dissociation.

10.3.2. Effect of Substrate

As shown in Figures 10.1 - 10.4 and summarized in Table 10.1, SAMs on Au/Ag(upd) and Au/Cu(upd) are more stable to exchange than SAMs on gold. Schlenoff et al. have proposed that a defect-rich surface stabilizes SAMs against desorption.[1] Nevertheless, none of our characterization methods suggests that the upd process roughens the surface or creates defects on the underlying gold. Roughness measurements performed on both gold and Au/Ag(upd) from AFM images revealed similar surface roughnesses for the two substrates (R_{ms} = 4 ± 2 Å). The

presence of any atomic-scale defects promoted by the upd process would likely affect the quality of the resulting SAMs. However, IR spectra for n-alkanethiols on Au/Ag(upd) indicate the formation of organized structures [as inferred from the position of $v_a(CH_2)$] that are as good or better than those observed for similar adsorbates on gold (Chapter 8).

A more likely explanation for the improved stability on upd-modified gold is that the thiol headgroup interacts more strongly with the silver(upd) and copper(upd) substrates than with gold. If dissociation from the surface controls the rate of exchange, a stronger substrate-adsorbate interaction would certainly slow the exchange process. Providing evidence for this hypothesis, the rate of exchange of $CF_3CF_2CH_2O(CH_2)_{11}S-$ with $C_{16}H_{33}SH$ is orders of magnitude greater on gold than on bulk silver (Figure 10.1), and the results of Chapter 9 indicated that alkanethiolate SAMs on silver and Au/Ag(upd) are more thermally stable than those on gold. These results suggest that thiols bind more strongly to silver than to gold. This improved stability for SAMs on silver may be the result of a S-Ag bond with more ionic character than a S-Au bond, as determined from Raman experiments.[19] Nevertheless, it is important to note that a surface of silver (or copper) upd on gold is chemically distinct from the outermost layer of a bulk silver (or copper) substrate, as evidenced by its more noble electrochemical characteristics and its enhanced resistance to oxidation. Thus, one can only hypothesize that the strength of a S-Ag(upd) interaction is similar to that of a S-Ag bond.

As shown in Figure 10.1, thiols on Au/Cu(upd) are more stable to exchange than either thiols on copper or gold. The rapid exchange of thiols on copper suggests that a thiol-copper interaction is no stronger than a thiol-gold interaction. However, results from temperature programmed desorption experiments indicate that SAMs of $n-C_{12}SH$ have considerably higher desorption energies on copper (32 kcal/mol) than on gold (26 kcal/mol).[20] The observed poor stability of SAMs on copper toward exchange is probably a function of the experimental conditions. For example, SAMs formed on copper from adsorptions of > 3 h duration are less ordered and exhibit greater contact angle hysteresis than those adsorbed for less than 1 h.[21] This disorder is likely the result of thiols corroding the underlying copper surface, and these additional pathways may contribute to the nature of the observed rapid exchange for thiol-based SAMs on copper. The self-assembly of thiols on Au/Cu(upd) appears to not be plagued by these corrosion problems (or to a dramatically reduced level) as the copper is only present in a single atomic layer and thus, exhibits enhanced stability to exchange.

10.3.3. Tail Group Effects on the Exchange Process

In contrast to SAMs on gold, the exchange of SAMs on upd-modified gold exhibits no clear dependence on tail group size (Table 10.1). This lack of dependence on monolayer packing could

be a function of the structure of the adsorbates within the SAM. For example, results from Chapter 8 suggested that SAMs composed of adsorbates with terminal groups that are smaller than the cross-section of the alkyl chain are more densely packed on silver, Au/Ag(upd), and Au/Cu(upd) than on gold. However, for adsorbates in which the level of packing depends on the packing of the tail groups rather than the alkyl chains [i.e. $FcCO(CH_2)_{10}SH$ and possibly $CF_3CF_2CH_2O(CH_2)_{11}SH$], the exchange rates on upd-modified gold are much lower than those on gold and are similar to those for adsorbates with small tail groups. This observation suggests that, although the density of defects for these bulkier SAMs on upd-modified gold and gold are comparable, the presence of these defects on upd-modified gold does not affect exchange to the same extent. In other words, the exchange process on upd-modified gold is less defect-mediated than on gold.

A mechanism consistent with these observations is one in which dissociation of the thiol from the upd-modified substrate strongly limits the exchange process. As the thiol-upd bond is perhaps stronger than the thiol-gold interaction, the dissociation energy for thiol adsorbates on upd-modified gold may be greater than that for thiols on gold. Whereas competing adsorbates may assist the dissociation of thiols from gold, their role in promoting dissociation from a upd substrate is hindered by the greater level of interaction between the adsorbate and substrate. This type of mechanism is consistent with the data on upd-modified gold (Figures 10.1 - 10.4). The higher degree of linearity for these data sets is expected if a first-order process is rate limiting. In contrast, the data sets for thiols on gold are more consistent with a mechanism in which dissociation is assisted by a displacement process caused by competing adsorbates that concentrate at defects and packing imperfections within the monolayer.

10.4. Conclusions

Modification of gold by an underpotentially deposited submonolayer of silver or copper before self-assembly results in systems that are more stable against exchange than SAMs on unmodified gold. The enhanced stability to exchange is consistent with the formation of a stronger metal-sulfur bond on upd-modified gold. On gold, adsorbates with terminal groups larger than the cross-section of the alkyl chain exchanged ~50 times more rapidly than those with methyl terminations. For upd-modified gold, the rates of exchange were relatively independent of the size of the terminal group. These results suggest that replacement of thiolates on gold is mediated by defects that allow competing adsorbates diffusional access to the underlying substrate while exchange on upd-modified gold is limited by dissociation of a stronger adsorbate-substrate bond between sulfur and copper or silver that is stronger than with gold.

10.5. Experimental

The preparation of upd-modified gold substrates is discussed in Chapter 8. The characterization of SAMs with wetting measurements, RAIRS, XPS, and electrochemistry is discussed in Chapter 8.

Exchange of F-tagged SAMs with $C_{16}SH$. Gold, silver, copper, Au/Ag(upd), and Au/Cu(upd) substrates were derivatized with $CF_3CF_2CH_2O(CH_2)_{11}SH$ (1 mM, ethanol) for 12 h. Upon removal from solution, the samples were rinsed with ethanol, dried with N_2, and placed in 1 mM solutions of n-$C_{16}H_{33}SH$ in ethanol. After allotted times, samples were removed from the exchanging solution, rinsed with isooctane and ethanol, dried with N_2, and characterized by XPS. The remaining coverage of the F-tagged SAM was determined by ratioing the F(1s) intensity for a partially exchanged SAM with that for a freshly prepared SAM on that substrate.

Exchange of HO_2C- and HO-terminated SAMs with $C_{12}SH$. Gold, Au/Ag(upd), and Au/Cu(upd) substrates were derivatized with $HO_2C(CH_2)_{10}SH$ or $HO(CH_2)_{11}SH$ (1 mM, ethanol) for 12 h. Upon removal from solution, the samples were rinsed with ethanol, dried with N_2, and placed in 1 mM solutions of n-$C_{12}H_{25}SH$ in ethanol. After removal from the exchanging solution, the samples were rinsed with isooctane and ethanol, dried in a stream of N_2, and characterized by wetting. The coverage of the polar component was determined by Cassie's equation (eq 10.1).

Exchange of Fc-terminated SAMs with $C_{12}SH$. Gold and Au/Ag(upd) samples were functionalized with $FcCO(CH_2)_{10}SH$ (1 mM, ethanol) for 12 h. After removal from solution, the samples were rinsed with ethanol and dried in a stream of N_2. The resulting assemblies were exposed to 1 mM solutions of n-$C_{12}H_{25}SH$ in ethanol for various periods of time. The samples were removed from solution, rinsed with isooctane and ethanol, dried in a stream of N_2, and characterized by cyclic voltammetry. The coverage of the ferrocene-terminated SAM was determined by ratioing the average integrated charge of the partially exchanged SAM to that of a freshly prepared $FcCO(CH_2)_{10}S$- SAM on the respective substrate.

Exchange of $C_{18}H_{37}S$- SAM with $C_{18}D_{37}SH$. Gold, Au/Ag(upd), and Au/Cu(upd) substrates were placed in 1 mM ethanolic solutions of octadecanethiol for 12 h. The exchange of the resulting octadecanethiolate SAM with octadecanethiol-d_{37} was monitored by IR. After exposure of Au/, Au/Ag(upd)/, and Au/Cu(upd)/$SC_{18}H_{37}$ samples to 1 mM ethanolic solutions of $C_{18}D_{37}SH$ for various periods of time, the samples were removed from solution, rinsed with isooctane and ethanol, dried in N_2, and characterized by IR. The integrated peak intensities of the asymmetric $[v_a(CH_2)]$ and symmetric $[v_s(CH_2)]$ methylene stretching vibrations for an exchanged sample were ratioed to those for an initially prepared sample to obtain coverage estimates of the remaining adsorbed non-deuterated thiol. The reported coverages were averages of the estimates obtained from ratios of both the $v_a(CH_2)$ and $v_s(CH_2)$ peaks.

174

10.5. References and Footnotes

1) Schlenoff, J. B.; Li, M.; Ly, H. *J. Am. Chem. Soc.* **1995**, *117*, 12528-12536.

2) Bain, C. D.; Troughton, E. B.; Tao, Y.-T.; Evall, J.; Whitesides, G. M.; Nuzzo, R. G. *J. Am. Chem. Soc.* **1989**, *111*, 321-335.

3) Jennings, G. K.; Laibinis, P. E. *Langmuir* **1996**, *12*, 6173-6175.

4) Chidsey, C. E. D.; Bertozzi, C. R.; Putsvinski, T. M.; Mujsce, A. M. *J. Am. Chem. Soc.* **1990**, *112*, 4301-4306.

5) Collard, D. M.; Fox, M. A. *Langmuir* **1991**, *7*, 1192-1197.

6) Scott, J. R.; Baker, L. S.; Everett, W. R.; Wilkins, C. L.; Fritsch, I. *Anal. Chem.* **1997**, *69*, 2636-2639.

7) Rowe, G. K.; Creager, S. E. *Langmuir* **1994**, *10*, 1186-1192.

8) Kumar, A.; Biebuyck, H. A.; Whitesides, G. M. *Langmuir* **1994**, *10*, 1498-1511.

9) Walczak, M. M.; Alves, C. A.; Lamp, B. D.; Porter, M. D. *J. Electroanal. Chem.* **1995**, *396*, 103-114.

10) Infrared spectra for SAMs on Au and Ag substrates that were exposed to air for 43 days exhibited methylene stretching positions and intensities that were almost identical to those for the initially prepared samples.

11) Jennings, G. K.; Laibinis, P. E. *J. Am. Chem. Soc.* **1997**, *118*, 5208-5214.

12) Laibinis, P. E.; Fox, M. A.; Folkers, J. P.; Whitesides, G. M. *Langmuir* **1991**, *7*, 3167-3173.

13) Laibinis, P. E.; Whitesides, G. M. *J. Am. Chem. Soc.* **1992**, *114*, 1990-1995.

14) The positions for the $v_a(CH_2)$ peaks in IR spectra of $HOC_{11}S$- and $HO_2CC_{10}S$-SAMs on gold are 2919 cm^{-1} and 2921 cm^{-1}, respectively.

15) Nuzzo, R. G.; Dubois, L. H.; Allara, D. L. *J. Am. Chem. Soc.* **1990**, *112*, 558-569.

16) Hickman, J. J.; Ofer, D.; Zou, C.; Wrighton, M. S.; Laibinis, P. E.; Whitesides, G. M. *J. Am. Chem. Soc.* **1991**, *113*, 1128-1132.

17) Jennings, G. K. *Electrochem. Soc. Interface* **1998**, *7*, 59.

18) Chang, S.-C.; Chao, I.; Tao, Y.-T. *J. Am. Chem. Soc.* **1994**, *116*, 6792-6805.

19) Bryant, M. A.; Pemberton, J. E. *J. Am. Chem. Soc.* **1991**, *113*, 8284-8293.

20) Jennings, G. K. *unpublished results* **1998**.

21) Laibinis, P. E.; Whitesides, G. M.; Allara, D. L.; Tao, Y.-T.; Parikh, A. N.; Nuzzo, R. G. *J. Am. Chem. Soc.* **1991**, *113*, 7152-7167.

Chapter 11. Structural Characterization of Self-Assembled n-Alkanethiolate Monolayers on Underpotentially Deposited Adlayers of Copper and Silver on Gold

11.1. Background

As mentioned in Chapter 1, self-assembled monolayers (SAMs) derived from n-alkanethiols provide perhaps the most flexible system for modifying the surface properties of many metals, including gold,[1,2] silver,[2,3] copper,[2] mercury,[4] and iron,[5] and other materials such as GaAs[6] and YBa$_2$CuO$_x$.[7] In the formation of n-alkanethiolate SAMs on these various substrates, energetic and geometric factors related to the metal-sulfur bonding control the resulting structure of the adsorbed organic assembly.[2] As each metal surface has distinct atomic-level features and provides differing levels of interaction with the adsorbing thiols, the structure of SAMs on these metals (and on different crystal faces of the same metal) can vary widely. For example, n-alkanethiols on mercury[4] orient almost normal to the surface while those on GaAs[6] tilt ~ 57° from the surface normal. These various structural conformations reflect the different densities of reactive sites on the metal surfaces and result from an interplay between the dominant metal-sulfur interaction and the less important energetics contributed by interchain interactions.

Alkanethiols on gold are the most widely studied class of SAMs due to the electrochemical inertness of gold and the flexibility offered by thiols in its surface modification.[8] The molecular details of the structure of these SAMs on gold have been probed with electron,[9] x-ray,[10] and He diffraction,[11] scanning probe microscopies,[12,13] and Raman [14] and IR spectroscopies.[2] Results from electron diffraction[9] and atomic force microscopy[13] suggest that the sulfur atoms bind in the three-fold-hollow sites on a Au(111) surface and form a ($\sqrt{3}$ x $\sqrt{3}$) R30° overlayer with an interchain spacing of 4.99 Å. Of these techniques, IR spectroscopy offers the most convenient method for assessing the phase state and conformation of the polymethylene chain of the SAM. In general, characterization by IR has focused on SAMs adsorbed onto polycrystalline gold, with the results from these studies often being confirmed later by diffraction studies of these assemblies on Au(111). Using the C-H stretching peaks in IR spectra, Porter et al. determined that the hydrocarbon chains of alkanethiolate SAMs on gold tilt ~30° on average from the surface normal and exist primarily in a crystalline state with a few gauche conformers present at the chain ends.[15] Efforts to control the molecular packing density within SAMs on gold have often involved the lengthy syntheses of adsorbates with bulky substituents,[16] rigid architectures,[17,18] or multiple ligating functionalities.[19] Although the lattice spacing on Au(111) (2.89 Å) is similar to that on Ag(111) (2.88 Å), SAMs on silver differ from those on gold in that the average cant of the adsorbates is only ~12°[2,3] or less.[20] This denser packing of the hydrocarbons on Ag(111) may

176

result from the lack of a clear site preference in which the binding of thiols to either on-top or three-fold-hollow sites is energetically feasible.[21] In short, the surface of Ag(111) provides a greater density of energetically favorable reactive sites than on Au(111).[22] These results suggest that the chemical modification of the outer atomic layer of gold to increase the number of reactive sites might offer a simple method to alter the packing density of SAMs on gold.

In this chapter, the atomic-level modification of gold by the underpotential deposition of copper and silver is demonstrated to affect the structure of an adsorbed SAM. As discussed in Chapter 8, n-alkanethiols chemisorb onto gold surfaces modified by the upd of silver or copper and produce oriented SAMs.[23] While these SAMs have similar wettabilities and thicknesses as those on gold, their molecular-level properties that are related to the nature of the metal-sulfur bonding are distinct. Specifically, SAMs formed on Au/Ag(upd) have greater thermal stabilities[24] than SAMs on gold (Chapter 9) while those on both Au/Ag(upd)[23] and Au/Cu(upd)[25] exhibit enhanced stability to exchange by competing adsorbates (Chapter 10). These enhanced stabilities are ascribed to a stronger sulfur-metal bond that is achieved by modification of the gold surface with upd. Besides the work reported here with SAMs on upd-modified gold, Burgess and Hawkridge have used the upd of silver on gold to reproducibly control the coverages of submonolayers of octadecanethiol.[26] Nishizawa et al. have studied the reversible deposition and stripping of copper upd layers through a SAM of propanethiol.[27] Zamborini et al. have recently reported that SAMs of hexadecanethiol on Au/Cu(upd) substrates effectively passivate the copper layer and that the combination of the SAM and upd layer significantly enhances the nobility of the underlying gold.[28] In Chapter 8, a upd adlayer of silver or copper was suggested to increase the packing density of an adsorbed octadecanethiolate SAM.[23] In this chapter, that finding is discussed in more detail by investigating the effect of upd adlayers of silver and copper on the structural properties of a series of n-alkanethiols (C_nSH; n = 15-20, 22). By using both odd- and even-chained thiols in this study, subtle variations in structure and bonding for the SAMs on these substrates were examined by using the methyl group as a spectoscopic tag. In addition, these studies provide a clear demonstration of the relationship between the microscopic, angstrom-level structure of a surface and its macroscopic properties as revealed by its wettability.

11.2. Results and Discussion

11.2.1. Infrared Spectra of SAMs on Native Metals and upd-Modified Gold

Evaporated gold films on silicon were derivatized with submonolayer amounts of silver or copper by underpotential deposition in a sulfate electrolyte and then functionalized by immersion in a 1 mM solution of an n-alkanethiol (C_nSH; n = 15-20, 22) for 16 h. Self-assembled monolayers

were prepared on gold, silver, and Au/Ag(upd) from isooctane while those on Au/Cu(upd) were prepared from ethanol. The SAMs formed by this procedure exhibited ellipsometric thicknesses and contact angles that were similar to those formed on native gold (Chapter 8). The coverages of silver and copper on the gold electrode after upd and subsequent thiol assembly were 0.60 ± 0.04 and 0.55 ± 0.05, respectively.

Figures 11.1a, b, c, and d shows grazing reflectance IR spectra of the C-H stretching region for SAMs formed from C_nSH (n = 15-20, 22) on substrates of gold, Au/Cu(upd), Au/Ag(upd), and silver, respectively. Spectra of these thiols on copper are similar to those on silver, as noted previously,[2] and are not shown here. The primary modes of the spectra are the asymmetric (r_a^-) and symmetric methyl modes—the latter split by Fermi resonance into r^+ and r^+(FRC) modes—and the asymmetric (d^-) and symmetric (d^+) methylene modes. The positions of these peaks—especially for the methylene modes—provide an indication of the phase state of the hydrocarbon chains. In these spectra, the positions of the asymmetric and symmetric methylene modes are 2918 - 2919 cm^{-1} and 2850-2851 cm^{-1}, respectively, both indicating formation of monolayers with crystalline hydrocarbon chains on these substrates. The spectra for SAMs on Au/Cu(upd) are superior to those reported previously by us[23] and reflect that higher quality SAMs can be formed on this substrate from ethanol (than from isooctane) with longer adsorption times, as shown by Zamborini et al.[28] For the other substrates, the IR spectra were observed to exhibit no solvent dependence. As discussed in Chapter 8, the greater susceptibility of Au/Cu(upd) to oxidation may affect the quality of the SAMs that can be formed on this substrate.[23]

The dipole moments of the methylene modes (d^- and d^+) are perpendicular to the axis of the hydrocarbon chain, and their intensities in a reflection infrared spectrum depend on the orientation of the adsorbates on the metal surface. Figure 11.2 shows the intensities of the asymmetric methylene (d^-) vibrational mode for SAMs of C_nSH on gold, silver, Au/Ag(upd), and Au/Cu(upd). As the chain length of the adsorbate increases from n = 15 to 22, the d^- intensity increases linearly for all systems, suggesting a common structure for the SAMs formed on a particular substrate for the different adsorbates. On all substrates, the lines exhibit a negative y-intercept reflecting the coupled nature of the polymethylene absorption, as noted previously.[2] For a common adsorbate, the d^- intensity was greatest on gold, of intermediate intensity on the upd-modified gold substrates, and smallest on silver (and copper). Combined with the symmetric methylene (d^+) intensities (not shown), these results suggest that the SAMs on upd-modified gold substrates are tilted less than those on gold and more than those on silver (vide infra). The data also suggest that the atomic-level modification of gold with upd of silver or copper before self-assembly can increase the packing density of SAMs on a gold suface. In addition, the dichroic ratios (d^-/d^+) for the spectra of
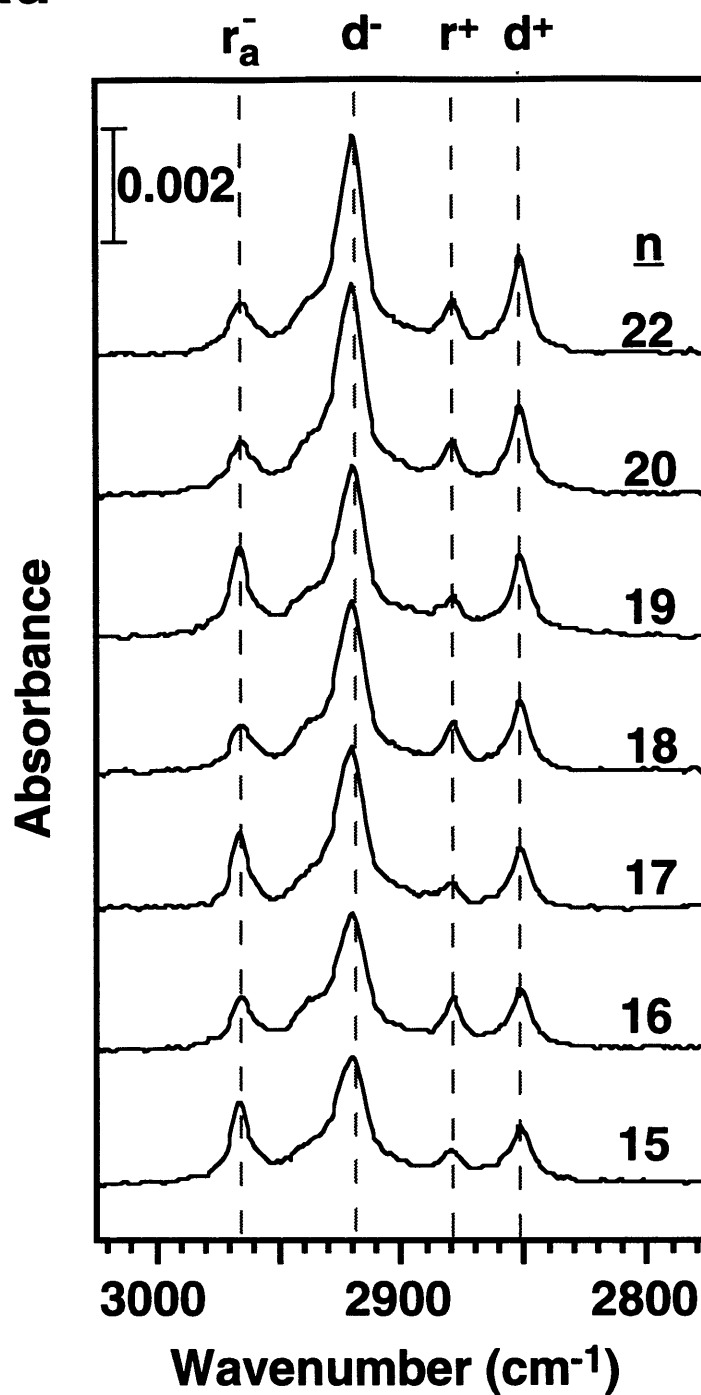
(a) Au

Figure 11.1. (a) Grazing reflectance IR spectra of monolayers derived from exposure of gold to n-alkanethiols (C_nSH; n = 15-20, 22).
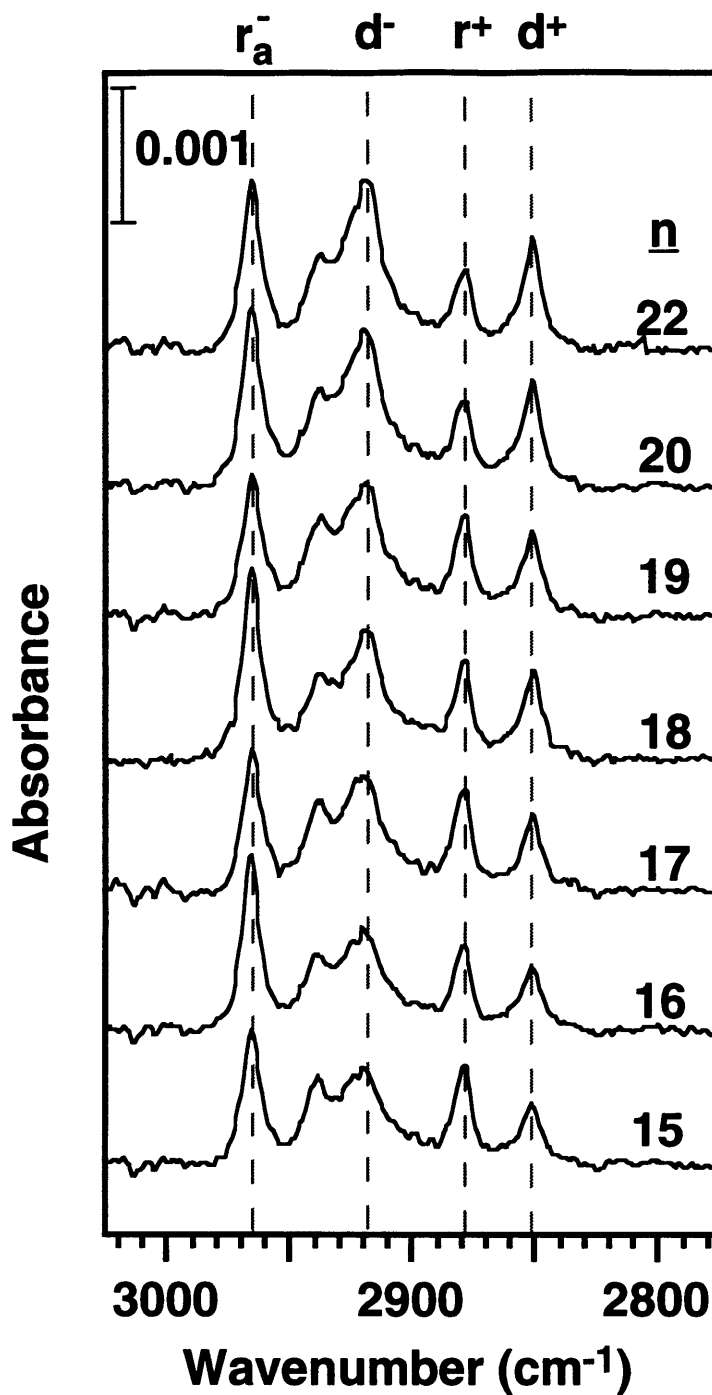
(b) Au/Cu(upd)

Figure 11.1. (b) Grazing reflectance IR spectra of monolayers derived from exposure of Au/Cu(upd) to n-alkanethiols (C_nSH; n = 15-20, 22).
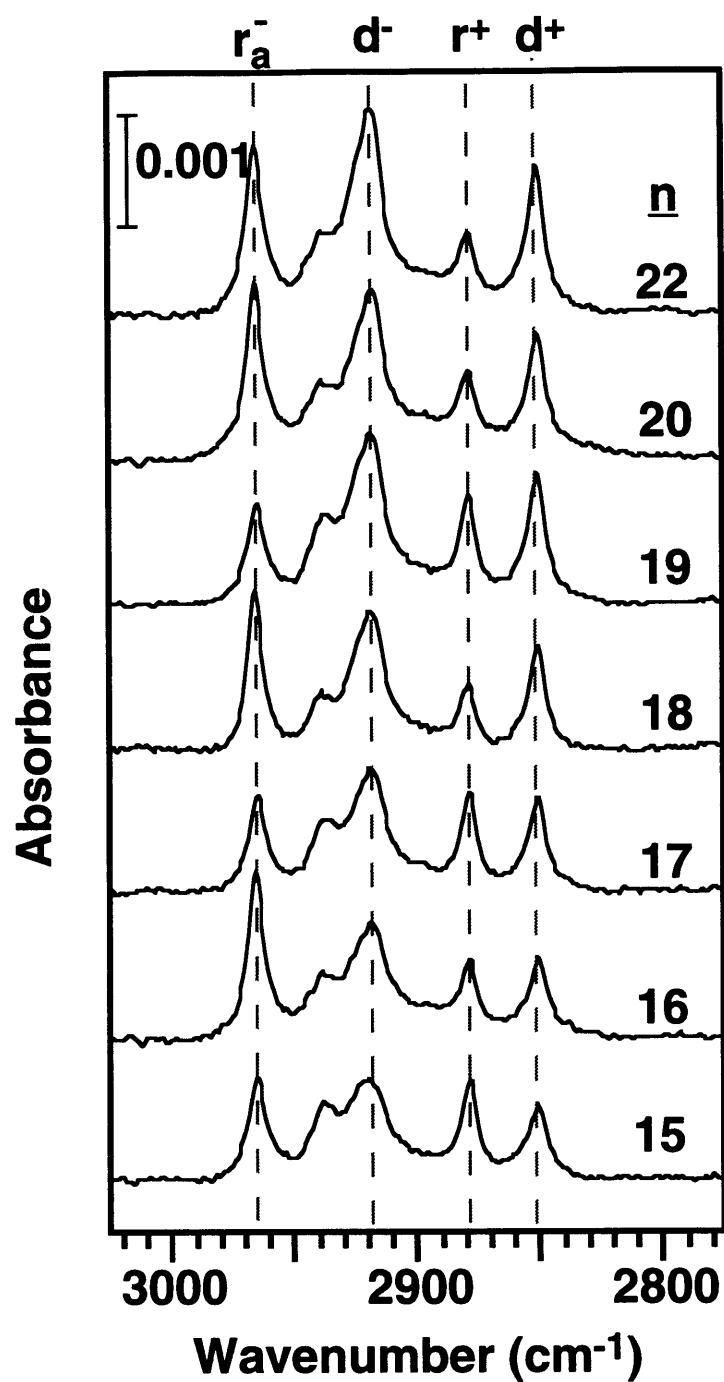
(c) Au/Ag(upd)

Figure 11.1. (c) Grazing reflectance IR spectra of monolayers derived from exposure of Au/Ag(upd) to n-alkanethiols (C_nSH; n = 15-20, 22).
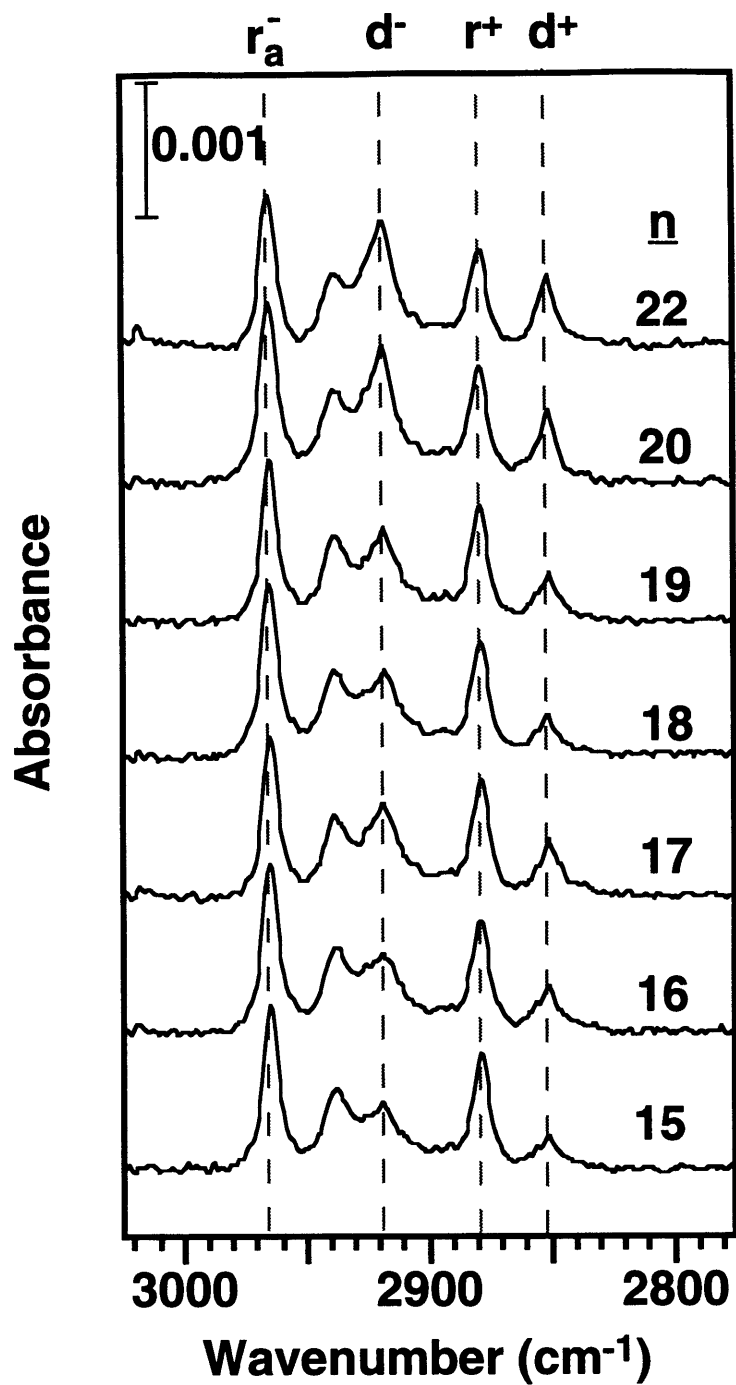
Figure 11.1. (d) Grazing reflectance IR spectra of monolayers derived from exposure of silver to n-alkanethiols (C_nSH; n = 15-20, 22).
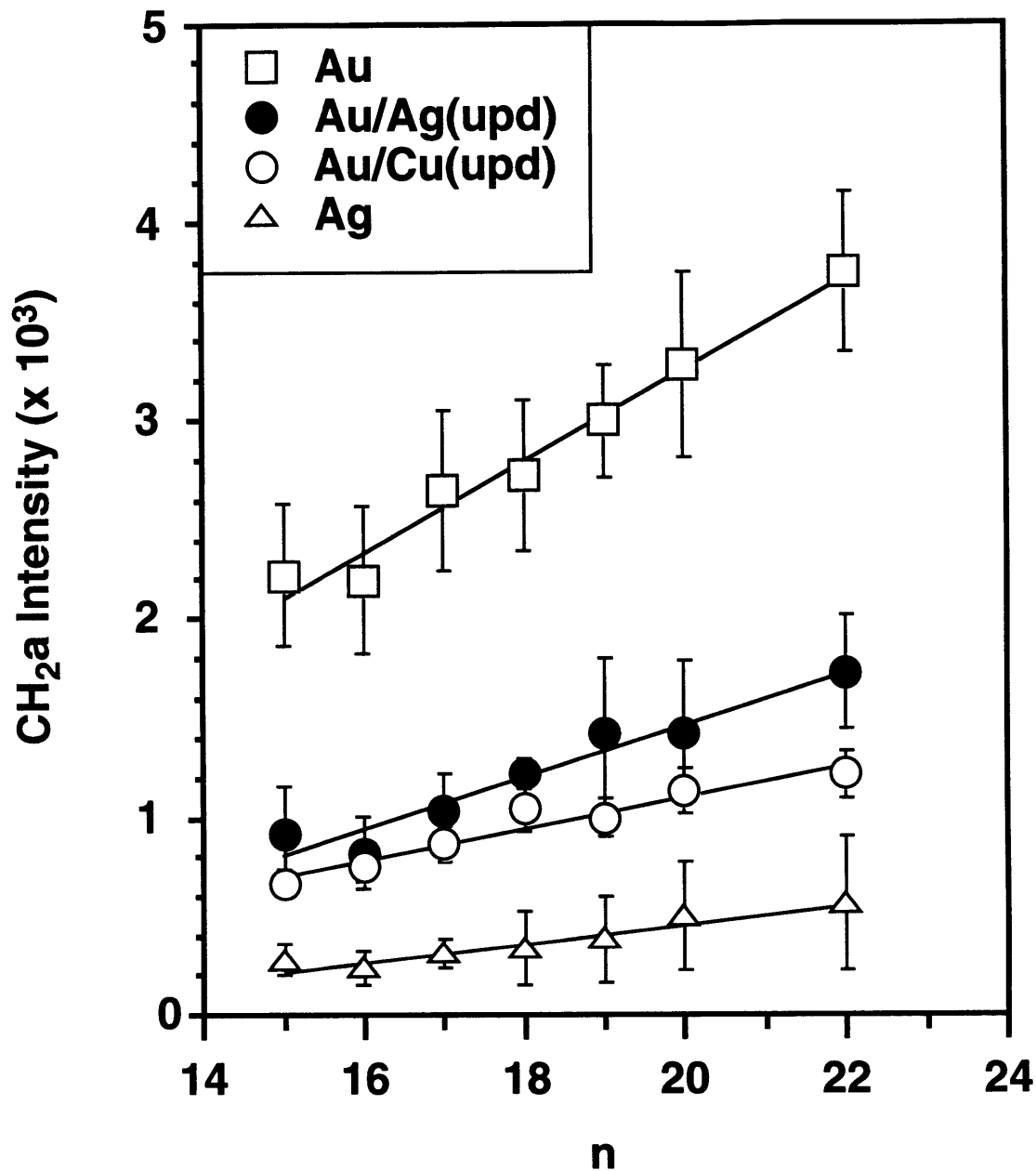
Figure 11.2. Intensities of the asymmetric methylene stretching mode (d⁻) for n-alkanethiols (C$_n$SH) adsorbed on gold, Au/Ag(upd), Au/Cu(upd), and silver surfaces. Intensities of d⁻ for n-alkanethiols adsorbed on copper are similar to those on silver. The lines are least-squares fits to the data.

SAMs on Au/Ag(upd) and Au/Cu(upd) are significantly lower than those for SAMs on gold or silver, suggesting a smaller twist of the adsorbates around the axis of the chain.

In the series of spectra for C_nSH on gold (Figure 11.1a), the asymmetric (r_a^-) and symmetric (r^+) methyl modes at ~2964 and ~2879 cm^{-1}, respectively, exhibit similar intensities for adsorbates with an even chain length but significantly different intensities for adsorbates with an odd chain length. Since these modes are orthogonal to each other, changes in intensity for one requires an opposite change in the other when comparing different spectra. This odd-even effect has been shown in SAMs by others[2,3,16] and indicates that the surface projection of the methyl group alternates between two different average orientations as the chain length is incrementally increased in these trans-extended molecular films. A remarkable feature of the spectra in Figure 11.1 is that the odd-even effect exhibited by n-alkanethiols on gold is opposite that (offset by one carbon) on Au/Cu(upd) and Au/Ag(upd). Figure 11.3 provides a simple illustration of this odd-even progression by showing the methyl mode intensities (r_a^- and r^+) as a function of the adsorbate chain length. The symmetric methyl intensity (r^+) is greater for even-chained adsorbates on gold and odd-chained adsorbates on upd-modified gold and to a much lesser degree on silver. In general, a greater symmetric methyl intensity indicates that the surface projection of the methyl group (i.e. the terminal C-C bond) is more normal to the surface. This result offers further evidence that subtle details of the molecular structure for SAMs on gold can be modified by pretreatment with a upd adlayer that alters its outermost atomic layer.

11.2.2. Calculation of Average Molecular Orientation for SAMs on Upd-Modified Gold

The intensities of the C-H absorptions in the IR spectra directly reflect the average orientation of the adsorbates on metal surfaces. Spectral simulations have been used to estimate the average structural orientation for SAMs on gold,[15] silver,[2] and copper.[2] The theoretical basis for these simulations—in addition to their application to other types of thin films—has been discussed in detail by Parikh and Allara[29] and will not be repeated here. In summary, the model uses an isotropic transmission spectrum of the bulk molecular species as input and scales this spectrum to that expected for an oriented film of molecular thickness using the projections of the transmission dipoles relative to the surface normal. The principal assumptions of the model for n-alkyl-based adsorbates are that the hydrocarbon chain is completely trans-extended and is oriented such that the structural conformation can be described by a cant (α) and twist (β) angle, as shown in Figure 11.4. Tilts or cants in the same direction as the S-C bond are positive while counterclockwise twists are positive.[30] For example, the spectrum for a SAM with $\alpha = 0$ would contain only methyl absorptions as the dynamic dipoles for the methylene modes would be perpendicular to the plane of
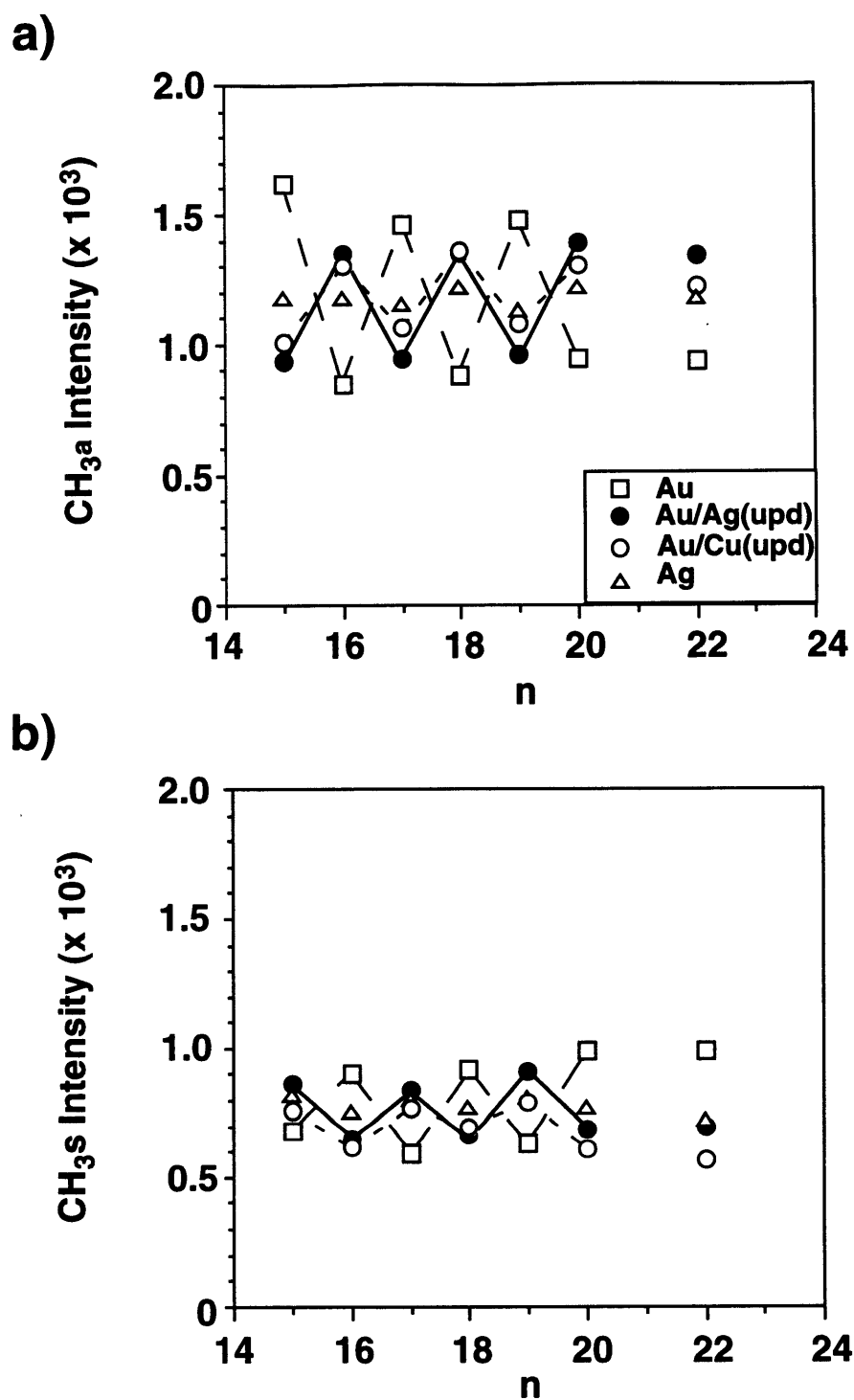
Figure 11.3. Intensities of the (a) asymmetric (r_a^-, CH_3a) and (b) symmetric (r^+, CH_3s) methyl modes for n-alkanethiols (C_nSH) adsorbed on gold, Au/Ag(upd), Au/Cu(upd), and silver surfaces. The lines serve as guides to the eye.

Figure 11.4. Schematic illustration of an all-trans chain in an n-alkanethiolate monolayer on a surface. The cant angle α and the chain twist β are shown along with their relationship to the surface coordinates.

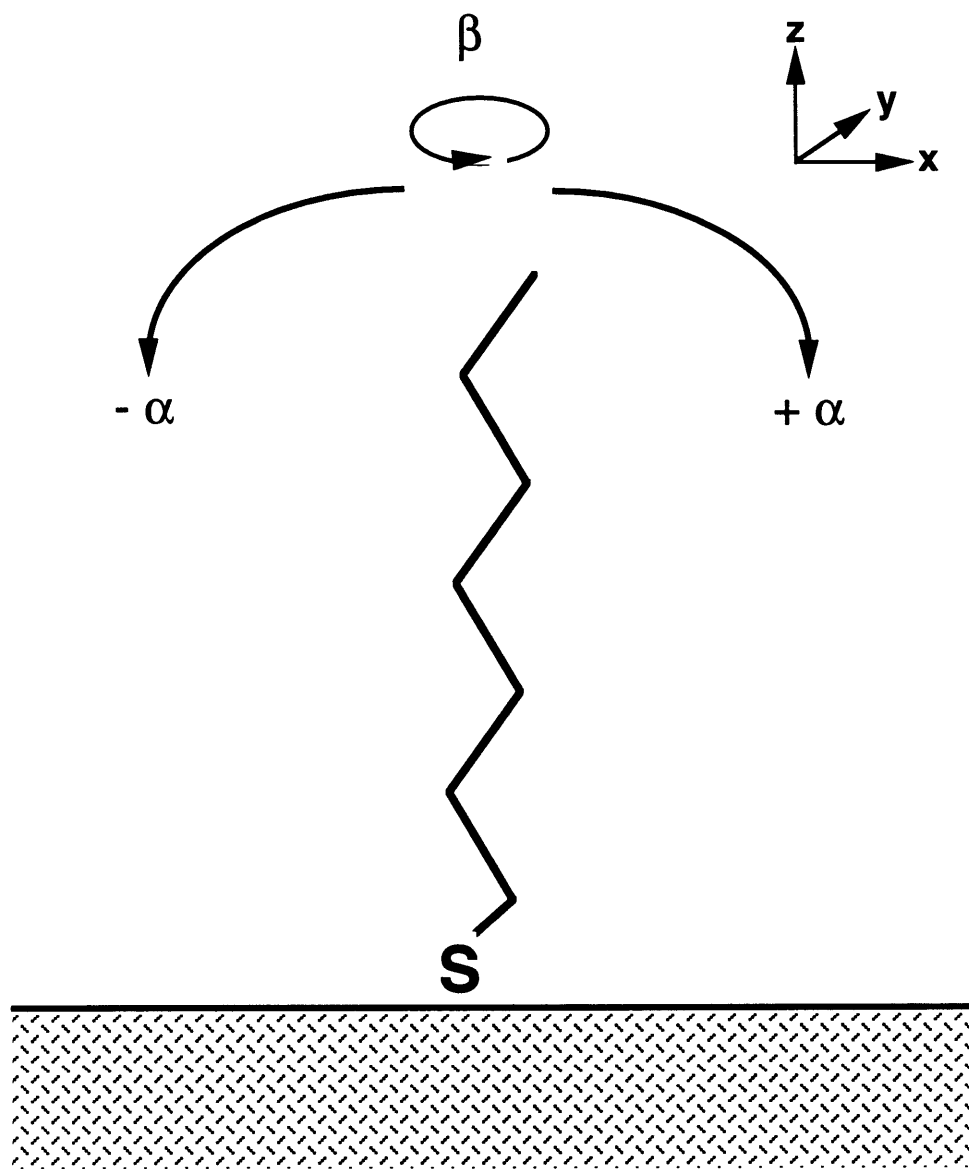the C-C backbone and would not interact with the electric field created by the reflected infrared beam. In general, as the chains tilt from the surface normal, the methylene modes increase in intensity due to a greater interaction of their dipoles with the electric field resulting in greater IR absorption. The remainder of this section focuses on the results of simulations of experimental infrared spectra for SAMs derived from $C_{18}SH$ on the native metals (gold and silver) and upd-modified gold. This adsorbate was studied because it is intermediate in chain length of those studied, it provides a simple comparison to the other adsorbates in the series, and SAMs derived from this n-alkanethiol have been the subject of greatest investigation.

11.2.2.1. $C_{18}SH$ on the Native Metals

The simulated spectra of SAMs formed from $C_{18}SH$ on gold and silver (and copper) have been discussed in great detail previously[2] and will be merely summarized here. In brief, Laibinis et al. reported that the IR spectra for SAMs on gold were consistent with a two-chain model (two different chain orientations within the SAM) consisting of chains canted at ~26° and twisted at either -48° or +50°.[2] In addition, to provide quality fits to the experimental spectra, the assumption of an all-trans chain was relaxed to allow gauche conformations at the terminal CH_2 groups of the chains, as consistent with molecular dynamics simulations.[31] For $C_{18}SH$ on silver, the experimental spectra were well described by a single-chain model consisting of chains canted at -13° and twisted at 42°. An interesting difference between SAMs on silver and gold is that both odd- and even-chained adsorbates were fit with a constant cant angle on gold to account for the alternating intensities of the methyl modes while the simulated cants on silver required variation between positive values for odd-chained adsorbates and negative values for even-chained adsorbates to allow for the lack of an odd-even progression in the experimental data. IR spectra on copper were sufficiently similar to those on silver to suggest that thiols formed a similar structure on the two metal surfaces.

The experimental spectra discussed here for $C_{18}SH$ on evaporated gold, silver, and copper films are similar to those obtained previously.[2] For $C_{18}SH$ on gold, simulated spectra with cants of 28° and twists of 48° provided excellent fits to the methylene modes. Nevertheless, an all-trans model was not sufficient to accurately fit the methyl modes due to the presence of gauche conformers in the terminal methylene units. As discussed above, a model that allows for gauche defects in these spectra can more effectively fit the methyl modes. Similar to previous results, a positive cant angle provided excellent fits to experimental spectra for SAMs containing either even- or odd-chained adsorbates. For $C_{18}SH$ on silver, simulated spectra for $\alpha = -12°$ and $\beta = 46°$ provided the best fits to the experimental spectra, agreeing with previous studies. On silver, a

single-chain, all-trans model provided good fits to the data. For odd-chained adsorbates, a cant of $+12°$ was required to account for the lack of an odd-even progression in methyl intensity.

11.2.2.2. SAMs on Au/Ag(upd) and Au/Cu(upd)

IR spectra for $C_{18}SH$ on both Cu- and Ag-upd modified gold are similar in that the methylene intensities are intermediate between those for SAMs on the native metals (Au and Ag or Cu) and that the odd-even progression in methyl intensity is opposite that exhibited on gold (Figures 11.1 and 11.3). These features of the spectra suggest that the cants for SAMs on both upd substrates are intermediate between those of the native metals and that the sign of the cant must be opposite that on gold. Figures 11.5a and b show both experimental and simulated IR spectra for $C_{18}SH$ on Au/Ag(upd) and Au/Cu(upd), respectively. The simulations are for SAMs with an all-trans chain and $\alpha = -18°$ and $-16°$ and $\beta = 45°$ and $43°$ on Au/Ag(upd) and Au/Cu(upd), respectively. Varying α and β by more than $1°$ from these values resulted in simulated spectra that provided clearly inferior fits to the experimental data. While the methylene modes are fit well in Figure 11.5, the methyl modes for the simulated spectra are less intense and slightly broader than those in the experimental spectra. These differences may reflect the different local environments for the methyl group in the SAM and the polycrystalline sample in KBr used as a basis for the simulated spectra. Nevertheless, the integrated intensities of the methyl modes are similar ($\pm 10\%$) for the experimental and simulated spectra. As for thiols on silver (and copper),[2] the spectra on the upd-modified gold are described well by a single-chain model. The negative cant exhibited for $C_{18}SH$ on upd-modified gold describes the structural orientation of odd-chained adsorbates, as well.

The intermediate cant for SAMs on upd-modified gold in comparison to those on the native metals might cause one to naively suggest that the structure of the SAM is an average of those on silver and gold. This suggestion would imply an underlying gold surface with regional areas of deposited silver and the presence of individual islands of SAMs on gold and silver. A close examination of the spectra in Figure 11.1 for $C_{18}SH$ on the various substrates suggests that the spectra of $C_{18}S/Ag(upd)/Au$ cannot result from a weighted averaging of the two spectra for $C_{18}SH$ on gold and silver. Specifically, the asymmetric methyl mode for $C_{18}SH$ on the Ag upd substrate is significantly greater than on either of the native metals. A similar analysis of the $C_{18}S/Cu(upd)/Au$ spectrum in comparison with those for $C_{18}SH$ on gold and copper leads to the same conclusion.
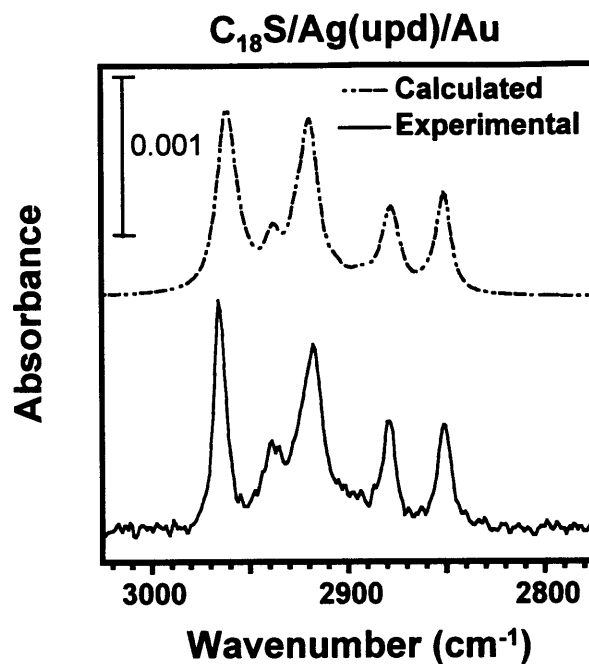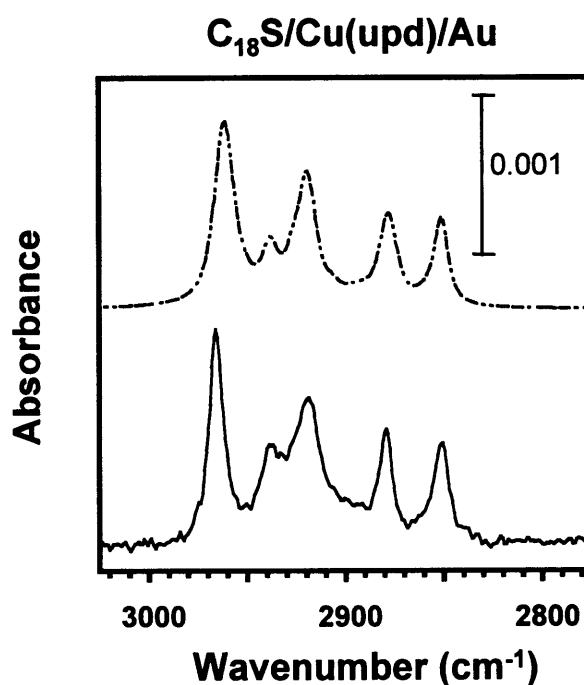
Figure 11.5. Experimental (solid) and calculated (dashed) IR spectra of SAMs derived from octadecanethiol on (a) Au/Ag(upd) and (b) Au/Cu(upd). The calculated spectra have cant angles, α, of (a) -18° and (b) -16° and twist angles, β, of (a) 45° and (b) 43°. The spectra have been offset vertically for clarity.

n = odd   **n = even**

$$\alpha = +28°$$

Gold   **Gold**

$$\alpha = -17°$$

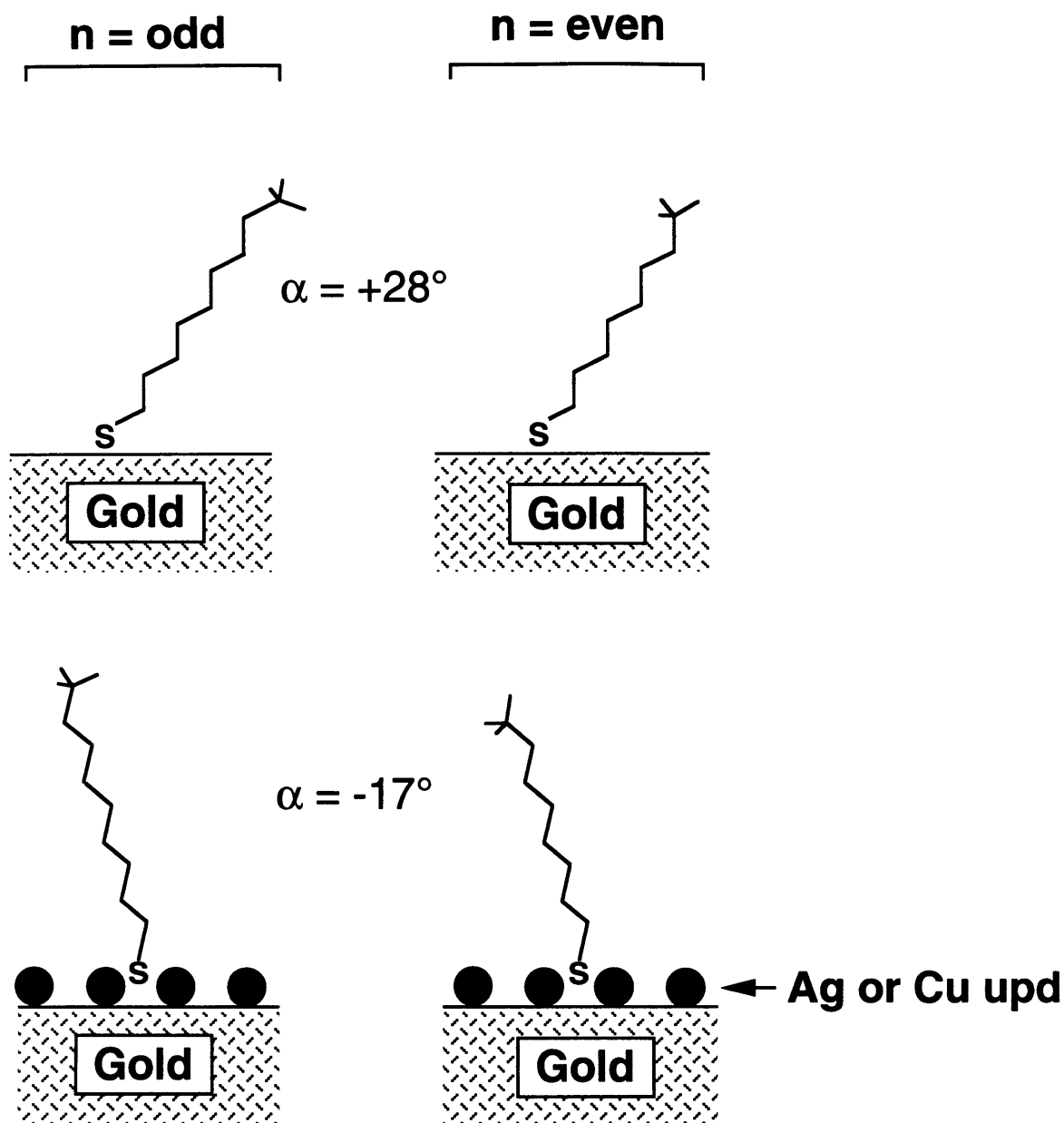**Gold**   **Gold**   ← **Ag or Cu upd**

Figure 11.6. Schematic illustration of the canted structures that form upon adsorption of n-alkanethiols (C_nSH) on gold, Au/Ag(upd), and Au/Cu(upd). The cant of -17° for SAMs on upd-modified gold is an average of the cants determined for Au/Ag(upd) (-18°) and Au/Cu(upd) (-16°). The structures formed on gold exhibit an odd-even modulation in the intensity of the methyl modes that is opposite that formed on upd-modified gold. This observation is consistent with the formation of a structure in which the cant angle (α) is positive for SAMs on gold and negative for SAMs on upd-modified gold.

11.2.3. Comparison of Binding and Structure for SAMs on upd and Native Metals

Figure 11.6 schematically illustrates the average orientations for SAMs of n-alkanethiols on the upd substrates and native metals prepared in our laboratory, as determined from IR spectra and spectral simulations. The smaller cants indicate that SAMs on upd metals are more densely packed than those on gold. This observation is the first report of a method to increase the packing density of SAMs on gold that does not involve chemical synthesis. Based on the structural orientation of the hydrocarbon chain in the SAMs on both upd metals, additional information can be inferred regarding the possible nature of the metal-sulfur binding and the overlayer structure of the SAMs enabling comparisons with the binding characteristics and structure for thiols on the native metals. For Au(111) substrates without upd modification, the sulfur head groups occupy three-fold hollow sites on the surface and form a ($\sqrt{3}$ x $\sqrt{3}$)R30° structure with an interchain distance of 4.99 Å.[1] The suggested sp^3 hybridization[21] of the sulfur on this surface results in a bond angle of 104° (or 76° from the surface normal) that is consistent with the odd-even progression in methyl intensity. On Ag(111), the thiols are suggested to form either an incommensurate overlayer by x-ray and helium diffraction[20] or a distorted ($\sqrt{7}$ x $\sqrt{7}$)[22] overlayer by STM with S adsorption favoring an sp hybridization. The reported interchain spacings for these SAMs vary from 4.61 Å (STM) to 4.67 Å (He diffraction) and 4.77 Å (x-ray diffraction).

For upd-modified gold substrates, the coverage and overlayer structure of the upd metal will likely affect the number of reactive sites for thiol adsorption. Gewirth's group has shown that the upd of silver onto Au(111) in sulfate electrolyte results in a 3 x 3 structure with a silver coverage of 0.44 by in situ AFM but a 5 x 5 structure with a silver coverage of 0.56 by LEED or Auger electron spectroscopy (AES).[32] The difference in these values may reflect the different modes of measurement or a change in structure upon removal from the electrochemical cell and subsequent analysis by vacuum techniques such as LEED or AES. The coverage of silver on our polycrystalline gold surface with a predominate Au(111) texture[33] is 0.60 by XPS and agrees well with the value of 0.56 obtained by Gewirth's group and attributed to a 5 x 5 adlayer structure of silver on Au(111). Based on these similarities, subsequent discussions assume that silver is present on these gold substrates in a 5 x 5 lattice with a corresponding interatomic spacing of 3.60 Å. Since the coverage of copper on these polycrystalline gold substrates is 0.55, copper may also form a 5 x 5 structure on gold. This structure has been identified for intermediate coverages of copper upd adlayers on Au(111) by in situ x-ray absorption spectroscopy.[34] Therefore, considering the similar cants for SAMs on either upd substrate, thiols on Au/Cu(upd) are assumed to adopt the same structure as that detailed for Au/Ag(upd) below.

Based on an average cant of 18°, the area occupied by each chain on Ag(upd)/Au is ~19.7 Å^2 and corresponds to an interchain spacing of 4.77 Å.[35] This area is greater than that occupied by each Ag adatom (11.2 Å^2) suggesting that binding in the three-fold hollow sites of the silver adlayer would produce too sparse a thiol adlayer. A possible structure for thiols on a 5 x 5 lattice of silver on gold is in every other three-fold hollow site of the silver adatoms, forming a ($\sqrt{7}$ x $\sqrt{7}$)R10.9° structure with an interchain spacing of 4.77 Å (Figure 11.7a). Interestingly, H_2S adsorbs onto Ag(111) in a similar ($\sqrt{7}$ x $\sqrt{7}$)R10.9° structure,[36] but alkanethiols cannot adopt this structure on the Ag(111) lattice due to steric limitations of the polymethylene chains. The greater spacing of silver adatoms on the Au/Ag(upd) surface may enable this arrangement of the thiols. Another possible structure for the thiols is a 4 x 4 overlayer with every fourth thiol constrained to a three-fold hollow site between silver adatoms (Figure 11.7b). The S-S nearest neighbor distance in this structure is 4.80 Å and would be consistent with the IR spectra. That the alternating, odd-even methyl orientation for SAMs on upd substrates is opposite that on gold (Figure 11.3) indicates that the sulfur-carbon bond is oriented more normal to the surface on the upd substrate. As the sulfurs are likely bound between the silver adatoms in two- or three-fold sites in either structure, steric limitations might force the C-S bond more normal to the surface; thereby, an sp^3 hybridization for the sulfur atom might result in SAMs with similar structural properties as those with sp hybridization for the adsorbed sulfur. Whether the hybridization of the sulfur is sp or sp^3 depends on the interaction between the sulfur and silver at the metal surface.

11.2.4. Effect on Wetting

The odd-even methyl orientation for SAMs on upd-modified gold can be probed by wetting measurements provided that the probe liquid is sensitive to the outer surface. As hexadecane (HD) is a liquid that interacts with solid surfaces solely through dispersive forces, the contact angle of HD (θ_{HD}) is extremely sensitive to the characteristics of the outermost 3 Å of a surface. [37,38] Figure 11.8 shows the wetting characteristics of the SAMs by HD as a function of the chain length of C_nSH adsorbed on gold, Au/Ag(upd), and Au/Cu(upd). On gold, the odd-even alternation in θ_{HD} is similar to that observed by others with even-chained SAMs being less wet by HD (greater θ_{HD}). The remarkable feature of Figure 11.8 is that the odd-even wetting trend for SAMs on gold is opposite that (offset by one carbon) for SAMs on either Au/Ag(upd) or Au/Cu(upd). A comparison of these data with the symmetric methyl intensities obtained from IR spectra (Figure 11.3) reveals that higher contact angles of HD are observed for SAMs that exhibit a stronger symmetric methyl intensity and a weaker asymmetric intensity in their IR spectrum. In other words, HD wets the surface less when the projection of the methyl group is more normal to the surface. Because HD completely wets methylene (-CH_2) surfaces,[39] the smaller values of θ_{HD}
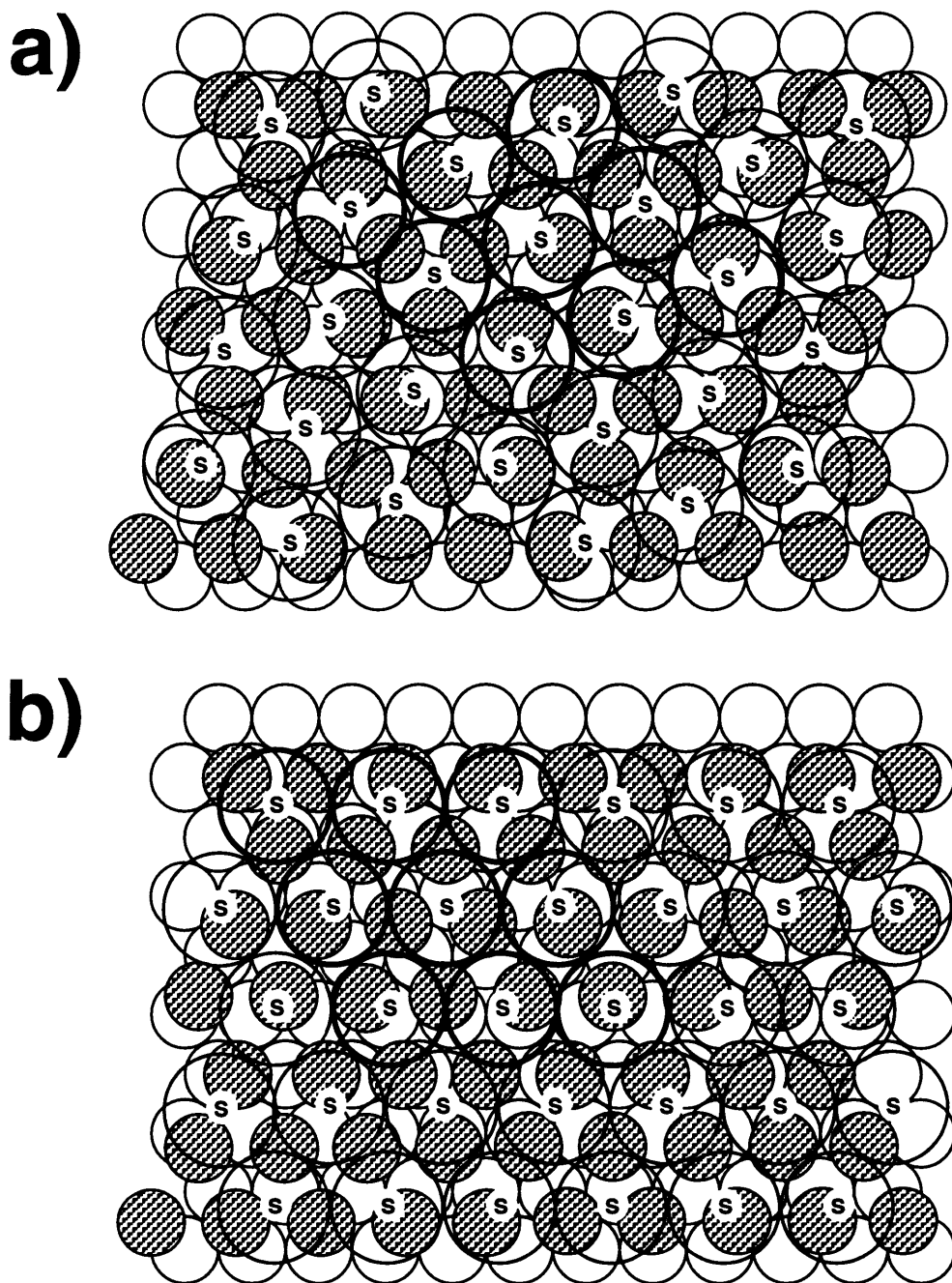
192

Figure 11.7. Possible structure and binding sites for n-alkanethiols on a Au/Ag(upd) substrate where the silver adlayer forms a 5 x 5 structure on the Au(111) surface with a coverage of 0.56: (a) a ($\sqrt{7}$ x $\sqrt{7}$)R10.9° structure for the thiol on the Ag adlayer with an interchain spacing of 4.77 Å and (b) a 4 x 4 structure for the thiol on the Ag adlayer with an interchain spacing of 4.80 Å. Based on the experimental and calculated IR spectra, the thiol is canted ~18° from the surface normal and exhibits an estimated interchain spacing is 4.77 ± 0.05 Å, which is consistent with the structures in both (a) and (b).
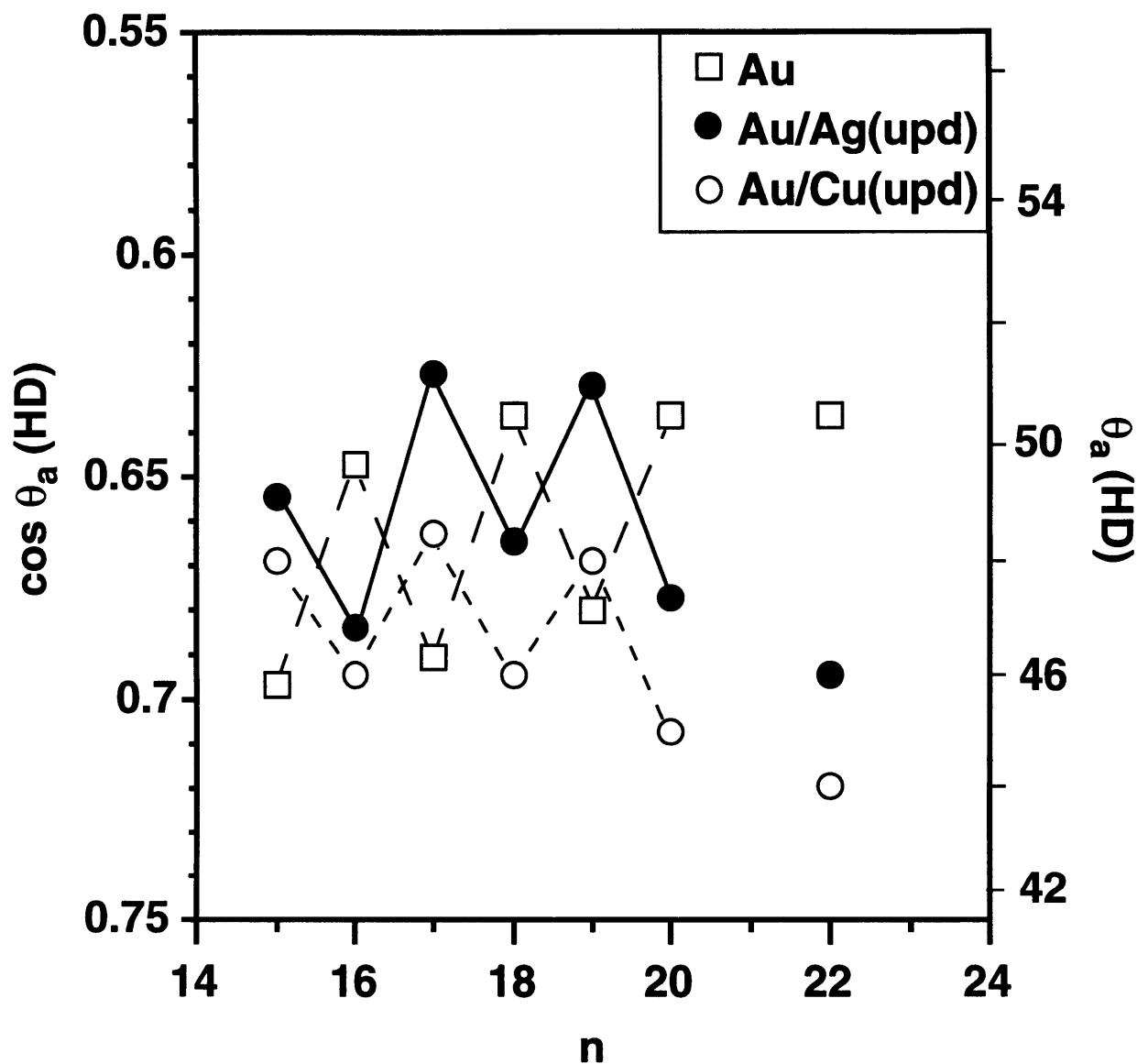
Figure 11.8. Wetting properties of SAMs formed from the adsorption of C_nSH (n = 15 - 20; 22) on gold, Au/Ag(upd), and Au/Cu(upd) as measured by the advancing contact angle of hexadecane $[\theta_a(HD)]$(right axis) or cos $\theta_a(HD)$ (left axis). The measured contact angles are accurate to within ±2° based on the average of measurements made on samples from independent preparations. The lines serve as guides to the eye. Wetting data for silver are not shown and exhibit no odd-even trend in the advancing hexadecane contact angle.

suggest a possible interaction between HD and the outermost -CH_2- units when the methyl groups orient away from the surface normal. In Figure 11.8, the odd-even wetting trend is most pronounced for thiols on gold and least prominent for thiols on Au/Cu(upd); the wetting results for SAMs on evaporated silver films (not shown) revealed no odd-even variation in θ_{HD}. These wetting results mirror the variations in the methyl mode intensities in Figure 11.3 as a more prominent odd-even progression is observed for thiols on gold, a more subtle effect is shown for thiols on Au/Cu(upd), and a significantly reduced effect (if any) is observed for thiols on silver. By pretreating the gold with upd layers of copper or silver before self-assembly, the S-metal binding and geometry are affected, thereby altering the orientation of the methyl group at the surface. That this effect is observable by wetting provides an notable example of how a molecular-level effect—such as the angstrom-level variation in the orientation of a methyl group—can influence a macroscopic surface property such as the wetting by a contacting liquid.

11.3. Conclusions

The underpotential deposition of silver or copper on polycrystalline gold modifies the outermost surface of the metal and alters the density of reactive sites for an adsorbing alkanethiol. SAMs formed by adsorption of n-alkanethiols on Au/Ag(upd) and Au/Cu(upd) exhibit different structures than on the native metals. In particular, SAMs on upd-modified gold are canted ~-17° from the surface normal and are more densely packed than those on gold which are canted ~28° from the surface normal. This cant is consistent with the thiols binding in primarily 3-fold and 2-fold sites on the silver or copper adlayer to form either a ($\sqrt{7}$ x $\sqrt{7}$)R10.9° or 4 x 4 structure. SAMs on upd-modified gold display an odd-even variation in the intensities of the methyl vibrational modes that is offset by one methylene unit from the odd-even modulation exhibited by SAMs on gold, suggesting that the upd alters the metal-S-C bonding geometry. These angstrom-level variations in the alternate orientations of the methyl groups can be detected macroscopically by measuring the contact angle of hexadecane. In particular, the methyl surface is wet less by hexadecane when the methyl units are oriented more normal to the surface, reflecting greater screening of the interaction between the liquid and the methylene groups nearest the surface.

11.4. Experimental

The preparation of gold/upd/SAM assemblies and their characterization by reflectance infrared spectroscopy and wetting were detailed in Chapter 8 and will not be repeated here. The odd-even wetting variations noted in Figure 11.8 were confirmed by double-blind experiments. Spectral simulations were performed using a computer program developed and provided by Atul Parikh

(LANL) and David L. Allara (Penn State).[29] The isotropic reference data required for the simulations of $C_{18}SH$ spectra were obtained from a file prepared by A. Parikh using $(C_{18}S)_2$ in a KBr matrix.

11.5 References and Footnotes

1) Ulman, A. *Chem. Rev.* **1996**, *96*, 1533-1544.

2) Laibinis, P. E.; Whitesides, G. M.; Allara, D. L.; Tao, Y.-T.; Parikh, A. N.; Nuzzo, R. G. *J. Am. Chem. Soc.* **1991**, *113*, 7152-7167.

3) Walczak, M. M.; Chung, C.; Stole, S. M.; Windrig, C. A.; Porter, M. D. *J. Am. Chem. Soc.* **1991**, *113*, 2370-2378.

4) Demoz, A.; Harrison, D. J. *Langmuir* **1993**, *9*, 1046-1050.

5) Volmer, M.; Stratmann, M.; Viefhaus, H. *Surf. Interface Anal.* **1990**, *16*, 278-282.

6) Sheen, C. W.; Shi, J. X.; Martensson, J.; Parikh, A. N.; Allara, D. L. *J. Am. Chem. Soc.* **1992**, *114*, 1514-1515.

7) Mirkin, C. R.; Chen, K.; Lo, R. K.; Zhao, J.; McDevitt, J. T. *J. Am. Chem. Soc.* **1995**, *117*, 6374-6375.

8) Laibinis, P. E.; Palmer, B. J.; Lee, S.-W.; Jennings, G. K. *The Synthesis of Organothiols and their Assembly into Monolayers on Gold*; in Thin Films, v. 24; Ulman, A., Ed.; Academic Press: Boston, 1998, pp 1-41.

9) Dubois, L. H.; Zegarski, B. R.; Nuzzo, R. G. *J. Chem. Phys.* **1993**, *98*, 678.

10) Fenter, P.; Eisenberger, P.; Liang, K. S. *Phys. Rev. Lett.* **1993**, *70*, 2447.

11) Camillone, N.; Chidsey, C. E. D.; Liu, G.-Y.; Scoles, G. *J. Chem. Phys.* **1993**, *1993*, 3503.

12) Poirier, G. E. *Chem. Rev.* **1997**, *97*, 1117-1127.

13) Xu, S.; Cruchon-Dupeyrat, S.; Garno, J. C.; Liu, G.-Y.; Jennings, G. K.; Yong, T.-H.; Laibinis, P. E. *J. Chem. Phys.* **1998**, *108*, 5002-5012.

14) Bryant, M. A.; Pemberton, J. E. *J. Am. Chem. Soc.* **1991**, *113*, 8284-8293.

15) Porter, M. D.; Bright, T. B.; Allara, D. L.; Chidsey, C. E. D. *J. Am. Chem. Soc.* **1987**, *109*, 3559-3568.

16) Chang, S.-C.; Chao, I.; Tao, Y.-T. *J. Am. Chem. Soc.* **1994**, *116*, 6792-6805.

17) Tour, J. M.; Jones, L.; Pearson, D. L.; Lamba, J. J. S.; Burgin, T. P.; Whitesides, G. M.; Allara, D. L.; Parikh, A. N.; Atre, S. V. *J. Am. Chem. Soc.* **1995**, *117*, 9529-9534.

18) Dhirani, A.-A.; Zehner, R. W.; Hsung, R. P.; Guyot-Sionnest, P. G.; Sita, L. R. *J. Am. Chem. Soc.* **1996**, *118*, 3319-3320.

19) Whitesell, J. K.; Chang, H. K. *Science* **1993**, *261*, 73-76.

20) Fenter, P.; Eisenberger, P.; Li, J.; Camillone, N.; Bernasek, S.; Scoles, G.; Ramanarayanan, T. A.; Liang, K. S. *Langmuir* **1991**, *7*, 2013-2016.

21) Sellers, H.; Ulman, A.; Shnidman, Y.; Eilers, J. *J. Am. Chem. Soc.* **1993**, *115*, 9389-9401.

22) Dhirani, A.; Hines, M. A.; Fisher, A. J.; Ismail, O.; Guyot-Sionnest, P. *Langmuir* **1995**, *11*, 2609-2614.

23) Jennings, G. K.; Laibinis, P. E. *J. Am. Chem. Soc.* **1997**, *118*, 5208-5214.

24) Jennings, G. K.; Laibinis, P. E. *Langmuir* **1996**, *12*, 6173-6175.

25) Jennings, G. K. *Electrochem. Soc. Interface* **1998**, *7*, 59.

26) Burgess, J. D.; Hawkridge, F. M. *Langmuir* **1997**, *13*, 3781-3786.

27) Nishizawa, M.; Sungawa, T.; Yoneyama, H. *Langmuir* **1997**, *13*, 5215-5217.

28) Zamborini, F. P.; Campbell, J. K.; Crooks, R. M. *Langmuir* **1998**, *14*, 640-647.

29) Parikh, A. N.; Allara, D. L. *J. Chem. Phys.* **1992**, *96*, 927-945.

30) The sign convention for the cant angle here is opposite that used in ref. 29.

31) Hautman, J.; Klein, M. L. *J. Chem. Phys.* **1989**, *91*, 4994-5001.

32) Mrozek, P.; Sung, Y.-E.; Han, M.; Gamboa-Aldeco, M.; Wieckowski, A.; Chen, C.-H.; Gewirth, A. A. *Electrochim. Acta* **1995**, *40*, 17-28.

33) Nuzzo, R. G.; Fusco, F. A.; Allara, D. L. *J. Am. Chem. Soc.* **1987**, *109*, 2358-2367.

34) Tadjeddine, A.; Guay, D.; Ladouceur, M.; Tourillon, G. *Phys. Rev. Lett.* **1991**, *66*, 2235-2238.

35) This value assumes that the interchain spacing for a SAM with 0° cant is the same as found in bulk paraffins: 4.65 Å.[1]

36) Schwaha, K.; Spencer, N. D.; Lambert, R. M. *Surf. Sci.* **1979**, *81*, 273-284.

37) Bain, C. D.; Whitesides, G. M. *J. Am. Chem. Soc.* **1988**, *110*, 6560-6561.

38) Laibinis, P. E.; Bain, C. D.; Nuzzo, R. G.; Whitesides, G. M. *J. Phys. Chem.* **1995**, *99*, 7663-7676.

39) Holmes-Farley, S. R.; Reamey, R. H.; McCarthy, T. J.; Deutch, J.; Whitesides, G. M. *Langmuir* **1985**, *1*, 725-740.

Appendix

Relationship between Adlayer Coverage and Relative XPS Intensities for the Adlayer and Underlying Substrate (Derivation of Eq 8.1)

The Au/upd layer/SAM system is modeled in Scheme A1 as a bulk substrate overlaid by two layers: the upd layer and the self- assembled monolayer (SAM). The XPS intensities for the

Scheme A1. Gold/upd Layer/SAM Assembly
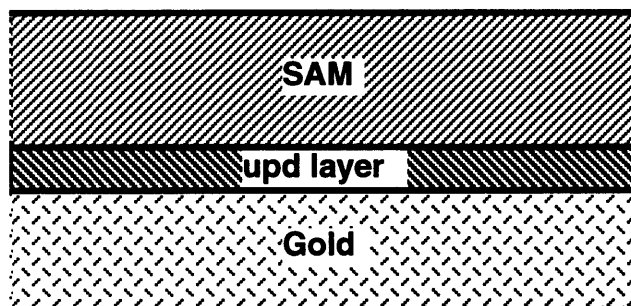
upd layer and the bulk substrate in this arrangement are described by eq A1 and A2, respectively,

$$I_{upd} = I^o_{upd} \left[1 - \exp\left(\frac{- d_{upd}}{\lambda_{upd(KE_{upd})} \cos\Theta} \right) \right] \exp\left(\frac{- d_{SAM}}{\lambda_{SAM(KE_{upd})} \cos\Theta} \right) \tag{A1}$$

$$I_{Au} = I^o_{Au} \exp\left(\frac{- d_{upd}}{\lambda_{upd(KE_{Au})} \cos\Theta} \right) \exp\left(\frac{- d_{SAM}}{\lambda_{SAM(KE_{Au})} \cos\Theta} \right) \tag{A2}$$

where I_{Au} and I_{upd} are the attenuated photoelectron intensities, I^o_{upd} and I^o_{Au} are the unattenuated intensities for bulk samples, d_{upd} and d_{SAM} are the thicknesses of the overlayers, $\lambda_{upd(KE_i)}$ is the inelastic mean free path through the upd adlayer for electrons of kinetic energy (KE) from the upd layer or the gold substrate, $\lambda_{SAM(KE_i)}$ is the inelastic mean free path through the SAM for electrons of kinetic energy (KE) from the upd layer or the gold substrate, and Θ is the angle of the detector to the surface normal. Eqs A1 and A2 apply for systems of homogeneous layers with uniform thickness.[1] As the upd layers have sub-monolayer coverages and should not be considered uniform, d_{upd} is replaced in these equations by the atomic thickness of the upd layer (a_{upd}) and the surface coverage of the upd layer (ϕ_{upd}). This replacement yields eq A3 and A4

199

$$I_{upd} = I^o_{upd} \ \phi_{upd} \left[1 - \exp\left(\frac{- a_{upd}}{\lambda_{upd(KE_{upd})} \cos\Theta} \right) \right] \exp\left(\frac{- d_{SAM}}{\lambda_{SAM(KE_{upd})} \cos\Theta} \right) \qquad (A3)$$

$$I_{Au} = I^o_{Au} \left[\left(1 - \phi_{upd} \right) + \phi_{upd} \exp\left(\frac{- a_{upd}}{\lambda_{upd(KE_{Au})} \cos\Theta} \right) \right] \exp\left(\frac{- d_{SAM}}{\lambda_{SAM(KE_{Au})} \cos\Theta} \right) \qquad (A4)$$

where a_{upd} is the diameter of the adatom and ϕ_{upd} is the fractional coverage of a monolayer for the upd layer.[1,2] Division of eq A3 by eq A4 yields eq A5 that relates the relative XPS intensities for the upd layer and underlying bulk substrate to the coverage of the upd layer, where C_{SAM} contains the effects of attenuation by the SAM on the upd and bulk signals (eq A6).

$$\frac{I_{upd}}{I_{Au}} = \frac{I^o_{upd}}{I^o_{Au}} \ \frac{\phi_{upd} \left[1 - \exp\left(\frac{- a_{upd}}{\lambda_{upd(KE_{upd})} \cos\Theta} \right) \right]}{\left(1 - \phi_{upd} \right) + \phi_{upd} \exp\left(\frac{- a_{upd}}{\lambda_{upd(KE_{Au})} \cos\Theta} \right)} \ C_{SAM} \qquad (A5)$$

$$C_{SAM} = \frac{\exp\left(\frac{- d_{SAM}}{\lambda_{SAM(KE_{upd})} \cos\Theta} \right)}{\exp\left(\frac{- d_{SAM}}{\lambda_{SAM(KE_{Au})} \cos\Theta} \right)} \qquad (A6)$$

Rearrangement of eq A5 yields the coverage of the upd layer as an explicit function (eq A7) of the measured relative intensities for the two XPS signals.

$$\phi_{upd} = \left\{ \left(\frac{I_{Au}}{I_{upd}} \right) \left(\frac{I^o_{upd}}{I^o_{Au}} \right) C_{SAM} \left[1 - \exp\left(\frac{- a_{upd}}{\lambda_{upd(KE_{upd})} \cos\Theta} \right) \right] + \left[1 - \exp\left(\frac{- a_{upd}}{\lambda_{upd(KE_{Au})} \cos\Theta} \right) \right] \right\}^{-1} \qquad (A7)$$

Footnotes and References

(1) Seah, M.P. In *Practical Surface Analysis: Volume 1. Auger and X-ray Photoelectron Spectroscopy*; Briggs, D., Seah, M.P., Eds.; Wiley: Chichester, 1990; p. 245.

(2) Eqs A3 and A4 are similar to those presented in ref 1 for thin or monoatomic overlayers. The equations developed here include additional attenuation factors due to the presence of the SAM or adventitious carbon.